Novel Bacterial Foraging Optimisation Algorithms with Application to Modelling and Control of Flexible Manipulator Systems

A thesis submitted to the University of Sheffield for the degree of Doctor of Philosophy

By
Heru Supriyono

Department of Automatic Control and Systems Engineering
The University of Sheffield
Mappin Street
Sheffield, S1 3JD
United Kingdom

February 2012

ABSTRACT

Biologically-inspired soft-computing algorithms, which were developed by mimicking evolution and foraging techniques of animals in nature, have attracted significant attention of researchers. The works are including the development of the algorithm itself, its modification and its application in broad areas. This thesis presents works on biologically-inspired algorithm based on bacterial foraging algorithm (BFA) and its performance evaluation in modelling and control of dynamic systems. The main aim of the research is to develop new modifications of BFA and its combination with other soft computing techniques and test their performances in modelling and control of dynamic systems. Modification of BFA focuses for improving its convergence in terms of speed and accuracy. The performances of modified BFAs are assessed in comparison to that of original BFA.

In the original BFA, in this thesis referred as standard BFA (SBFA), bacteria use constant chemotactic step size to head to global optimum location. Very small chemotactic step size around global optimum location will assure bacteria find the global optimum point. However, a large number of steps is needed for the whole optimisation process. Moreover, there is potential for the algorithm to be trapped in one of the local optima. On the contrary, big chemotactic step size will assure bacteria have faster convergence speed but the literature shows that it results oscillation around global optimum point and the algorithm potentially missing the global optimum point and leading to oscillation around the point. Thus SBFA can be improved by applying adaptable chemotactic step size which could change: very large when bacteria are in locations far away from the global optimum location, to speed up the convergence, and very small when bacteria are in the locations near the global optimum so that bacteria able to find global optimum point without oscillation.

Here, four novel adaptation schemes allowing the chemotactic step size to depending on the cost function value have been proposed. The adaptation schemes are developed based on linear, quadratic and exponential functions as well as fuzzy logic (FL). Then, the proposed BFAs with adaptable chemotactic step size, i.e. linearly adaptable BFA (LABFA), quadratic adaptable BFA (QABFA), exponentially adaptable BFA (EABFA) and fuzzy adaptable chemotactic step size (FABFA), are validated by using them to find global minimum point of seven well-known benchmark functions commonly used in development of optimisation techniques development. The results show that all ABFAs achieve better accuracy and speed compared to those of SBFA.

The ABFAs are then used in modelling and control of a single-link flexible manipulator system. This includes modelling (based on linear model structures, neural network (NN), and fuzzy logic (FL)), optimising joint-based collocated (JBC) proportional-derivative (PD) control, and optimising both PD and proportional integral derivative (PID) control of end-point acceleration feedback for vibration reduction of a single-link flexible manipulator. The results show that ABFAs outperform SBFA in terms of convergence speed and accuracy. Since all SBFA and ABFAs use the same general parameters and bacteria are initially placed randomly across the nutrient media (cost function), the superiority better performance of ABFAs are attributed to the proposed adaptable chemotactic step size.

PUBLICATIONS

Part of the work presented in this thesis has either been published or submitted or accepted for publication. These are listed below:

A. Journal papers

1. **H. Supriyono** and M.O. Tokhi, "Fuzzy modelling of a flexible manipulator with bacterial foraging algorithms", submitted to *IEEE Transactions on Evolutionary Computation* (January 2012).
2. **H. Supriyono** and M. O. Tokhi, "Parametric modelling approach using bacterial foraging algorithms for modelling of flexible manipulator systems", submitted in revised to *Engineering Applications of Artificial Intelligence* (January 2012).
3. **H. Supriyono**, and M.O. Tokhi, (2011), "Adaptation schemes of chemotactic step size of bacterial foraging algorithm for faster convergence", Journal of Artificial Intelligence, **4**(4), pp. 207-219. DOI: 10.3923/jai.2011.207.219.

B. Conference Papers

1. **H. Supriyono** and M.O. Tokhi, "Dynamic neuro-modelling using bacterial foraging optimisation with fuzzy adaptation", *Third International Conference on Intelligent Systems, Modelling and Simulations, ISMS 2012, Kota Kinabalu, Malaysia, 8-10 February 2012*. (A**ccepted**)
2. **H. Supriyono**, M.O. Tokhi and B.A. Md Zain, (2011), "Modelling of flexible manipulator systems using bacterial foraging algorithms", *Proceedings of CLAWAR 2011: The 14th International Conference on Climbing and Walking Robots and the Support Technologies for Mobile Machines (CLAWAR2011), Paris, France, 6-8 September 2011*, pp. 157-165.
3. **H. Supriyono**, M.O. Tokhi and B.A. Md Zain, (2010), "Control of a single-link flexible manipulator using improved bacterial foraging algorithm", *Proceedings of 2010 IEEE Conference on Open Systems (ICOS2010), Kuala Lumpur, Malaysia. 5-7 December 2010*, pp. 68-73, DOI: 10.1109/ICOS.2010.5720066.
4. **H. Supriyono**, M.O. Tokhi and B.A. Md Zain, (2010), "Adaptive biologically-inspired algorithm-based controller tuning for input tracking control of flexible

manipulators", *Proceedings of 9th IEEE International Conference On Cybernetic Intelligent Systems, Reading, United Kingdom, 1-2 September 2010*, pp. 2-7, DOI: 10.1109/UKRICIS.2010.5898150.

5. **H. Supriyono** and M.O. Tokhi, (2010), "Bacterial foraging algorithm with adaptable chemotactic step size", *Proceedings of Second International Conference on Computational Intelligence, Communication Systems and Networks 2010 (CICSyN2010)*, Liverpool, United Kingdom, 29-30 July 2010, pp. 72-77, Digital Object Identifier: 10.1109/CICSyN.2010.52.

ACKNOWLEDGEMENT

All praise and glory are due to Allah, Whose mercy and blessings have been bestowed constantly upon the author. Peace and blessings be upon Prophet Muhammad.

Firstly, I would like to express my bottomless gratitude for Dr. M. Osman Tokhi for his warm welcome since the first day I joined his group, supervision, deep discussion, encouragement and guidance. I have been learning a lot of things in the group, both academic and non-academic, especially on how supervisor treats students. I enjoyed very much the environment in the group and possibly suitable to be adopted in my home department once I return back to my home university.

Secondly, I would like to thank my sponsors who have provided full financial support during my study. The first sponsor, the main sponsor, is the Ministry of National Education and Culture of Republic of Indonesia who has provided funding and the second sponsor is my home university, Universitas Muhammadiyah Surakarta (UMS), who manage the day-to-day scholarship program. The efforts of human resources department (HRD) of UMS are marvellous and I really appreciate them.

Also, I would like to thank all of my friends in the group for their suggestion, support and discussion during the study in the group. The atmosphere is very fantastic. All these experiences have enriched my perception and widen my horizon. Besides, I also would express my gratitude to all academics and staff at the Department of ACSE for their help, support and knowledge.

Moreover I would like to thank Professor David Al Dabass and Professor Mahdi Mahfouf, external and internal examiners respectively for their suggestions and advices for further improvement.

Finally, I would like to express my deepest gratitude to my parents, my wife and my daughters. Thanks for their support and prayers over years of my study.

TABLE OF CONTENTS

Title

Abstract i

Publications iii

Acknowledgement v

Table of Contents vi

List of Figures xi

List of Tables xix

Chapter 1: Introduction 1

1.1. Background 1

1.2. Aim of the research 7

1.3. Research objectives 7

1.4. Contributions of the research 8

1.5. Organisation of the thesis 11

Chapter 2: Bacterial Foraging Algorithm: An Overview 13

2.1. Introduction 13

2.2. The original bacterial foraging algorithm 13

2.2.1. Basic concept of bacteria movement 13

2.2.2. Optimisation technique based on bacterial foraging 15

2.2.3. The original BFA computation algorithm 19

2.3. Current applications and modifications 21

2.3.1. Application of SBFA 21

2.3.2. Modifications and improvements of BFA 23

2.4. Parameters choosing and their impacts on convergence and accuracy 28

2.4.1. Overall foraging of bacteria illustration 30

2.4.2. Impact of bacteria population size 35

2.4.3. Impact of chemotactic step number 38

2.4.4. Impact of maximum continuous swim number 39

2.4.5. Impact of reproduction steps 41

2.4.6. Impact of elimination and dispersal event 43

2.4.7. Impact of chemotactic step size 46
2.4.8. Impact of probability value which bacteria will be eliminated/dispersed 48
2.4.9. Impact of initial positions of bacteria 50
2.5. Summary 52

Chapter 3: Flexible Manipulator System: An Overview 53
3.1. Introduction 53
3.2. Structure of flexible manipulator system 53
3.3. Previous works on modelling of flexible manipulator system 56
3.3.1. Introduction 56
3.3.2. Mathematical or analytical approaches 58
3.3.3. Parametric modelling approaches 62
3.3.4. Non-parametric modelling approaches 62
3.4. Previous works on control of flexible manipulator system 63
3.5. Preliminary motion dynamics experiment 64
3.6. Summary 65

Chapter 4: Bacterial Foraging Algorithm with Adaptable Chemotactic Step Size 67
4.1. Introduction 67
4.2. Adaptation mechanism of chemotactic step size 67
4.2.1. Linearly adaptive bacterial foraging algorithm 69
4.2.2. Quadratic adaptive bacterial foraging algorithm 70
4.2.3. Exponentially adaptive bacterial foraging algorithm 70
4.2.4. Chemotactic step size adaptation using fuzzy logic 71
4.3. Computation steps ABFAs 74
4.4. Results and discussions 77
4.4.1. Test function 1: Rosenbrock function 78
4.4.2. Test Function 2: sphere function 82
4.4.3. Test function 3: Rastrigin’s function 6 85
4.4.4. Test function 4: Schwefel’s function 7 88
4.4.5. Test function 5: Ackley function 91

4.4.6. Test function 6: weighted sphere function 95
4.4.7. Test function 7: Schwefel's function 1.2 97
4.4.8. Comparison 101
4.5. Summary 101

Chapter 5: Using Parametric Modelling of Flexible Manipulator with Bacterial Foraging Algorithms 102
5.1. Introduction 102
5.2. Preliminary experimentation 103
5.3. Model structure formulation 103
5.4. ABFA-based modelling 104
5.5. Model Validation 105
5.6. Results and Discussion 106
5.6.1. Preliminary simulation: empirical cost functions comparison 107
5.6.2. Hub-angle model 110
5.6.3. Hub-velocity modelling 120
5.6.4. End-point acceleration 131
5.7. Summary 142

Chapter 6: Modelling of Flexible Manipulator Using Neural Networks Optimised by Bacterial Foraging Algorithms 144
6.1. Introduction 144
6.2. Brief fundamentals of neural network 146
6.3. NN-based modelling computation 149
6.3.1. Model structure formulation 149
6.3.2. Computation steps of NN-based model 150
6.3.3. Model validation for BFA-NN models 151
6.4. FL-based modelling computation 152
6.4.1. Model structure formulation 152
6.4.2. Computation steps of BFA-FL 154
6.4.3. Model validation for BFA-FL models 155
6.5. Protocol and preliminary computation 156
6.5.1. Protocol computation 156

6.5.2. Preliminary simulation: empirical comparison of cost functions 157
6.6. Results and discussion: BFA-NN models 160
6.6.1. Hub-angle model 160
6.6.2. Hub-velocity model 171
6.6.3. End-point acceleration model 180
6.7. Results and discussion: BFA-FL models 192
6.7.1. Hub-angle model 192
6.7.2. Hub-velocity model 201
6.7.3. End-point acceleration model 210
6.8. Summary 220

Chapter 7: Control of Flexible Manipulator System Using Bacterial Foraging Algorithms 222
7.1. Introduction 222
7.2. Brief overview of PID control 224
7.3. Single-link flexible manipulator model 224
7.4. Hub-angular reference tracking control 225
7.4.1. ABFA-JBC PD control structure and computation 225
7.4.2. Protocol of simulation and experimentation 226
7.4.3. Preliminary simulation: empirical cost function comparison 229
7.4.4. Closed-loop simulation using J_2 232
7.5. Vibration control using end-point acceleration feed back 237
7.5.1. Controller structure and computation 237
7.5.2. Protocol of simulations and experimentations 238
7.5.3. Open-loop simulation 239
7.5.4. End-point acceleration feedback with PD control 240
7.5.5. End-point acceleration feedback with PID control 247
7.6. Summary 254

Chapter 8: Conclusion and Future Work 255
8.1. Summary and Conclusion 255
8.2. Future work 257
8.2.1. Applications BFAs for vibration control of a single-link flexible

manipulator systems and other flexible structures 257
8.2.2. Application of BFAs for modelling and control of a multi-link flexible manipulator systems 258
8.2.3. Applications of BFAs for robotic modelling and control 258
8.2.4. Applications of BFAs in modelling and control paradigms for paraplegic mobility 258
8.2.5. Hybridization of BFA with other biologically-inspired soft computing techniques 258
8.2.6. Application of BFA in the real-time 258
8.2.7. Multi-objective BFA 259
8.2.8. Ensemble computation using BFA 259
8.2.9. Application of BFA in grid computing 259

References 260

LIST OF FIGURES

Figure 1.1: Biologically-inspired algorithms taxonomy block diagram (Brabazon, 2010) 4

Figure 1.2: The possible configuration of the three algorithms considered in the work 6

Figure 2.1: An illustration figure of E. Coli bacterium structure (Passino, 2002, 2005) 14

Figure 2.2: Illustration of chemotaxis pattern of E. Coli bacterium (Passino, 2002, 2005) 15

Figure 2.3: Flowchart of original BFA (Passino, 2002) 21

Figure 2.4: Plot of nutrient media function used in (Passino, 2002) 29

Figure 2.5: Illustration of bacteria's chemotaxis from their initial positions in the nutrient media 30

Figure 2.6: Bacteria trajectories in the first elimination and dispersal event: 2D view 31

Figure 2.7: Bacteria trajectories in the second elimination and dispersal event: 2D view 32

Figure 2.8: Bacteria trajectories in the third elimination and dispersal event: 2D view 33

Figure 2.9: Bacteria trajectories in the first elimination and dispersal event: 1D view 33

Figure 2.10: Bacteria trajectories in the second elimination and dispersal event: 1D view 34

Figure 2.11: Bacteria trajectories in the third elimination and dispersal event: 1D view 34

Figure 2.12: Convergence plot of SBFA 35

Figure 2.13: Convergence plots of SBFA with various population sizes with $C(i)$ equal to 0.01 37

Figure 2.14: Convergence plots of SBFA for different bacteria population size with $C(i)$ equal to 0.1 37

Figure 2.15: Convergence plots of SBFA for various N_c values 39

Figure 2.16: Convergence of SBFA for different N_s values 40

Figure 2.17: Convergence plots of SBFA for different N_{re} values with chemotactic step size ($C(i)$) equal to 0.01 42

Figure 2.18: Convergence plots of SBFA for various N_{re} value with chemotactic step size ($C(i)$) equal to 0.05 43

Figure 2.19: Convergence of SBFA for various N_{ed} values with chemotactic step size is equal to 0.01 44

Figure 2.20: Convergence of SBFA for various N_{ed} values with chemotactic step size is equal to 0.1 46

Figure 2.21: Convergence plots of SBFA for various ($C(i)$) values 48

Figure 2.22: Convergence plots of SBFA for various probability threshold (p_{ed}) values 49

Figure 2.23: Various predetermined initial positions of bacteria in the nutrient media and their convergence plots 51

Figure 3.1: The laboratory-scale single-link flexible manipulator rig 53

Figure 3.2: Schematic diagram of the experimental rig (Azad, 1994) 54

Figure 3.3: Outline of the flexible manipulator system (Azad, 1994) 55

Figure 3.4: Representation of the flexible manipulator system (Azad, 1994) 55

Figure 3.5: General concept of system identification 57

Figure 3.6: The system identification loop (Ljung, 1999) 57

Figure 3.7: Simulation block diagram using SIMULINK with state-space formulation (Azad, 1994; Poerwanto, 1998) 62

Figure 3.8: Experimental results of flexible manipulator 66

Figure 4.1: Bacteria trajectories in finding minimum value of cost function from peak initial position, where θ is the bacterium's position and $J(\theta)$ is the corresponding nutrient value 68

Figure 4.2: Overall construction of fuzzy logic model (picture adopted from Sivanandam et al. (2007) and then modified) 72

Figure 4.3: Fuzzy logic-based adaptable chemotactic step size construction 73

Figure 4.4: Fuzzy input with seven Gaussian membership functions: ES is extremely small, VS is very small, S is small, M is medium, B is big, VB is very big and EB is extremely big 73

Figure 4.5: Illustration of relation between nutrient value $J(i)$ and

adaptable chemotactic step size $C_a(i)$ 77
Figure 4.6: Two-variable Rosenbrock function 79
Figure 4.7: Fuzzy membership functions and surface of FABFA for Rosenbrock test function 80
Figure 4.8: Simulation results of algorithms with Rosenbrock test function 82
Figure 4.9: Two-variable sphere function 82
Figure 4.10 Fuzzy membership functions and surface of FABFA for five-dimension sphere test function 84
Figure 4.11: Simulation results of all algorithms for five-dimension sphere test function 85
Figure 4.12: Two-variable Rastrigin's function 6 86
Figure 4.13 Fuzzy membership functions and surface of FABFA for 30-dimension Rastrigin's function 87
Figure 4.14: Simulation results of algorithms for 30-dimension Rastrigin's function 6 88
Figure 4.15: Two-dimension Schwefel's function 7 89
Figure 4.16: Fuzzy membership functions and surface of FABFA for Schwefel's function 7 90
Figure 4.17: Simulation results of algorithms for two-dimension Schwefel's function 7 91
Figure 4.18: Two-dimension Ackley function 92
Figure 4.19: Fuzzy membership functions and surface of FABFA for Ackley test function 93
Figure 4.20: Simulation results of the algorithms for two-dimension Ackley test function 94
Figure 4.21: Two-dimension weighted sphere function 95
Figure 4.22: Fuzzy membership functions and surface of FABFA for 30-dimension weighted sphere test function 96
Figure 4.23: Simulation results of all algorithms for 30-dimension weighted sphere test function 97
Figure 4.24: Two-variable Schwefel's function 1.2 98
Figure 4.25: Fuzzy membership functions and surface of FABFA for two-dimension Schwefel's function 1.2 test function 99

Figure 4.26: Simulation results of all algorithms for Schwefel function 1.2 101
Figure 5.1: ABFA-based ARX model structure for flexible manipulator modelling 104
Figure 5.2: ARX modelling process using BFA 105
Figure 5.3: Overall modelling sequence 106
Figure 5.4: Simulation results of SBFA-ARX based models using all cost function in modelling phase 108
Figure 5.5: Time-domain hub-angle response of SBFA-ARX based models using all cost function in validation phase 109
Figure 5.6: Fuzzy membership function and surface of FABFA for hub-angle model in the modelling phase 111
Figure 5.7: Simulation results for hub-angle model in the modelling phase 113
Figure 5.8: Simulation results of the algorithms for hub-angle model in the validation phase 115
Figure 5.9: Validation test for SBFA-ARX for hub-angle model 116
Figure 5.10: Validation test for LABFA-ARX for hub-angle model 117
Figure 5.11: Validation test for QABFA-ARX for hub-angle model 118
Figure 5.12: Validation test for EABFA-ARX for hub-angle model 119
Figure 5.13: Validation test of FABFA-ARX for hub-angle model 120
Figure 5.14: Fuzzy membership functions and surface of FABFA for hub-velocity model in modelling phase 122
Figure 5.15: Simulation results of all algorithms for hub-velocity model in modelling phase 124
Figure 5.16: Simulation results of all algorithms for hub-velocity model in validation phase 126
Figure 5.17: Validation test for SBFA-ARX for hub-velocity modelling 127
Figure 5.18: Validation test for LABFA-ARX for hub-velocity modelling 128
Figure 5.19: Validation test for QABFA-ARX for hub-velocity modelling 129
Figure 5.20: Validation test for EABFA-ARX for hub-velocity modelling 130
Figure 5.21: Validation test for FABFA-ARX for hub-velocity modelling 131
Figure 5.22: Fuzzy membership function and surface of FABFA for end-point acceleration models for all algorithms in modelling phase 133
Figure 5.23: Simulation results of end-point acceleration model for all

algorithms in modelling phase 135
Figure 5.24: Simulation results of end-point acceleration model for all algorithms in validation phase 137
Figure 5.25: Validation test for SBFA-ARX for end-point acceleration model 138
Figure 5.26: Validation test for LABFA-ARX for end-point acceleration model 139
Figure 5.27: Validation test for QABFA-ARX for end-point acceleration model 140
Figure 5.28: Validation test for EABFA-ARX for end-point acceleration model 141
Figure 5.29: Validation test for FABFA-ARX model for end-point acceleration 142
Figure 6.1: General structure of MLP: three input in input layer, 2 hidden layers and two output in output layer 147
Figure 6.2: Single neuron of NN 147
Figure 6.3: Activation functions used by NN 148
Figure 6.4: Basic diagram of NARX model identification with NN-ABFA 150
Figure 6.5: Optimisation process of NN with BFA 151
Figure 6.6: Flowchart of overall modelling sequence for NN-based modelling 152
Figure 6.7: Basic diagram of modelling of single-link flexible manipulator systems using ABFA-FL: K_1, K_2 and K_3 are the scaling factors for input and output 153
Figure 6.8: Fuzzy input with five Gaussian membership functions: NB is negative big, NS is negative small, ZO is zero, PS is positive small and PB is positive big 154
Figure 6.9: BFA-FL computation steps flowchart 155
Figure 6.10: Flowchart of overall modelling sequence for FL-based modelling 156
Figure 6.11: Simulation results of hub-angle model using different cost functions in the training phase 159
Figure 6.12: Simulation results of hub-angle models using different cost

functions in the validation phase 160
Figure 6.13: Fuzzy membership functions and surface of FABFA for hub-angle model in the training phase 162
Figure 6.14: Simulation results of hub-angle BFA-NN models in modelling phase 163
Figure 6.15: Simulation results of hub-angle BFA-NN models in validation phase 165
Figure 6.16: Correlation tests of hub-angle SBFA-NN model 166
Figure 6.17: Correlation tests of hub-angle LABFA-NN model 167
Figure 6.18: Correlation tests of hub-angle QABFA-NN model 168
Figure 6.19: Correlation tests of hub-angle EABFA-NN model 169
Figure 6.20: Correlation tests of hub-angle FABFA-NN model 170
Figure 6.21: Fuzzy membership function and surface of FABFA for hub-velocity model in the training phase 172
Figure 6.22: Simulation results of hub-velocity BFA-NN models in modelling phase 173
Figure 6.23: Simulation results of hub-velocity BFA-NN models in validation phase 175
Figure 6.24: Correlation tests of hub-velocity SBFA-NN model 176
Figure 6.25: Correlation tests of hub-velocity LABFA-NN model 177
Figure 6.26: Correlation tests of hub-velocity QABFA-NN model 178
Figure 6.27: Correlation tests of hub-velocity EABFA-NN model 179
Figure 6.28: Correlation tests of hub-velocity FABFA-NN model 180
Figure 6.29: Fuzzy membership function and surface of FABFA for end-point acceleration models in modelling phase 182
Figure 6.30: Simulation results of end-point acceleration BFA-NN model in modelling phase 184
Figure 6.31: Simulation results of end-point acceleration BFA-NN model in validation phase 186
Figure 6.32: Correlation tests of end-point acceleration SBFA-NN model 187
Figure 6.33: Correlation tests of end-point acceleration LABFA-NN model 188
Figure 6.34: Correlation tests of end-point acceleration QABFA-NN model 189
Figure 6.35: Correlation tests of end-point acceleration EABFA-NN model 190

Figure 6.36: Correlation tests of end-point acceleration FABFA-NN model 191
Figure 6.37: Fuzzy membership functions of BFAs-FL for hub-angle model 193
Figure 6.38: Simulation results of hub-angle BFA-FL models in the training phase 195
Figure 6.39: Fuzzy surfaces of hub-angle BFA-FL models 196
Figure 6.40: Simulation results of hub-angle BFA-FL models in the validation phase 197
Figure 6.41: Correlation tests of hub-angle SBFA-FL model 198
Figure 6.42: Correlation tests of hub-angle LABFA-FL model 199
Figure 6.43: Correlation tests of hub-angle QABFA-FL model 200
Figure 6.44: Correlation tests of hub-angle EABFA-FL model 201
Figure 6.45: Fuzzy membership functions of hub-velocity BFA-FL model 203
Figure 6.46: Simulation results of hub-velocity BFA-FL models in the training phase 204
Figure 6.47: Fuzzy surfaces of hub-velocity BFA-FL models 205
Figure 6.48: Simulation results of hub-velocity BFA-FL models in the validation phase 206
Figure 6.49: Correlation tests of hub-velocity SBFA-FL model 207
Figure 6.50: Correlation tests of hub-velocity LABFA-FL model 208
Figure 6.51: Correlation tests of hub-velocity QABFA-FL model 209
Figure 6.52: Correlation tests of hub-velocity EABFA-FL model 210
Figure 6.53: Fuzzy membership function of BFA-FL for end-point acceleration models 212
Figure 6.54: Simulation results of end-point acceleration BFA-FL models in modelling phase 214
Figure 6.55: Surfaces of fuzzy models for end-point acceleration models 215
Figure 6.56: Simulation results of end-point acceleration BFA-FL models in the validation phase 216
Figure 6.57: Correlation tests of end-point acceleration SBFA-FL model 217
Figure 6.58: Correlation tests of end-point acceleration LABFA-FL model 218
Figure 6.59: Correlation tests of end-point acceleration QABFA-FL model 219
Figure 6.60: Correlation tests of end-point acceleration EABFA-FL model 220
Figure 7.1: ABFA-tuned JBC PD control of flexible manipulator 225

Figure 7.2: Flowchart of JBC PD-BFA computation steps 226
Figure 7.3: A bang-bang input with 75 degree magnitude for reference input 227
Figure 7.4: Overall simulation and experiment sequence 229
Figure 7.5: Simulation results with SBFA-JBC PD for step input using J_1 and J_2 230
Figure 7.6: Simulation results with bang-bang input using J_1 and J_2 231
Figure 7.7: Fuzzy membership functions and surface of FABFA for JBC PD control 234
Figure 7.8: Simulation results with BFA-JBC PD controls 235
Figure 7.9: Experimental time-domain hub-angle responses 236
Figure 7.10: End-point acceleration feedback for vibration reduction 237
Figure 7.11: Open-loop end-point acceleration response to bang-bang input 240
Figure 7.12: Fuzzy membership function and surface of FABFA-PD of end-point acceleration feedback 242
Figure 7.13: Simulations results for PD end-point acceleration feedback controls 243
Figure 7.14: Experimental results of end-point acceleration responses 246
Figure 7.15: Fuzzy membership function and surface of FABFA PID end-point acceleration feedback control 249
Figure 7.16: Simulation results of BFA PID end-point acceleration feedback controls 250
Figure 7.17: Experimental results of BFA PID end-point acceleration feedback controls 253

LIST OF TABLES

Table 2.1: Numerical data of nutrient media used by Passino (2002) 29

Table 2.2: Numerical result of optimisation process using SBFA for nutrient media 35

Table 2.3: Numerical results of SBFA with various population sizes with chemotactic step size ($C(i)$) is equal to 0.01 36

Table 2.4: Numerical results of SBFA with various population sizes with chemotactic step size ($C(i)$) is equal to 0.1 38

Table 2.5: Numerical results of SBFA for different N_c values 39

Table 2.6: Numerical results of SBFA for different N_s values 41

Table 2.7: Numerical results of SBFA for various N_{re} values with chemotactic step size ($C(i)$) equal to 0.01 42

Table 2.8: Numerical results of SBFA for various N_{re} values with chemotactic step size ($C(i)$) equal to 0.05 43

Table 2.9: Numerical results of SBFA for various values of N_{ed} with chemotactic step size is equal to 0.01 45

Table 2.10: Numerical results of SBFA for various values of N_{ed} with chemotactic step size is equal to 0.1 46

Table 2.11: Numerical results of SBFA for various $C(i)$ with initial positions of bacteria at [11, 15] 48

Table 2.12: Numerical results of SBFA for various p_{ed} values 50

Table 2.13: Numerical results of SBFA with various initial positions of bacteria 51

Table 3.1: Physical parameters of experimental flexible manipulator rig 55

Table 4.1: Numerical results of simulation with Rosenbrock test function (2 dimensions) 81

Table 4.2: Numerical results of simulation with five-dimension sphere test function 85

Table 4.3 Numerical results of simulation with 30-dimension Rastrigin test function 88

Table 4.4: Numerical results of simulation with two-dimension Schwefel's function 7 test function 91

Table 4.5 Numerical results of simulation with two-dimension Ackley test function 94

Table 4.6. Numerical simulation results with 30-dimension weighted sphere test function 97

Table 4.7 Numerical simulation results with two-dimension Schwefel's function 1.2 test function 100

Table 5.1: Numerical results of the cost functions in the modelling phase 109

Table 5.2: Numerical results of the cost functions in the validation phase 110

Table 5.3: Numerical results of hub-angle models for the algorithms in the modelling phase 112

Table 5.4: Numerical results of hub-angle models for the algorithms in the validation phase 114

Table 5.5: Numerical results of hub-velocity models for the algorithms in modelling phase 123

Table 5.6: Numerical results of hub-velocity models for the algorithms in validation phase 125

Table 5.7: Numerical results of end-point acceleration models for the algorithms in modelling phase 134

Table 5.8: Numerical results of end-point acceleration models for the algorithms in validation phase 136

Table 6.1: Numerical result of hub-angle BFA-NN model using different cost functions in the training phase 159

Table 6.2: Numerical result of hub-angle models using different cost functions in validation phase 160

Table 6.3: Numerical results of hub-angle BFA-NN models in the training phase 164

Table 6.4: Numerical results of hub-angle BFA-NN models in the validation phase 164

Table 6.5: Numerical results of hub-velocity BFA-NN models in the training phase 173

Table 6.6: Numerical result of hub-velocity BFA-NN models in the validation phase 174

Table 6.7:	Numerical results of end-point acceleration BFA-NN models in the training phase	183
Table 6.8:	Numerical results of end-point acceleration BFA-NN models in the validation phase	185
Table 6.9:	Fuzzy rules for hub-angle model	193
Table 6.10:	Numerical results of hub-angle BFA models in the training phase	194
Table 6.11:	Numerical results of hub-angle BFA-FL models in the validation phase	197
Table 6.12:	Fuzzy rules of hub velocity BFA-FL model	202
Table 6.13:	Numerical results of hub-velocity BFA-FL models in the training phase	204
Table 6.14:	Numerical results of hub-velocity BFA-FL models in validation phase	206
Table 6.15:	Fuzzy rules for end-point acceleration model	211
Table 6.16:	Numerical results of end-point acceleration BFA-FL models in the training phase	213
Table 6.17:	Numerical results of end-point acceleration BFA-FL models in the validation phase	216
Table 7.1:	Effects of each parameter of PID control	224
Table 7.2:	Performance of controllers for step input using J_1 and J_2	231
Table 7.3:	Optimal results of SBFA-JBC PD using J_1 and J_2	232
Table 7.4:	Time-domain responses of SBFA-JBC PD using J_1 and J_2	232
Table 7.5:	Numerical results of optimum J of the controllers	235
Table 7.6:	Time-domain hub-angle responses of the controllers	236
Table 7.7:	Experimental time-domain hub-angle responses parameters with BFA-JBC PD controls	237
Table 7.8:	Numerical results of end-point acceleration response in open-loop (F is frequency (Hz) and M is magnitude ($m/sec^2/Hz$))	240
Table 7.9:	Numerical results for PD end-point acceleration feedback controls	244
Table 7.10:	Spectral attenuation at resonance modes with BFA-PD end-point acceleration feedback controls against open-loop control	

($m/sec^2/Hz$) 244

Table 7.11: Spectral attenuation at resonance modes with BFA PD end-point acceleration feedback controls against EABFA JBC PD without feedback loop ($m/sec^2/Hz$) 245

Table 7.12: Experimental results of time-domain end-point acceleration responses 245

Table 7.13: Spectral attenuations achieved at resonance modes with BFA-PD end-point acceleration feedback controls against open-loop control ($m/sec^2/Hz$). 246

Table 7.14: Spectral attenuations achieved at resonance modes with BFA-PD end-point acceleration feedback controls against EABFA JBC PD without feedback loop ($m/sec^2/Hz$). 247

Table 7.15: Numerical results for BFA PID end-point acceleration feedback controls 251

Table 7.16: Spectral attenuations achieved at resonance modes with BFA-PID end-point acceleration feedback controls against open-loop control ($m/sec^2/Hz$) 251

Table 7.17: Spectral attenuations achieved at resonance modes with BFA-PID end-point acceleration feedback controls against EABFA JBC PD without feedback loop ($m/sec^2/Hz$) 252

Table 7.18: Experimental results for BFA PID end-point acceleration feedback controls 252

Table 7.19: Spectral attenuations achieved at resonance modes with BFA-PID end-point acceleration feedback controls against open-loop control ($m/sec^2/Hz$) 253

Table 7.20: Spectral attenuations achieved at resonance modes with BFA-PID end-point acceleration feedback controls against EABFA JBC PD without feedback loop ($m/sec^2/Hz$) 254

CHAPTER 1
INTRODUCTION

1.1. Background

Computing methodologies of various levels of sophistication are present behind modern industrial and commercial applications such as control, voice processing, system identification and estimation, fault diagnosis, pattern recognition, image processing, etc. Generally, the computing methodologies are hidden from the end user who, probably, will not be aware of the computing side of the application. For years, researchers and engineers have been developing and applying computing methods based on conventional or traditional computing techniques. These computing methods are referred to as "hard computing" (HC) methodologies or simply called as "computing" by most people. The disadvantages of HC methodologies are that they need high precision and accurate information of the system. Meanwhile, in real world problems the system is always not ideal. Also, HC methodologies usually need excessive development time. However, HC methodologies have well-known numerical stability and their effects as part of a larger system have been well-analyzed (Ovaska et al., 2002, 2006). In control, linear quadratic Gaussian (LQG) and root locus are two examples of HC that are widely used by researchers and engineers.

In contrast to HC, "soft computing" (SC) methodologies can be utilised in situations where there is imprecision, uncertainty, partial truth that might be caused by complexity, nonlinearity, time variation, or disturbances of the system to achieve robustness, tractability with low cost solution (Suzuki et al., 2000). These superiorities over HC make SC widely used in industrial applications such as aerospace, communication systems, consumer appliances and electric power systems (Dote and Ovaska, 2001). The original definition of SC has been made by Professor Lotfi A. Zadeh as quoted from (Ovaska et al., 2006):

> *"Soft computing differs from conventional (hard) computing in that, unlike hard computing, it is tolerant of imprecision, uncertainty, partial truth, and approximation. In effect, the role model for soft computing is: Exploit the tolerance for imprecision, uncertainty, partial truth, and approximation to achieve tractability, robustness and low solution cost.*

At this juncture, the principal constituents of soft computing (SC) are fuzzy logic (FL), neural computing (NC), genetic computing (GC) and probabilistic reasoning (PR), with the latter subsuming belief networks, chaos theory and parts of learning theory. What is important to note is that soft computing is not a melange. Rather, it is a partnership in which of the partners contributes a distinct methodology for addressing problems in its domain. In this prospective, the principal constituent methodologies in SC are complementary rather than competitive."

Although not mentioned in the original definition above, currently developed algorithms such as swarm intelligence, chaos theory, perceptron, etc can also be included as constituents of SC. For most researchers and engineers, the term "computational intelligence" is more frequently used instead of SC. Thus, the term computational intelligence and SC are usually used interchangeably. For all constituents of SC include FL, NC, GC, and PR, it can be noted that, in an application, the use of combination of these constituents give better results than only using individually FL, NC, GC, and PR. In order to make SC more widespread for different applications, three essential principal requirements are needed (Goldberg, 2002; Ovaska et al., 2006):

- Scalable results
- Practicality
- Little models or theory

In an application, SC could be used either to replace HC or to complement HC. A few examples of HC and SC are combination of LQG with FL, LQG with GA, and root locus with FL.

In an optimisation problem where the task is to find global optimum in the search space, there are several challenging properties such as there may be many local optima, the size of the search space may be so large that may impact on computation time of the search process. Various numerical analysis based tools have been developed and proposed to find an acceptable solution. Most of them are based on gradient of cost function as guidance to the global optimum solution. These techniques are efficiently applied with convex cost functions which are continuous and without nonlinearities in the cost function and its constraints (Eldred, 1998), however the drawback is that there is high possibility to be trapped at a local optimum point.

Global optimisation algorithms attempt to find the global optimum in the search space by either using deterministic or heuristic approach. Deterministic algorithms search the global optimum point using a certain pattern while heuristic approaches search the global optimum based on experience. The advantages of deterministic techniques are that they have high possibility to find global optimum. However, they usually need long computational time and high computational resources. Heuristic approaches are usually developed based on non-deterministic or stochastic techniques. By using this concept, they can search the optimisation space randomly so that the global optimum point can be found within acceptable computation time and using reasonable computation resources. However, because the random process produces unlimited number possible solutions, in the highly complex or highly nonlinear systems, the computation time also significantly increases in such cases.

In general, biologically-inspired algorithms comprise computational algorithms that have been developed by mimicking biological processes that occur in the nature such as evolution and natural selection, human brain and reasoning, social systems and foraging with the main aim is to seek potential and possible alternative techniques or tools for solving highly complex problems that may not be achieved by using existing computational methods such as dynamic programming, linear programming, nonlinear programming, gradient descent based methods. Every natural process has its own mechanism which is usually self-organized, very efficient and very optimal. Some examples of natural processes, to mention a few, are natural selection where the fittest species will survive while weaker species will die, foraging (mechanism for food locating, handling, and ingesting) of species like birds, fishes, ants, and bacteria. Several existing biologically inspired algorithms are outlined in the taxonomy block diagram depicted in Figure 1.1. All these algorithms are not based on gradient of cost function so they do not need to calculate the gradient and are less susceptible to problems of local optimum that arise with multimodal error surfaces.

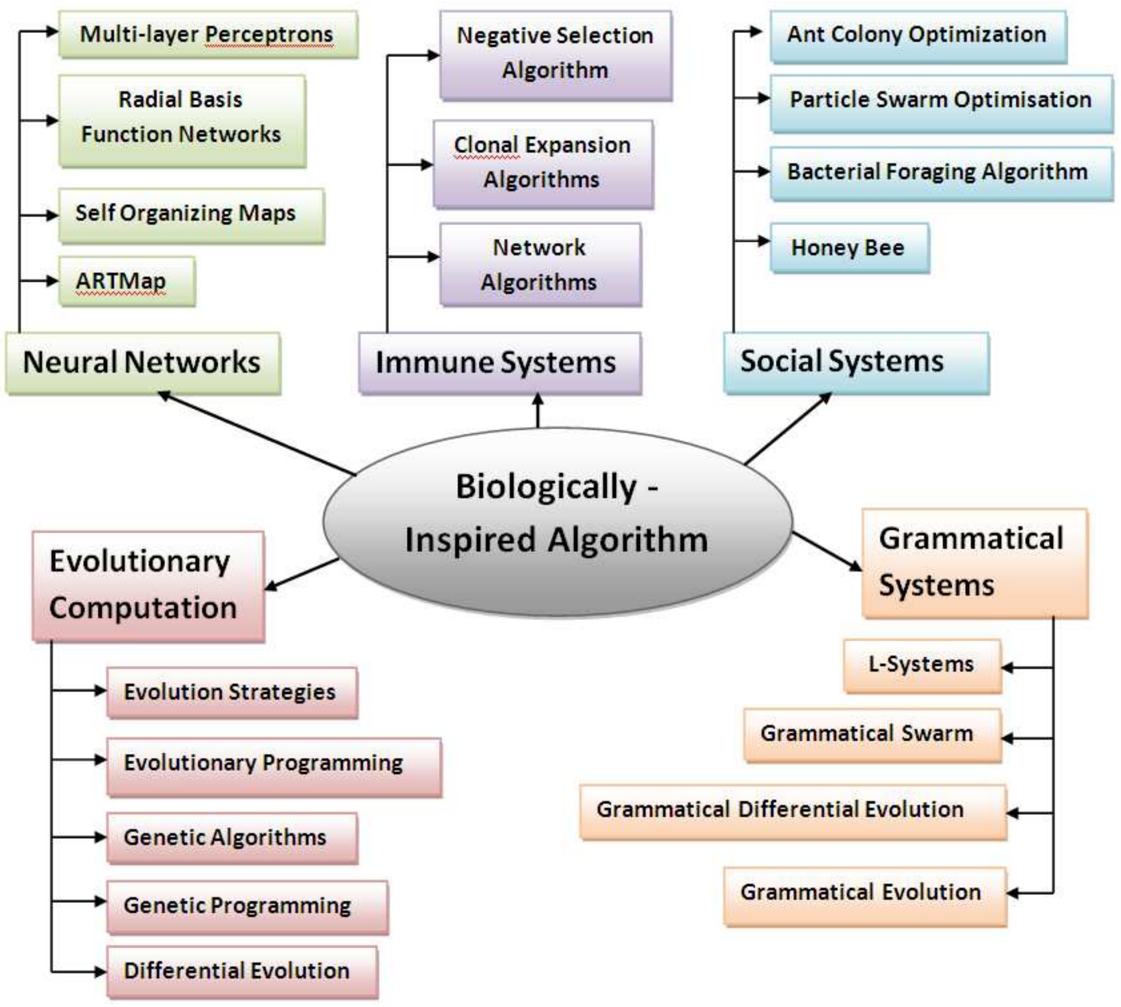

Figure 1.1: Biologically-inspired algorithms taxonomy block diagram (Brabazon, 2010).

Social systems-based algorithms were developed by modelling the behaviour of animals in doing something collectively, for example foraging in groups, rather than individually (Passino, 2002). Bacterial foraging algorithm (BFA) (Passino, 2002), which has been developed based on foraging strategies of E. Coli bacteria, emerged as one of relatively the most newly developed biologically-inspired optimisation methods. E. Coli bacteria always try to find a place which has high level of nutrition and avoid a place which has noxious substance. From the optimisation point of view, the optimum value is the place which has the highest nutrient level. The initial position of bacteria could be set in certain predetermined position or dispersed randomly across the nutrient media (search space). Bacteria will move towards global optimum position by applying “biased” random walk called chemotaxis in constant “step size”. After performing a predetermined number of chemotactic steps, the health of bacteria is sorted based on the nutrient level they get. Half of the population with high nutrient level, the healthy bacteria, will reproduce (every bacterium splits into two bacteria) and takes the same place of their mother while the remaining half with lower nutrient level, unhealthy bacteria, will die. By using this mechanism, the number of bacteria in the population will remain constant. Because of external factors, the number of bacteria in the population could be decreased sharply or dispersed to other regions of nutrient media. This event makes bacteria able to explore most parts or whole regions of nutrient media.

The constant chemotactic step size of random walk of bacteria in original BFA (Passino, 2002) has two consequences, bigger step size makes bacteria able to heading to optimum location faster but with risk to miss the global optimum on the other hand very small step size ensure bacteria to find global optimum but to require a lot of chemotactic steps to converge to the optimum value. Investigations on the chemotactic step size which will result in faster convergence without sacrificing accuracy need to be carried out.

Artificial neural networks referred to here as neural networks (NNs) are initiated by Hebb (1949) and then have been enhanced by Hopfield (1982), Rumellhart et al. (1986), Grossberg (1982) and Widrow (1987). Since their introduction, NNs have attracted significant attention of researchers because of their advantages for example parallelism, distributed representation and computation, generalization ability, adaptability and inherent contextual information processing as well as their learning capability (Jain and Mohiuddin, 1996).

Fuzzy logic (FL) is a concept firstly introduced by Lotfi Zadeh base (1965, 1973) to model human reasoning in the decision making based on imprecise and incomplete information in the form of rule base. Simply speaking, FL can be viewed as a way of incorporating human experiences and knowledge and then breaking it down into certain computation steps to produce output from given input. Because it has been developed based on human logic-like, it can deal with nonlinearity of systems.

The three concepts, namely BFA, NN and FL can be combined to build hybrid technique(s) to solve problems more accurately than by each one individually. Since BFA is an optimisation algorithm, it could be utilised to find optimal parameters of NN and FL. Alternatively, FL which has been developed based on human reasoning can be used to enhance BFA's performance so that BFA will have faster convergence and better accuracy and then may be applied it to optimising NN. Thus the possible configuration of combination of these three algorithms considered in this work is as shown in Figure 1.2.

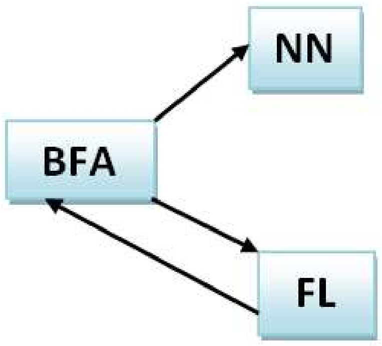

Figure 1.2: The possible configuration of the three algorithms considered in the work.

Compared to rigid manipulators, the use of flexible manipulators has several advantages (Azad, 1994; Book and Majette, 1983):

a. It needs lower energy consumption
b. It requires smaller actuator
c. It has safer operation due to reduced inertia
d. It has compliant structure
e. It has possible elimination of gearing
f. It has less bulky design
g. It has low mounting strength and rigidity requirements

All these advantages allow flexible manipulators to be used in various applications such as in sophisticated robotic assistants for the disabled (Gharooni et al., 2001), for reducing the space-launch cost in space exploration (Yamano et al., 2000), and for handling hazardous waste material in hazardous plants (Jamshidi et al., 1998).

Besides its advantages, the oscillatory behaviour of a flexible manipulator system during its operation needs special consideration. The flexible nature and distributed characteristic of a flexible manipulator system leads to complex system dynamics. Another problem is that the coupling between the rigid dynamics and the flexible dynamics of the link may also cause stability problems (Talebi et al., 2002). This makes the task of controlling flexible manipulator systems including: finding accurate model of the system, setting precise position, and suppressing its vibration due to system flexibility and non-minimum phase characteristics of the system (Piedboeuf et al., 1993; Yurkovich, 1992) becomes very challenging. Thus, finding an accurate model which represents whole dynamics of both rigid and flexible factors to design an accurate control system is very challenging task.

It can be noted from the literature that BFA has not been applied in the area of a single-link flexible manipulator system, either for modelling or control. Thus, the application of BFA, either its original algorithm or upgraded version, and its combination with NN and FL for modelling and control of a single-link flexible manipulator system would be very interesting.

1.2. Aim of the research

From the literature, it can be noted that, since it is still relatively newly developed optimisation technique, there are still spaces that can be explored on the modification of BFA especially to increase its convergence speed and accuracy and also its possible combination with other soft computing techniques such as FL and NN. Moreover, despite its potential, BFA has not been reported yet for modelling and control of flexible manipulator systems. The main aim of the research is to develop new modifications of BFA and its combination with other soft computing techniques and test their performances in modelling and control of dynamic systems, exemplified by a single-link flexible manipulator system. Modification of BFA is focusing on improving its convergence in terms of speed and accuracy. The performance of modified BFA will be compared to that of the original BFA, referred as standard BFA (SBFA).

1.3. Research objectives

The main aim of the research can be broke down into several objectives as follows:

1. To investigate the development of modified BFA for better convergence and better global optimum value with due consideration of computational complexity in comparison to the original BFA.
2. To investigate the performances of the modified BFAs in modelling a single-link flexible manipulator system based on parametric modelling approach, in comparison to that of SBFA based on the optimum nutrient value achieved, convergence speed and time-domain response.
3. To investigate potential soft-computing techniques that combine BFAs, NN, and FL in non-parametric modelling and control of a single-link flexible manipulator system and validate the developed model and control strategies experimentally within a flexible manipulator rig. Possible permutations which will be considered throughout the work include:
   a. Combination of BFAs and FL. This will include:

    - Using FL for modifying BFA so that the BFA will have faster convergence and better accuracy.
    - Using BFAs for optimising FL

   b. Combination of BFAs and NN. BFAs will be used for finding optimal parameters of NN, i.e. weights, biases and parameters of activation functions.
   c. Combination of BFAs, FL and NN. The modified BFA based on FL will be used to optimise NN, i.e. to find optimal weights, biases and parameters of activation functions.

4. To investigate the performances of modified BFAs in finding optimal controller parameters for a single-link flexible manipulator: for hub-angular movement control and vibration reduction of end-point flexible arm. The performances of modified BFAs will then be compared to that of SBFA based on the optimum nutrient value achieved, convergence speed and time-domain response.

1.4. Contributions of the research

The contributions arising from this thesis include the following:

- **Contribution 1: bacterial foraging algorithm with linearly adaptable chemotactic step size (LABFA).**

  The chemotactic step size has been made adaptable regarding the nutrient value by utilising linear function of nutrient level. The algorithm has been validated in finding optimum point of several benchmark functions and the results have been assessed in comparison to that of SBFA.

- **Contribution 2: bacterial foraging algorithm with quadratic adaptable chemotactic step size (QABFA).**

  The chemotactic step size has been made adaptable regarding the nutrient value by utilising quadratic function of nutrient level. The algorithm has been validated in finding optimum point of several benchmark functions and the results have been assessed in comparison to that of SBFA.

- **Contribution 3: bacterial foraging algorithm with exponentially adaptable chemotactic step size (EABFA).**

  The chemotactic step size was has been adaptable regarding the nutrient value by utilising exponential function of nutrient level. The algorithm has been validated in finding optimum point of several benchmark functions and the results have been assessed in comparison to that of SBFA.

- **Contribution 4: bacterial foraging algorithm with fuzzy adaptable chemotactic step size (FABFA).**

  A Mamdani type fuzzy logic has been used for the adaptation mechanism of chemotactic step size so that the chemotactic step size is changed according to the nutrient level. The algorithm has been validated in finding optimum point of several benchmark functions and the results have been assessed in comparison to that of SBFA.

- **Contribution 5: Parametric approach using bacteria foraging algorithms with adaptable chemotactic step size (ABFAs) for modelling of flexible manipulator system.**

  In the investigation, a linear structure model which represented flexible manipulator system is optimised by BFAs. The modelling process involves:

  a. Preliminary experimentation. Empirical comparison of three cost function alternatives, i.e. sum of absolute error (SAE), mean of absolute error (MAE) and mean of squared error (MSE), for modelling process has been performed. The results show that MSE has been the most suitable cost function for modelling process.

  b. Optimisation process. Three single-input single-output (SISO) models based on autoregressive with exogenous input (ARX) model structure optimised by LABFA, QABFA, EABFA and FABFA have been developed and their results have been assessed in comparison to that of SBFA. The comparison has been made based on the optimum cost function value achieved, convergence speed and time-domain and frequency-domain responses.

- **Contribution 6: Non parametric modelling approach using neural network (NN) optimised by ABFAs for modelling of flexible manipulator system.**

  Here, NN optimised by BFAs are used for modelling of flexible manipulator. The modelling process involves following steps:

  a. Preliminary experimentation. Empirical comparison of three cost function alternatives, i.e. sum of absolute error (SAE), mean of absolute error (MAE) and mean of squared error (MSE) and root mean square error (RMSE) has been performed in the modelling process. The results show that RMSE was the most suitable cost function for modelling process based on NN.
  b. Optimisation process. Three NNs optimised by LABFA, QABFA, EABFA and FABFA based SISO have been developed and the results assessed in comparison to that of SBFA. The comparison has been made based on the optimum cost function value achieved, convergence speed and time-domain and frequency-domain responses.

- **Contribution 7: Non parametric modelling approach using fuzzy logic (FL) optimised by ABFAs for modelling of flexible manipulator system.**

  In this work, three SISO models based on BFAs-optimised FL have been developed for modelling the hub-angle, hub-velocity and end-point acceleration responses of the manipulator. The performances of LABFA, QABFA, EABFA and FABFA have been assessed in comparison to that of SBFA based on optimum cost function value achieved, convergence speed and time-domain and frequency-domain responses.

- **Contribution 8: Using ABFAs for optimising joint-based collocated (JBC) proportional derivative (PD) control for input tracking of flexible manipulator system.**

  There are two parameters of JBC PD controller to optimise, i.e. proportional (K_p) and derivative (K_v). The investigation in this work involves two steps:

  a. Preliminary experimentation. Empirical comparison of two cost function alternatives. Two cost function alternatives i.e. mean of squared error (MSE) and MSE plus weighted maximum overshoot/undershoot have been considered. The results show that MSE plus weighted maximum overshoot /

undershoot is more suitable to be used because the overshoot / undershoot can be suppressed better than with MSE.

b. Optimisation process. LABFA, QABFA and EABFA are used to tune these two parameters and MSE plus weighted maximum overshoot / undershoot has been chosen as the nutrient media. The results have been assessed in comparison to that of SBFA based on optimum of cost function achieved, convergence speed and time-domain responses.

- **Contribution 9: Using ABFAs PD and proportional integral and derivative (PID) control with end-point acceleration feedback for vibration reduction of end-point flexible arm.**

  The investigations involving following steps:

  a. The best ABFAs 1 based controller in the input tracking control discussed in sub chapter 8.3 is used as the input tracking control. The selection is based on the cost function J value achieved because smallest J means it has the smallest error.
  b. For each payload attached in the end-point of flexible arm, PD and PID controllers are optimised using ABFAs 2. The performances of controller with end-point acceleration feedback are compared to open loop control and JBC-PD control without controller with end-point acceleration feedback based on the J_α value, time-domain and frequency-domain responses.
  c. The performances of ABFAs are compared to SBFA based on the optimum J_α achieved, convergence speed, time-domain and frequency responses of end-point acceleration.

1.5. Organisation of the thesis

The rest of the thesis is organized as follow:

Chapter 2: Presents a detailed overview of BFA: its algorithm, applications, modifications and empirical investigation on parameter selection and its impact on convergence and accuracy.

Chapter 3: Describes the experimental flexible manipulator rig used in this work: its technical specifications, previous work on modelling and control and preliminary experimentation for collecting input-output data pairs.

Chapter 4: Presents the development of chemotactic step size adaptation mechanisms, i.e. LABFA, QABFA, EABFA and FABFA. The proposed algorithms are validated in finding optimum value of several well-known benchmark functions. The performances of ABFAs are then compared to that of SBFA based on convergence speed and optimum cost function value achieved.

Chapter 5: Discusses the application of ABFAs developed and discussed in Chapter 4 in parametric modelling of a single-link flexible manipulator system, from input torque to hub-angle, hub velocity and end-point acceleration outputs. ABFAs are used to find optimum parameters of an ARMA structure model representing the dynamics of a single-link flexible manipulator system and their performances are assessed in comparison to that of SBFA.

Chapter 6: Presents the application of ABFAs developed and discussed in Chapter 4 for optimising NN and FL in modelling of flexible manipulator system and their comparative performance assessment with that of SBFA. Three SISO models are developed for modelling hub-angle, hub-velocity and end-point acceleration responses of the system.

Chapter 7: Discusses the application of ABFAs developed in Chapter 4 for tuning JBC PD controller for input tracking control and for tuning PD and PID controller with end-point acceleration feedback for vibration reduction of end point of flexible arm and their performances comparison with SBFA.

Chapter 8: Presents the concluding remarks of the work and the possible future work.

CHAPTER 2
BACTERIAL FORAGING ALGORITHM: AN OVERVIEW

2.1. Introduction

In this chapter, the applications and current modifications of bacterial foraging algorithm (BFA) are surveyed. The objective of the investigation is to study the characteristics of the original BFA, survey previous modifications and applications and study the impact of its parameter changes. Firstly, the concept of chemotaxis and original algorithm are discussed in detail. Secondly, the applications of the original BFA in various areas are overviewed. Moreover, previous modifications proposed, developed and used by researchers on original BFA are outlined. Finally, the impact of BFA's parameter selection on convergence and its accuracy is studied.

2.2. The original bacterial foraging algorithm

2.2.1. Basic concept of bacteria movement

BFA (Passino, 2000; Passino, 2002) is an optimisation method developed based on the foraging strategy of Escherichia Coli (E. Coli) bacteria, bacteria that live in the human intestine. Foraging strategy is a method of animals for locating, handling and ingesting their food. The structure of E. Coli bacteria is such that it has a "body" which is constructed from a plasma membrane, cell wall and capsule that contains the cytoplasm and nucleoid. Furthermore, E. Coli bacteria have flagella that can move in a rotation manner and used for locomotion: if the flagella moves counter clockwise it makes bacteria to move forward with large displacement namely "swim" and if the flagella moves clockwise it makes the bacteria move in an uncertain direction with very small displacement called "tumble". The size of E. Coli bacterium itself is very tiny, about 1 μm in diameter, 2 μm in length, 1 picogram in weight with about 70 % of it being water. An illustration figure of E. Coli bacterium structure is depicted in Figure 2.1.

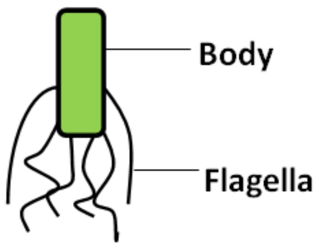

Figure 2.1: An illustration of E. Coli bacterium structure (Passino, 2002, 2005)

In general, in their lifetime in the media, E. Coli bacteria always try to find the place which has a high nutrient level and avoid noxious places using certain motion pattern namely “taxes”. In moving towards nutrient value, every bacterium releases chemical substances of attractant when heading to a nutritious place and repellent when they are near a noxious place. Thus, the motion pattern of E. Coli in finding nutrient is called “chemotaxis”. If E. Coli bacteria are moving towards higher nutrient level than their previous position, they will move forward (swim or run) continuously. However, if bacteria arrive at a place with a lower nutrient level than the previous position, they will tumble.

The cartoon illustrations of bacteria in swim and tumble are depicted in Figure 2.2. In Figure 2.2(a) the bacterium moves from its initial position P_1 to new position P_2 and then the nutrient values of P_1 and P_2 is compared. Because nutrient level of P_2 is higher than P_1, the bacterium then moves forward in the same direction as previous movement namely swim or run to the new position P_3. Then, the same process is performed until the last bacteria’s lifetime. The bacteria’s chemotaxis which involves both swimming and tumbling is illustrated in Figure 2.2(b). The bacterium moves from its initial position P_1 to the new position P_2. Because the nutrient level in P_2 is lower than that in P_1, the bacterium does not continue to move toward in the same direction as previous movement but moves in another uncertain direction with very small displacement called tumbling to new position P_3. Also because the nutrient level of P_3 is lower than that in P_2, the bacterium will tumbling and arrive at the new position P_4. Now, the nutrient level in P_4 is higher than that in P_3 thus the bacterium is swimming in the same direction as previous movement to the new position P_5. In the nutritious media, bacteria spend more time swimming than tumbling. On the contrary, in a media which has a low nutrient level, the bacteria will tumble more frequently than swim.

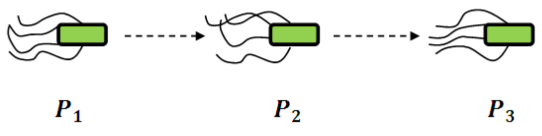

(a) Moving forward continuously (swim)

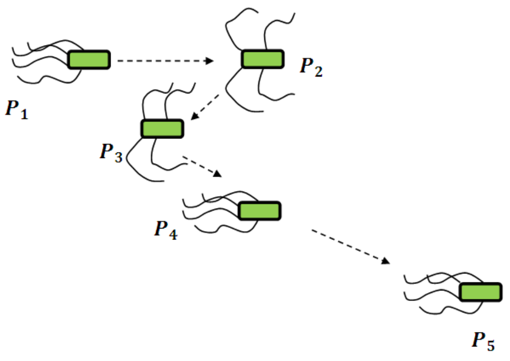

(b) Moving forward-tumbling-swim

Figure 2.2: Illustration of chemotaxis pattern of E. Coli bacterium (Passino, 2002, 2005)

Thus, the chemotaxis of bacteria in the nutrient media for their lifetime can be summarised as follows (Passino, 2002, 2005):

a. In the noxious place: combination of tumble and swim to move away from the noxious place and try to find nutritious place
b. In the neutral place (there are neither nutrient nor poison): more frequent tumble to find nutritious place (searching)
c. In the nutritious place: swim as long as possible in the direction of up nutrient gradient

2.2.2. Optimisation technique based on bacterial foraging

From the E. Coli bacteria's mechanism in finding places with high nutrient value and avoiding noxious places an optimisation technique that models this process, namely bacterial foraging algorithm (BFA), is developed (Passino, 2002). For example, suppose that it is desired to find the global minimum of $J(\theta), \theta \in \Re^p$ with θ is the position of a bacterium and $J(\theta)$ represents the nutrient media level at θ where there is no measurement or there is no analytical description of the gradient $\nabla J(\theta)$. This minimisation problem can be solved using non-gradient optimisation technique adopted from foraging of E. Coli bacteria. There are three possibilities of $J(\theta)$ value: $J(\theta) < 0, J(\theta) = 0$ and $J(\theta) > 0$ indicating that the bacterium at location θ is in nutrient-rich, neutral, and noxious environments, respectively. E. Coli bacteria will apply biased random walk to climb up the nutrient concentration (find lower and lower values of $J(\theta)$), avoid noxious substances (the place where $J(\theta) > 0$), and search for ways out of neutral media (location where $J(\theta) = 0$).

The optimisation steps from beginning to the end that model how E. Coli bacteria find food can be divided into four main parts, namely chemotaxis, swarming, reproduction and elimination and dispersal.

a. Chemotaxis

The position and its corresponding nutrient value (usually called as cost function value in optimisation) of i-th bacterium at the j-th chemotactic step, k-th reproduction step, and l-th elimination and dispersal event can be denoted as $\theta(i,j,k,l)$ and $J(i,j,k,l)$ respectively with $i = 1,2,...,S$ and $\theta(i,j,k,l) \in \Re^p$. From its current position, bacteria will walk heading to the position that has lower $J(i,j,k,l)$ value. The "speed" of the walk is determined by the value of chemotactic step size $C(i) > 0, i = 1,2,...,S$. The bacteria's chemotaxis could be a combination of:

- Continuous swim
- Swim followed by tumble
- Tumble followed by tumble
- Tumble followed by swim

A unit length random direction $\phi(j)$ on the range [-1,1] is generated to define the direction of movement after tumble. Thus, the movement of bacteria from one position to another position can be formulated as:

$$\theta(i,j+1,k,l) = \theta(i,j,k,l) + C(i)\phi(j) \tag{2.1}$$

If at bacteria position $\theta(i,j+1,k,l)$ the cost function value $J(i,j+1,k,l)$ is lower than $J(i,j,k,l)$ then the bacteria will move one step with the same direction as the previous direction with the step size $C(i)$. Another step with the same direction is taken if the next cost function is lower. The maximum number of continuous swim in the same direction taken is N_s. After N_s swim, bacteria have to tumble.

b. Swarming

In the walking process bacteria could release chemical substances to attract other bacteria (attractants) so that other bacteria could swarm together. Besides bacteria could release chemical substances to repel other bacteria (repellent) so that other bacteria move away because two bacteria cannot be in the same location at the same time and keep a certain distance between two bacteria. This process is called cell-to-cell signalling via attractant and repellent (swarming). The swarming process for every bacterium is formulated as:

$$J_{cc}(\theta, P(j,k,l)) = \sum_{i=1}^{S} J_{cc}(\theta, \theta(i,j,k,l)) \tag{2}$$

$$J_{cc}(\theta, P(j,k,l)) = \begin{array}{l} \sum_{i=1}^{S}\left[-d_{attract}\exp\left(-\omega_{attract}\sum_{m_p=1}^{p}\left(\theta_{m_p}-\theta_{m_p}(i)\right)^2\right)\right]+ \\ \sum_{i=1}^{S}\left[h_{repellent}\exp\left(-\omega_{repellent}\sum_{m_p=1}^{p}\left(\theta_{m_p}-\theta_{m_p}(i)\right)^2\right)\right] \end{array} \tag{3}$$

where:

- $\theta = [\theta_1, \theta_2, ..., \theta_p]^T$ is a point on the optimisation domain
- $\theta_{m_p}(i)$ is position of the m_p-th component of the i-th bacterium
- $d_{attract}$ is the depth of attractant released by the cell (a quantification of how much attractant is released)
- $\omega_{attract}$ is a measure of the width of the attractant signal (a quantification of the diffusion rate of the chemical)
- $h_{repellent}$ is the height of the repellent effect (magnitude of its effect)
- $\omega_{repellent}$ is a measure of the width of the repellent.

Thus, in the optimisation, the nutrient media in which bacteria will find the optimum place is the cost function value plus cell-to-cell signalling (swarming effect) as:

$$J(i,j,k,l) + J_{cc}(\theta, P(j,k,l)) \tag{4}$$

In order to get optimal nutrient media landscape the cost function value J and cell-to-cell signalling value J_{cc} have to be balanced because if the attractant width is high and very deep, the cells will have a strong tendency to swarm, and they may even avoid going after nutrients and favour swarming. In contrast, if the attractant width is small and the depth shallow, there will be little tendency to swarm and each cell will search on its own.

c. Reproduction

In a rich nutrient media bacteria will reproduce very fast and the number of bacteria will increase significantly and in a poor nutrient media bacteria will die so that the population size will decrease significantly. To model the reproduction mechanism, after N_c chemotactic step size, the health of all bacteria is then sorted in ascending order based on their accumulated cost function value;

$$J_{health} = \sum_{j=1}^{N_c+1} J(i, j, k, l) \tag{2.5}$$

In the minimisation process, the highest cost function value means the least healthy bacteria and bacteria which have the lowest cost function value means the healthiest bacteria. Based on their health, the bacteria population is divided into two halves:

$$S_r = \frac{S}{2} \tag{6}$$

The S_r least healthy bacteria die and the other S_r healthiest bacteria reproduce (every bacterium splits into two bacteria) and placed at the same location with their mother. This reproduction mechanism keeps the bacteria population constant. After reproduction, bacteria will continue the chemotaxis process until achieve maximum chemotactic number N_c and then other reproduction events will be performed.

d. Elimination and dispersal

The population of E. Coli bacteria in the nutrient media can be reduced or replaced instantly because of external factors such as catastrophe that will make nutrient media poisoned instantly. In the modelling, after performing N_{re} reproduction steps there are elimination and dispersal events. Bacteria which have probability value (between 0 and 1) lower than certain threshold value (p_{ed}) are eliminated and dispersed to another location and bacteria which have probability value higher than p_{ed} keep their current position and are not dispersed. After elimination and dispersal event, bacteria will start chemotaxis until achieve reproduction steps N_{re} and then followed by other elimination and dispersal events. This routine is done until maximum elimination and dispersal events N_{ed} achieved.

2.2.3. The original BFA computation algorithm

In the optimisation algorithm development, there are several parameters that should be defined in advance involving:

- p as dimension of the search space (number of parameters to optimise)
- S as the number of bacteria in the population (for simplicity, S as chosen for even number)
- N_c as the number of chemotactic steps per bacterium lifetime between reproduction steps
- N_s as maximum number of swim of bacteria in the same direction
- N_{re} as the number of reproduction steps
- N_{ed} as the number of elimination and dispersal events
- p_{ed} as the probability that each bacteria will be eliminated/dispersed.
- $i = 1, 2, \dots, S$ as the index for the bacterium
- $j = 1, 2, \dots, N_c$ as the index for chemotactic step
- $k = 1, 2, \dots, N_{re}$ as the index for reproduction step
- $l = 1, 2, \dots, N_{ed}$ as the index of elimination and dispersal event
- $m_s = 1, 2, \dots, N_s$ as the index for number of swim

In search for nutritious places, bacteria will continuously perform random walk without stopping until their life is over. The life of bacteria is determined as a total number of steps which is calculated as $N_c \times N_{re} \times N_{ed}$. Finally, the bacterium which has the highest nutrient level after all steps carried out is determined as the optimisation result. Thus, original BFA (Passino, 2002) that models bacterial population chemotaxis, swarming, reproduction, elimination, and dispersal (initially, $j = k = l = 0$) can be formulated in the algorithm below (note that updates to the θ^i automatically result in updates to P):

```
1. Elimination-dispersal loop: for $l = 1,2,\dots,N_{ed}$, do $l = l + 1$
2. Reproduction loop: for $k = 1,2,\dots,N_{re}$, do $k = k + 1$
3. Chemotaxis loop: for $j = 1,2,\dots,N_c$, do $j = j + 1$
   a. For $i = 1,2,3,\dots,S$, take a chemotactic step for bacterium $i$:
```

b. Compute the nutrient media (cost function) value $J(i,j,k,l)$. Calculate $J(i,j,k,l) = J(i,j,k,l) + J_{cc}\left(\theta^i(j,k,l), P(j,k,l)\right)$ (i.e., add on the cell-to-cell attractant effect to the nutrient concentration). If there is no swarming effect then $J_{cc}\left(\theta^i(j,k,l), P(j,k,l)\right) = 0$.

c. Put $J_{last} = J(i,j,k,l)$ to save this value since a better cost via a run may be found.

d. Tumble: Generate a random vector $\Delta(i) \in \Re^p$ with each element $\Delta_{m_p}(i), m_p = 1,2,\dots,p$, a random number on the range $[-1,1]$.

e. Move: Compute

$$\theta^i(j+1,k,l) = \theta^i(j,k,l) + C(i)\frac{\Delta(i)}{\sqrt{\Delta^T(i)\Delta(i)}}$$

This results in a step of size $C(i)$ in the direction of the tumble for bacterium i.

f. Compute the nutrient media (cost function) value $J(i,j+1,k,l)$, and calculate $J(i,j+1,k,l) = J(i,j+1,k,l) + J_{cc}\left(\theta^i(j+1,k,l), P(j+1,k,l)\right)$. If there is no swarming effect then $J_{cc}\left(\theta^i(j+1,k,l), P(j+1,k,l)\right) = 0$.

g. Swim (note that an approximation has been used since swimming behaviour of each cell is decided as if the bacteria numbered $\{1,2,\dots,i\}$ have moved and $\{i+1, i+2,\dots,S\}$ have not; this is much simpler to simulate than simultaneous decisions about swimming and tumbling by all bacteria at the same time):

   i. Put $m_s = 0$ (counter for swim length)

   ii. While $m_s < N_S$ (if have not climbed down too long)

   - Count $m_s = m_s + 1$
   - If $J(i,j+1,k,l) < J_{last}$ (if doing better), then $J_{last} = J(i,j+1,k,l)$ and calculate

$$\theta^i(j+1,k,l) = \theta^i(j+1,k,l) + C(i)\frac{\Delta(i)}{\sqrt{\Delta^T(i)\Delta(i)}}$$

     This results in a step of size $C(i)$ in the direction of the tumble for bacterium i. Use this $\theta^i(j+1,k,l)$ to compute the new $J(i,j+1,k,l)$ as in sub step f above.
   - Else, $m = N_s$ (the end of the while statement).

h. Go to next bacterium $(i+1)$ if $i \neq S$ (i.e., go to sub step b above) to process the next bacterium.

4. If $j < N_c$, go to step 3.
5. Reproduction:

a. For the given k and l, and for each $i = 1,2,3,\dots,S$, let

$$J^i_{health} = \sum_{j=1}^{N_c+1} J(i,j,k,l)$$

Be the health of bacterium i (a measure of how many nutrients it got over its lifetime and how successful it was at avoiding noxious substances). Sort bacteria and chemotactic parameters $C(i)$ in order of ascending cost J_{health} (higher cost means lower health).

b. The S_r bacteria with the highest J_{health} values die and the other S_r bacteria with the best values split (and the copies that are made are placed at the same location as their parent).

6. If $k < N_{re}$, go to step 2.
7. Elimination-dispersal: for $i = 1,2,3,\dots,S$, eliminate and disperse each bacterium which has probability value less than p_{ed}. If one bacterium is eliminated then it is dispersed to random location of nutrient media. This mechanism makes computation simple and keeps the number of bacteria in the population constant.

```
    For $m = 1:S$
        if $p_{ed>rand}$ (Generate random number for each bacterium and if the generated number
        is smaller than $p_{ed}$ then eliminate/disperse the bacterium)
                Generate new random positions for bacteria
        else
                Bacteria keep their current position (bacteria are not dispersed)
        end
    end
8.  If $l < N_{ed}$, then go to step 1; otherwise end.
```

The original BFA algorithm above can be presented as a flowchart in Figure 2.3.

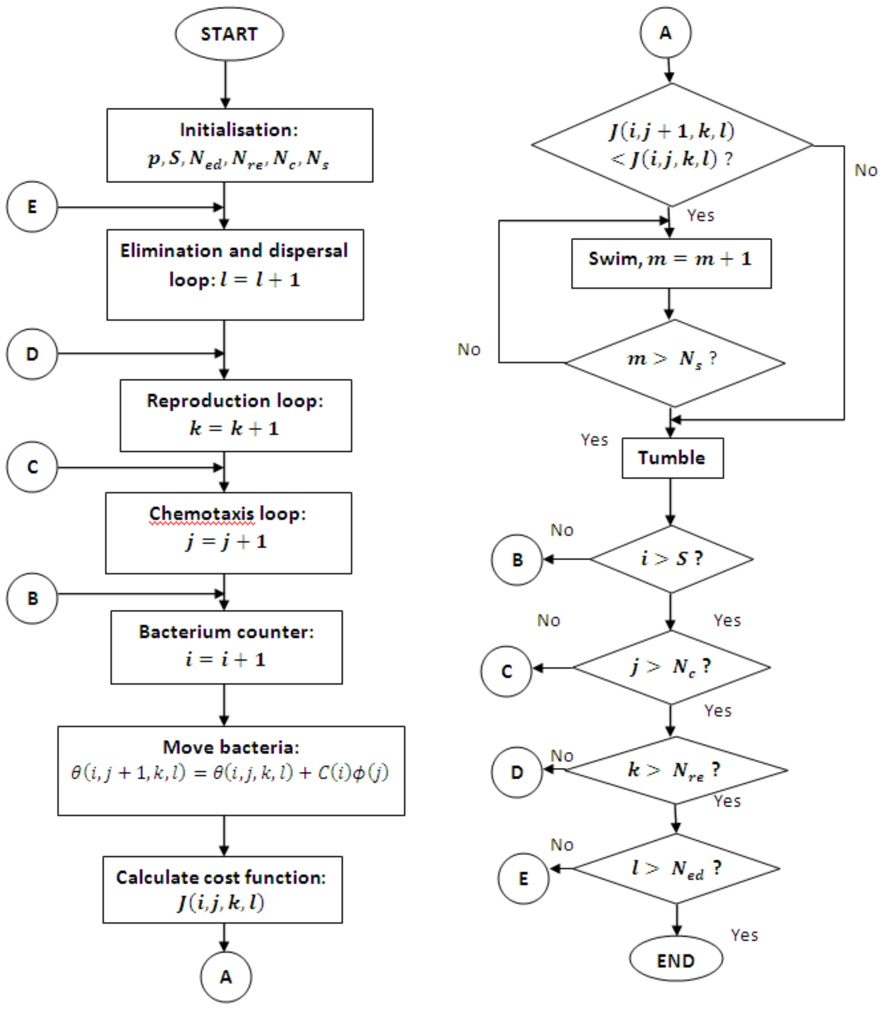
START
Initialisation: $p, S, N_{ed}, N_{re}, N_c, N_s$
E
Elimination and dispersal loop: $l = l + 1$
D
Reproduction loop: $k = k + 1$
C
Chemotaxis loop: $j = j + 1$
B
Bacterium counter: $i = i + 1$
Move bacteria: $\theta(i, j+1, k, l) = \theta(i, j, k, l) + C(i)\phi(j)$
Calculate cost function: $J(i, j, k, l)$
A
A
$J(i, j+1, k, l) < J(i, j, k, l)$?
No
Yes
Swim, $m = m + 1$
No
$m > N_s$?
Yes
Tumble
No
B
$i > S$?
No
Yes
C
$j > N_c$?
Yes
D
No
$k > N_{re}$?
Yes
No
E
$l > N_{ed}$?
Yes
END

Figure 2.3: Flowchart of original BFA (Passino, 2002)

2.3. Current applications and modifications

2.3.1. Application of SBFA

Since its introduction, the original BFA (Passino, 2000, 2002), in this work referred as standard BFA (SBFA), has attracted significant attention from researchers in broad areas of applications as highlighted below:

A. Power systems

In the area of power systems, SBFA has been used for designing multiple optimal power system stabilizers (Das et al. 2008), estimating resistive and inductive parameters in electric systems (Noriega et al., 2010), estimating parameters of single phase core type transformer model (Padma and Subramanian, 2010), tuning PID controller for power oscillation suppression of load frequency control (Ali and Abd-Elazim; 2010), optimising weights and biases of a neural network (NN) for load forecasting of power systems application (Ulagammai et al., 2007), optimising NN for image compression applications (Ying et al. 2008), tuning multiband power system stabilizers of power systems (Sumanbabu, et al., 2007), enhancing voltage profile and minimising losses in transmission line of power systems (Kumar and Renuga, 2010), tuning parameters of power system stabilizers (Ghoshal et al., 2009), and optimising PI controller for active power filter application (Mishra and Bhende, 2007).

B. Controller tuning for complex systems

SBFA has also been applied for controller tuning for complex systems, i.e. tuning PID controller for multivariable systems (Kim and Cho, 2005), finding optimum PID controllers for different-order systems (Niu et al., 2006), optimising PID controller's parameters for various order systems (Ali and Majhi, 2006), and tuning PD-PI controller (Jain and Nigam, 2008a, 2008b).

C. Communication systems

In the communication systems, SBFA has been utilised for suppressing inference of linear antenna arrays (Guney and Basbug, 2008), designing optimal array of Yagi-Uda antennas (Mangaraj et al., 2010), designing nonlinear channel equalizers (Majhi and Panda, 2006), and calculating resonant frequency of rectangular microstrip antenna (Gollapudi et al., 2008).

D. Image processing and pattern recognition

In the areas of image processing and pattern recognition, SBFA has been employed for designing optimal filter for face classification (Sinha, 2007), enhancing peak signal-to-noise ratio in image processing (Bakwad et al., 2009a), optimising membership function parameter of fuzzy model for handwritten Hindi numerals recognition (Hanmandlu et al., 2007), and solving independent component analysis (ICA) problems (Acharya et al., 2007).

E. General systems

Besides the applications above, SBFA has been used for finding the optimum point of dynamic cost function environments (Ramos, et al., 2007), developing system identification for nonlinear dynamic systems (Majhi and Panda, 2010), developing Hammerstein model (Lin and Liu, 2006), and improving extended Kalman filter to solve simultaneous localization and mapping problems for mobile robots and autonomous vehicles (Chatterjee and Matsuno, 2006).

2.3.2. Modifications and improvements of BFA

In order to improve SBFA's performance, modifications on some aspects of SBFA have been proposed. The modifications have been made to improve SBFA's performance in various aspects such as its convergence to the optimum value, computation time, and accuracy.

A. Modification 1: adaptable chemotactic step size

One improvement concept is how to accelerate the convergence of SBFA. With SBFA (Passino, 2002), to find places with high nutrient level, bacteria use random walk with certain constant chemotactic step size for whole computational process regardless of the nutrient value. This makes bacteria walk with constant speed heading to the optimum value. If the step size is set to a small value, bacteria need more iteration to find the optimum value. To speed up the bacteria's walk and reduce the iterations needed, bigger step size can be used.

However, a mathematical analysis of the chemotactic step in SBFA based on classical gradient descent search approach in (Dasgupta et al., 2008, Dasgupta et al., 2009a) suggests that chemotaxis employed by SBFA usually results in sustained oscillation when close to the global optimum especially on relatively flat landscape nutrient media. Thus, the chemotactic step size needs to be selected as small as possible. Such condition makes a trade-off between speeding up bacteria's walk and minimising the oscillation around the global optimum point. Making adaptable chemotactic step size, i.e. the value of chemotactic step size changed to follow certain conditions, will solve the problem.

Several attempts have been made by researchers to propose adaptable chemotactic step size for BFA. Dasgupta et al. (2008; Dasgupta et al., 2009a; Das et al., 2009) have proposed simple linear functions of nutrient value of every bacterium and have tested these on several well known benchmark functions as well as applied to a parameter estimation problem. This algorithm has also been used in for several areas, such as forecasting stock market indices (Majhi et al., 2009), detecting circle in a digital image (Dasgupta et al., 2010), and designing optimal three-phase energy efficient induction motor (Sakthivel et al., 2010).

Datta et al. (2008) have proposed an alternative chemotactic step size adaptation mechanism, where an adaptive delta modulation principle is used to control the step size. They have applied the algorithm to optimisation of array of antennas. Coelho and Silveira (2006) proposed an adaptable chemotactic step size by adopting several probability distribution functions such as uniform, Gaussian and Cauchy, and have applied the algorithm to tuning PID controller of robotic manipulator systems. Chen et al. (2009) proposed a modified BFA called cooperative bacterial foraging optimization (CBFO). The algorithm has been divided into two stages, one stage with big chemotactic step size and then continued with another stage with smaller step size. Big step size in the first phase has been used to locate possible region of optimum solution without being trapped into local optima and smaller step size in the second phase used to find the optimum point. They have validated the algorithm in finding the optimum value of several benchmark functions.

Farhat and El-Hawary (2010) have proposed modification of SBFA by introducing nonlinear decreasing chemotactic step size and stopping criteria. Thus, the optimisation process is stopped after the cost function has reached a pre-specified value. They have applied the algorithm to solve economic dispatch with valve-point effects and wind power of power systems. On one hand the stopping criteria regarding pre-specified value is able to save computation iteration but in the other hand it could not show that the predetermined value is the real global optimum point. Mishra (2005) has been combined SBFA with FL to solve harmonic estimation problems, where Sugeno-type FL is used for adaptation of chemotactic step size. The input of FL is the minimum of cost function value and its output is the step size value. By using this algorithm, the chemotactic step size is changed adaptively according to cost function value.

B. Modification 2: health sorting and swarming

Among the first modification on SBFA is the swarming computation formula (Liu and Passino, 2002), where the swarming formula has been reformulated so that its value is changed depending on the cost function value to replace constant value of SBFA. Tripathy et al. (2006) proposed three modifications of SBFA, where

- In the reproduction steps, the health of bacteria is sorted based on the minimum value instead of accumulation value.
- In the swarming formulation, the distances of all bacteria are measured from the global optimum instead of the distance of each bacterium.

This algorithm has been used for designing robust controller for unified power flow control (UPFC) of power systems. The algorithm has further been used to solve various problems such as optimising both real power loss and voltage stability of UPFC (Tripathy and Mishra, 2007), finding optimal angle of v-dipoles antenna (Mangaraj et al., 2008), finding both optimal location and amount of series injected voltage for UPFC of power systems (Tripathy et al., 2006). A new modification with the same concept but with adaptable chemotactic step size has also been proposed (Hota et al. 2010), where the chemotactic step size is made adaptive in a pre-determined range. The algorithm has been applied to find optimal solution of economic emission load dispatch of power systems.

C. Modification 3: hybridizing with other algorithms

Besides stand-alone, SBFA may also be combined with other algorithms. A hybrid algorithm combining SBFA and Nelder-Mead has been proposed by Panigrahi and Pandi (2008), where Nelder-Mead algorithm is used to evaluate the optimum value which will be compared to optimum value of BFA for every chemotaxis step. If the optimum value of BFA is better than that of Nelder-Mead algorithm then update it otherwise use optimum value of Nelder-Mead algorithm as the best optimum value. They have also made chemotactic step size adaptive with certain formula. They have applied the algorithm to solving the problem of economic load dispatch of power system, and to optimising the congestion cost of power system (Panigrahi and Pandi, 2009).

Biswas et al. (2007a) have proposed a hybrid algorithm combining differential evolution (DE) and SBFA where mutation, crossover and selection of DE concept is adopted to model chemotaxis of BFA while reproduction steps and elimination and dispersal events are discarded. The chemotactic step size has also been changed according to cost function value using a special formula. They have validated the algorithm in finding optimum point of several well-known benchmark functions. The algorithm has also been applied to solving congestion management problem in power systems (Pandi et al., 2009).

A hybrid of PSO and SBFA has been proposed by (Korani, 2008), where PSO is used to model the social environment. In order to accelerate convergence to global optimum point, the concept of position of every swarm and its velocity is adopted for bacteria to replace the random walk approach in SBFA. The algorithm has been applied to tune PID controllers for various testing systems. This algorithm has also been applied to finding global optimum of benchmark functions (Shen et al., 2009).

Another hybrid algorithm of PSO and SBFA has been proposed by Saber and Venayagamoorthy, (2008), where movement principle in PSO is adopted to replace random walk of SBFA. The algorithm has been used to solve economic load dispatch problems of power systems. Almost the same concept of hybrid algorithm between PSO and SBFA has also been proposed by Gollapudi et al. (2009) where movement concept of PSO has been used to replace random walk of BFA. The algorithm has been used in resonance frequency calculation of rectangular microstrip antenna. This algorithm has also been validated using several benchmark functions (Gollapudi et al., 2011).

Chu et al. (2008) proposed a hybrid algorithm combining PSO and BFA, where the movement idea of PSO is adopted for chemotaxis to replace random walk of BFA. Also the chemotactic step size was reduced as long as the index reproduction and elimination and dispersal increase. They have validated the algorithm in finding optimum point of several benchmark functions.

Yong et al. (2009) have proposed hybrid of PSO and BFA, where PSO operator has been used to perform mutation of every bacterium after every chemotactic step before reproduction steps. By using the movement steps, bacterium will always be attracted towards the global optimum position for entire population every time. The algorithm has been used to solve parameter optimisation of power system stabilizer.

Biswas et al. (2007b) proposed hybrid algorithm between PSO and BFA where movement concept in PSO has been adopted to update position and velocity of bacteria after chemotaxis step while elimination and dispersal events have been discarded. They have validated the algorithm in finding optimum point of various benchmark functions. Alavandar et al. (2010) have also proposed the same concept of hybrid between PSO and

BFA and applied it to optimising fuzzy logic for controlling two- link rigid-flexible manipulator.

A hybrid algorithm combining PSO, BFA and Nelder-Mead has been proposed by Mahmoud, (2010). PSO has been adopted to replace random walk concept of SBFA. After the last elimination and dispersal events, Nelder-Mead algorithm is used to find the final optimum point. The algorithm has been used in designing optimal bow-tie antenna for 2.45 GHz RFID readers. Kim and Cho (2006) and Kim et al., (2007) have proposed a hybrid algorithm combining GA and BFA and have tested the algorithm with several benchmark functions and have used it to tune PID controller for automatic voltage regulator (AVR) systems.

Jain et al. (2009) have proposed hybrid algorithm combining GA, PSO and BFA, where selection, crossover, and mutation operators of GA are used to increase diversity of the search and movement concept of PSO is utilised to replace random walk concept of SBFA. Finally, in the elimination and dispersal events, the eliminated bacteria are not dispersed to new random position but generated via mutation. The algorithm has been used to tune PD-like fuzzy pre-compensated control for two-link rigid-flexible manipulator.

D. Modification 4: simplification and chemotaxis

Ramirez-llanos and Quijano (2009) have proposed a simplification of SBFA by only using chemotaxis and discarding both reproduction steps and elimination and dispersal events in order to make BFA suitable for real-time application. In the end of algorithm, the best bacterium is defined as bacterium which has minimum of accumulation cost function value for all of chemotaxis steps. Then the proposed algorithm was used for reducing of pressure of valves control in a water distribution system.

Dasgupta et al. (2009b) have proposed a modification of BFA by introducing some simplifications in SBFA. In the simplified BFA algorithm, namely micro-BFA, there are only three bacteria used. After all chemotaxis steps, those three bacteria are ranked based on their cost function value. Bacterium with the best cost function value is kept unaltered, the second best bacterium is moved to a place near the best bacterium and the worst is dispersed in another random location by using standard elimination and dispersal events. Reproduction steps are discarded. The algorithm has been validated in finding optimum value of several high dimensional benchmark functions.

Rashtchi et al. (2009) have proposed modifications of SBFA by introducing an adaptable chemotactic step size and tumble method. Chemotactic step size is reduced as exponential function of elimination and dispersal index. For tumble method, if bacteria are found with the cost function value of current position worse than that of previous position then bacteria will not move to random direction but keep previous position. The algorithm has been validated in finding optimum point of various benchmark functions.

In order to reduce computation time, simplifications of SBFA have been proposed by researchers. In parallel bacterial foraging optimisation (PBFO) (Bakwad et al., 2009) the best optimum point is evaluated during the chemotaxis step fitness function evaluations to replace health sorting concept of SBFA. Also, a threshold value is added to the position computation to accelerate computation time. Moreover, a mutation operator is performed by adding social component to bacteria position computation while elimination and dispersal events are discarded. PBFO has been computed using multiprocessor nodes and applied to video compression. The algorithm, also referred to as synchronous bacterial foraging optimization, has been used in various applications such as finding optimum value of several benchmark functions (Bakwad et al., 2010), and tuning parameters of fuzzy PID controller (Su et al., 2010).

2.4. Parameters selection and their impact on convergence and accuracy

In the optimisation process, computation parameters have to be determined in advance. In order to get optimum result with minimum computation cost, the parameters values have to be chosen properly in accordance with nutrient media landscape. The choice of parameter selection and their impact on convergence and accuracy are studied in this section. In order to observe the characteristic of SBFA in relation to parameters changes, simulations are conducted on SBFA to find optimum point of given nutrient media. The nutrient media is taken from the nutrient media used by Passino (2002) which can be formulated as follows:

$$\begin{aligned} J(x) \quad = \quad & 5e^{-0.1((x_1-15)^2+(x_2-20)^2)} - 2e^{-0.08((x_1-20)^2+(x_2-15)^2)} \\ & +3e^{-0.08((x_1-25)^2+(x_2-10)^2)} + 2e^{-0.1((x_1-10)^2+(x_2-10)^2)} \\ & -2e^{-0.5(x_1-5)^2+(x_2-10)^2} - 4e^{-0.1((x_1-15)^2+(x_2-5)^2)} \\ & -2e^{-0.5((x_1-8)^2+(x_2-25)^2)} - 2e^{-0.5((x_1-21)^2+(x_2-25)^2)} \\ & +2e^{-0.5((x_1-25)^2+(x_2-16)^2)} + 2e^{-0.5((x_1-5)^2+(x_2-14)^2)} \end{aligned} \tag{2.7}$$

The nutrient media is a two-dimension search space with two variables: x_1 and x_2. The nutrient function has one global maximum at J equal to 5 when variables $[x_1, x_2]$ are equal to $[15, 20]$, four local maxima, four local minima and one global minimum at J equal to 4 when variables $[x_1, x_2]$ are equal to $[15, 4]$. The detailed numerical data of all peaks is presented in Table 2.1. The 3D and 2D plots of the test function are shown in the Figure 2.4 with the range of parameters x_i in $(0, 30)$. Since the nutrient function has one global maximum, four local maxima, four local minima and one global minimum, it is very risky for the optimization algorithm to be trapped in one of the local minima.

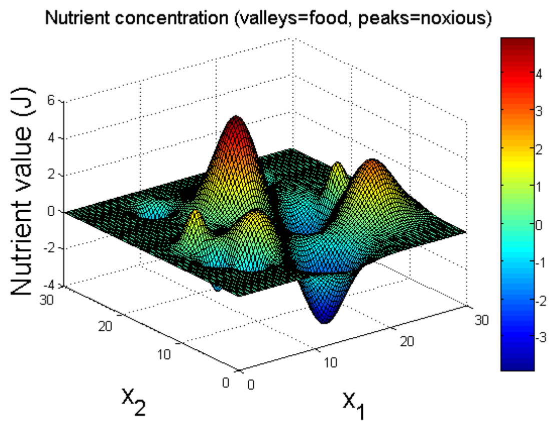

(a) 3D view

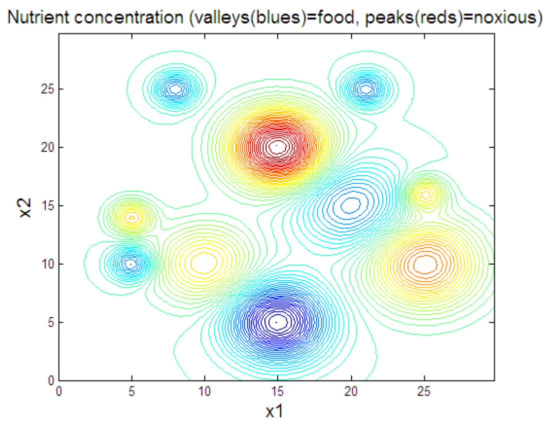

(b) 2D view

Figure 2.4: Plot of nutrient media function used in (Passino, 2002)

Table 2.1: Numerical data of nutrient media used by Passino (2002)

Maxima/minima	x_1	x_2	**Nutrient value J**
Global maximum	15	20	5
Local minimum	20	15	-2
Local maximum	25	10	3
Local maximum	10	10	2
Local minimum	5	10	-2
Global minimum	15	5	-4
Local minimum	8	25	-2
Local minimum	21	25	-2
Local maximum	25	16	2
Local maximum	5	14	2

Here, the nutrient media above is viewed as minimisation problem, which means the task is to find the global minimum point of the nutrient media. From the SBFA's point of view, the global minimum point is the place which has the highest nutrient level.

2.4.1. Overall foraging of bacteria

To know how the algorithm works, here SBFA is used to find optimum (minimum) point of nutrient media formulated in equation (2.7). In the simulation, the SBFA used the following parameter values:

❖ $p = 2$	❖ $N_c = 40$	❖ $N_{re} = 4$	❖ $N_{ed} = 3$
❖ $S = 20$	❖ $N_s = 4$	❖ $S_r = {}^{S}/_{2}$	❖ $p_{ed} = 0.25$

The chemotactic step size $C(i)$ was chosen as 0.2. Those parameters were chosen so that the BFA will be able to find the optimum point of the nutrient media. The initial positions of bacteria can be placed either at certain predetermined positions or randomly in the nutrient media. If bacteria were placed randomly, they can fall anywhere across the nutrient media with the probability that a part of them will fall near the food. In contrast, if bacteria were placed in certain pre-determined place, they will begin the search from the same initial point. The chemotaxis process of bacteria from their initial positions, random and predetermined position $[x_1, x_2]$ at $[11, 15]$, is illustrated in Figure 2.5.

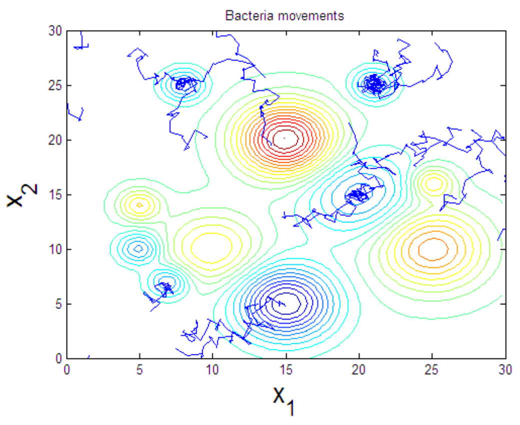

(a) Placed randomly

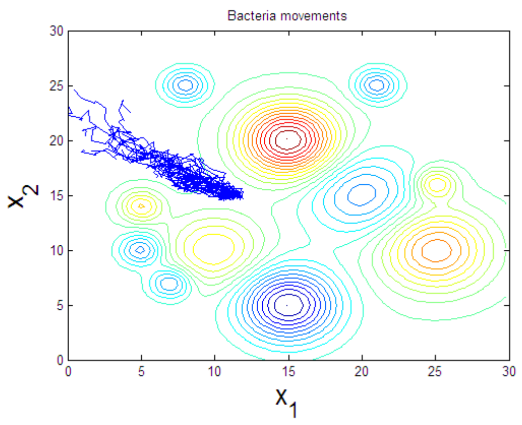

(b) Placed at $[11, 15]$

Figure 2.5: Illustration of bacteria's chemotaxis from their initial positions in the nutrient media

From their initial positions, bacteria will find food (in this minimisation problem means place which has lower nutrient media value) by using biased random walk; they will move to random direction but will move forward continuously in the same direction (swim) if they find the correct path. For purposes of illustration, in this section the initial positions of bacteria were chosen in the neutral position in the nutrient media, e.g. at $[11, 15]$. This initial position was chosen because it was "neutral" position (the nutrient value is nearly equal to zero) and it lies between peaks and valleys. Bacteria will move away from peaks toward valleys. After all chemotaxis steps, reproduction steps are performed. In the reproduction step, half of bacteria, which are less healthy will die and the remaining half (healthier bacteria) will reproduce (split into two bacteria and new bacteria has the same place with their mother). With this mechanism only the healthiest bacteria (bacteria in the richest food) will survive.

The simulation results in Figure 2.6 show that after all four reproduction steps, all bacteria were trapped in one of the local minima. Elimination and dispersal events, which are performed soon after all reproduction steps have taken place is a mechanism that makes bacteria to be distributed in other parts of the nutrient media.

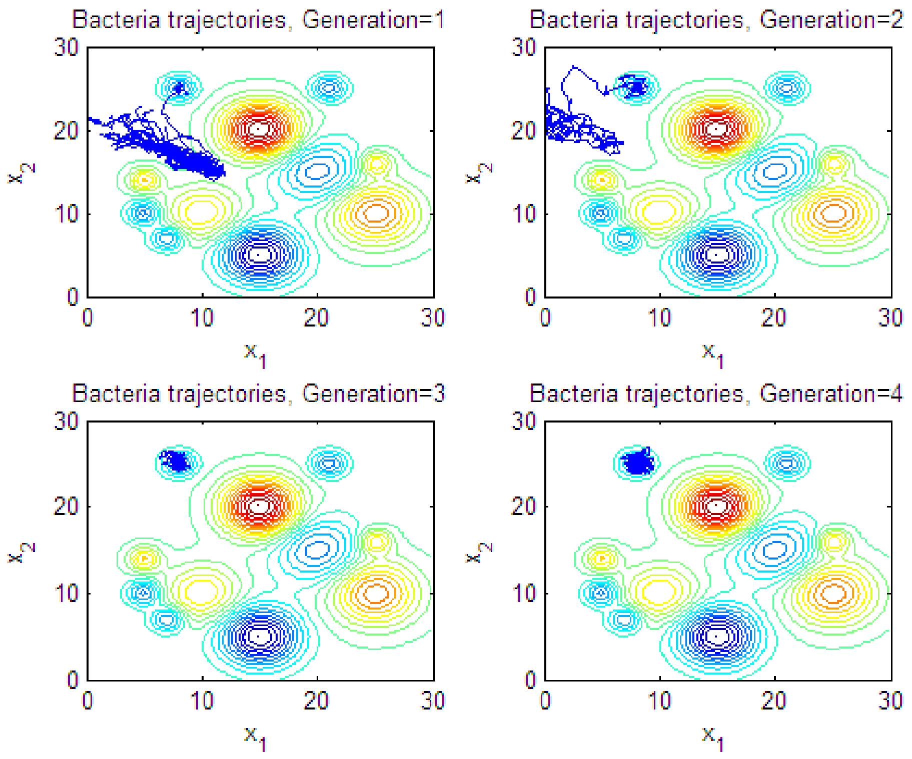

Figure 2.6: Bacteria trajectories in the first elimination and dispersal event: 2D view

Figure 2.7 shows that after one elimination and dispersal event, a part of bacteria fall into the valley where the global minimum exists. In the fourth reproduction of second elimination and dispersal event, bacteria grouped in the global valley and local valley.

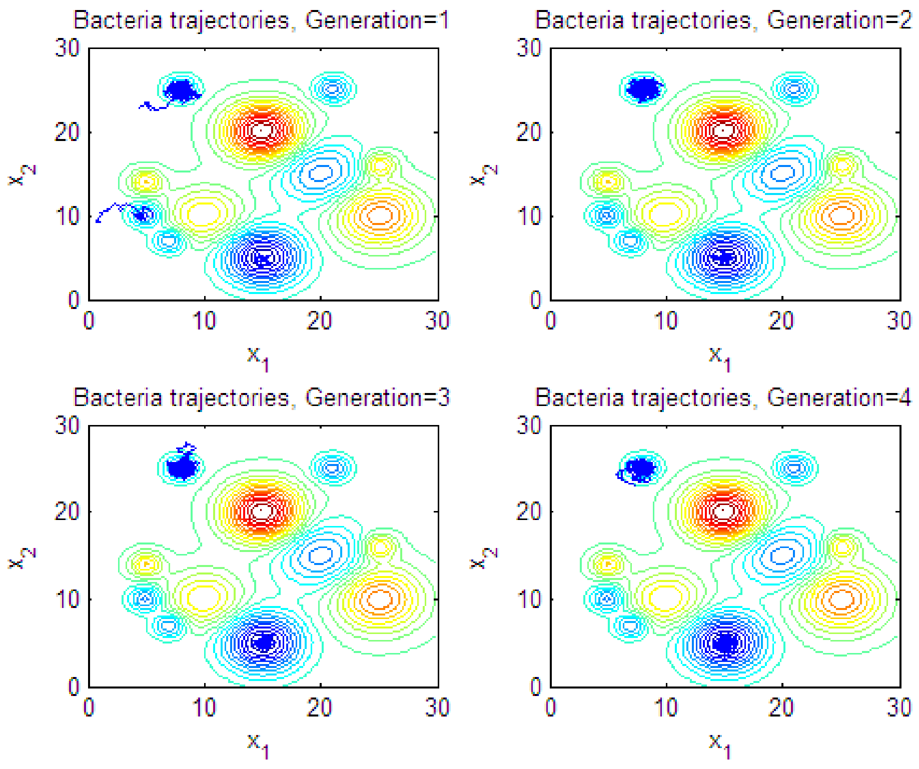

Figure 2.7: Bacteria trajectories in the second elimination and dispersal event: 2D view

Plots in Figure 2.8 show that in the final elimination and dispersal event all bacteria were able to find the global valley. Every movement of bacteria will result new positions which in turn will result new corresponding coordinate $[x_1, x_2]$. The trajectories of x_1 and x_2 for all bacteria in all simulation steps are depicted in Figure 2.9 – Figure 2.11.

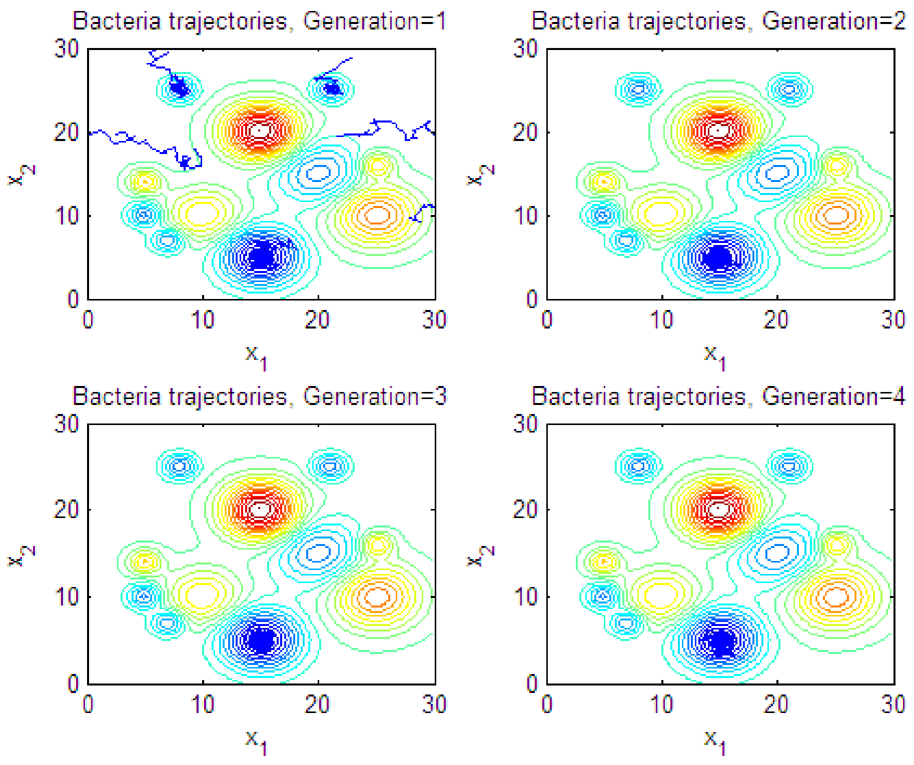

Figure 2.8: Bacteria trajectories in the third elimination and dispersal event: 2D view

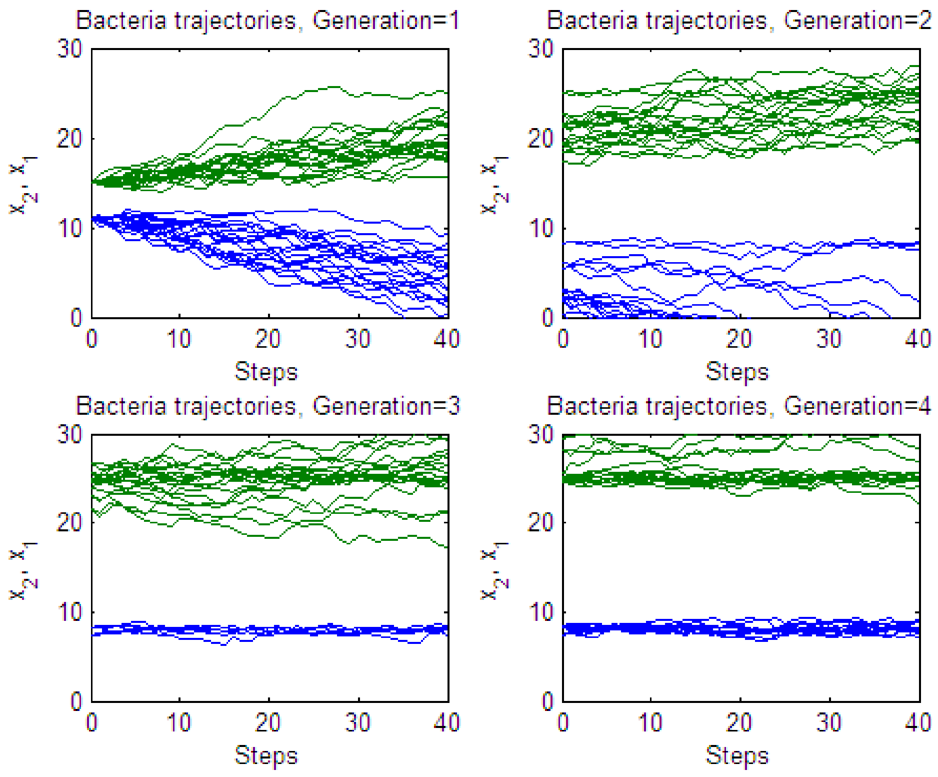

Figure 2.9: Bacteria trajectories in the first elimination and dispersal event: 1D view

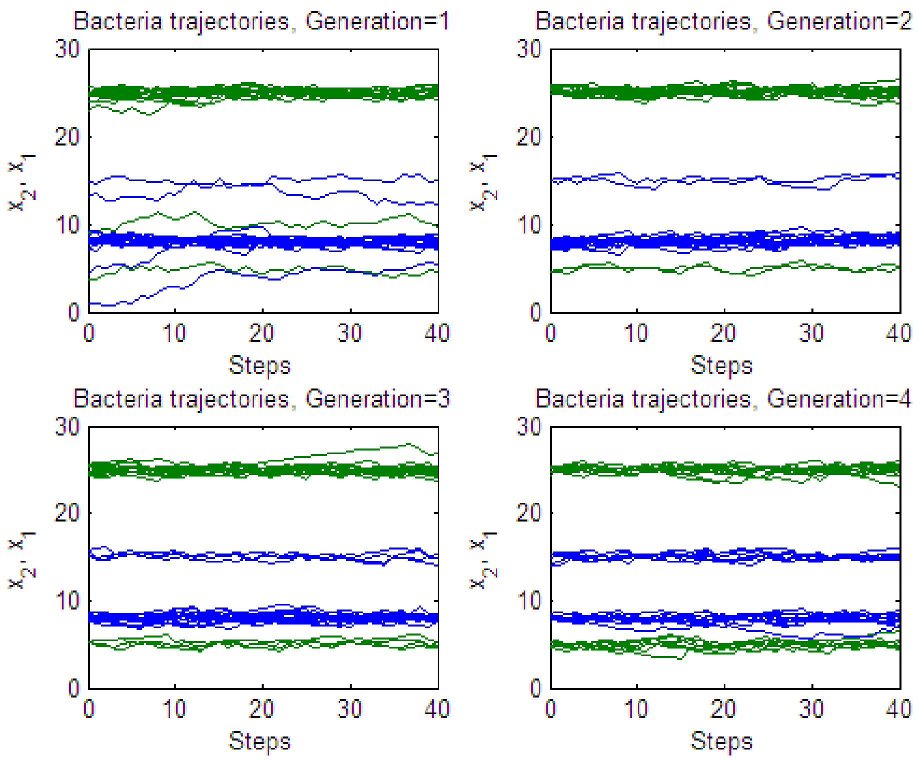

Figure 2.10: Bacteria trajectories in the second elimination and dispersal event: 1D view

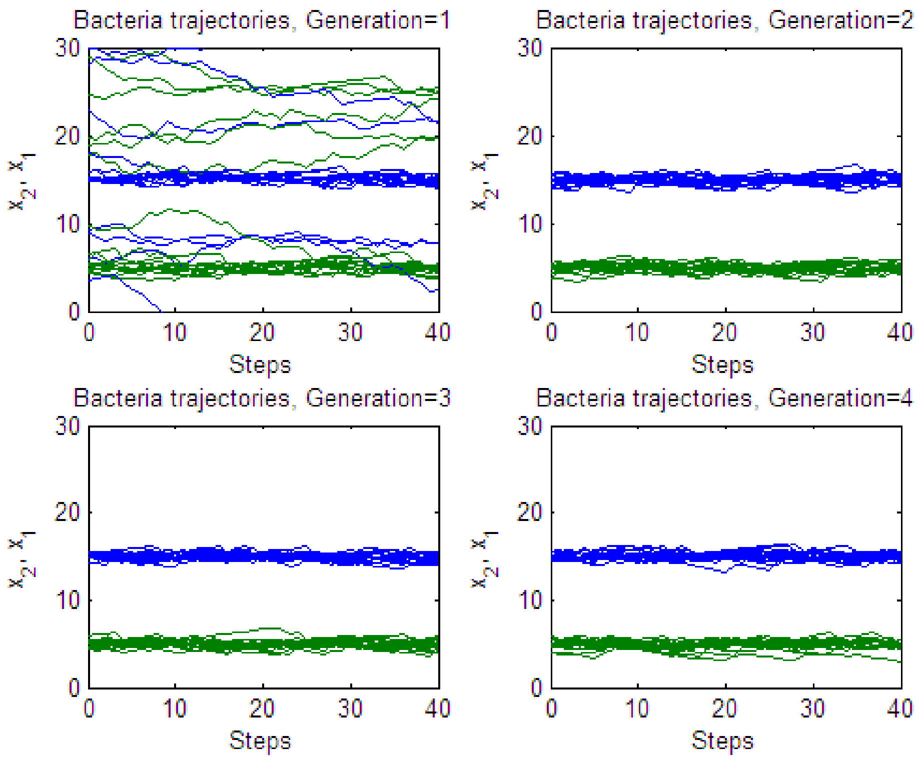

Figure 2.11: Bacteria trajectories in the third elimination and dispersal event: 1D view

Convergence plot of SBFA is depicted in Figure 2.12. The plot presents the minimum nutrient value achieved by all bacteria for each step. SBFA converges to optimum value in 200 steps. The numerical results are presented in Table 2.2.

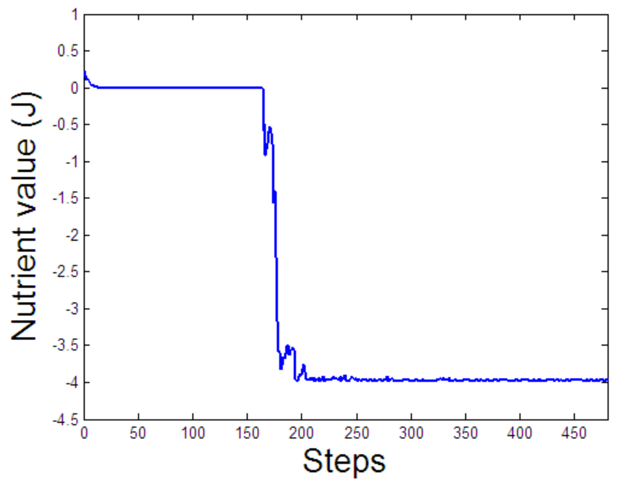

Figure 2.12: Convergence plot of SBFA

Table 2.2: Numerical result of optimisation process using SBFA for nutrient media

Initial positions of bacteria	**Initial J**	**Optimum x_1**	**Optimum x_2**	**Optimum J**	**Convergence speed (steps)**
$[11, 15]$	0.2283	14.9071	4.9442	-3.9813	203

2.4.2. Impact of bacteria population size

Large number of bacteria population size (S) has advantage that more bacteria searching in the nutrient media mean they can search and explore more parts of nutrient media. Besides, in the randomly distributed initial positions, more bacteria mean there is high probability that bacteria fall near the optimum value. The drawback of large population size is it will increase the computation complexity. In this section, the impact of S is investigated. SBFA with various S is used to find global minimum of the cost function formulated in equation (2.7). In the simulation, the following SBFA parameters values were used:

❖ $p = 2$	❖ $N_c = 40$	❖ $N_{re} = 4$	❖ $N_{ed} = 3$
	❖ $N_s = 4$	❖ $S_r = S/2$	❖ $p_{ed} = 0.25$

The chemotactic step size ($C(i)$) values were chosen at 0.01 and 0.1 while initial positions of bacteria were selected at $[11, 15]$ and randomly across the nutrient media.

Numerical results for chemotactic step size ($C(i)$) equal to 0.01 presented in Table 2.3 show that to reduce the population size makes bacteria to be trapped in one of local minima. However, with initial positions of bacteria spread randomly across the nutrient media, SBFA was able to find place near the global optimum when bacteria population size was 10 or above compared to population size equal to 100 when placed at $[11, 15]$. When bacteria reach a place near the global point, the optimum point achieved was the same for all S. The convergence plots depicted in Figure 2.13 show that by spreading bacteria across the nutrient media, SBFA was able to converge faster than placed at $[11, 15]$. Also the larger population size, the faster SBFA converge to optimum value.

Table 2.3: Numerical results of SBFA with various population sizes with chemotactic step size ($C(i)$) is equal to 0.01

Initial positions of bacteria	S	**Optimum** x_1	**Optimum** x_2	**Optimum** J	**Convergence speed (steps)**
At $[11, 15]$	4	-0.3308	1.1083	1.7022×10^{-8}	258
	10	19.9754	15.0206	-1.9116	362
	50	21.0061	25.0081	-1.9895	196
	100	15.0154	4.9836	-3.9867	353
Randomly in nutrient media	4	19.9826	15.0250	-1.9116	449
	10	15.0635	4.9287	-3.9845	466
	50	15.0145	4.9836	-3.9867	203
	100	15.0159	4.9851	**-3.9867**	**109**

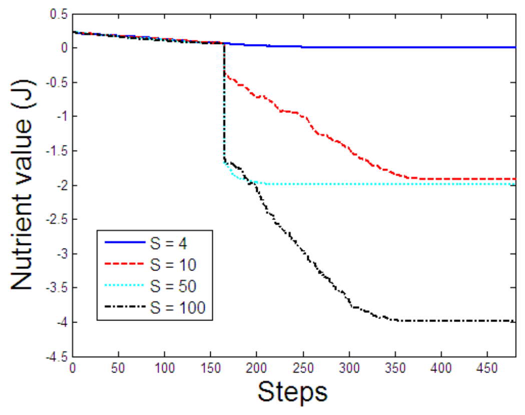

(a) Initial positions: at $[11, 15]$

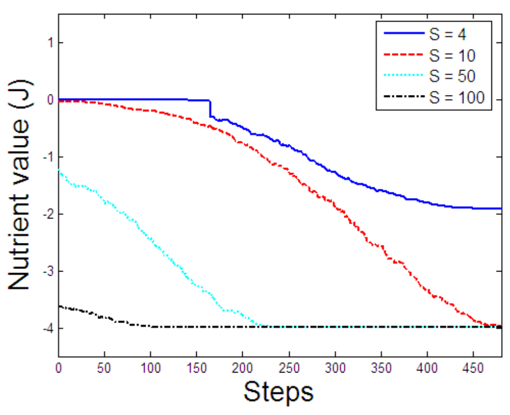

(b) Initial positions: random

Figure 2.13: Convergence plots of SBFA with various population sizes with $C(i)$ equal to 0.01

For chemotactic step size equal to 0.1, numerical results presented in Table 2.4 show that the bacteria population size had very little effect on the optimum nutrient value achieved. Similar to small step size, here, the convergence plots depicted in Figure 2.14 show that larger population size resulted SBFA convergence faster to the optimum value.

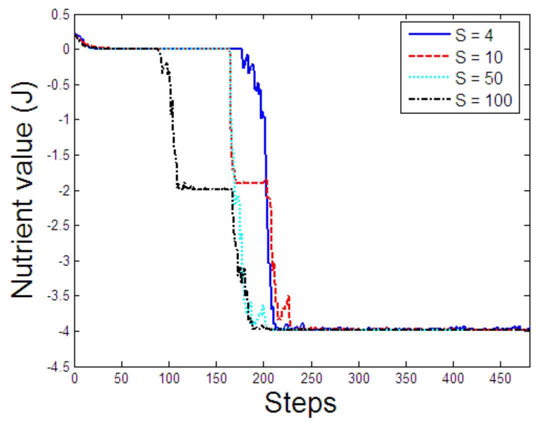

(a) Initial positions: at $[11, 15]$

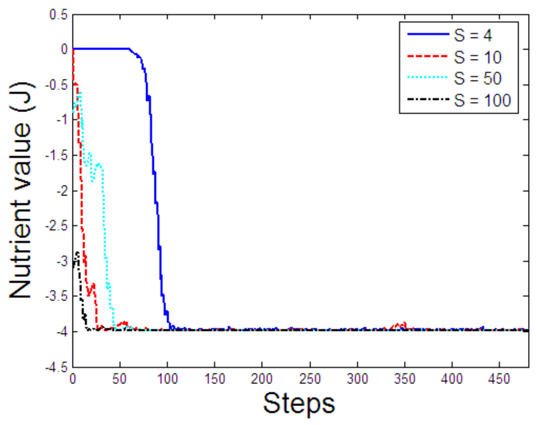

(b) Initial positions: randomly

Figure 2.14: Convergence plots of SBFA for different bacteria population size with $C(i)$ equal to 0.1

Table 2.4: Numerical results of SBFA with various population sizes with chemotactic step size ($C(i)$) equal to 0.1

Initial positions of bacteria	S	**Optimum** x_1	**Optimum** x_2	**Optimum** J	**Convergence speed (steps)**
At $[11, 15]$	4	15.0347	4.9579	-3.9863	245
	10	14.9978	4.9407	-3.9858	264
	50	15.0054	4.9400	-3.9859	207
	100	15.0046	4.9887	-3.9866	203
Randomly in the nutrient media	4	14.9981	4.9780	-3.9866	108
	10	14.9695	5.0052	-3.9856	68
	50	15.0224	4.9932	-3.9866	46
	100	15.0218	4.9657	**-3.9866**	**16**

2.4.3. Impact of chemotactic step number

If the number of chemotactic step (N_c) is set too small, bacteria will not have enough steps to converge to the optimum value so that bacteria will face the risk of getting trapped at local minima. Large N_c will give high probability for bacteria to reach the optimum point. However, large N_c will increase computation complexity and computation time. In this section, SBFA with various N_c values is used to find global optimum value of nutrient media. The objective of the investigation is to reveal the impact of N_c value, on both convergence and accuracy of SBFA. The parameters used in the simulation were:

❖ $p = 2$	❖ $N_s = 4$	❖ $N_{re} = 4$	❖ $N_{ed} = 3$
❖ $S = 20$		❖ $S_r = S/2$	❖ $p_{ed} = 0.25$

Chemotactic step size ($C(i)$) was set to 0.05 while the initial positions of bacteria were selected at $[11, 15]$ and randomly across the nutrient media.

The convergence plots depicted in Figure 2.15 show that the N_c value affected the convergence of SBFA when bacteria were initially placed at $[11, 15]$. However, it did not give much effect when bacteria were initially placed randomly across the nutrient media. Numerical results presented in Table 2.5 show that SBFA needed longer chemotaxis steps (bigger N_c value) to find the global minimum when bacteria were placed at $[11, 15]$. However, with the initial positions of bacteria placed randomly selected across the nutrient media the N_c only had little effect because parts of bacteria were landed near the optimum point. Another consequence of bigger N_c value is that the computation time will be longer.

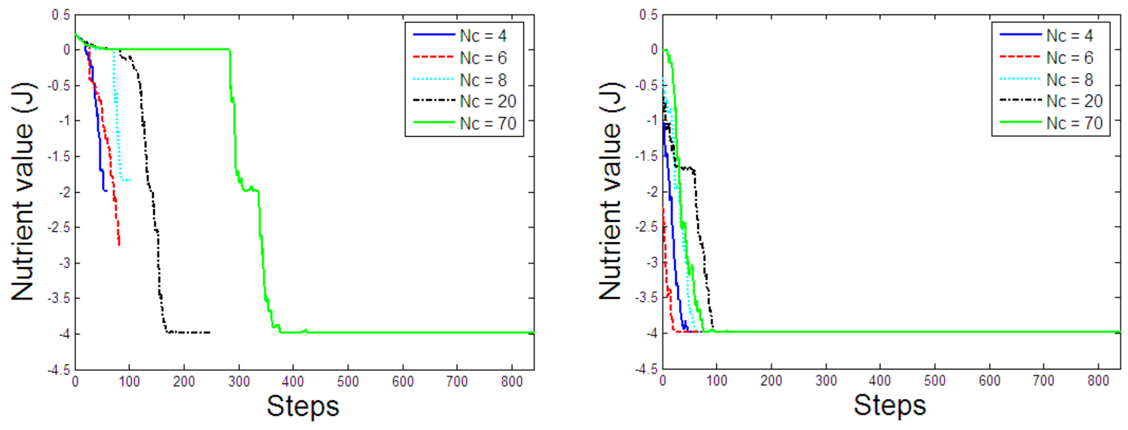

(a) Initial positions: at $[11, 15]$ (b) Initial positions: random

Figure 2.15: Convergence plots of SBFA for various N_c values

Table 2.5: Numerical results of SBFA for different N_c values

Initial positions of bacteria	N_c	**Optimum** x_1	**Optimum** x_2	**Optimum** J	**Chemotactic steps**	**Convergence speed (steps)**
At $[11, 15]$	4	7.9314	24.9892	-1.9924	48	-
	6	15.3316	3.1119	-2.7689	72	-
	8	4.8911	9.9831	-1.8428	96	-
	20	15.0193	4.9909	-3.9867	240	170
	70	15.0252	4.9799	-3.9867	840	378
Randomly in nutrient media	4	14.9930	4.9575	-3.9862	48	50
	6	14.9874	4.9681	-3.9863	72	26
	8	15.0006	4.9756	-3.9866	96	65
	20	15.0153	4.9746	-3.9867	240	96
	70	15.0059	4.9766	-3.9866	840	78

2.4.4. Impact of maximum continuous swim number

Large maximum continuous swim number (N_s) enables bacteria to swim continuously directly heading to the optimum value which means bacteria will only need fewer iterations to achieve global optimum point. However, if the N_s value is too large bacteria will face the risk of moving to and being trapped in local minima. Here, SBFA with various N_s is used to find optimum point of the nutrient media formulated in equation (2.7). The objective of the investigation is to disclose the effect of N_s on the convergence and accuracy of SBFA. In the simulation, the BFA parameters were selected as:

❖ $p = 2$	❖ $N_c = 40$	❖ $N_{re} = 4$	❖ $N_{ed} = 3$
❖ $S = 20$		❖ $S_r = {}^{S}/_{2}$	❖ $p_{ed} = 0.25$

Chemotactic step size was chosen equal to 0.05 while the initial positions of bacteria were selected at $[11, 15]$ and randomly across the nutrient media.

The convergence plots depicted in Figure 2.16 show that the longer N_s the faster SBFA will converge to optimum point. However, too big N_s value results in a delay in the convergence because bacteria will swim toward local optimum point. Numerical results outlined in Table 2.6 show that N_s values only slightly influence the optimum value achieved by SBFA but it impacts on the convergence speed.

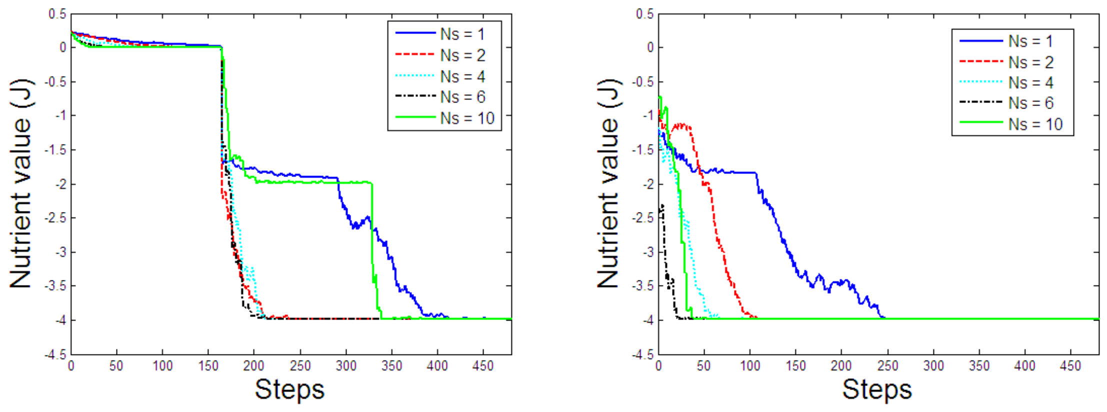

(a) Initial positions: at [11; 15] (b) Initial positions: random

Figure 2.16: Convergence of SBFA for different N_s values

Table 2.6: Numerical results of SBFA for different N_s values

Initial positions of bacteria	N_s	Optimum x_1	Optimum x_2	Optimum J	Convergence speed (steps)
At $[11, 15]$	1	15.0170	4.9903	-3.9867	413
	2	15.0134	4.9730	-3.9866	238
	4	15.0227	4.9955	-3.9866	213
	6	15.0016	5.0060	-3.9864	215
	10	15.0343	5.0100	-3.9863	372
Randomly in the nutrient media	1	15.0176	4.9834	-3.9867	248
	2	15.0281	4.9782	-3.9866	109
	4	15.0142	4.9953	-3.9866	75
	6	14.9949	4.9994	-3.9864	47
	10	15.0368	4.9998	-3.9864	39

2.4.5. Impact of reproduction steps

During reproduction steps, only healthiest bacteria will survive and the other least healthy bacteria will be discarded. In the BFA algorithm, with small number of reproduction steps (N_{re}) bacteria may converge prematurely to local optima. With large N_{re} the bacteria will be able to concentrate to good regions using healthiest bacteria only and ignore lower-nutrient regions. However, clearly, larger N_{re} increases computational complexity and computational time. In this section, SBFA with various N_{re} values is used to find optimum point of the nutrient media formulated in equation (2.7). The objective of the investigation is to discover the impact of N_{re} on the convergence and accuracy of BFA. In the simulation, the following BFA parameters were used:

❖ $p = 2$	❖ $N_c = 40$	❖ $S_r = S/2$	❖ $N_{ed} = 3$
❖ $S = 20$	❖ $N_s = 4$		❖ $p_{ed} = 0.25$

Chemotactic step size ($C(i)$) values were selected equal to 0.01 and 0.05 while the initial positions of bacteria were selected at $[11, 15]$ and randomly across the nutrient media.

With a step size of to 0.01, the converge plots depicted in Figure 2.17 show that, in general, large N_{re} value makes SBFA to converge slower than a small N_{re} value. For the accuracy, numerical results presented in Table 2.7 show that SBFA needs enough N_{re} to be able find the place near the optimal point. The introduction of N_{re} automatically increases chemotaxis steps and this in turn increases computational load and time. Similarly with chemotactic step size of 0.05 the convergence plots depicted in Figure 2.18 show that smaller N_{re} values result in faster convergence. Also, numerical results presented in Table 2.8 show that N_{re} values give little impact on the accuracy.

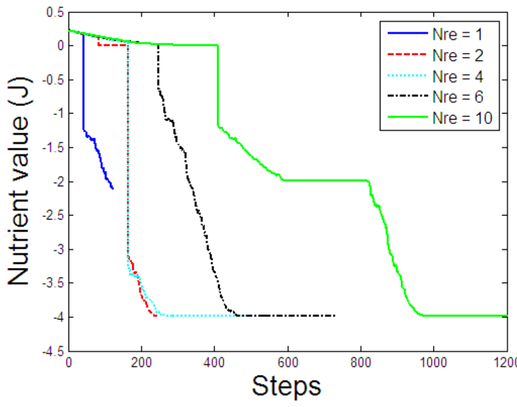

(a) Initial positions: at $[11, 15]$

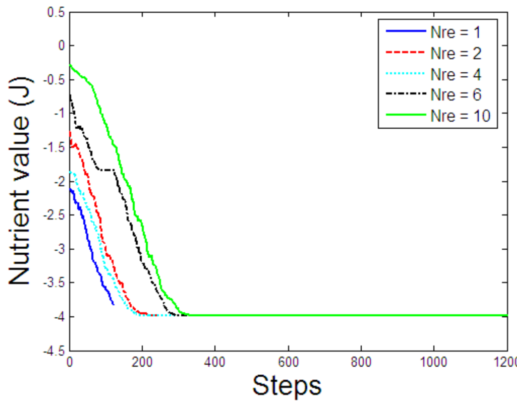

(b) Initial positions: random

Figure 2.17: Convergence plots of SBFA for different N_{re} values with chemotactic step size ($C(i)$) equal to 0.01

Table 2.7: Numerical results of SBFA for various N_{re} values with chemotactic step size ($C(i)$) equal to 0.01

Initial positions of bacteria	N_{re}	**Optimum x_1**	**Optimum x_2**	**Optimum J**	**Chemotactic steps**	**Convergence speed (steps)**
At $[11, 15]$	1	13.8592	2.7395	-2.1045	120	-
	2	14.9285	5.0630	-3.9809	240	-
	4	15.0163	4.9846	-3.9867	480	269
	6	15.0164	4.9823	-3.9867	720	464
	10	15.0159	4.9878	-3.9867	1200	972
Randomly across nutrient media	1	15.5702	5.3337	-3.8188	120	-
	2	15.0163	4.9913	-3.9867	240	223
	4	15.0174	4.9826	-3.9867	480	196
	6	15.0207	4.9867	-3.9867	720	293
	10	15.0149	4.9867	-3.9867	1200	330

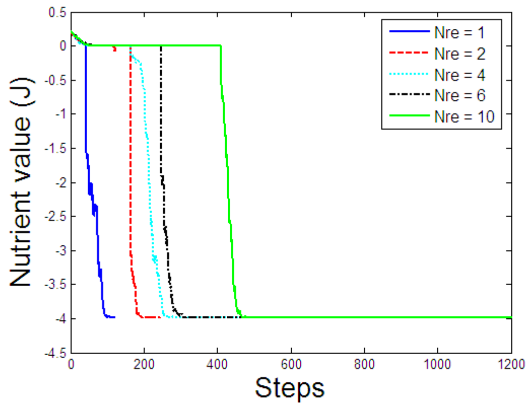

(a) Initial positions: at $[11, 15]$

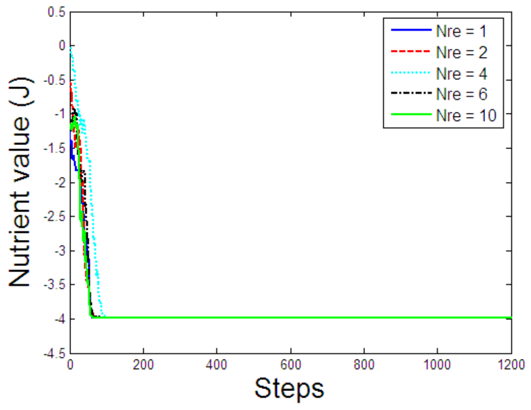

(b) Initial positions: random

Figure 2.18: Convergence plots of SBFA for various N_{re} value with chemotactic step size $(C(i))$ equal to 0.05

Table 2.8: Numerical results of SBFA for various N_{re} values with chemotactic step size $(C(i))$ equal to 0.05

Initial positions of bacteria	N_{re}	**Optimum** x_1	**Optimum** x_2	**Optimum** J	**Chemotactic steps**	**Convergence speed (steps)**
At $[11, 15]$	1	14.9880	5.0137	-3.9860	120	109
	2	15.0384	5.0039	-3.9863	240	194
	4	15.0344	4.9888	-3.9866	480	263
	6	15.0195	4.9558	-3.9864	720	307
	10	14.9986	4.9862	-3.9866	1200	469
Randomly in nutrient media	1	15.0557	4.9764	-3.9860	120	61
	2	15.0219	4.9972	-3.9866	240	69
	4	15.0026	4.9783	-3.9866	480	98
	6	15.0281	4.9911	-3.9866	720	75
	10	15.0000	4.9947	-3.9865	1200	63

2.4.6. Impact of elimination and dispersal event

Elimination and dispersal event makes bacteria dispersed in another region of nutrient media. This event results bacteria to possibly fall into a region near the optimum point. Thus, a large value of elimination and dispersal number (N_{ed}) will assure bacteria explore all regions of nutrient media, with increased computational complexity and time as the side effect. With small value of N_{ed} and especially with small population size, the bacteria may not explore the whole nutrient media. In this section, SBFA with various N_{ed} values is utilised to find optimal point of the nutrient media formulated in equation (2.7). The objective of the work is to study the impact of N_{ed} value on the convergence and accuracy of the algorithm. In the simulation, the following SBFA parameters values were used:

❖ $p = 2$	❖ $N_c = 40$	❖ $N_{re} = 4$	
❖ $S = 20$	❖ $N_s = 4$	❖ $S_r = S/2$	❖ $p_{ed} = 0.25$

The chemotactic step size $(C(i))$ values were selected equal to 0.01 and 0.1 while the initial positions of bacteria were selected at $[11, 15]$ and randomly in the nutrient media.

For a step size of 0.01, the convergence plots depicted in Figure 2.19 show that in general smaller N_{ed} values result in faster convergence. For the initial positions of bacteria at $[11, 15]$, the numerical results presented in Table 2.9 show that SBFA needed enough N_{ed}, e.g. 3 to find a place near the optimum point. For initial positions of bacteria selected randomly in the nutrient media, the BFA was able to find locations near the optimum point with only one elimination and dispersal event because part of bacteria initially fell near the optimum point. Large N_{ed} values increase the number of chemotaxis steps and in turn increase the computation load and time. These conditions also apply to chemotactic step size equal to 0.1.

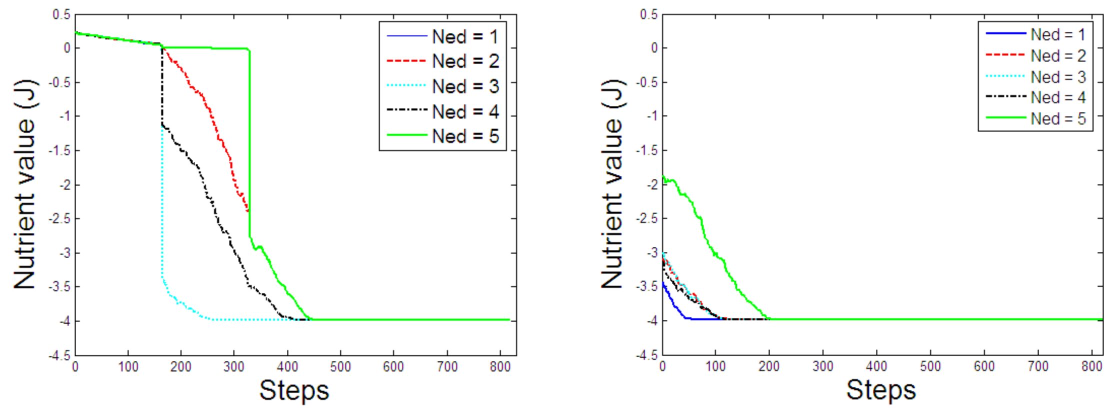

(a) Initial positions: at $[11, 15]$ (b) Initial positions: random

Figure 2.19: Convergence of SBFA for various N_{ed} values with chemotactic step size equal to 0.01

Table 2.9: Numerical results of SBFA for various values of N_{ed} with chemotactic step size equal to 0.01

Initial positions of bacteria	N_{ed}	**Optimum x_1**	**Optimum x_2**	**Optimum J**	**Chemotactic steps**	**Convergence speed (steps)**
At $[11, 15]$	1	8.4477	16.5802	0.0421	160	-
	2	14.7798	7.1715	-2.3939	320	-
	3	15.0143	4.9797	-3.9867	480	258
	4	15.0136	4.9804	-3.9867	640	416
	5	15.0144	4.9787	-3.9867	800	453
Randomly in nutrient media	1	15.0134	4.9822	-3.9867	160	55
	2	15.0175	4.9841	-3.9867	320	122
	3	15.0168	4.9815	-3.9867	480	114
	4	15.0199	4.9792	-3.9867	640	118
	5	15.0152	4.9840	-3.9867	800	205

Similar to small chemotactic step size, Table 2.10 shows that, with initial positions of bacteria selected at $[11, 15]$ in the nutrient media, using chemotactic step size equal to 0.1 the BFA needed N_{ed} values, of two or above to converge. However, with the initial positions of bacteria selected randomly, the BFA was able to find locations near the optimum point with only one elimination and dispersal event. Also, larger N_{ed} value resulted in a larger number of chemotaxis steps and longer computation time. The convergence plots depicted in Figure 2.20 show that N_{ed} values did not impact on the convergence of SBFA.

Table 2.10: Numerical results of SBFA for various values of N_{ed} with chemotactic step size equal to 0.1

Initial positions of bacteria	N_{ed}	**Optimum** x_1	**Optimum** x_2	**Optimum** J	**Chemotactic steps**	**Convergence speed (steps)**
At $[11, 15]$	1	-15.3647	27.7284	6.2863×10^{-42}	160	-
	2	15.0253	4.9891	-3.9867	320	219
	3	15.0411	4.9876	-3.9864	480	200
	4	15.0097	4.9308	-3.9855	640	208
	5	15.0456	4.9699	-3.9863	800	211
Randomly across nutrient media	1	14.9760	4.9777	-3.9860	160	95
	2	15.0315	4.9694	-3.9865	320	96
	3	15.0205	4.9709	-3.9866	480	41
	4	15.0069	5.0002	-3.9865	640	44
	5	15.0316	4.9344	-3.9856	800	80

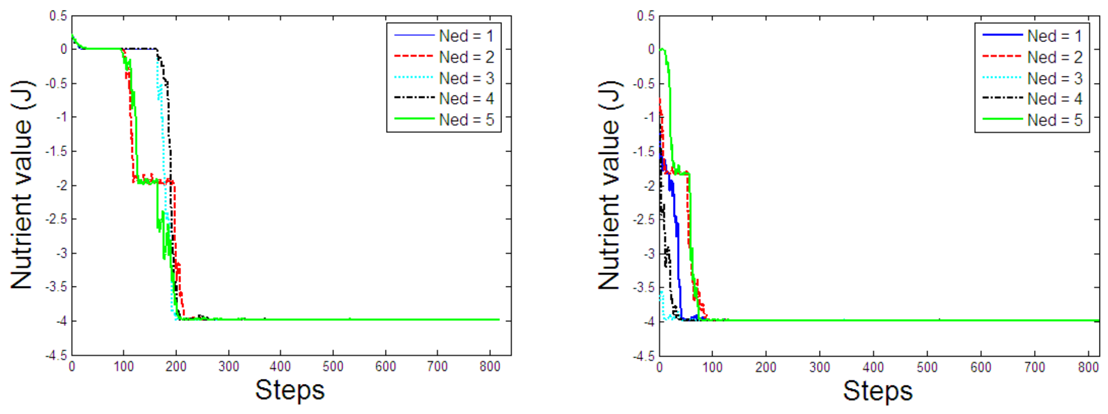

(a) Initial positions: at $[11, 15]$ (b) Initial positions: random

Figure 2.20: Convergence of SBFA for various N_{ed} values with chemotactic step size equal to 0.1

2.4.7. Impact of chemotactic step size

Chemotactic step size, $C(i)$, value determines the length of one chemotaxis step.

- If $C(i)$ is very small, bacteria will be able to find on optimal point very close to the theoretical optimum point. However, the convergence will be very slow so that large number of steps will be needed. Also too small $C(i)$ will make bacteria have high probability of being trapped at local optima.

- If $C(i)$ is very large, bacteria will be able to converge to optimum value very fast and possibly able to miss possible local optima by swimming through them without stopping. However, if the optimum value lies in a valley then it will get risk to jump over the valley.

In order to reveal the impact of chemotactic step size ($C(i)$) on the convergence and accuracy, in this section BFA with various $C(i)$ values is used to find optimum point of nutrient media formulated in equation (2.7). In the simulation, the SBFA used the parameters values:

❖ $p = 2$	❖ $N_c = 40$	❖ $N_{re} = 4$	❖ $N_{ed} = 3$
❖ $S = 20$	❖ $N_s = 4$	❖ $S_r = S/2$	❖ $p_{ed} = 0.25$

The initial positions of bacteria were selected at $[11, 15]$ and randomly across the nutrient media.

Convergence plots depicted in Figure 2.21 show that bigger chemotactic step size results BFA to converge to optimum point faster than that with smaller step size and too small step size makes SBFA either not reaching a place near optimum point. However, too big chemotactic step size makes bacteria oscillate around optimum point. In addition, SBFA is able to converge faster if the initial positions of bacteria are chosen randomly because part of bacteria fall in the area near to the optimum value than if placed at $[11, 15]$. Numerical results outlined in Table 2.11 show that if the chemotactic step size is too small SBFA could not achieve nutrient value close to optimum point but if the step size is too big SBFA may achieve nutrient value farther from optimum point. With initial positions of bacteria placed randomly in the nutrient media, SBFA could achieve a location near the optimum point using smaller step size.

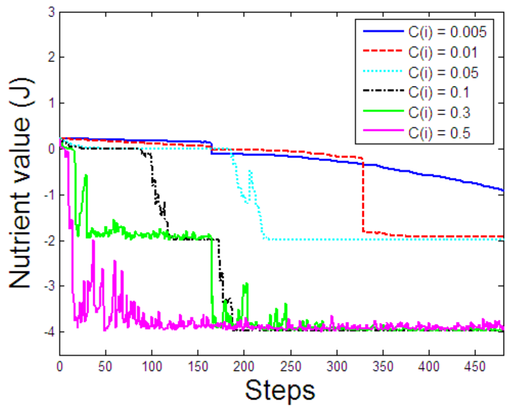

(a) Initial positions: at [11; 15]

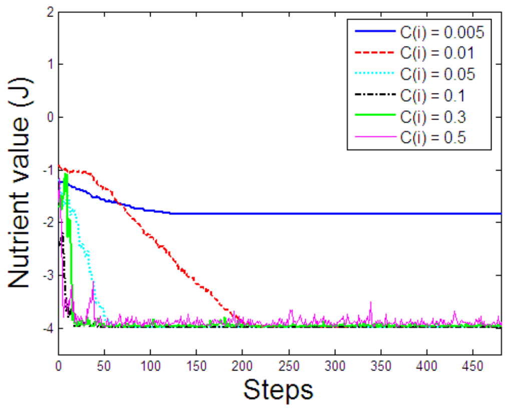

(b) Initial positions: random

Figure 2.21: Convergence plots of SBFA for various $C(i)$ values

Table 2.11: Numerical results of SBFA for various $C(i)$ with initial positions of bacteria at $[11, 15]$

Initial positions of bacteria	$\boldsymbol{C(i)}$	**Optimum** $\boldsymbol{x_1}$	**Optimum** $\boldsymbol{x_2}$	**Optimum** $\boldsymbol{J}$	**Convergence speed (steps)**
At $[11, 15]$	0.005	18.4859	3.6244	-0.9782	-
	0.01	19.9765	15.0175	-1.9116	374
	0.05	7.9853	25.0029	-1.9968	236
	0.1	15.0521	4.9860	-3.9862	220
	0.3	14.9795	4.8436	-3.9783	333
	0.5	15.0602	4.7878	-3.8903	217
Randomly in nutrient media	0.005	4.9252	9.9929	-1.8441	142
	0.01	15.0130	4.9818	-3.9867	245
	0.05	15.0142	4.9953	-3.9866	75
	0.1	15.0448	4.9335	-3.9853	45
	0.3	15.0673	4.9467	-3.9151	18
	0.5	14.8269	4.9370	-3.8714	45

2.4.8. Impact of probability value which bacteria will be eliminated/dispersed

In the BFA algorithm, probability value which bacteria will be eliminated/dispersed (p_{ed}) determines the threshold condition that bacteria will be eliminated and dispersed and in turn determines how many bacteria will be eliminated/dispersed. Larger p_{ed} values mean larger number of bacteria will be eliminated and dispersed and vice versa.

The advantage of large p_{ed} value is that more bacteria are dispersed to other parts of the nutrient media so that BFA can search almost all parts of the nutrient media, and in turn avoid getting trapped at local optima and also further to accelerate the convergence. However, the negative impact of large p_{ed} value is that it may degrade the algorithm to random exhaustive search. In this section, SBFA with various p_{ed} values is used to find optimum point of the nutrient media formulated in equation (2.7). The objective of the investigation is to study the impact of p_{ed} on the convergence and accuracy of BFA. In the simulation, the BFA used the following parameter values:

❖ $p = 2$	❖ $N_c = 40$	❖ $N_{re} = 4$	❖ $N_{ed} = 3$
❖ $S = 20$	❖ $N_s = 4$	❖ $S_r = S/2$	

The chemotactic step size $(C(i))$ was selected equal to 0.01 with the initial positions of bacteria selected at $[11, 15]$ and randomly across the nutrient media.

The convergence plots depicted in Figure 2.22 show that large p_{ed} values result in faster convergence. The numerical results presented in Table 2.12 show that with initial positions of bacteria at $[11, 15]$ and too small a p_{ed} value the SBFA could not achieve a location closest to the optimum point. This is likely because there were not enough bacteria to be eliminated and dispersed to other area so that bacteria were trapped in one of the local minima. For computation time, there was no trends either increasing or decreasing due to changes in p_{ed} value.

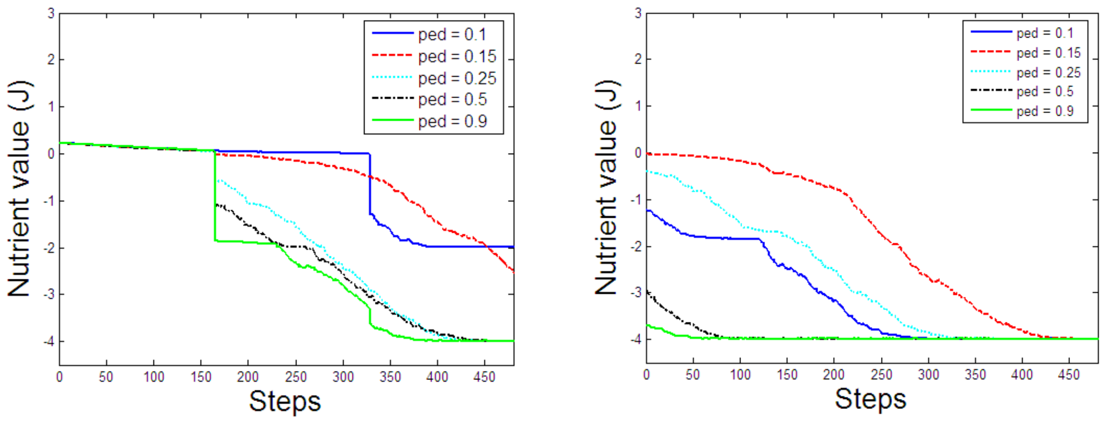

(a) Initial positions: at $[11, 15]$ (b) Initial positions: random

Figure 2.22: Convergence plots of SBFA for various probability threshold (p_{ed}) values

Table 2.12: Numerical results of SBFA for various p_{ed} values

Initial positions of bacteria	p_{ed}	Optimum x_1	Optimum x_2	Optimum J	Convergence speed (steps)
At $[11, 15]$	0.1	21.0075	25.0036	-1.9895	392
	0.15	16.5141	3.6822	-2.6726	484
	0.25	15.0165	4.9796	-3.9867	434
	0.5	15.0200	4.9796	-3.9867	444
	0.9	15.0143	4.9828	-3.9867	383
Randomly in the nutrient media	0.1	15.0141	4.9829	-3.9867	294
	0.15	15.0181	4.9805	-3.9867	445
	0.25	15.0135	4.9841	-3.9867	349
	0.5	15.0152	4.9838	-3.9867	111
	0.9	15.0130	4.9821	-3.9867	58

2.4.9. Impact of initial positions of bacteria

In the BFA optimisation process, the initial positions of bacteria could be selected at certain position or just placed randomly in the nutrient media. If the region of global optimum in the nutrient media is known, the initial positions of bacteria could be placed in the region to accelerate convergence and achieve nutrient value as close as possible with global optimum. In this section SBFA with different initial positions of bacteria is used to find optimum point of the nutrient media formulated in equation (2.7). The objective of the investigation is to study the impact of initial positions of bacteria on convergence and accuracy. In the simulation, the SBFA used the following parameter values:

❖ $p = 2$	❖ $N_c = 40$	❖ $N_{re} = 4$	❖ $N_{ed} = 3$
❖ $S = 20$	❖ $N_s = 4$	❖ $S_r = {}^{S}/_{2}$	❖ $p_{ed} = 0.25$

Thus every bacterium will have 480 steps in their lifetime. The chemotactic step size was selected equal to 0.05. The initial positions of bacteria were selected in seven pre-determined positions, e.g. $[3, 20]$, $[2, 2]$, $[28, 2]$, $[28, 28]$, $[15, 28]$, $[15, 10]$, and $[11, 15]$ and randomly in the nutrient media as depicted in Figure 2.23(a).

The convergence plots depicted in Figure 2.23(b) show that the fastest convergence was achieved with initial positions of bacteria at $[15, 10]$, which is very close to the global optimum point.

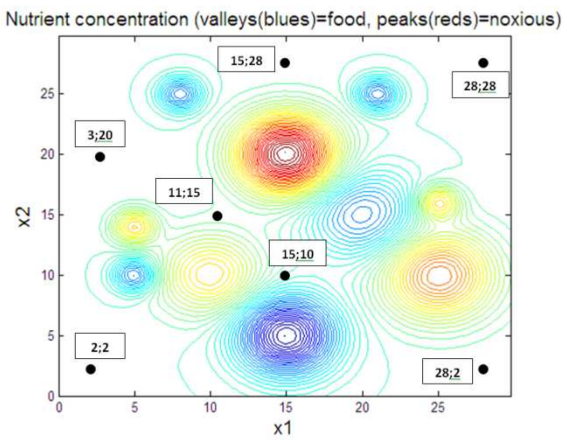

(a) Various initial positions

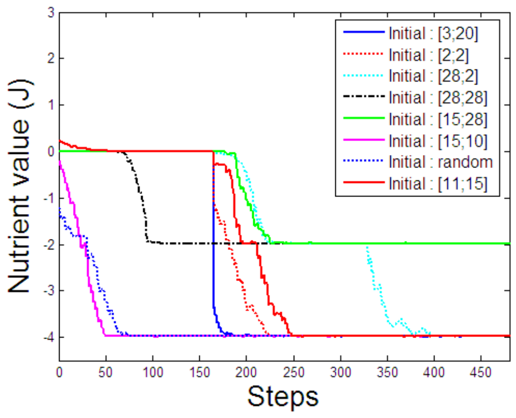

(b) Convergence plots

Figure 2.23: Various predetermined initial positions of bacteria in the nutrient media and their convergence plots

It can be noticed that the convergence of SBFA with initial positions of bacteria selected randomly in the nutrient media was slightly slower than with $[15, 10]$ but faster than with all the other rest predetermined initial positions. Numerical results presented in Table 2.13 show that the SBFA was able to converge to the global optimum point for most of the initial positions of bacteria except for $[15, 28]$ and $[28, 28]$ in 480 steps.

Table 2.13: Numerical results of SBFA with various initial positions of bacteria

Initial positions of bacteria	**Initial J**	**Optimum x_1**	**Optimum x_2**	**Optimum J**	**Convergence speed (steps)**
[3, 20]	3.4672×10^{-6}	15.0013	4.9913	-3.9866	316
[2, 2]	5.4471×10^{-6}	15.0047	5.0071	-3.9864	326
[28, 2]	0.0087	14.9907	4.9753	-3.9844	415
[28, 28]	-1.5674×10^{-8}	21.0133	25.0216	-1.9892	109
[15, 28]	0.0083	20.9845	25.0194	-1.9888	241
[15, 10]	-0.1996	15.0106	4.9991	-3.9866	53
Random	-	15.0215	4.9831	-3.9867	75
[11, 15]	0.2283	15.0275	4.9822	-3.9856	252

2.5. Summary

The original BFA proposed by Passino (2000, 2002) has been described in detail together with its current applications and proposed modifications. Although the original BFA performed well in the various applications, the modifications have improve its performance in several aspects such as convergence to the optimum value, convergence speed, etc. The previous modifications proposed, developed and used by researches give an overview of the potential open space for further modification and its application. Finally, the impact of parameter selection in the original BFA on convergence and accuracy has been studied.

It can be noted that the most influential factors on convergence are initial positions of bacteria and chemotactic step size ($C(i)$) while the most influential factors for accuracy are N_c, N_{re}, N_{ed} and chemotactic step size ($C(i)$). If the initial positions of bacteria are chosen randomly in the nutrient media and adequate N_c, N_{re} and N_{ed} values are provided, then the most influential factor for both convergence and accuracy is the chemotactic step size ($C(i)$). Hybridization of BFA with other techniques such as FL and NN need further study to reveal its potential, possibility, and performance. Chapter 3 will present an overview of a single-link flexible manipulator considered in this work.

CHAPTER 3
FLEXIBLE MANIPULATOR SYSTEMS: AN OVERVIEW

3.1. Introduction

The flexible manipulator system utilised in the research is overviewed in this chapter. First of all, the structure of available experimental rig is described. Secondly, current works on modelling and control of the flexible manipulator are discussed. Finally, the experimental input-output data pairs gathered from the flexible manipulator rig is presented.

3.2. Structure of flexible manipulator system

The flexible manipulator rig considered in this work is a laboratory-scale facility depicted in Figure 3.1 (Azad, 1994; Tokhi and Azad, 1997).

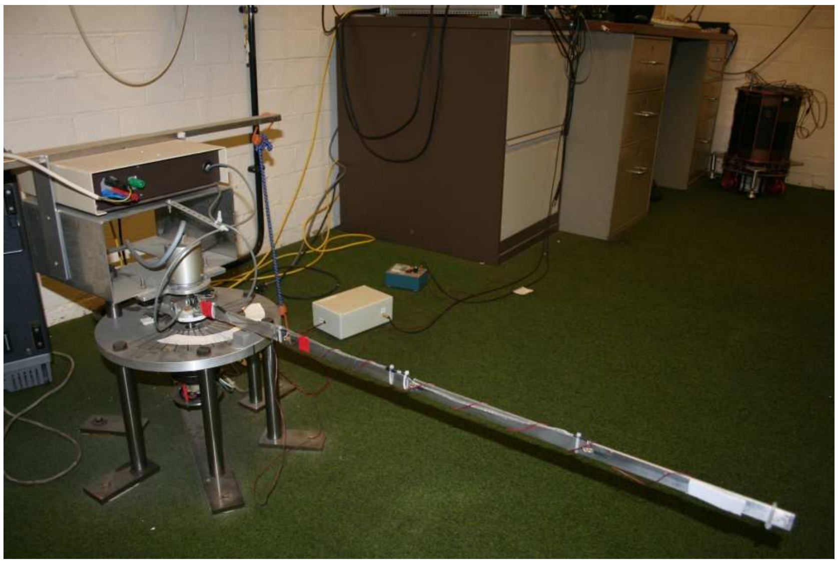
Figure 3.1: The laboratory-scale single-link flexible manipulator rig

The experimental rig consists of a thin beam attached on the hub actuator. The actuator is a U9M4AT type printed circuit motor driving the flexible manipulator with a bi-directional motor drive amplifier (LA5600 manufactured by Electro-Craft Corporation). The three measuring devices used to record the responses of the manipulator are shaft encoder, tachometer and accelerometer. For shaft encoder, a transducer used for measuring hub-angular displacement, with a resolution of 2048 pulses/revolution manufactured by Heidenhain is been selected. The tachometer is used for measurement of the hub angular velocity of the manipulator. The accelerometer, located at the end-point of the flexible arm mounted using epoxy adhesive, is used for measuring the end-point acceleration. The instrument used for accelerometer is integrated circuit piezoelectric (ICP) accelerometer 303A03. This device has advantages such as its lightweight, small size, can cover the range of frequencies involved in these investigations with voltage sensitivity of 1.02 mV/ms^{-2} and has low impedance output that allows the use of long cables without an appreciable signal loss or distortion. A precision interface circuit PCL 818G is used to interface the flexible manipulator system with a computer, currently a personal computer (PC) with a Pentium Celeron-500 MHz is utilised. A direct interface between the processor, the actuator and sensors can be handled by this board (Azad, 1994; Tokhi and Azad, 1997). MATLAB/SIMULINK environment is developed in the PC and used to communicate with the manipulator so that all data from the manipulator can be recorded and a controller can be designed and applied. The block diagram of the experimental rig is depicted in Figure 3.2.

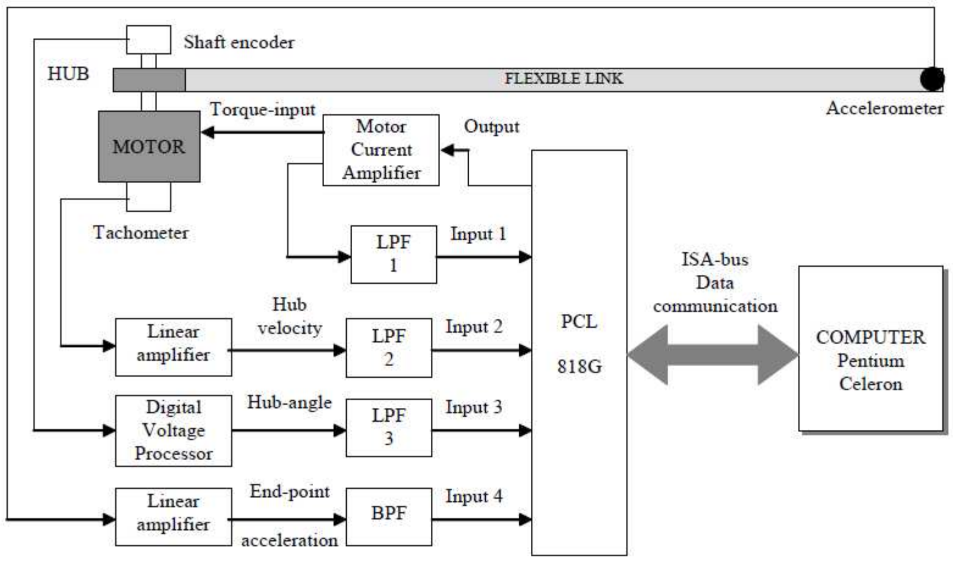

Figure 3.2: Schematic diagram of the experimental rig (Azad, 1994)

The arm of the manipulator is a beam made from aluminium material. An outline of the mechanical model of the flexible manipulator is depicted in Figure 3.3 (Azad, 1994; Tokhi and Azad, 1997). In the schematic representation of the flexible manipulator in Figure 3.4(a): the stationary and moving coordinates are represented by POQ and

$P'OQ'$ respectively, θ is the hub-angular displacement, τ is the applied torque at the hub by a drive motor, M_p represents a payload mass, I_h is the hub inertia, I_p is inertia associated with the payload. The physical parameters of the flexible arm used in this work are outlined in Table 3.1. In this work, the impact of gravity is neglected. The operational range of the flexible manipulator rig is in the range of ± 80 degrees as depicted in Figure 3.4(b).

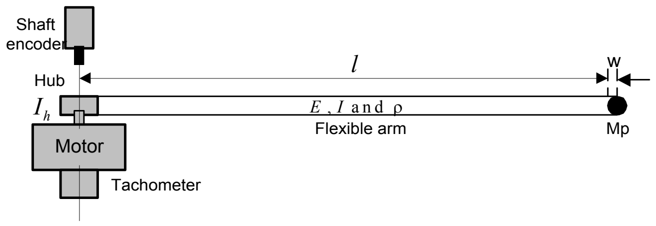

Figure 3.3: Outline of the flexible manipulator system (Azad, 1994)

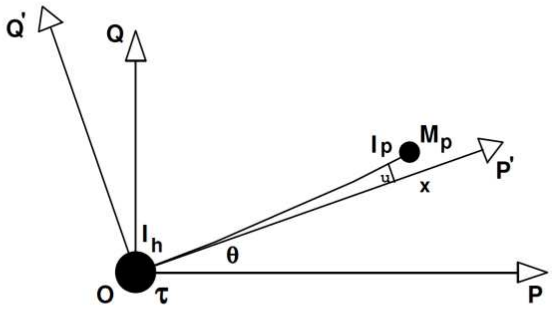

(a) Schematic representation

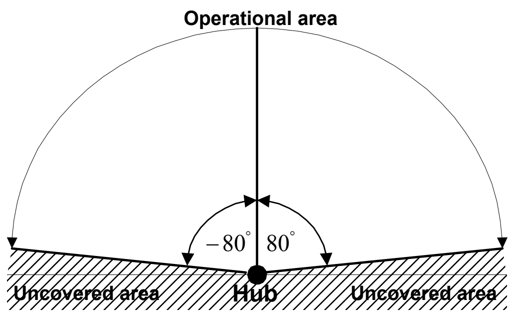

(b) Operational range

Figure 3.4: Representation of the flexible manipulator system (Azad, 1994)

Table 3.1: Physical parameters of experimental flexible manipulator rig

Physical parameters	**Value**
Length (l)	960 mm
Width (w)	19.008 mm
Thickness (h)	3.2004 mm
Mass density per unit volume (ρ)	2710 $K_g m^{-3}$
The second moment of inertia (I)	5.1924×10^{-11} m^4
The young modulus (E)	71×10^9 Nm^{-2}
Moment of inertia (I_b)	0.04862 $K_g m^2$
The hub inertia (I_h)	5.86×10^{-4} $K_g m^2$

3.3. Previous works on modelling of flexible manipulator system

3.3.1. Introduction

In general, system modelling is the process of developing a structure that represents the dynamics of system under study. Several methods such as mathematical method and numerical analysis have been proposed, developed and used by researchers (Azad, 1994; Poerwanto, 1998). By using a mathematical analysis, the flexible manipulator dynamics can be represented as a partial differential equation (PDE). The modelling of flexible manipulator using numerical analysis method involves representation of flexible manipulator dynamics by solving the PDE using finite difference (FD) or finite element (FE) methods.

Flexible manipulator systems can also be modelled by using certain methods that avoid solving dynamics/kinematics of the system. These include parametric and non-parametric identification techniques (Shaheed and Tokhi, 2002). With these approaches, model of the system is derived based on input-output data pairs collected at input-output terminals of the system. As a consequence, the accuracy of the model is highly dependent on the accuracy of the collected data from the experimentation steps (Ljung, 1999). There are two steps for these approaches. Firstly, qualitative operations which define the structure of the model such as type and order of the differential/difference equation that relate the input to the output have to be performed. This step is called characterization. Then, the numerical values of the structural parameters are determined, which minimize the residual/error between actual system and the model. This step is known as identification. Construction of a model based on input-output data pair involves three main components (Ljung, 1999):

a. The input-output data available gathered from experiment
b. A set of candidate models.
c. An assessment mechanism to determine the best model

Furthermore, the system modelling problem can be considered as an optimisation task where the objective is to find parameters of the model that minimise the prediction error between the system's actual output (the measured data) and the predicted output (model's output). The general concept of system identification can be described as in Figure 3.5, where $u(k)$ is the actual input, $y(k)$ is the actual output, $\hat{y}(k)$ is the predicted output and $e(k)$ is the error;

$$e(k) = y(k) - \hat{y}(k) \tag{3.1}$$

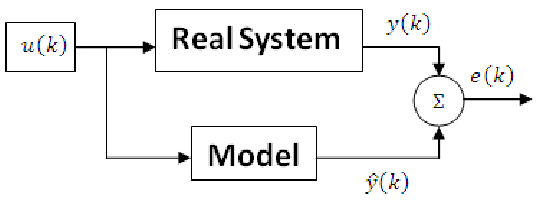

Figure 3.5: General concept of system identification

The model is fitted to the real system using the procedure described as:

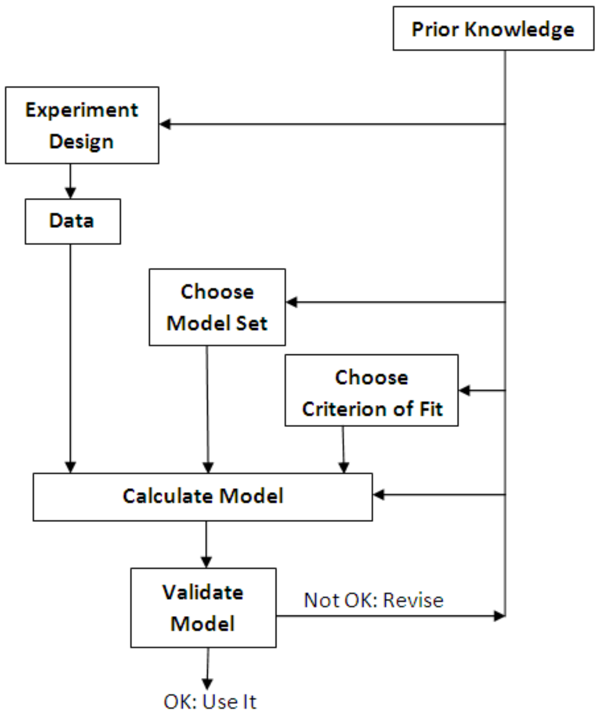

Figure 3.6: The system identification loop (Ljung, 1999)

Following the modelling phase, the validation phase is carried out. Firstly the resulted model must be stable. Secondly, the model shall predict the system response to given excitation. To validate predictive capability of the model the experimental data is split into two sets: estimation set (modelling set) and test set (prediction set). Normally, the data set is divided into two halves. Finally, if the developed model is adequate, the prediction errors should not contain any information about the past errors, inputs or outputs of the system. The adequacy of the model can be checked by using a set of the correlation tests described below (Billings and Voon, 1986), where $\varepsilon(t)$ is the prediction error (residual), $u(t)$ is the input, $\phi_{u\varepsilon}(\tau)$ represents the cross-correlation function between $u(t)$ and $\varepsilon(t)$, $\varepsilon u(t) = \varepsilon(t+1)u(t+1)$, and $\delta(\tau)$ is an impulse function:

$$\phi_{\varepsilon\varepsilon}(\tau) = E[\varepsilon(t-\tau)\varepsilon(t)] = \delta(\tau)$$
$$\phi_{u\varepsilon}(\tau) = E[u(t-\tau)\varepsilon(t)] = 0,\ \forall\tau$$
$$\phi_{u^2\varepsilon}(\tau) = E[(u^2(t-\tau) - \bar{u}^2(t))\varepsilon(t)] = 0,\ \forall\tau \qquad (3.2)$$
$$\phi_{u^2\varepsilon^2}(\tau) = E[(u^2(t-\tau) - \bar{u}^2(t))\varepsilon^2(t)] = 0,\ \forall\tau$$
$$\phi_{\varepsilon(\varepsilon u)}(\tau) = E[\varepsilon(t)\varepsilon(t-1-\tau)u(t-1-\tau)] = 0,\ \tau \geq 0$$

The correlations will never be exactly zero for all lags and the 95% confidence bands are used to indicate if the estimated correlations are significant or not. However, for linear time-invariant models, the first two correlation tests of equation (3.2) are applicable (Billings and Voon, 1986).

3.3.2. Mathematical or analytical approaches

Mathematical analysis for solving the partial differential equation (PDE) to characterise the dynamic behaviour of flexible manipulator systems have been proposed (Azad, 1994) such as Book (1984), Cannon and Schmitz (1984) and Hasting and Book (1987). Another method is by using numerical analysis based on finite difference (FD) (Azad, 1994; Poerwanto, 1998; Tokhi et al., 1997) and Finite element (FE) (Martins et al., 2003; Menq and Chen, 1988; Mohamed, 2003; Tokhi and Azad, 1995; Tokhi et al., 2001; Tokhi and Mohamed, 1999; Tokhi et al., 1995; Tokhi et al., 1997; Usoro et al., 1986) methods to solve the PDE.

A. Mathematical formulation of systems dynamics

A schematic description of the single-link flexible manipulator system considered in this work is depicted in Figure 3.4(a) (Azad, 1994), where the stationary and moving coordinates are represented by POQ and $P'OQ'$ respectively, $\tau(t)$ is the applied torque at the hub, M_P is the payload mass, I_h is the hub inertia, E is the Young modulus, I is the second moment of inertia and ρ is the mass density per unit length of the manipulator respectively. With the gravity effects are neglected, the motion of the manipulator is confined to the $P'OQ'$ plane only.

A pinned-free flexible beam, which incorporating inertia at the hub and payload mass at the end-point, can be considered as a representation of flexible manipulator system model. The displacement $y(x,t)$ of a point along the manipulator at a distance x

from the hub can be described as a function of both the rigid body motion $\theta(t)$ and elastic deflection $u(x,t)$ measured from the line OP';

$$y(x,t) = x\theta(t) + u(x,t) \tag{3.3}$$

where θ is the angular displacement and u is the elastic deflection. By ignoring the effects of rotary inertia and shear deformation, the motion of the manipulator can be represented as a fourth order PDE as (Azad, 1994):

$$EI\frac{\partial^4 u(x,t)}{\partial x^4} + \rho\frac{\partial^2 u(x,t)}{\partial t^2} = -\rho x\ddot{\theta} \tag{3.4}$$

With boundary conditions are;

- The displacement at the hub $\{u(0,t)\}$ must be zero,
- The total forces at the hub must be the same with the applied torque,
- The shear force at the end-point must be equal to $M_P\frac{\partial^2 u(x,t)}{\partial t^2}$ (Tse et.al, 1980).
- The stress at the end-point must be zero, that is, no force should be present at the free end;

$$\begin{aligned} u(0,t) &= 0 \\ I_h\frac{\partial^3 u(0,t)}{\partial t^2\partial x} - EI\frac{\partial^2 u(0,t)}{\partial x^2} &= \tau(t) \\ M_p\frac{\partial^2 u(l,t)}{\partial t^2} - EI\frac{\partial^3 u(l,t)}{\partial x^3} &= 0 \\ EI\frac{\partial^2 u(l,t)}{\partial x^2} &= 0 \end{aligned} \tag{3.5}$$

where l is the length of the manipulator. The whole derivation of the system's equations in details can be found in (Azad, 1994, Poerwanto, 1998). Finally, the governing dynamic equation of the system with damping can be formulated as (Poerwanto, 1998)

$$EI\frac{\partial^4 u(x,t)}{\partial x^4} + \rho\frac{\partial^2 u(x,t)}{\partial t^2} - D_S\frac{\partial^3 u(x,t)}{\partial x^2\partial t} = -\rho x\ddot{\theta} \tag{3.6}$$

where D_S is the resistance to strain velocity (rate of change of strain) and $D_S\frac{\partial^3 u(x,t)}{\partial x^2\partial t}$ is the resulting damping moment dissipated in the manipulator structure during its dynamic operation. The corresponding boundary conditions are given as in equation (3.5).

B. Finite difference-based modelling

Here, the FD method is used to solve the PDE in equation (3.6) numerically, and hence develop a simulation algorithm characterising the behaviour of the system. There are two steps in FD discretisation: dividing the structure into a set of equal-length sections and considering the deflection of end of each section (grid-point) over time. The derivation (Azad, 1994, Poerwanto, 1998) results in a set of difference equations which can be connected into a concise form of matrix representation as:

$$\mathbf{Y}_{i,j+1} = \mathbf{A}\mathbf{Y}_{i,j} + \mathbf{B}\mathbf{Y}_{i,j-1} + \mathbf{C}\mathbf{F} \tag{3.7}$$

where $\mathbf{Y}_{i,j+1}$ is the displacement of grid points $i = 1,2,\cdots,n$ of the manipulator at time step $j+1$, $\mathbf{Y}_{i,j}$ and $\mathbf{Y}_{i,j-1}$ are the corresponding displacements at time steps j and $j-1$ respectively. **A** and **B** are constant $n \times n$ matrices and **C** is a constant matrix related to the given input torque and **F** is an $n \times 1$ matrix related to the time step Δt and mass per unit length of the flexible manipulator;

$$\mathbf{Y}_{i,j+1} = \begin{bmatrix} y_{1,j+1} \\ y_{2,j+1} \\ \vdots \\ y_{n,j+1} \end{bmatrix}, \quad \mathbf{Y}_{i,j} = \begin{bmatrix} y_{1,j} \\ y_{2,j} \\ \vdots \\ y_{n,j} \end{bmatrix}, \quad \mathbf{Y}_{i,j\text{-}1} = \begin{bmatrix} y_{1,j\text{-}1} \\ y_{2,j\text{-}1} \\ \vdots \\ y_{n,j\text{-}1} \end{bmatrix} \tag{3.8}$$

$$\mathbf{A} = \begin{bmatrix} K_1 & K_2 & K_3 & 0 & 0 & \cdots & 0 & 0 \\ (b+d) & (a\text{-}2d) & (b+d) & \text{-}c & 0 & \cdots & 0 & 0 \\ \text{-}c & (b+d) & (a\text{-}2d) & (b+d) & \text{-}c & \cdots & 0 & 0 \\ \vdots & \ddots & \ddots & \ddots & \ddots & \ddots & \ddots & \vdots \\ 0 & 0 & \cdots & \text{-}c & b+d & a\text{-}2d & b+d & \text{-}c \\ 0 & 0 & \cdots & 0 & K_7 & K_8 & K_9 & K_{10} \\ 0 & 0 & \cdots & 0 & 0 & K_{14} & K_{15} & K_{16} \end{bmatrix} \tag{3.9}$$

$$\mathbf{B} = \begin{bmatrix} K_4 & K_5 & 0 & 0 & 0 & \cdots & 0 & 0 \\ -d & 2d-1 & -d & 0 & 0 & \cdots & 0 & 0 \\ 0 & -d & 2d-1 & -d & 0 & \cdots & 0 & 0 \\ \vdots & \ddots & \ddots & \ddots & \ddots & \ddots & \ddots & \vdots \\ 0 & 0 & \cdots & 0 & -d & 2d-1 & -d & 0 \\ 0 & 0 & \cdots & 0 & 0 & K_{11} & K_{12} & K_{13} \\ 0 & 0 & \cdots & 0 & 0 & 0 & 0 & K_{17} \end{bmatrix} \tag{3.10}$$

$$\mathbf{C} = \tau(j); \; \mathbf{F} = \begin{bmatrix} K_6 & 0 & \cdots & 0 \end{bmatrix}^T \tag{3.11}$$

where

$$a = 2 - \frac{6EI\Delta t^2}{\rho\Delta x^4} \; ; \; b = \frac{4EI\Delta t^2}{\rho\Delta x^4} \; ; \; c = \frac{EI\Delta t^2}{\rho\Delta x^4} \; ; \; d = \frac{D_S\Delta t}{\rho\Delta x^2}$$

$$K_1 = \frac{c\Delta t^2 EI + 2c\Delta x I_h + (a-2d)\Delta t^2 EI}{\Delta t^2 EI + c\Delta x I_h} \qquad K_4 = -\frac{c\Delta x I_h + (1-2d)\Delta t^2 EI}{\Delta t^2 EI + c\Delta x I_h}$$

$$K_2 = \frac{(b+d)\Delta t^2 EI}{\Delta t^2 EI + c\Delta x I_h} \qquad K_5 = -\frac{d\Delta t^2 EI}{\Delta t^2 EI + c\Delta x I_h}$$

$$K_3 = -\frac{c\Delta t^2 EI}{\Delta t^2 EI + c\Delta x I_h} \qquad K_6 = \frac{c\Delta x^2 \Delta t^2}{\Delta t^2 EI + c\Delta x I_h}$$

$$K_7 = -c \qquad K_{11} = -d$$

$$K_8 = (b+d) \qquad K_{12} = -(1-2d)$$

$$K_9 = (a+c-2d) \qquad K_{13} = -d$$

$$K_{10} = -(2c-b-d)$$

$$K_{14} = \frac{-2c\Delta t^2 EI}{\Delta t^2 EI + 2c\Delta x^3 M_P}$$

$$K_{15} = \frac{4c\Delta t^2 EI}{\Delta t^2 EI + 2c\Delta x^3 M_P}$$

$$K_{16} = \frac{\Delta t^2 EI}{\Delta t^2 EI + 2c\Delta x^3 M_P}\left\{a + 2b - 4c + \frac{4c\Delta x^3 M_P}{\Delta t^2 EI}\right\}$$

$$K_{17} = \frac{-\Delta t^2 EI}{\Delta t^2 EI + 2c\Delta x^3 M_P}\left\{\frac{2c\Delta x^3 M_P}{\Delta t^2 EI} + 1\right\}$$

Moreover, the dynamic equation of the manipulator can be simulated in a state-space form by referring to the matrix formulation as:

$$\begin{aligned} x(n+1) &= \mathbf{P}x(n) + \mathbf{Q}u \\ y(n) &= \mathbf{R}x(n) + \mathbf{S}u \end{aligned} \qquad (3.12)$$

where

$$\mathbf{P} = \left[\begin{array}{c|c} \mathbf{A} & \mathbf{B} \\ \hline I_{\mathrm{NxN}} & 0_{\mathrm{NxN}} \end{array}\right], \quad \mathbf{Q} = \left[\begin{array}{c} \mathbf{C} \\ \hline 0_{\mathrm{N\times1}} \end{array}\right], \quad \mathbf{R} = \begin{bmatrix} I_{\mathrm{N}} & 0_{\mathrm{N}} \end{bmatrix}, \quad \mathbf{S} = \begin{bmatrix} 0_{2\mathrm{N}} \end{bmatrix}$$

$$u = \begin{bmatrix} \tau & 0 & \cdots & 0 \end{bmatrix}^{\mathrm{T}}, \ y(n) = \begin{bmatrix} x(1,n) \cdots x(N,n)\ ,\ x(1,n-1) \cdots x(N,n-1) \end{bmatrix}$$

With N is the number of sections. Finally, the state space formulation can be implemented in the MATLAB/SIMULINK as depicted in Figure 3.7 (Azad, 1994; Poerwanto, 1998).

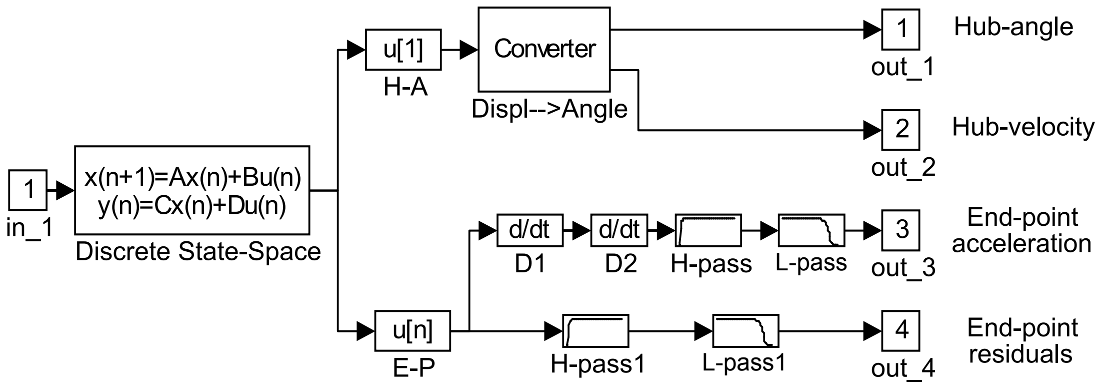

Figure 3.7: Simulation block diagram using SIMULINK with state-space formulation (Azad, 1994; Poerwanto, 1998)

This state-space formulation of dynamic motion representation has been widely used for control development purpose prior to real experimentation (Md Zain and Tokhi, 2009a; Md Zain et al., 2009c; Poerwanto, 1998; Tokhi and Azad, 1995; Tokhi et al., 1995; Tokhi et al., 1997).

3.3.3. Parametric modelling approaches

Parametric modelling is a linear system identification technique which formulates the model of the plant as a linear mathematical function that relates the input to output usually in form of partial differential/difference equation or transfer function. Various estimation methods have been used by researchers for example least mean square (LMS) and recursive least squares (RLS) (Md Zain et al., 2009a; Poerwanto, 1998; Shaheed and Tokhi, 2002), as well as intelligent optimisation techniques such as genetic algorithm (GA) (Md Zain, 2011; Md Zain et al., 2009a; Shaheed et al., 2001) and particle swarm optimisation (PSO) (Alam and Tokhi, 2007; Md zain 2011; Md Zain et al., 2009b) for modelling the single-link flexible manipulators.

3.3.4. Non-parametric modelling approaches

Non-parametric modelling is an attempt to represent plant with an input-output behavioural box, not as an explicit mathematical function. Literature shows that neural networks (NNs) have been proposed for modelling flexible manipulator systems. Talebi et al. (1998) used recurrent NN for modelling flexible manipulator for space application. Also, multilayer perceptron (MLP) NN with backpropagation learning algorithm and radial basis function (RBF) NN have been utilised for modelling single-link flexible manipulator (Shaheed and Tokhi, 2002).

3.4. Previous works on control of flexible manipulator systems

Generally, there are two control objectives for a flexible manipulator, i.e. to control the hub-angular displacement (input tracking) and to suppress vibration at the end point of the manipulator. Hub-angular displacement control is aimed to place the flexible arm in a desired position and vibration control is aimed to minimise the vibration arising during the movement.

Some works on hub-angular displacement control of single-link flexible manipulator have been proposed by researchers. A proportional-derivative (PD)-like control referred to as joint-based collocated (JBC), here cited as JBC PD control, has been used (Poerwanto, 1998). There are only two parameters to tune in JBC PD control, i.e. proportional gain in the feed-forward path of hub-angle reference input and derivative gain in hub-velocity feedback path. Proportional integral derivative (PID) control has also reported for hub-angular control of flexible manipulators (Md Zain and Tokhi, 2009a; Md Zain et al., 2009c), where the three parameters have been optimised using genetic algorithm (GA). Siddique and Tokhi (2006) proposed a hybrid control approach combining GA, neural network and fuzzy logic, referred to as GA-based neuro-fuzzy control system, for hub-angle control of single link flexible manipulator system. In the proposed controller, neural network was used for tuning both the inputs and output gains of fuzzy control. The weights, threshold value and activation function parameter of neural network were optimised using GA.

Sharma et al. (2003) proposed a modular neural network (MNN) for hub-angle control of single-link flexible manipulator control. In the MNN, three single neural networks were proposed to process three feedback signals: hub-angle, hub velocity and end-point acceleration. The outputs of the NNs were then combined to produce one control signal for the flexible manipulator system. GA was used to find optimal NN architecture, weights, threshold values and parameters of activation function.

Various techniques, in combination with hub-angular movement control, have been proposed to reduce vibration at the end-point of flexible arm. The JBC PD control has been proposed in combination with iterative learning control (ILC) where JBC PD control has been used for hub-angular control (Md Zain et al., 2005; Tokhi and Md Zain, 2006). In the proposed algorithm, the JBC PD control has been designed by using root locus technique and ILC were optimised by GA. The same control architecture but with input shaping optimised by GA has been proposed (Md Zain, 2006). Hybrid control strategies combining JBC PD, ILC, input shaping and PID have been proposed for flexible manipulator systems (Tokhi et al., 2004), where JBC PD has been used for hub-angle control while input shaping, ILC and PID with acceleration feedback has been used for vibration control. Parameters of JBC PD have been tuned using root locus technique. Mohamed et al. (2005) proposed a hybrid control structure combining JBC PD control, input shaping, and strain feedback where JBC PD control has been used for controlling the hub-angular movement while input shaping and strain feedback has been used for vibration suppression. The parameters of JBC PD controller have been deduced using root locus analysis.

Alam and Tokhi (2007) proposed a hybrid control structure combining fuzzy logic (FL) and command shaping (CS) where PD-like FL control was used for hub-angle control while CS has been used for vibration suppression. GA has been used to optimise both FL control and CS. Shaheed et al. (2005) proposed a hybrid control structure comprising adaptive JBC control and adaptive neuro-inverse-dynamic active vibration control, where adaptive JBC control was applied to control hub-angular movement and adaptive neuro-inverse-dynamic active vibration control was used for vibration suppression.

The application of BFA in the modelling and control of a single-link flexible manipulator systems have not been reported yet. A hybrid BFA and particle swarm optimisation (PSO), however, has been used for optimising a hybrid fuzzy pre-compensated PD controller in trajectory control of a two-link rigid flexible manipulator (Alavandar et al., 2010). More complete previous work on modelling and control of flexible manipulator can be found in Tokhi and Azad (2008).

3.5. Preliminary motion dynamics experiment

In this section, a preliminary experimentation is carried out to determine the dynamic response characteristics of the system. A random signal with maximum amplitude $\pm$ 0.3 Nm is applied as torque input to excite the flexible manipulator system. The sampling time used is 0.001 seconds. This sampling time will cover the system dynamics over a frequency range up to 500 Hz. The single-link flexible manipulator is a single-input multiple-output (SIMO) system with the input as a torque applied at the hub and the three outputs are measured from the three sensors of flexible manipulator: hub-angle, hub velocity and end-point acceleration.

Experimental results are depicted in Figure 3.8. There are 6400 data samples in total for a random input and each of the three outputs. The experimental hub-angle response depicted in Figure 3.8(b) shows that, because there is no control action, the flexible manipulator does not follow the random signal input and the output increases with very small oscillation. The variation in gradient of hub-angle response is evident in the hub-angle velocity, widely cited as hub-velocity for short, response depicted in Figure 3.8(c) with very small amplitude oscillatory signal. The time-domain end-point acceleration is depicted in Figure 3.8(d). From the spectral density of end-point acceleration depicted in Figure 3.8(e) it can be noted that frequencies of the first three resonance modes of the system were at 11.67 Hz, 36.96 Hz and 64.22 Hz for the 1st , 2nd , and 3rd mode respectively.

3.6. Summary

The technical specifications of flexible manipulator considered in the research have been described. Also previous works on modelling and control of flexible manipulator have been outlined so that they can be used as a guide for future work. Preliminary experiment has been performed to determine dynamics characteristics of the system and highlight its main dynamic features. The data collected from the experiment will be used in subsequent chapters to model the system using BFAs.

The development of bacterial foraging algorithm with adaptable chemotactic step size and its test using seven benchmark functions will be presented in Chapter 4.

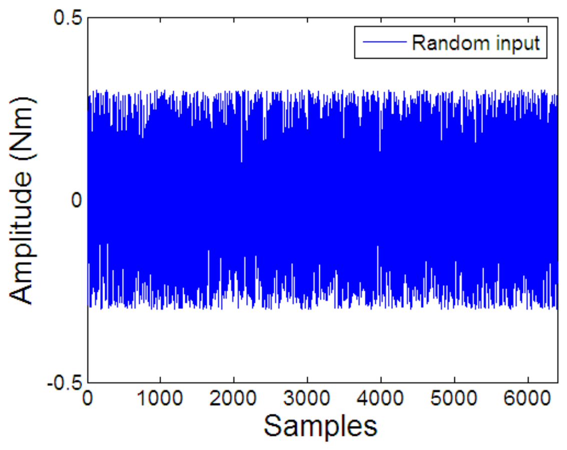

(a) Random torque input

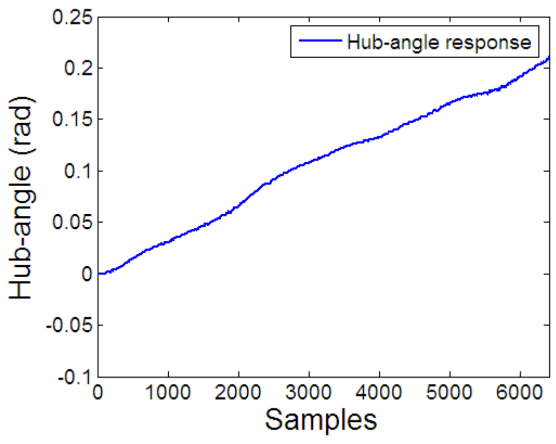

(b) Time-domain hub-angle

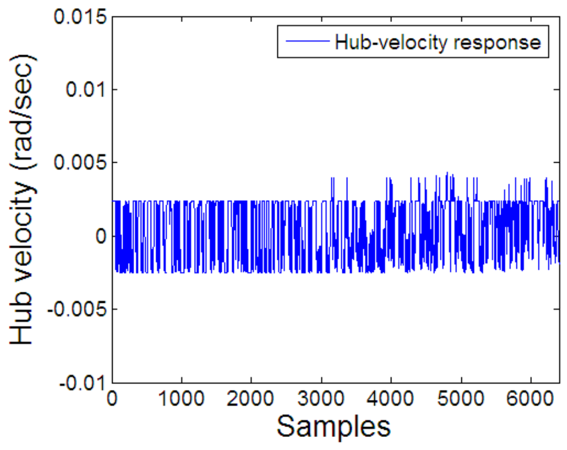

(c) Time-domain hub velocity

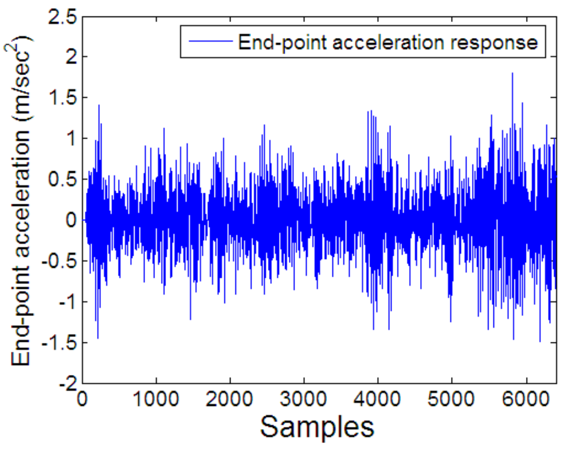

(d) Time-domain end-point acceleration

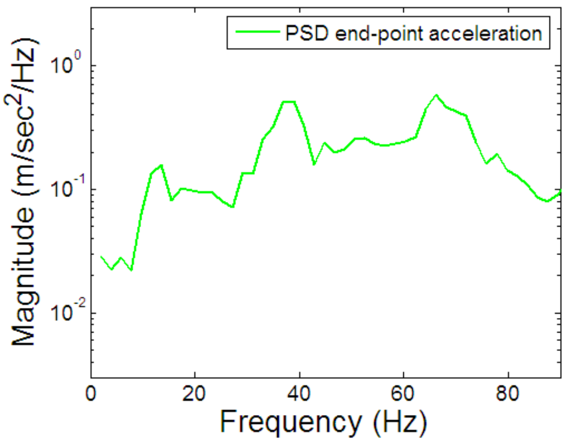

(e) Spectral density of end-point acceleration

Figure 3.8: Experimental results of flexible manipulator

CHAPTER 4
BACTERIAL FORAGING ALGORITHM WITH ADAPTABLE CHEMOTACTIC STEP SIZE

4.1. Introduction

With SBFA (Passino, 2002), bacteria use random walk with a fixed value during the whole computational process regardless of the nutrient value to find locations with high nutrient level. The chemotactic step size can be made adaptive, i.e. the chemotactic step size changes to follow some conditions. The objective of the work in this chapter is to investigate the adaptation schemes in the BFA so that the chemotactic step size may change depending on the nutrient value. Four approaches, namely using linear function, quadratic function, exponential function and fuzzy logic (FL) are presented. In the full BFA algorithm, the four proposed approaches will be used as the new chemotactic step size instead of a constant value. In order to validate their effectiveness, the proposed adaptation mechanisms are tested to find global optimum point of several well-known benchmark functions, commonly used in testing of new optimisation algorithms. The performances of BFA with adaptable chemotactic step size are then assessed in comparison to that of SBFA. The comparison is made based on the convergence and optimum nutrient value (accuracy) achieved.

4.2. Adaptation mechanism of chemotactic step size

The works reported in the literature show that with adaptable chemotactic step size, BFA is able to converge faster. Suppose SBFA is used to find optimum value of the nutrient value (cost function) depicted in Figure 4.1 subject to minimisation, and the initial position of bacterium is at the peak of cost function (P_1). The bacterium will move down the hill heading for the minimum of cost function (point P_n) constantly according to the determined chemotactic step size. The bigger step size the faster the bacterium will move down the hill. However, a mathematical analysis of the chemotactic step in standard BFA based on classical gradient descent search approach in (Dasgupta et al., 2009) suggests that chemotaxis employed by standard BFA usually results in sustained oscillation when close to the global minimum especially on flat landscape nutrient media. In order to damp the oscillation, very small chemotactic step size is needed around the global optimum. Thus large step size will lead to the bacterium oscillating around the optimum point and probably miss the minimum value. Small step size will ensure the bacterium to find the minimum value but will require large number of iterations to find the minimum point from. Empirical simulation results discussed in Chapter 2 confirm these phenomena.

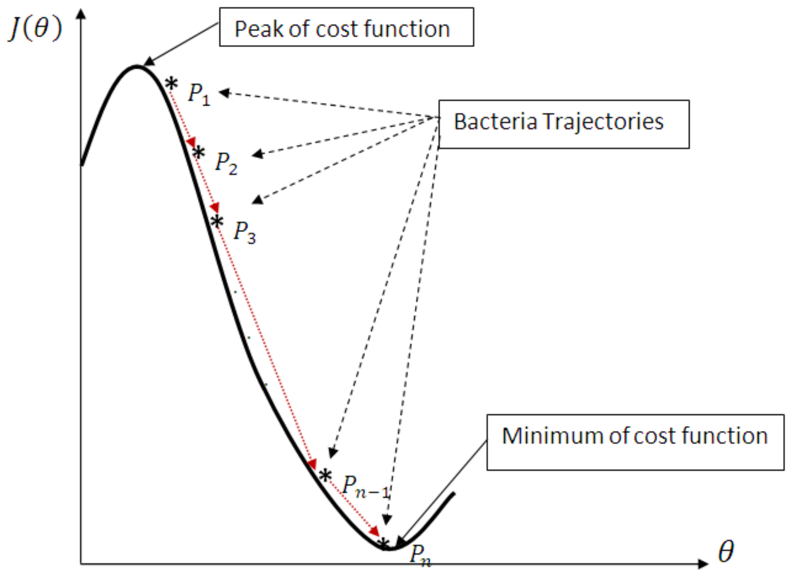

Figure 4.1: Bacteria trajectories in finding minimum value of cost function from peak initial position, where θ is the bacterium's position and $J(\theta)$ is the corresponding nutrient value

A strategy to overcome this problem is to apply large step size when the cost function value is large so that the bacterium moves down the hill faster and then apply very small step size when the bacterium is near the optimum point to ensure the bacterium is able to find the optimum point. Thus the chemotactic step size can be made adaptive, i.e. the value of chemotactic step size changed based on the nutrient value; if the nutrient value is high then the step size is large and if the nutrient value is low then the step size is small. By applying this mechanism, the adaptive BFA (ABFA) will be faster in convergence and will also be able to find the global optimum.

In this work, investigations are carried out to make the chemotactic step size adaptable by incorporating nutrient value of every bacterium into four mechanisms: using three functions namely linear, quadratic, and exponential and using a FL approach. The four approaches are adopted because of their simplicity so that the computational complexity of the algorithm is not increased. The basic assumption used in the ABFA development in this work is that the global minimum solution of the nutrient media has to be non-negative. By using this assumption, when the nutrient value is high it means the bacteria are still far away from the global minimum position so that large step size is needed to approach the global minimum faster and when the nutrient value is low it means the bacteria are close to the global minimum value thus small step size is needed so that bacteria will not miss the global minimum point.

4.2.1. Linearly adaptive bacterial foraging algorithm

The first adaptation mechanism proposed in this work is referred to as linearly ABFA (LABFA), where a linear function of nutrient value of every bacterium is used for updating the chemotactic step size. The use of simple linear function for updating chemotactic step size of BFA has been previously reported (Majhi et al., 2009; Pandi et al., 2009; Dasgupta et al., 2009). The disadvantage of the adaptation is that the maximum chemotactic step size of unity is likely to be too big for some of optimisation tasks with global minimum point equal to zero.

In order to make the maximum chemotactic step size more flexible according to the nature of optimisation task, in this work a tuneable maximum step size is introduced instead of unity. Moreover, in order to control of changes in the chemotactic step size, tuneable scaling factor for absolute nutrient value is introduced here. Thus changes in the chemotactic step size depend on the two tuneable factors. By using this strategy, changes in the chemotactic step size can be made steeper so that to lead to faster convergence. This results in a new linear adaptation scheme with flexibility in the optimisation task according to the nature of the problem. The new linear adaptive chemotactic step size is, thus, formulated as follows:

$$C_{al}(i) = \frac{c_{max}}{1+\frac{b}{d|J(i)|}} \tag{4.1}$$

where, $C_{al}(i)$ is linearly adaptive chemotactic step size for every bacterium, c_{max} is tuneable maximum chemotactic step size, b is tuneable positive factor, d is tuneable positive scaling factor and $|J(i)|$ is absolute of cost function of every bacterium. Larger $|J(i)|$ will result in smaller $\frac{b}{d|J(i)|}$, and this in turn, with determined c_{max}, will produce larger $C_{al}(i)$ and vice versa. The scaling factor d is used to scale $|J(i)|$ so that $C_{al}(i)$ is not very big. This strategy is very useful in the application where the maximum nutrient value is very big. Using such a formulation, the chemotactic step size will change in the range [0, c_{max}] linearly depending on the nutrient (cost function) value as:

- If $J(i)$ is big then the term $\frac{b}{d|J(i)|}$ of equation (4.1) will approach zero, and this will lead to $C_{al}(i)$ to approach c_{max}
- If $J(i)$ is small and approaching zero then the term $\frac{b}{d|J(i)|}$ of equation (4.1) will become a very large value (infinity), and this will lead to $C_{al}(i)$ to approach zero

4.2.2. Quadratic adaptive bacterial foraging algorithm

The adaptation mechanism formulated in equation (4.1) can be accelerated by introducing a mechanism that boosts $|J(i)|$ value using a quadratic function. The quadratic ABFA (QABFA) uses quadratic function of nutrient value of every bacterium for updating the chemotactic step size. The chemotactic step size is thus formulated as follows:

$$C_{aq}(i) = \frac{c_{max}}{1+\frac{b}{d\left((gJ(i))^2+|gJ(i)|\right)}} \tag{4.2}$$

where $C_{aq}(i)$ is quadratic adaptive step size for every bacterium, g is tuneable scaling factor, and $J(i)$ is the nutrient value for every bacterium. The quadratic function of $|J(i)|$ will result in extremely big denominator value $\frac{b}{d\left((gJ(i))^2+|gJ(i)|\right)}$, and this in turn, will make this function approach zero and thus $C_{aq}(i)$ to approach C_{max}. By using this formula, QABFA will be able to converge to the optimum point faster than LABFA because it has bigger chemotactic step size for the same $|J(i)|$ value. In order to prevent $C_{aq}(i)$ being too big, the scaling factors d and g are introduced. These factors will helpful to maintain the chemotactic step size very large when the nutrient value is large but very small when the nutrient value is small so that bacteria will be able to head to the global optimum without oscillation. In this case, the chemotactic step size will change in a quadratic manner in the range of [0, c_{max}], depending on the nutrient value.

4.2.3. Exponentially adaptive bacterial foraging algorithm

The adaptation mechanism formulated in equation (4.1) can also be further accelerated by applying exponential function of the nutrient media. The use of exponential function of nutrient media will result in larger chemotactic step size for the same nutrient media than LABFA and QABFA. The exponentially ABFA (EABFA) uses an exponential function for updating the chemotactic step size, as follows:

$$C_{ae}(i) = \frac{c_{max}}{1+\frac{b}{de^{(g|J(i)|)}}} \tag{4.3}$$

where $C_{ae}(i)$ is exponentially adaptive step size for every bacterium. Similar to LABFA and QABFA, larger $|J(i)|$ will make the value of $de^{(g|J(i)|)}$ become very large and as a result the value of $\frac{b}{de^{(g|J(i)|)}}$ will become very small or approach zero, and this in turn will make $C_{ae}(i)$ to approach c_{max}. On the contrary, if $|J(i)|$ is very small or close to zero the value of $de^{g|J(i)|}$ will be very small, leading to the value of $\frac{b}{de^{(g|J(i)|)}}$ becoming very big, and this in turn will lead to $C_{ae}(i)$ to become very small or approach zero. The positive scaling factor g will ensure the value $e^{(g|J(i)|)}$ not be too large when $|J(i)|$ is very large and the positive scaling factor d will make $\frac{b}{de^{(g|J(i)|)}}$ to become very small or to approach zero to ensure bacteria achieve nearest positions to the global optimum point and do not oscillate. As a result, the chemotactic step size will change exponentially according to nutrient value in the range [0, c_{max}].

4.2.4. Chemotactic step size adaptation using fuzzy logic

In this section a further approach for chemotactic step size adaptation is presented using fuzzy logic (FL). As referred to in the literature review presented in Chapter 2, Mishra (2005) proposed the use of a Sugeno type FL with four trapezoidal membership functions for adaptation scheme of chemotactic step size, where minimum of the nutrient media was used as the input of the FL and the output of FL as a minimum of nutrient value times a constant related to the membership function. Because the new chemotactic step size only depends on the minimum value of nutrient media, all bacteria will use the same chemotactic step size regardless their own nutrient value. The resulted chemotactic step size is suitable only for bacteria which have smallest nutrient value at every step but not for other bacteria because it will be too small for bacteria which lie in the positions that have big nutrient value (still far away from the nutrient media). The probability of such negative impact is that most bacteria will not search wide area of the nutrient media and even may get trapped in local minima for complex nutrient media. This disadvantage can be solved by making the chemotactic step size of every bacterium dependent on its own nutrient value. Also instead of using trapezoidal membership function, here

Gaussian membership function is used because it is able to represent uncertainty in measurements most adequately (Kreinovich et al., 1992).

The FL concept was first introduced by Lotfi Zadeh to model human reasoning from imprecise and incomplete information by giving definitions to vague terms and allowing construction of rule base (Zadeh, 1965, 1968, 1973). The FL will map from input to output by using human-like reasoning in the form of rule base. The general FL model construction is depicted in Figure 4.2.

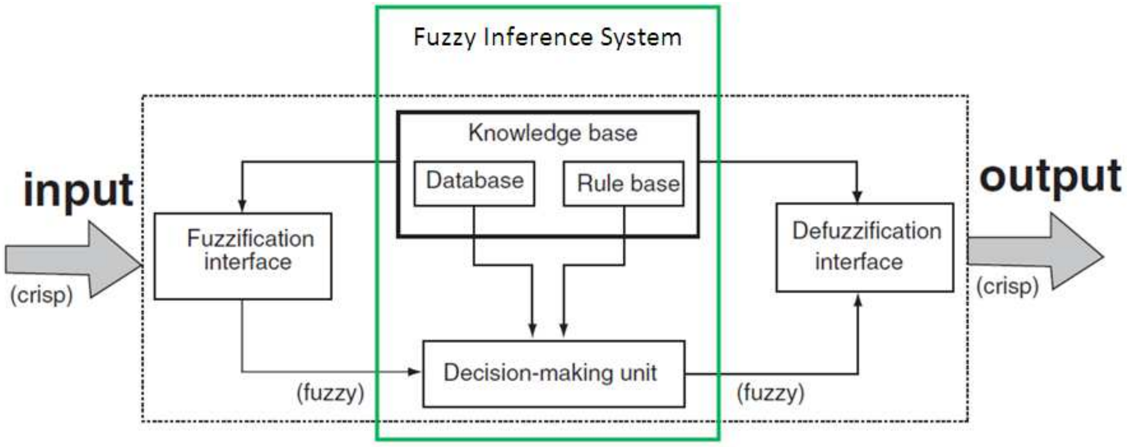

Figure 4.2: Overall construction of fuzzy logic model (picture adopted from Sivanandam et al. (2007) and then modified)

The input of the FL model is crisp value. This is then converted into fuzzy linguistic variable through the process of fuzzification. The result is set into the fuzzy inference system (FIS) which inaugurates the decision making unit with the rule base and associated database. The outcome of the FIS is transformed to crisp values through the defuzzification process. For further details of fundamentals of fuzzy logic see (Jang et al., 1997; Sivanandam et al. 2007; Zadeh, 1965, 1968, 1973).

Because of its advantages such as intuitive, widespread acceptance and well suited to human input (Sivanandam et al., 2007), Mamdani fuzzy model (Mamdani and Assilian, 1974) with centre of area (COA) defuzzification method is used throughout this work. Initially, Sugeno fuzzy model (Takagi and Sugeno, 1985; Sugeno and Kang, 1988) was also considered and used. However Mamdani fuzzy model was able to produce better results than Sugeno fuzzy model. Thus, FL construction for adaptable chemotactic step size, depicted in Figure 4.3, with one-input one-output fuzzy model was considered as follows: the input of FL is the absolute of nutrient media value of every bacterium

($|J(i)|$) and its output is the fuzzy adaptable chemotactic step size of every bacterium ($C_{af}(i)$).

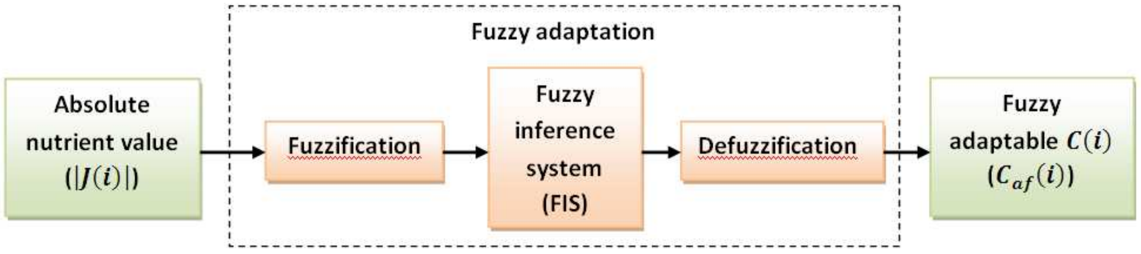
Fuzzy adaptation
Absolute nutrient value ($|J(i)|$)
Fuzzification
Fuzzy inference system (FIS)
Defuzzification
Fuzzy adaptable $C(i)$ ($C_{af}(i)$)

Figure 4.3: FL-based adaptable chemotactic step size construction

To ensure the chemotactic step size will be very big when the cost function value is large and will be very small or approaching zero when the cost function value is very small or approaching zero, seven membership functions are applied both for input and output. Four and five membership functions were also considered, however seven membership functions gave better results. Gaussian membership function, which is formulated in equation (4.4), was chosen for the chemotactic step size to change smoothly. Moreover, uncertainty in measurements can be represented most adequately with Gaussian membership function (Kreinovich et al., 1992). The fuzzy input with seven Gaussian membership functions is depicted in Figure 4.4.

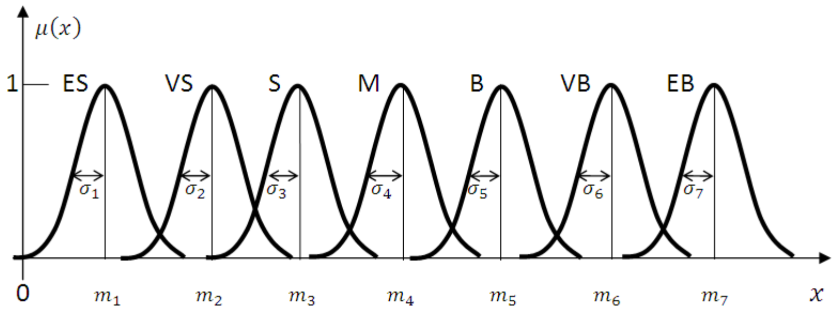

Figure 4.4: Fuzzy input with seven Gaussian membership functions: ES is extremely small, VS is very small, S is small, M is medium, B is big, VB is very big and EB is extremely big

$$\mu(x) = exp\left(-\frac{1}{2}\left(\frac{x-m}{\sigma}\right)^2\right) \tag{4.4}$$

Both the two Gaussian memberships parameters (means $m_1, \dots, m_7$ and standard deviations $\sigma_1, \dots, \sigma_7$) for input and output were chosen by trial and error. The FL produces output from the input by using human-like reasoning in the form of fuzzy rules which are constructed from a set of IF-THEN operations. Parameters which can be changed to get optimal FL construction are fuzzy rules and the weight of every fuzzy rule output (usually between zero and one). The weight value determines the strength of the output of related fuzzy rule: when the weight is zero it means the output of the fuzzy rule is zero and when the output is one it means the output of fuzzy rule is in full scale. The FL-based adaptable chemotactic step size can be formulated as:

$$C_{af}(i) = \mathcal{F}(|J(i)|) \tag{4.5}$$

where $C_{af}(i)$ is the fuzzy adaptable chemotactic step size for every bacterium and $\mathcal{F}(\cdot)$ is a FL structure mapping from cost function value as an input to step size as an output. In the FL structure, the universe of discourse of Gaussian membership functions of input and output are chosen adequately so that to cover the range of both input and output. The general form of fuzzy rule for adaptation can be formulated as:

$$\text{IF } |J(i)| \text{ is } A \text{ THEN } C_{af}(i) \text{ is } B \quad (weight) \tag{4.6}$$

So that the output level of consequence part is B scaled by $weight$. Thus by using this strategy if $|J(i)|$ is very big then $C_{af}(i)$ is very big and if $|J(i)|$ is very small then $C_{af}(i)$ is very small or approaching zero so that bacteria would be able to approach the global optimum point without oscillation.

Because there is only one to one relation from input ($|J(i)|$) and output ($C_{af}(i)$) of FL structure, for seven Gaussian membership function of fuzzy input and output, there will be seven fuzzy rules. The correlation between $|J(i)|$ and $C_{af}(i)$ is dependent on the fuzzy rules and their corresponding weights. So that users have freedom to define the chemotactic step size in accordance with the nature of cost function of optimisation problem, to find better accuracy without oscillation around global optimum point.

With those adaptable formulated in equation (4.1) – equation (4.3) and equation (4.5) above, the movement of bacteria from one position to another position can be formulated in equation (1) can now be formulated as:

$$\theta(i, j+1, k, l) = \theta(i, j, k, l) + C_a(i)\phi(j) \tag{4.7}$$

where $C_a(i)$ is $C_{al}(i), C_{aq}(i), C_{ae}(i)$ and $C_{af}(i)$ for LABFA, QABFA, EABFA and FABFA respectively.

4.3. Computation steps of ABFAs

The major computation steps of ABFAs are exactly the same as computation of SBFA (Passino, 2002) discussed in Chapter 2. The difference in the ABFAs is that the chemotactic step sizes of bacteria are adaptable types $C_{al}(i), C_{aq}(i), C_{ae}(i)$ and $C_{af}(i)$ as formulated in equations (4.1)-equation (4.3) and equation (4.5) for LABFA, QABFA, EABFA and FABFA respectively. The detailed computation steps of ABFAs that model bacterial population chemotaxis, swarming, reproduction, elimination, and dispersal (initially, $j = k = l = 0$) in finding the optimum value of nutrient media can be seen in the algorithm below (note that updates to the θ^i automatically result in updates to P) (Passino, 2002):

1. Elimination-dispersal loop: for $l = 1,2, \dots, N_{ed}$, do $l = l + 1$
2. Reproduction loop: for $k = 1,2, \dots, N_{re}$, do $k = k + 1$
3. Chemotaxis loop: for $j = 1,2, \dots, N_c$, do $j = j + 1$
    a. For $i = 1,2,3, \dots, S$, take a chemotactic step for bacterium i:
    b. Compute the nutrient value of every bacterium ($J(i,j,k,l)$). Calculate $J(i,j,k,l) = J(i,j,k,l) + J_{cc}\left(\theta^i(j,k,l), P(j,k,l)\right)$. If there is no swarming effect then $J_{cc}\left(\theta^i(j,k,l), P(j,k,l)\right) = 0$.
    c. Put $J_{last} = J(i,j,k,l)$ to save this value since a better cost via a run may be found.
    d. Tumble: Generate a random vector $\Delta(i) \in \Re^p$ with each element $\Delta_m(i), m = 1,2, \dots, p$, a random number on $[-1.1]$.
    e. Move: Compute

    $$\theta^i(j+1,k,l) = \theta^i(j,k,l) + C_a(i)\frac{\Delta(i)}{\sqrt{\Delta^T(i)\Delta(i)}}$$

    This results in a step of size $C_a(i)$ in the direction of the tumble for bacterium i. In this work $C_a(i)$ is equal to constant value for SBFA and are equal to the proposed adaptable chemotactic step size: $C_{al}(i), C_{aq}(i), C_{ae}(i)$ and $C_{af}(i)$ for LABFA, QABFA, EABFA and FABFA respectively.
    f. Compute the nutrient value of every bacterium ($J(i,j+1,k,l)$). Calculate $J(i,j+1,k,l) = J(i,j+1,k,l) + J_{cc}\left(\theta^i(j+1,k,l), P(j+1,k,l)\right)$. If there is no swarming effect then $J_{cc}\left(\theta^i(j+1,k,l), P(j+1,k,l)\right) = 0$.
    g. Swim:
        i. Put $m = 0$ (counter for swim length)
        ii. While $m < N_S$ (if have not climbed down too long)
            - Count $m = m + 1$
            - If $J(i,j+1,k,l) < J_{last}$ (if doing better), then $J_{last} = J(i,j+1,k,l)$ and calculate

            $$\theta^i(j+1,k,l) = \theta^i(j+1,k,l) + C_a(i)\frac{\Delta(i)}{\sqrt{\Delta^T(i)\Delta(i)}}$$

            This results in a step of size $C_a(i)$ in the direction of the tumble for bacterium i. In this work $C_a(i)$ is equal to constant value for SBFA and is equal to the proposed adaptable chemotactic step size: $C_{al}(i), C_{aq}(i), C_{ae}(i)$ and $C_{af}(i)$ for LABFA, QABFA, EABFA and FABFA respectively. Use this $\theta^i(j+1,k,l)$ to compute the new $J(i,j+1,k,l)$ as in sub step f above.
            - Else, $m = N_s$ (the end of the while statement).
    h. Go to next bacterium $(i+1)$ if $i \neq S$ (i.e., go to sub step b above) to process the next bacterium.
4. If $j < N_c$, go to step 3.
5. Reproduction:

a. For the given k and l, and for each $i = 1,2,3,\dots,S$, let

$$J_{health}^{i} = \sum_{j=1}^{N_c+1} J(i,j,k,l)$$

be the health of bacterium i. Sort bacteria and chemotactic parameters $C_a(i)$ in order of ascending cost J_{health} (higher cost means lower health).

b. The S_r bacteria with the highest J_{health} values die and the other S_r bacteria with the best values split (and the copies that are made are placed at the same location as their parent).

6. If $k < N_{re}$, go to step 2.
7. Elimination-dispersal: for $i = 1,2,3,\dots,S$, eliminate and disperse each bacterium which has probability value less than p_{ed}. If one bacterium is eliminated then it is dispersed to random location of nutrient media. This mechanism makes computation simple and keeps the number of bacteria in the population constant.

```
for $m = 1:S$
    if $p_{ed>rand}$ (Generate random number for each bacterium and if the generated random
    number is smaller than $p_{ed}$ then eliminate/disperse the bacterium)
        Generate new random positions for bacteria
    else
        Bacteria keep their current position (bacteria are not dispersed)
    end
end
```

8. If $l < N_{ed}$, then go to step 1; otherwise end.

The relation between nutrient value of every bacterium $J(i)$ and adaptable chemotactic step size $C_a(i)$, where $C_a(i)$ is $C_{al}(i), C_{aq}(i), C_{ae}(i)$ and $C_{af}(i)$ for LABFA, QABFA, EABFA and FABFA respectively, is illustrated in Figure 4.5. The figure illustrates that the height of chemotactic step size is up and down regarding the nutrient value according to adaptation mechanism formulated in equations (4.1)-equation (4.3) and equation (4.5).

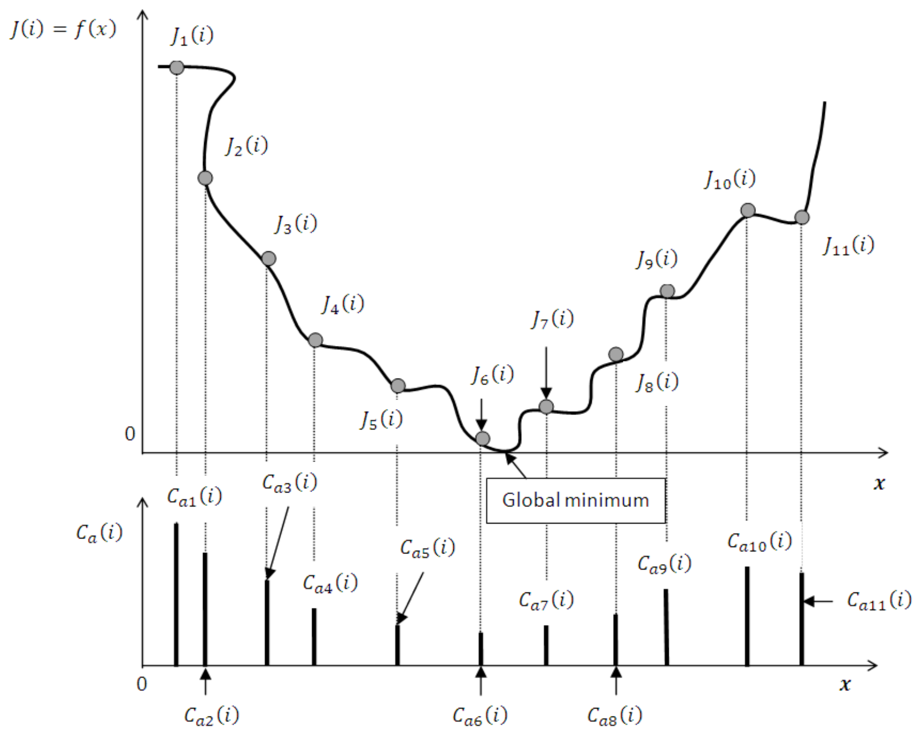

Figure 4.5 Illustration of the relationship between the nutrient value $J(i)$ and the adaptable chemotactic step size $C_a(i)$

4.4. Results and discussions

In order to evaluate and assess their performances, the developed ABFAs are tested with seven well-known benchmark test functions commonly used in the evaluation of new optimization algorithms. Thus, the seven benchmark test functions become nutrient media in which bacteria will find locations with the highest nutrient value. Since the global optimum point of benchmark functions is equal to zero, the location which has the highest nutrient value is thus equal to zero. Those benchmark functions have different characteristics allowing the ABFAs to be evaluated over a range of different characteristics. The following protocol is followed in the simulations:

1. Various chemotactic step size values and settings of SBFA, LABFA, QABFA, EABFA and FABFA are considered with each bench mark function. All algorithms use the same general parameters which are selected so that bacteria have enough chemotaxis steps towards the global minimum point, enough reproduction steps so that the bacteria can refine the best nutrient value and enough elimination and dispersal events and probability threshold so that bacteria can search almost the whole nutrient media without too much computation complexity. Bacteria will try to find the global optimum point from their initial

positions until their lifetime finish. For all algorithms, as mentioned in Chapter 2, the life time of bacteria is determined by the total number of steps they have, which is calculated as $N_c \times N_{re} \times N_{ed}$.

2. Using the step size values and the settings which resulted in the best nutrient value, for every benchmark function, 50 independent runs for each the five algorithms, i.e. SBFA, LABFA, QABFA, EABFA and FABFA are performed. The optimum nutrient values of each algorithm for all the 50 runs are recorded and then compared with each other for: the best, mean and standard deviation of optimum nutrient value. The mean and standard deviation of optimum nutrient value are defined as:

$$\bar{J} = \frac{\sum_{k=1}^{N} J(k)}{N} \tag{4.8}$$

$$\sigma_J = \sqrt{\frac{\sum_{k=1}^{N} \left(J(k)\right)^2}{N} - (\bar{J})^2} \tag{4.9}$$

where: $\bar{J}$ is the mean of optimum nutrient value J, N is the total number of runs and σ_J is the standard deviation of J. The best optimum nutrient value shows the closest position that can be achieved by the algorithm and the mean optimum nutrient value, gives information on mean nutrient value that can be achieved by the algorithm. The standard deviation is measured as variation of the data from its mean. Small standard deviation means that the data point is close to the mean and high standard deviation shows that the data point is spread over a large range.

3. The convergence of the run which results the best optimum nutrient value for each algorithm is recorded and compared. The comparison is made by counting how many steps are needed by the algorithm to achieve nearest location to the global minimum point. The convergence is plotted in one dimension graph with the x-axis representing the steps and the y-axis representing the minimum nutrient value achieved by bacteria in every step. Also the oscillation phenomenon of bacteria around the global minimum point is studied.

4.4.1. Test function 1: Rosenbrock function

The well known classical Rosenbrock function is formulated as:

$$J(x) = \sum_{i=1}^{n}(100 \times (x_{i+1} - x_i^2)^2 + (1 - x_i)^2) \tag{4.10}$$

In the tests the variables $x_i = x_{i+1}$ are in the range of $[-2.048, 2.048]$. The 3D and 2D views of the two-variable Rosenbrock function are depicted in Figure 4.6.

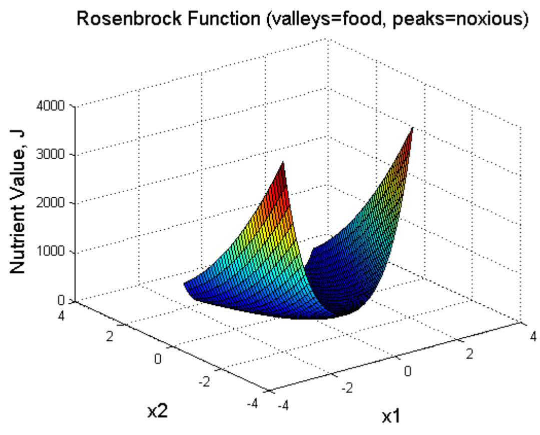

(a) 3D view

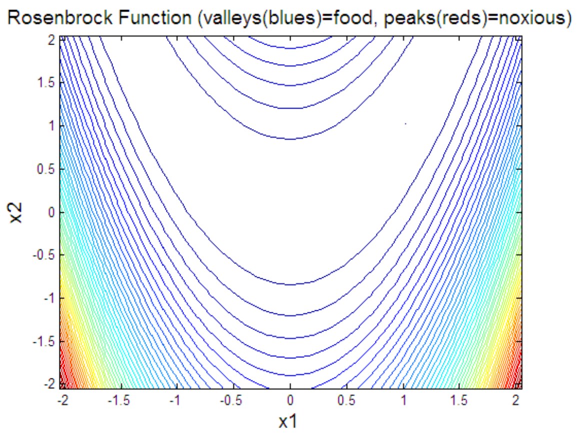

(b) 2D view

Figure 4.6: Two-variable Rosenbrock function

It is noted that the global minimum of the Rosenbrock function lies inside a long-narrow-parabolic shaped valley. In this investigation, the Rosenbrock function is simulated for 2 dimensions. The global minimum point is $J(x)$ equal to zero when variable $x_i = x_{i+1} = 1$. In these tests, the following parameter values were used with all the algorithms:

❖ $p = 2$	❖ $N_c = 40$	❖ $N_{re} = 4$	❖ $N_{ed} = 3$
❖ $S = 10$	❖ $N_s = 4$	❖ $S_r = {}^{S}/_{2}$	❖ $p_{ed} = 0.25$

The initial positions of bacteria were selected randomly across the nutrient media. Various chemotactic step size values were selected by trial and error and applied for SBFA, and the best optimum nutrient value was achieved when the step size was equal to 0.0075. For LABFA, QABFA and EABFA, all parameters settings, i.e. c_{max}, b, d and g were chosen by trial and error. The chemotactic step sizes for LABFA, QABFA and EABFA were formulated as:

$$C_{al}(i) = \frac{0.1}{1+\frac{10}{|J(i)|}} \tag{4.11}$$

$$C_{aq}(i) = \frac{0.1}{1+\frac{100}{(J(i))^2+|J(i)|}} \tag{4.12}$$

$$C_{ae}(i) = \frac{0.1}{1+\frac{21}{e^{(|J(i)|)}}} \tag{4.13}$$

For FABFA, the fuzzy membership function parameters, i.e. universe of discourse, m and σ were selected heuristically. The fuzzy membership functions of input and output are depicted in Figure 4.7(a) and 4.7(b) respectively. The fuzzy surface for FABFA shown in Figure 4.7(c) was obtained using the fuzzy rules formulated as follows:

$$\begin{array}{lll} R_1 & : & \text{IF } |J(i)| \text{ is ES THEN } C_{af}(i) \text{ is ES} \quad (1) \\ R_2 & : & \text{IF } |J(i)| \text{ is VS THEN } C_{af}(i) \text{ is S} \quad (1) \\ R_3 & : & \text{IF } |J(i)| \text{ is S THEN } C_{af}(i) \text{ is M} \quad (1) \\ R_4 & : & \text{IF } |J(i)| \text{ is M THEN } C_{af}(i) \text{ is B} \quad (1) \\ R_5 & : & \text{IF } |J(i)| \text{ is B THEN } C_{af}(i) \text{ is EB} \quad (1) \\ R_6 & : & \text{IF } |J(i)| \text{ is VB THEN } C_{af}(i) \text{ is EB} \quad (1) \\ R_7 & : & \text{IF } |J(i)| \text{ is EB THEN } C_{af}(i) \text{ is EB} \quad (1) \end{array} \tag{4.14}$$

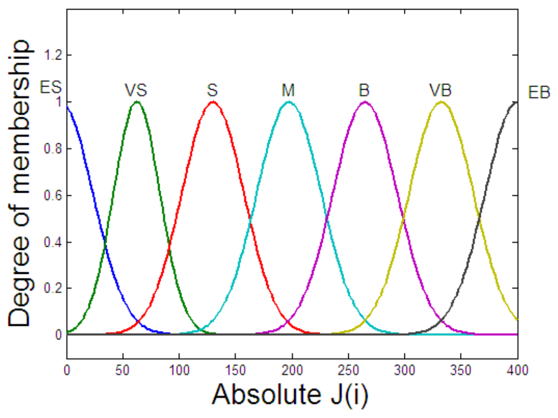

(a) Input: $|J(i)|$

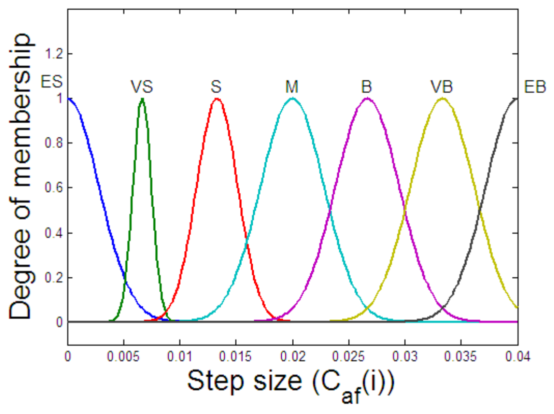

(b) Output $C_{af}(i)$

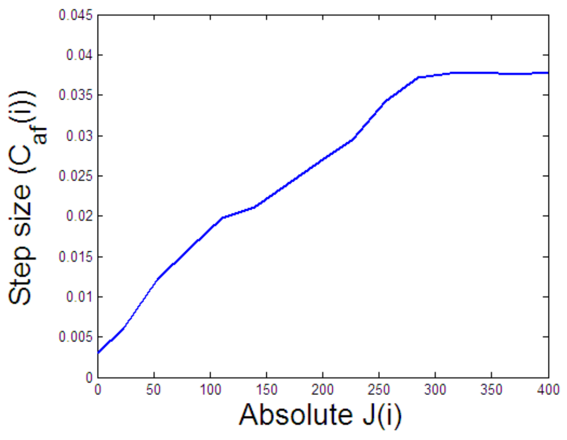

(c) Fuzzy surface

Figure 4.7: Fuzzy membership functions and surface of FABFA for Rosenbrock test function

The numerical results shown in Table 4.1 demonstrate that, using adaptable chemotactic step size, all the four proposed algorithms outperformed the SBFA in reaching the optimum nutrient value, and FABFA achieved the lowest nutrient value, i.e. 1.2154×10^{-6} among them. Also, FABFA achieved the best mean and standard deviation of optimum nutrient value J. Since all BFAs used the same general parameters, the difference of nutrient value achieved is mainly caused by the chemotactic step size.

Table 4.1: Numerical results of simulation with Rosenbrock test function (2 dimensions)

Algorithm	**Best optimum J**	$\bar{J}$	σ_J	$C(i)$ **range**	**Convergence (steps)**
SBFA	224.8601×10^{-6}	0.6420	2.0633	0.0075	54
LABFA	9.7765×10^{-6}	0.0151	0.0149	$[2.1433 \times 10^{-7}, 0.1]$	9
QABFA	50.1061×10^{-6}	0.1059	0.1591	$[1.1202 \times 10^{-6}, 0.1]$	10
EABFA	5.0282×10^{-6}	0.0162	0.0423	[0.0046, 0.1]	**7**
FABFA	$\mathbf{1.2154 \times 10^{-6}}$	$\mathbf{6.4053 \times 10^{-5}}$	$\mathbf{1.0223 \times 10^{-4}}$	[0.0025, 0.037]	26

The convergence plots in Figure 4.8(a) show that all the four proposed algorithms were faster in convergence, since they reached the optimum point using 9, 10, 7 and 26 steps for LABFA, QABFA, EABFA and FABFA respectively, whereas SBFA used 54 steps of SBFA. Since the initial positions of bacteria were selected randomly in the nutrient media, the nutrient value of each algorithm in the first step was different and the bacteria with EABFA fell in locations near the global minimum point while bacteria with QABFA fell far away from the global minimum. A comparative view of the best optimum nutrient value achieved by the algorithms is depicted in Figure 4.8(b).

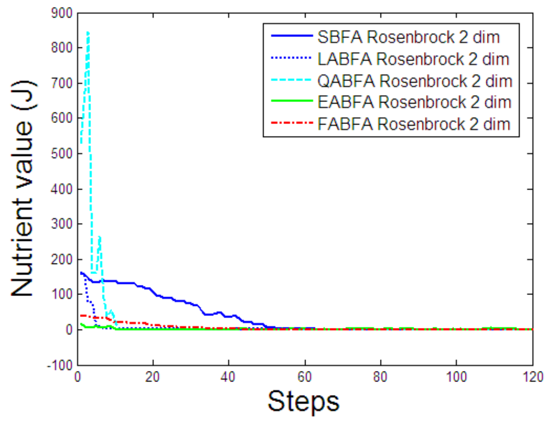

(a) Convergence plots

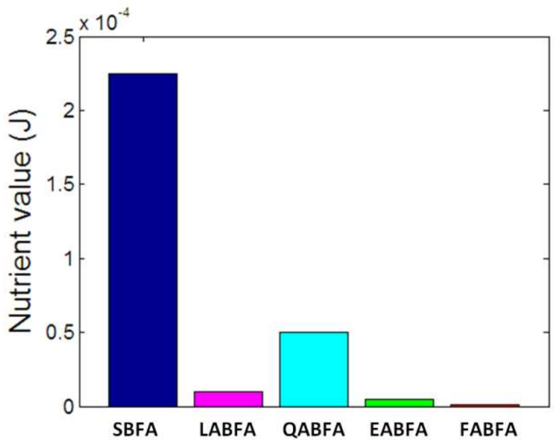

(b) The best optimum J

Figure 4.8: Simulation results of algorithms with Rosenbrock test function.

4.4.2. Test Function 2: sphere function

The sphere function can be formulated as:

$$J(x) = \sum_{i=1}^{n} x_i^2 \tag{4.15}$$

The characteristics of the sphere function is that it is continuous, convex, and unimodal. In the tests carried out here the variables x_i are considered in the range $[-5.12, 5.12]$. The global minimum in this case is $J(x)$ equal to zero which is reached when all variables x_i are equal to zero. The 3D and 2D views of the two-variable sphere function are shown in Figure 4.9. The plots show that the test function only has one valley with one global minimum point and there are no local minima. Thus, it is trivial for the algorithm (bacteria) to find the down direction rather than climbing in the opposite direction of the valley. However, it is very difficult to find the global minimum value.

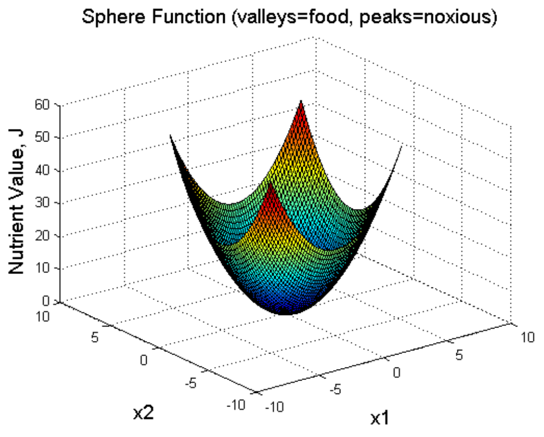

(a) 3D view

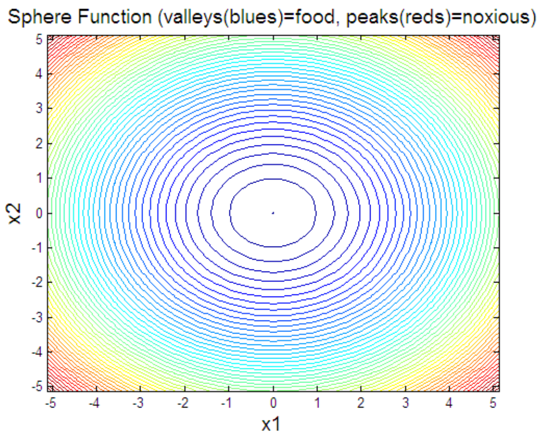

(b) 2D view

Figure 4.9: Two-variable sphere function

In the investigation, a five-dimension sphere function was used and all algorithms used the parameter values:

❖ $p = 5$	❖ $N_c = 40$	❖ $N_{re} = 5$	❖ $N_{ed} = 5$
❖ $S = 10$	❖ $N_s = 4$	❖ $S_r = {}^{S}/_{2}$	❖ $p_{ed} = 0.25$

The initial positions of bacteria were selected randomly in the nutrient media. Various chemotactic step size values were chosen and applied in the simulation of SBFA and the best optimum nutrient value achieved was equal to 3.7057×10^{-5} when the chemotactic step size was equal to 0.01. For LABFA, QABFA and EABFA, all parameters settings, i.e. c_{max}, b, d and g were chosen by trial and error. Chemotactic step size for LABFA, QABFA and EABFA were formulated as:

$$C_{al}(i) = \frac{0.1}{1+\frac{8}{|J(i)|}} \tag{4.16}$$

$$C_{aq}(i) = \frac{0.1}{1+\frac{8}{0.95\left((J(i))^2+|J(i)|\right)}} \tag{4.17}$$

$$C_{ae}(i) = \frac{0.1}{1+\frac{20}{e^{(0.0880|J(i)|)}}} \tag{4.18}$$

For FABFA, the fuzzy membership function parameters, i.e. universe of discourse, m and σ were selected heuristically. The membership functions of FABFA for input and output are depicted in Figure 4.10(a) and Figure 4.10(b) respectively. The fuzzy rules formulated as:

$$\begin{array}{lll l}
R_1 & : & \text{IF } |J(i)| \text{ is ES THEN } C_{af}(i) \text{ is ES} & (1) \\
R_2 & : & \text{IF } |J(i)| \text{ is VS THEN } C_{af}(i) \text{ is S} & (1) \\
R_3 & : & \text{IF } |J(i)| \text{ is S THEN } C_{af}(i) \text{ is M} & (1) \\
R_4 & : & \text{IF } |J(i)| \text{ is M THEN } C_{af}(i) \text{ is EB} & (1) \\
R_5 & : & \text{IF } |J(i)| \text{ is B THEN } C_{af}(i) \text{ is EB} & (1) \\
R_6 & : & \text{IF } |J(i)| \text{ is VB THEN } C_{af}(i) \text{ is EB} & (1) \\
R_7 & : & \text{IF } |J(i)| \text{ is EB THEN } C_{af}(i) \text{ is EB} & (1)
\end{array} \tag{4.19}$$

map the input – output relation into the fuzzy surface depicted in Figure 4.10(c). In the fuzzy surface plot, the fuzzy adaptable chemotactic step size $C_{al}(i)$ remained high, e.g. around 0.09, for $|J(i)|$ higher than 50, and then decreased sharply to a very small value, e.g. below 0.01, lower than SBFA's step size, around global minimum point.

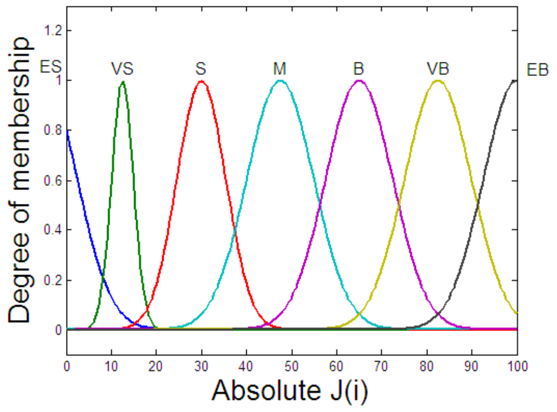

(a) Input: $|J(i)|$

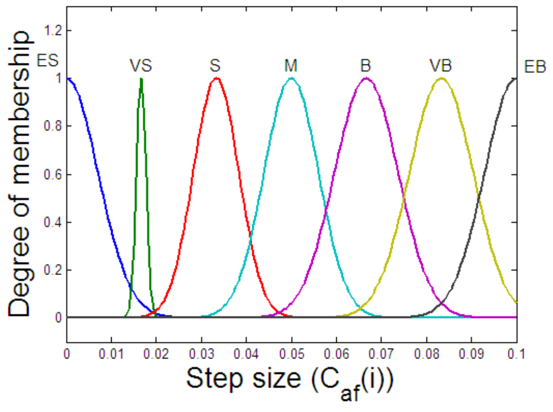

(b) Output: $C_{af}(i)$

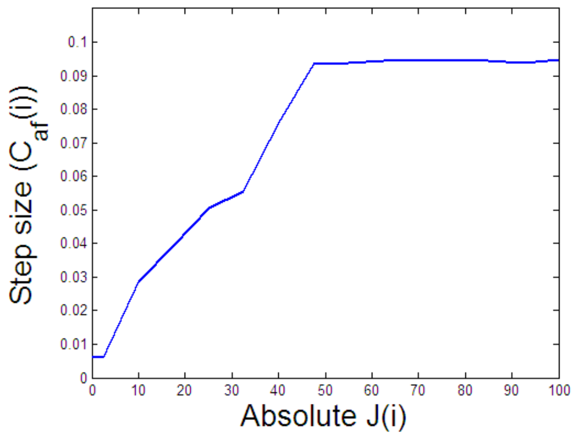

(c) Fuzzy surface

Figure 4.10: Fuzzy membership functions and surface of FABFA for five-dimension sphere test function

The numerical results presented in Table 4.2 show that the four proposed algorithms outperformed the SBFA in finding the global optimum with the best nutrient value achieved by LABFA, as 1.8301×10^{-6}. Also, LABFA achieved the smallest mean optimum J, of 3.3956×10^{-5}, while EABFA achieved the best standard deviation value, of 1.7525×10^{-5}. The convergence plots presented in Figure 4.11 show that all the four proposed algorithms were faster in convergence than SBFA, and among them QABFA had the fastest convergence speed; it only needed 95 steps to converge. A comparison of the optimum J values achieved by the algorithms is depicted in Figure 4.11(b).

Table 4.2: Numerical results of simulation with five-dimension sphere test function

Algorithm	**The best optimum *J***	$\bar{J}$	σ_J	$C(i)$ **range**	**Convergence (steps)**
SBFA	37.0571×10^{-6}	23.0109×10^{-5}	10.3612×10^{-5}	0.01	500
LABFA	$\mathbf{1.8301 \times 10^{-6}}$	$\mathbf{3.3956 \times 10^{-5}}$	2.7472×10^{-5}	$[1.4025 \times 10^{-6}, 0.1]$	100
QABFA	3.2594×10^{-6}	4.2199×10^{-5}	2.4692×10^{-5}	$[3.8720\times 10^{-8}, 0.1]$	**95**
EABFA	12.6040×10^{-6}	5.0845×10^{-5}	$\mathbf{1.7525 \times 10^{-5}}$	[0.0048, 0.1]	190
FABFA	18.4170×10^{-6}	5.8373×10^{-5}	1.8266×10^{-5}	[0.0057, 0.095]	190

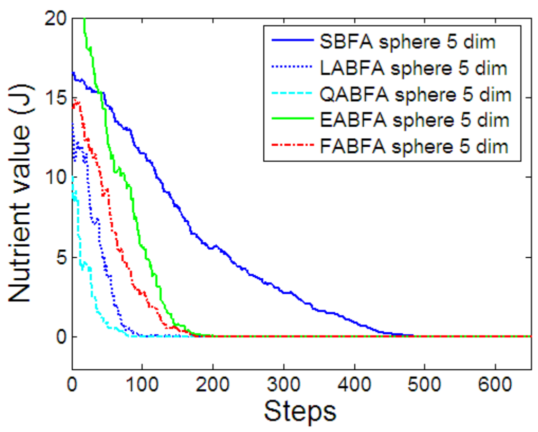

(a) Convergence plots

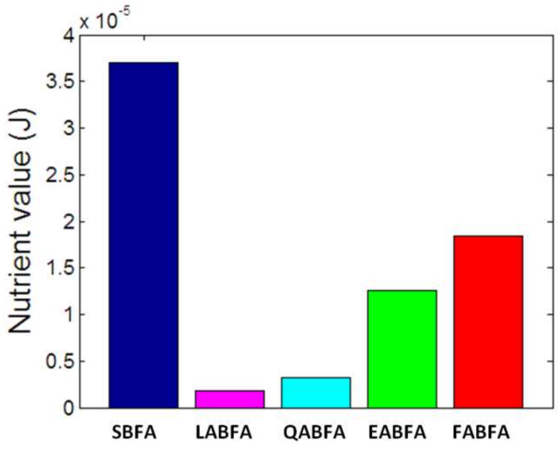

(b) The best optimum J

Figure 4.11: Simulation results of all algorithms for five-dimension sphere test function

4.4.3. Test function 3: Rastrigin's function 6

The general form of Rastrigin's function 6 is given as:

$$J(x) = 10n + \sum_{i=1}^{n} \left(x_i^2 - 10cos(2\pi x_i) \right) \tag{4.20}$$

This function has one global minimum only and many local minima (is highly multimodal) with the locations of minima regularly distributed. The difficulty with this test function is that, since there are a lot of local minima, it is very risky for the algorithm as it may get trapped in one of local minima. In the tests, simulations are carried out with the variables x_i in the range $[-5.12, 5.12]$. The function has global minimum equal to zero at x_i equal to zero. Figure 4.12 shows 3D and 2D plots of a two-variable Rastrigin's function 6.

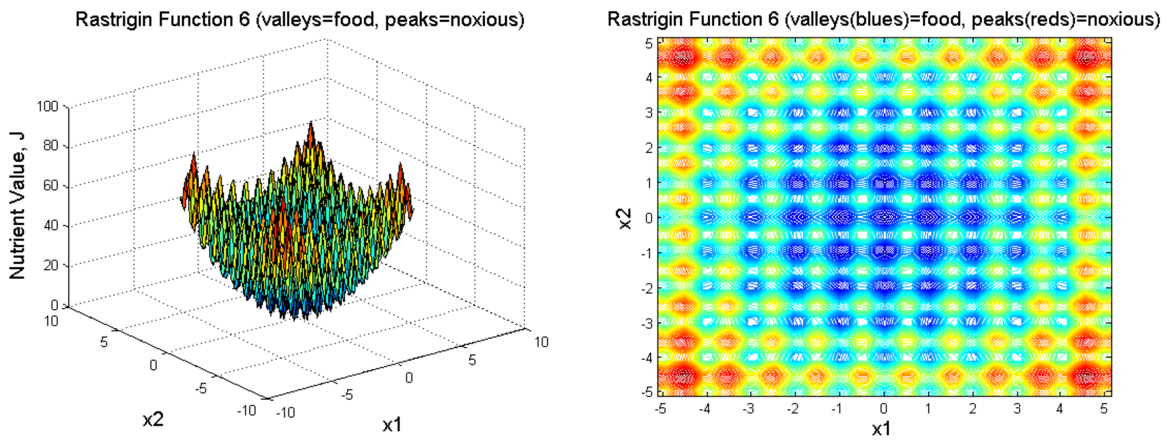

(a) 3D view (b) 2D view

Figure 4.12: Two-variable Rastrigin's function 6

Here, the investigation was carried out for 30 dimensions Rastrigin's function. The general parameters of BFAs used in the simulation are:

❖ $p = 30$	❖ $N_c = 40$	❖ $N_{re} = 4$	❖ $N_{ed} = 4$
❖ $S = 10$	❖ $N_s = 4$	❖ $S_r = {}^{S}/_{2}$	❖ $p_{ed} = 0.25$

The initial positions of bacteria were selected randomly across the nutrient media. Among various chemotactic step size values of SBFA used in the simulation, the best nutrient value, of 162.9286, was achieved when the chemotactic step size was equal to 0.025. All parameters and settings for LABFA, QABFA, EABFA and FABFA were chosen by trial and error. The chemotactic step sizes for LABFA, QABFA and EABFA were formulated as:

$$C_{al}(i) = \frac{0.2}{1+\frac{1}{5\times10^{-4}|J(i)|}} \tag{4.21}$$

$$C_{aq}(i) = \frac{0.2}{1+\frac{1}{2.5\times10^{-6}\left((J(i))^2+|J(i)|\right)}} \tag{4.22}$$

$$C_{ae}(i) = \frac{0.25}{1+\frac{1}{0.023e^{(0.005|J(i)|)}}} \tag{4.23}$$

The fuzzy membership functions of FABFA for input and output are depicted in Figure 4.13(a) and Figure 4.13(b). The associated fuzzy rules formulated as:

$$\begin{array}{lll l} R_1 & : & \text{IF } |J(i)| \text{ is ES THEN } C_{af}(i) \text{ is ES} & (1) \\ R_2 & : & \text{IF } |J(i)| \text{ is VS THEN } C_{af}(i) \text{ is VS} & (0.8) \\ R_3 & : & \text{IF } |J(i)| \text{ is S THEN } C_{af}(i) \text{ is S} & (0.5) \\ R_4 & : & \text{IF } |J(i)| \text{ is M THEN } C_{af}(i) \text{ is M} & (1) \\ R_5 & : & \text{IF } |J(i)| \text{ is B THEN } C_{af}(i) \text{ is B} & (1) \\ R_6 & : & \text{IF } |J(i)| \text{ is VB THEN } C_{af}(i) \text{ is VB} & (1) \\ R_7 & : & \text{IF } |J(i)| \text{ is EB THEN } C_{af}(i) \text{ is EB} & (1) \end{array} \tag{4.24}$$

results in the fuzzy surface of FABFA depicted in Figure 4.13(c).

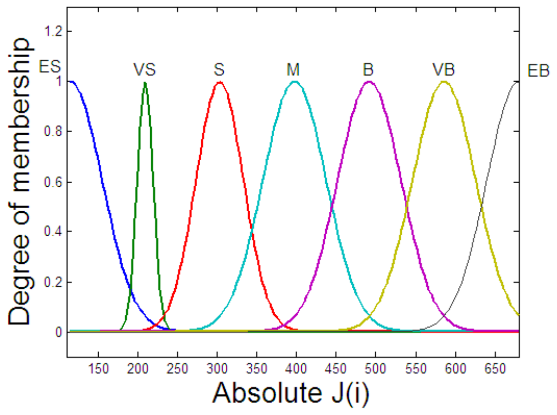

(a) Input: $|J(i)|$

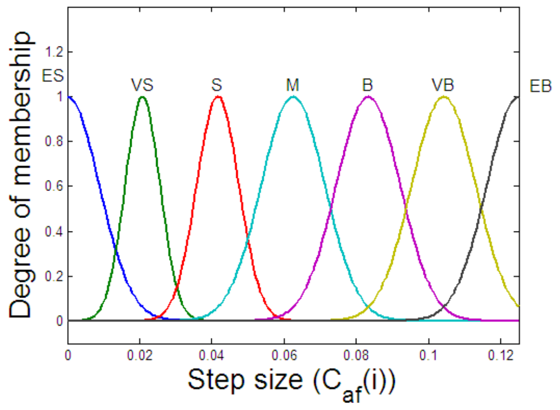

(b) Output: $C_{af}(i)$

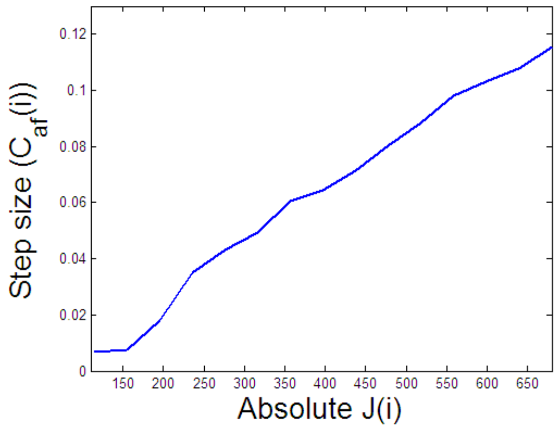

(c) Fuzzy surface

Figure 4.13: Fuzzy membership functions and surface of FABFA for 30-dimension Rastrigin's function 6

The convergence plots in Figure 4.14(a) show that all the five BFA algorithms had almost the same convergence speed, and converged in around 500 steps. The graphs after 500 steps were not exactly flat but decreasing with only very small gradient. It is interesting to note that all the four proposed algorithms converged to lower nutrient values than SBFA. The numerical results presented in Table 4.3 show that all the four proposed algorithms were able to achieve better optimum values than that of SBFA with the best optimum J value 122.2388 achieved by FABFA. Also, FABFA achieved the best mean J value, of 160.6510 while the best standard deviation of J 17.7094 was achieved by QABFA. A comparison of the best optimum J values is depicted in Figure 4.14(b).

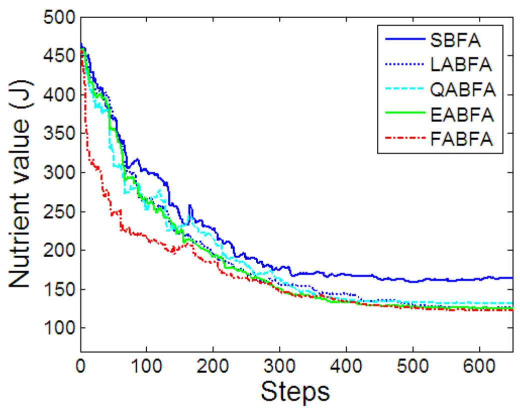

(a) Convergence plots

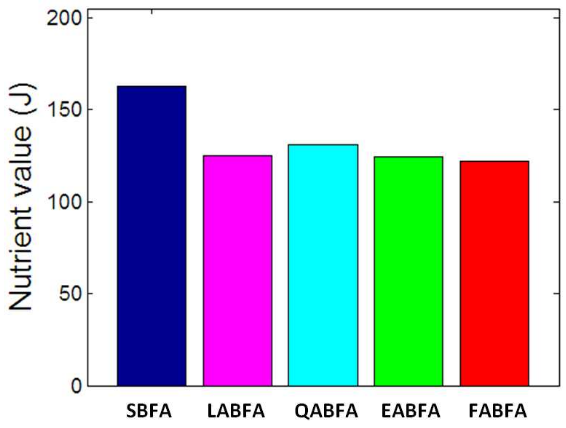

(b) The best optimum J

Figure 4.14: Simulation results of algorithms for 30-dimension Rastrigin's function 6

Table 4.3 Numerical results of simulation with 30-dimension Rastrigin test function

Algorithm	**The best optimum J**	$\bar{J}$	σ_J	$C(i)$ **range**	**Convergence (steps)**
SBFA	162.9286	206.3566	24.7710	0.025	500
LABFA	125.2555	169.2364	18.5067	[0.0120, 0.2]	500
QABFA	130.9555	170.2937	**17.7094**	[0.0083, 0.2]	500
EABFA	124.4501	172.3045	19.6060	[0.0103, 0.25]	500
FABFA	**122.2388**	**160.6510**	23.4752	[0.0067, 0.118]	500

4.4.4. Test function 4: Schwefel's function 7

The general formula for Schwefel's function 7 is given as:

$$J(x) = 418.9829 \times n - \sum_{i=1}^{n} x_i sin\left(\sqrt{|x_i|}\right) \tag{4.25}$$

The characteristic of this function is that the global minimum lies geometrically distant, over the parameter space, from the next best local minima. Therefore, the search algorithms are potentially prone to convergence in the wrong direction. In the test, the variables x_i were in the range $[-500, 500]$. The function has a global minimum of $J(x)$ equal to zero when all variables x_i are equal to 420.9687. Figure 4.15 shows 3D and 2D plots of a two-variable Schwefel's function 7.

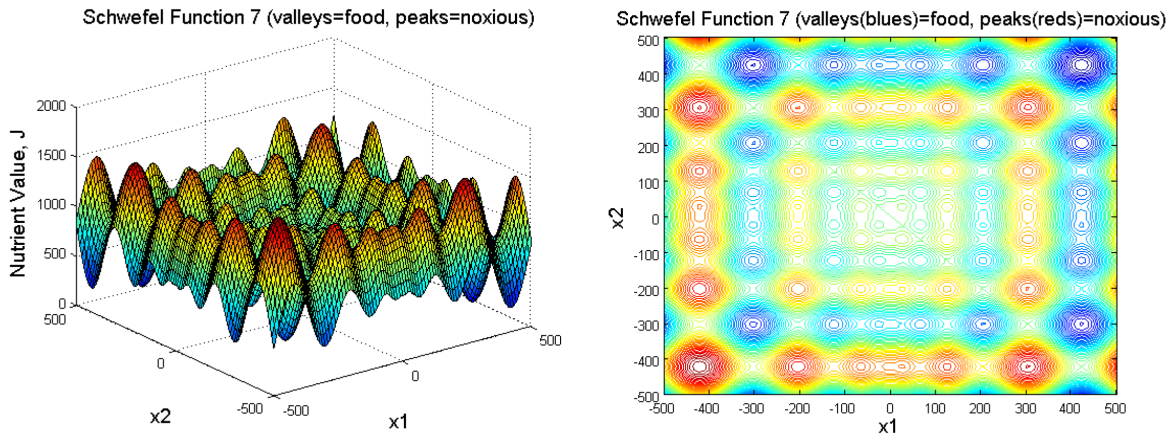

a. 3D view b. 2D view

Figure 4.15: Two-dimension Schwefel's function 7.

In the investigations carried out, a two-dimension Schwefel's function 7 was used. In the simulation, the BFA parameters were set as:

❖ $p = 2$	❖ $N_c = 50$	❖ $N_{re} = 4$	❖ $N_{ed} = 4$
❖ $S = 30$	❖ $N_s = 4$	❖ $S_r = S/2$	❖ $p_{ed} = 0.25$

The initial positions of bacteria were selected randomly across the nutrient media. After various trial and error efforts in choosing chemotactic step size for SBFA, it was noticed that the best optimum J was achieved equal to 4.2722×10^{-4} when the chemotactic step size was equal to 0.6. All the parameter settings for LABFA, QABFA, EABFA and FABFA were chosen by trial and error. The chemotactic step sizes for LABFA, QABFA and EABFA were formulated as:

$$C_{al}(i) = \frac{2}{1+\frac{150}{|J(i)|}} \tag{4.26}$$

$$C_{aq}(i) = \frac{2}{1+\frac{2}{7.5\times10^{-6}\left((J(i))^2+|J(i)|\right)}} \tag{4.27}$$

$$C_{ae}(i) = \frac{2}{1+\frac{4.1}{e^{\left(10^{-6}|J(i)|\right)}}} \tag{4.28}$$

For FABFA, the fuzzy membership functions of input and output can be seen in Figure 4.16(a) and Figure 4.16(b) respectively. The associated fuzzy rules were formulated as:

$$\begin{array}{lll l}
R_1 & : & \text{IF } |J(i)| \text{ is ES THEN } C_{af}(i) \text{ is ES} & (1) \\
R_2 & : & \text{IF } |J(i)| \text{ is VS THEN } C_{af}(i) \text{ is S} & (1) \\
R_3 & : & \text{IF } |J(i)| \text{ is S THEN } C_{af}(i) \text{ is EB} & (1) \\
R_4 & : & \text{IF } |J(i)| \text{ is M THEN } C_{af}(i) \text{ is EB} & (1) \\
R_5 & : & \text{IF } |J(i)| \text{ is B THEN } C_{af}(i) \text{ is EB} & (1) \\
R_6 & : & \text{IF } |J(i)| \text{ is VB THEN } C_{af}(i) \text{ is EB} & (1) \\
R_7 & : & \text{IF } |J(i)| \text{ is EB THEN } C_{af}(i) \text{ is EB} & (1)
\end{array} \tag{4.29}$$

The corresponding fuzzy surface resulting from the fuzzy rules is depicted in Figure 4.16(c).

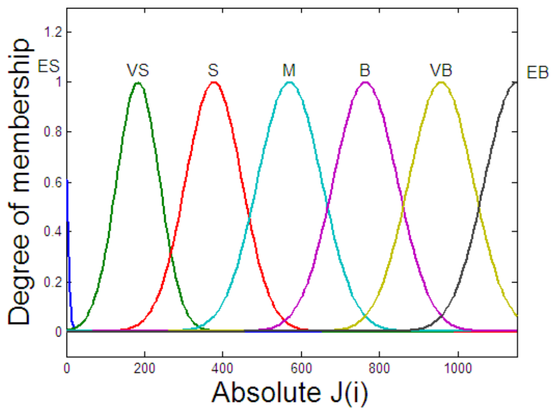

(a) Input: $|J(i)|$

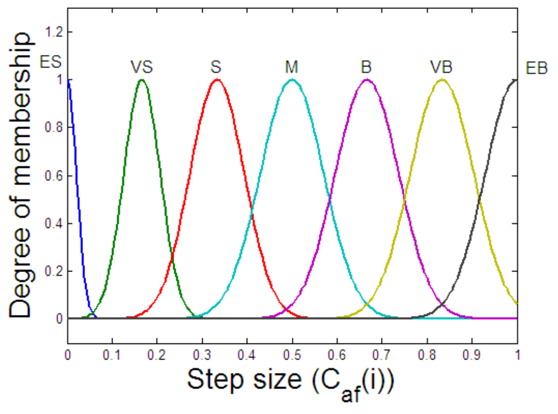

(b) Output: $C_{af}(i)$

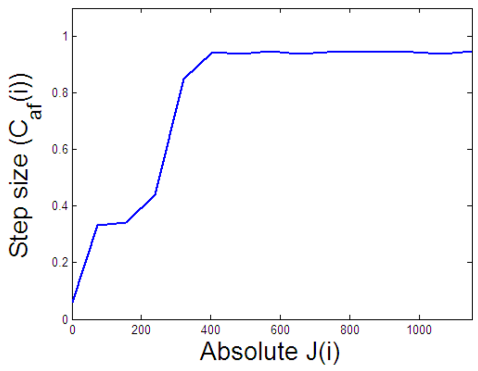

(c) Fuzzy surface

Figure 4.16: Fuzzy membership functions and surface of FABFA for Schwefel's function 7

The numerical results presented in Table 4.4 show that the three proposed algorithms were able to reach better global optimum values than that of SBFA with the best optimum J 2.5566×10^{-5} was achieved by QABFA. However, the best mean and standard deviation of optimum J were achieved by FABFA, as 3.2859×10^{-4} and 0.0011 respectively.

Table 4.4: Numerical results of simulation with two-dimension Schwefel's function 7 test function

Algorithm	**Optimum value**	$\bar{J}$	σ_J	$C(i)$ **range**	**Convergence (Steps)**
SBFA	42.7220×10^{-5}	125.0224	90.9566	0.6	130
LABFA	2.9029×10^{-5}	0.0077	0.0148	$[4.3280 \times 10^{-7}, 2]$	**55**
QABFA	$\mathbf{2.5566 \times 10^{-5}}$	0.0233	0.0556	$[7.4662 \times 10^{-6}, 2]$	60
EABFA	4.0509×10^{-5}	0.0026	0.0032	$[0.3925, 2]$	70
FABFA	2.5703×10^{-5}	$\mathbf{3.2859 \times 10^{-4}}$	**0.0011**	$[0.0373, 0.95]$	60

The convergence of the algorithms in Figure 4.17(a) shows that all the four proposed algorithms converged faster to the optimum J with LABFA as the fastest among them (55 steps). A comparison of the optimum J achieved by the algorithms is shown in Figure 4.17(b).

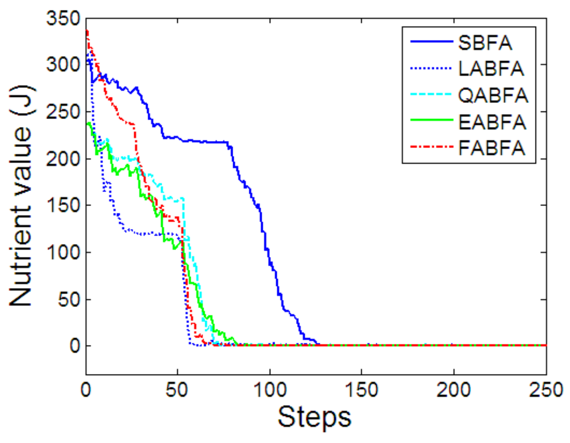

(a) Convergence plots

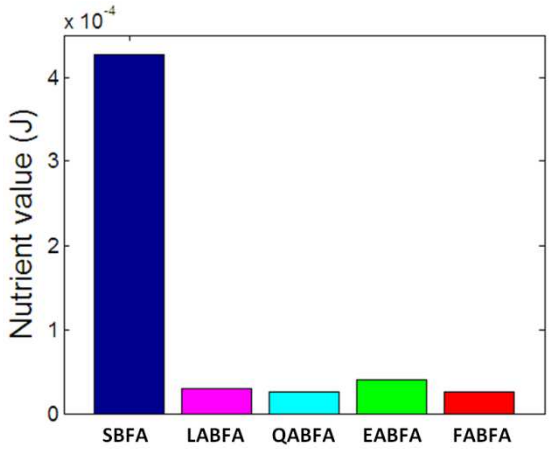

(b) The best optimum J

Figure 4.17: Simulation results of algorithms for two-dimension Schwefel's function 7

4.4.5. Test function 5: Ackley function

The general form of Ackley function is given as:

$$J(x) = 20 + e - 20e^{-0.2\sqrt{\frac{1}{n}\sum_{i=1}^{n} x_i^2}} - e^{\frac{1}{n}\sum_{i=1}^{n} cos(2\pi x_i)} \tag{4.30}$$

The Ackley function has many local maxima with one global minimum surrounded by several local minima. In the test, variables x_i were set in the range $[-32.768, 32.768]$. The Ackley function has one global minimum $J(x)$ equal to zero which is achieved when all of variables x_i are equal to zero. Figure 4.18 shows 3D and 2D plots of a two-variable Ackley function.

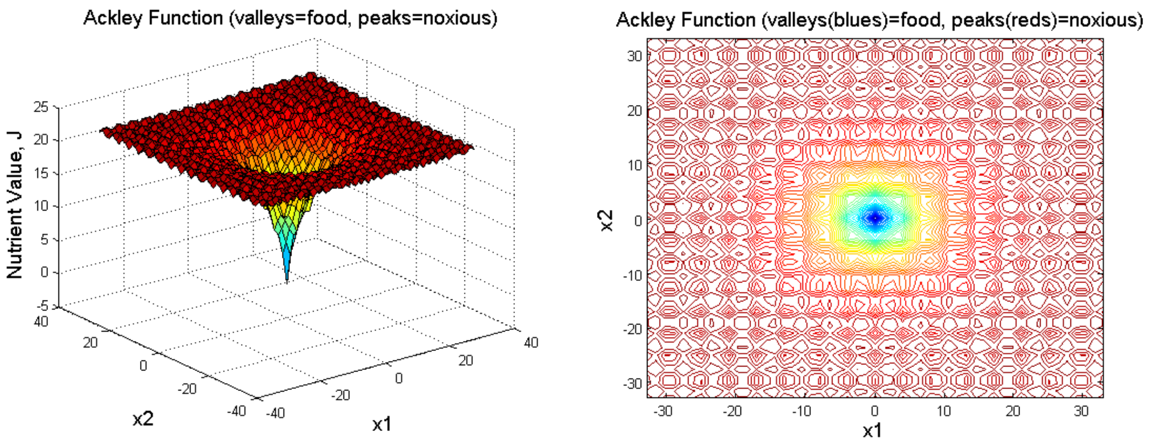

(a) 3D view (b) 2D view

Figure 4.18: Two-dimension Ackley function

The two-dimension Ackley function was used in the investigations in this work. The BFA parameters used in the simulation were:

❖ $p = 2$	❖ $N_c = 40$	❖ $N_{re} = 4$	❖ $N_{ed} = 4$
❖ $S = 10$	❖ $N_s = 4$	❖ $S_r = S/_2$	❖ $p_{ed} = 0.25$

The initial positions of bacteria were selected randomly across the nutrient media. Various chemotactic step sizes were tried in the simulation of SBFA and the best optimum J result (1.5691×10^{-4}) was achieved when the chemotactic step size was equal to 4.5000×10^{-4}. The of parameter settings of LABFA, QABFA, EABFA and FABFA were chosen manually by trial and error. The chemotactic step sizes for LABFA, QABFA and EABFA were formulated as:

$$C_{al}(i) = \frac{2}{1+\frac{3}{0.1|J(i)|}} \tag{4.31}$$

$$C_{aq}(i) = \frac{2}{1+\frac{2.5}{0.01\left((J(i))^2+|J(i)|\right)}} \tag{4.32}$$

$$C_{ae}(i) = \frac{2}{1+\frac{1.75}{10^{-5}e^{(|J(i)|)}}} \tag{4.33}$$

For FABFA, the fuzzy membership functions of input and output are depicted in Figure 4.19(a) and Figure 4.19(b) respectively. With these fuzzy membership functions, fuzzy rules formulated as:

$$\begin{array}{lll} R_1 : & \text{IF } |J(i)| \text{ is ES THEN } C_{af}(i) \text{ is ES} & (1) \\ R_2 : & \text{IF } |J(i)| \text{ is VS THEN } C_{af}(i) \text{ is VS} & (0.1) \\ R_3 : & \text{IF } |J(i)| \text{ is S THEN } C_{af}(i) \text{ is B} & (1) \\ R_4 : & \text{IF } |J(i)| \text{ is M THEN } C_{af}(i) \text{ is EB} & (1) \\ R_5 : & \text{IF } |J(i)| \text{ is B THEN } C_{af}(i) \text{ is EB} & (1) \\ R_6 : & \text{IF } |J(i)| \text{ is VB THEN } C_{af}(i) \text{ is EB} & (1) \\ R_7 : & \text{IF } |J(i)| \text{ is EB THEN } C_{af}(i) \text{ is EB} & (1) \end{array} \tag{4.34}$$

result in fuzzy surface depicted in Figure 4.19(c).

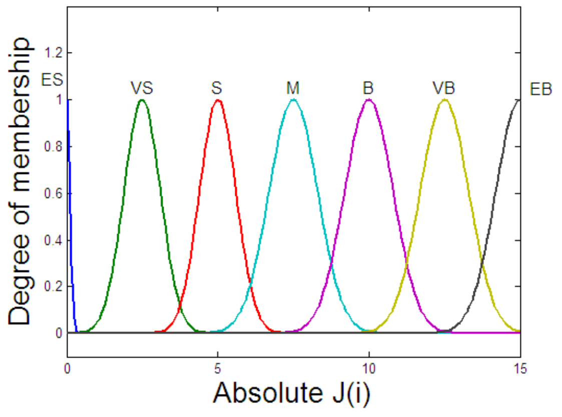

(a) Input: $|J(i)|$

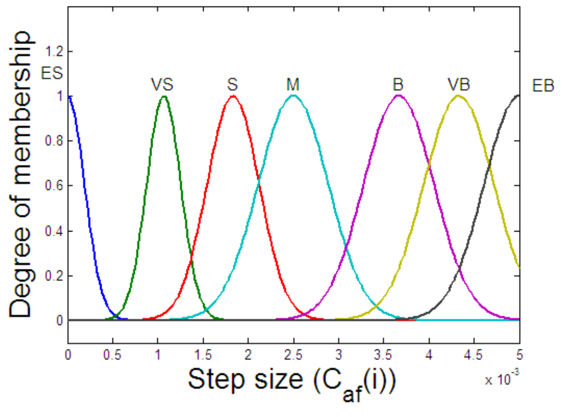

(b) Output: $C_{af}(i)$

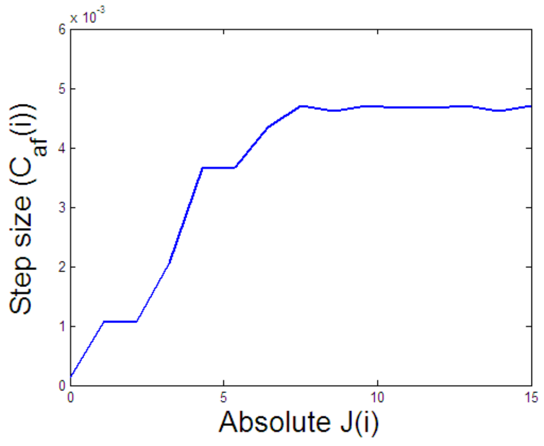

(c) Fuzzy surface

Figure 4.19: Fuzzy membership functions and surface of FABFA for Ackley test function

The numerical results presented in Table 4.5 show that all the four proposed algorithms were able to find better global optimum value than SBFA with the best optimum J achieved by LABFA as 8.8818×10^{-16} while the best mean and standard deviation were achieved by QABFA as 3.5127×10^{-5} and 1.1116×10^{-4} respectively.

Table 4.5 Numerical results of simulation with two-dimension Ackley test function

Algorithm	**Optimum value**	$\bar{J}$	σ_J	$C(i)$ **range**	**Convergence (Steps)**
SBFA	1.5691×10^{-4}	3.2271	1.5189	4.5000×10^{-4}	245
LABFA	$\mathbf{8.8818 \times 10^{-16}}$	0.0051	0.0129	$[7.6975 \times 10^{-16}, 2]$	28
QABFA	3.4683×10^{-12}	$\mathbf{3.5127 \times 10^{-5}}$	$\mathbf{1.1116 \times 10^{-4}}$	$[1.3903 \times 10^{-12}, 2]$	**15**
EABFA	3.4277×10^{-6}	0.0128	0.0212	$[1.1429 \times 10^{-5}, 2]$	90
FABFA	2.0163×10^{-5}	0.0021	0.0031	$[1.3603 \times 10^{-4}, 4.800 \times 10^{-3}]$	95

The convergence plots in Figure 4.20(a) show that in the initial iterations, bacteria of all the four proposed algorithms were in locations far from the global minimum while bacteria of SBFA were in locations closer to the global minimum. However, all the proposed algorithms were able to head to the global minimum faster than SBFA with QABFA as the fastest among them, able to converge in 15 steps. A comparison of the optimum J values achieved by the algorithms is depicted in Figure 4.20(b).

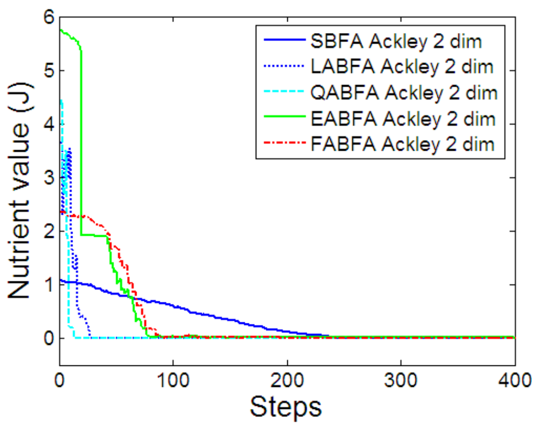

(a) Convergence plots

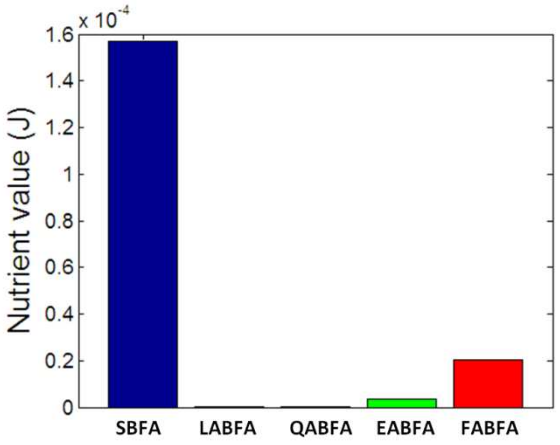

(b) The best optimum J

Figure 4.20: Simulation results of the algorithms for two-dimension Ackley test function

4.4.6. Test function 6: weighted sphere function

The general form of weighted sphere function is given as:

$$J(x) = \sum_{i=1}^{n} i \times x_i^2 \qquad (4.35)$$

This is a continuous, convex, and unimodal function. In the test, x_i span in the interval $[-5.12, 512]$. The function has a global minimum value $J(x)$ equal to zero when all variables x_i are equal to zero. The 3D and 2D plots of a two-variable weighted sphere function is depicted in the Figure 4.21.

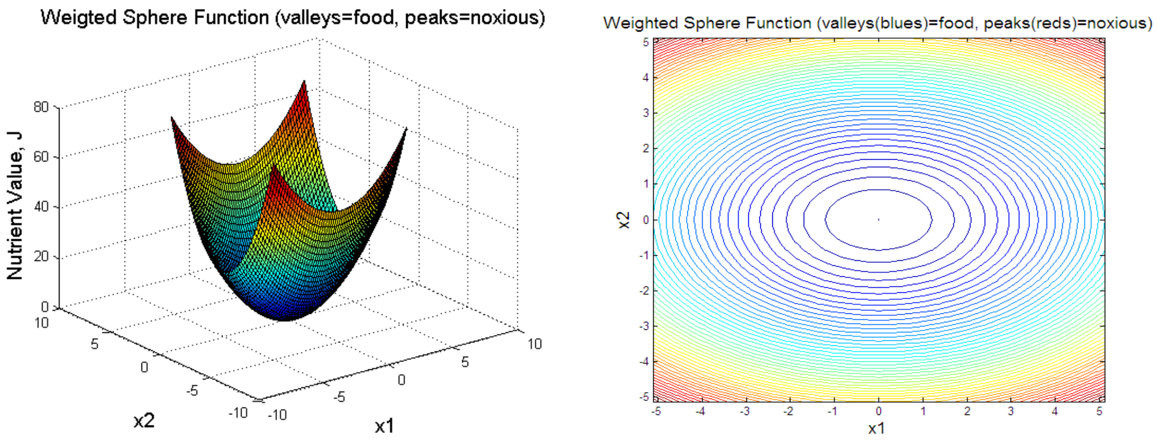

(a) 3D view (b) 2D view

Figure 4.21: Two-dimension weighted sphere function

A 30-dimension weighted sphere function was used in the investigation. The BFA parameters were set to:

❖ $p = 30$	❖ $N_c = 40$	❖ $N_{re} = 5$	❖ $N_{ed} = 5$
❖ $S = 20$	❖ $N_s = 4$	❖ $S_r = S/2$	❖ $p_{ed} = 0.25$

The initial positions of bacteria were selected randomly in the nutrient media. In the investigations, it was noticed that, for SBFA, the best optimum J achieved was 3.8373 when the chemotactic step size was equal to 0.07. The parameters and settings for LABFA, QABFA, EABFA and FABFA were chosen by trial and error. The chemotactic step sizes for LABFA, QABFA and EABFA were formulated as:

$$C_{al}(i) = \frac{0.2}{1+\frac{20}{0.1|J(i)|}} \qquad (4.36)$$

$$C_{aq}(i) = \frac{0.2}{1+\frac{20}{0.006\left((J(i))^2+|J(i)|\right)}} \qquad (4.37)$$

$$C_{ae}(i) = \frac{0.2}{1+\frac{21}{e^{(0.009|J(i)|)}}} \tag{4.38}$$

For FABFA, the fuzzy membership functions of input and output are depicted in Figure 4.22(a) and Figure 4.22(b) respectively. The fuzzy rules formulated as:

$$\begin{array}{lll l} R_1 & : & \text{IF } |J(i)| \text{ is ES THEN } C_{af}(i) \text{ is ES} & (1) \\ R_2 & : & \text{IF } |J(i)| \text{ is VS THEN } C_{af}(i) \text{ is S} & (1) \\ R_3 & : & \text{IF } |J(i)| \text{ is S THEN } C_{af}(i) \text{ is M} & (1) \\ R_4 & : & \text{IF } |J(i)| \text{ is M THEN } C_{af}(i) \text{ is EB} & (1) \\ R_5 & : & \text{IF } |J(i)| \text{ is B THEN } C_{af}(i) \text{ is EB} & (1) \\ R_6 & : & \text{IF } |J(i)| \text{ is VB THEN } C_{af}(i) \text{ is EB} & (1) \\ R_7 & : & \text{IF } |J(i)| \text{ is EB THEN } C_{af}(i) \text{ is EB} & (1) \end{array} \tag{4.39}$$

will map the input to output in the form of fuzzy the surface depicted in Figure 4.22(c).

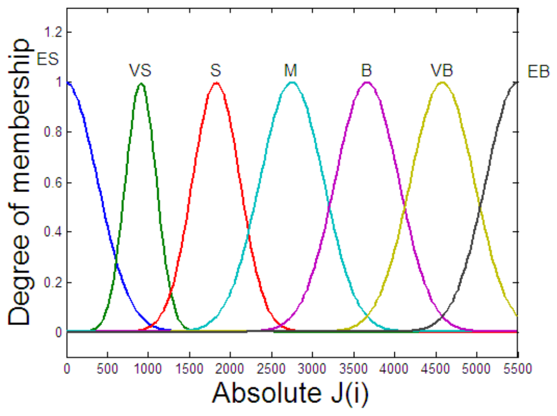

(a) Input: $|J(i)|$

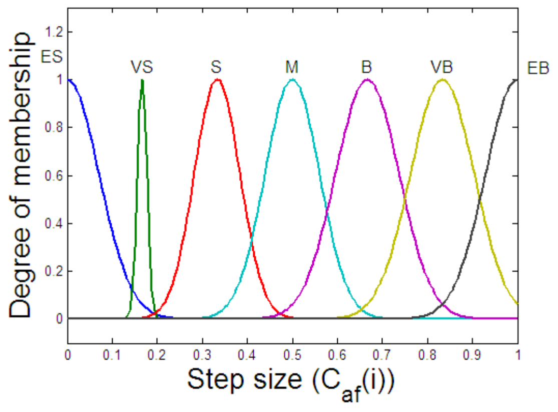

(b) Output: $C_{af}(i)$

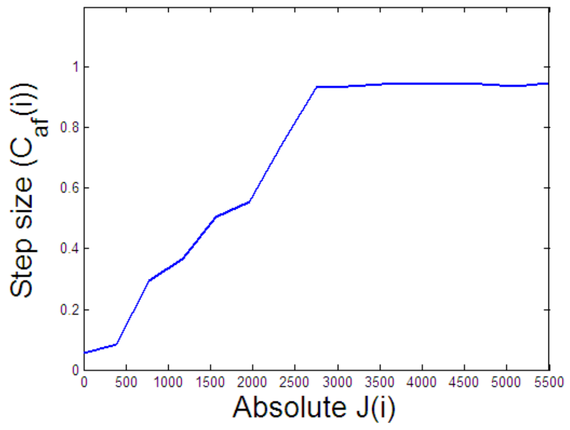

(c) Fuzzy surface

Figure 4.22: Fuzzy membership functions and surface of FABFA for 30-dimension weighted sphere test function

The numerical results in Table 4.6 show that all the four proposed algorithms were able to achieve better optimum J than SBFA with the best optimum J (0.3486) achieved by LABFA. LABFA also achieved the best mean optimum J while FABFA had the best standard deviation of optimum J.

Table 4.6. Numerical simulation results with 30-dimension weighted sphere test function

Algorithm	**Optimum value**	$\bar{J}$	σ_J	$C(i)$ **range**	**Convergence (steps)**
SBFA	3.8373	6.9009	1.6235	0.07	680
LABFA	**0.3486**	**1.6879**	0.9372	$[7.9523 \times 10^{-4}, 0.2]$	520
QABFA	1.3051	2.1652	0.4766	$[2.2585 \times 10^{-4}, 0.2]$	520
EABFA	0.5578	1.9526	1.0263	[0.0092, 0.2]	520
FABFA	2.1179	2.9460	**0.4168**	[0.0534, 0.95]	520

The convergence plots depicted in Figure 4.23(a) show that all the four proposed algorithms were faster in convergence (all the four algorithms converged in 520 steps), than SBFA which converged in 680 steps. A comparison of the best optimum J of all algorithms is depicted in Figure 4.23(b).

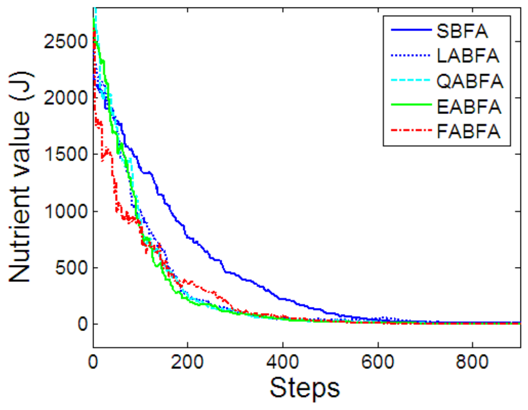

(a) Convergence plots

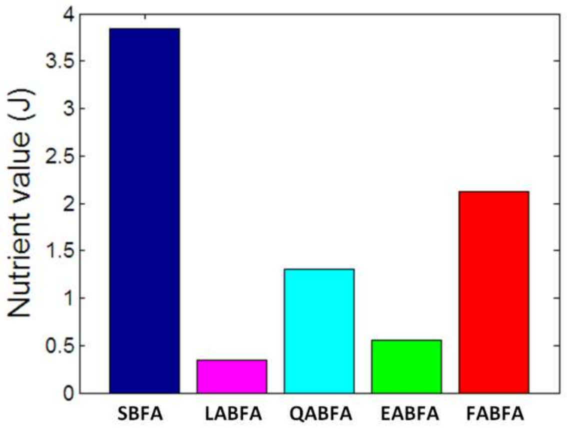

(b) The best optimum J

Figure 4.23: Simulation results of all algorithms for 30-dimesion weighted sphere test function

4.4.7. Test function 7: Schwefel's function 1.2

The general form of Schwefel's function 1.2 is given as:

$$J(x) = \sum_{i=1}^{n} \left(\sum_{j=1}^{n} x_i \right)^2 \tag{4.40}$$

The Schwefel's function 1.2 is characterised by rotated hyper ellipsoids. In the test, variables x_i were in the interval $[-65.536, 65.536]$. The function has a global minimum $J(x)$ equal to zero at variables x_i equal to zero. Figure 4.24 shows 3D and 2D views of a two-variable Schewefel's function 1.2.

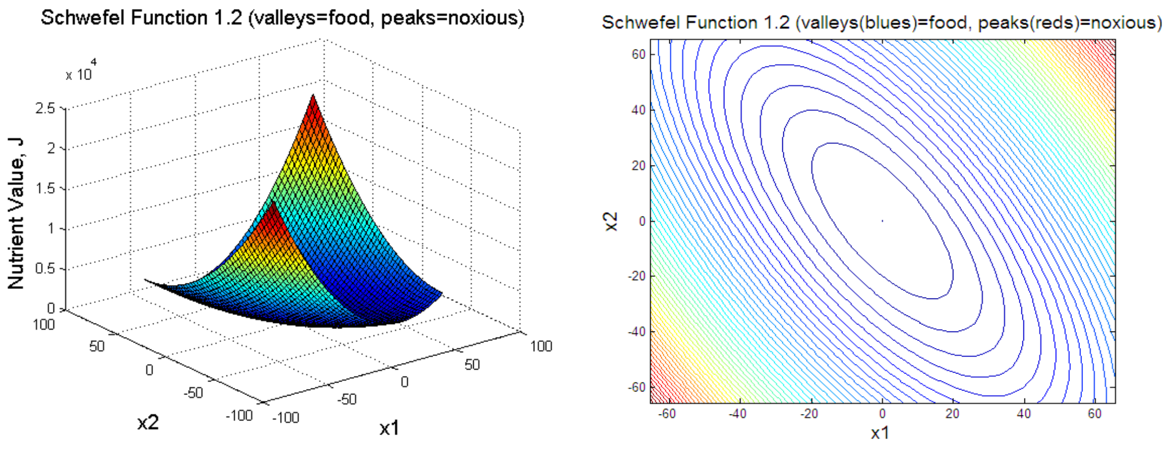

(a) 3D view (b) 2D view

Figure 4.24: Two-variable Schwefel's function 1.2

A two-dimension Schwefel's function 1.2 was used in the investigation carried out here. In the simulation, the BFA parameters were set as:

❖ $p = 2$	❖ $N_c = 40$	❖ $N_{re} = 4$	❖ $N_{ed} = 4$
❖ $S = 10$	❖ $N_s = 4$	❖ $S_r = S/2$	❖ $p_{ed} = 0.25$

The initial positions of bacteria were selected randomly in the nutrient media. Among various chemotactic step sizes chosen for SBFA, the best optimum J value, of 4.0258×10^{-6}, was obtained with the chemotactic step size $C(i)$ equal to 0.009. The parameter settings of LABFA, QABFA, EABFA and FABFA were chosen by trial and error. The chemotactic step sizes for LABFA, QABFA and EABFA were formulated as:

$$C_{al}(i) = \frac{0.2}{1+\frac{1}{0.1|J(i)|}} \tag{4.41}$$

$$C_{aq}(i) = \frac{0.2}{1+\frac{5}{(J(i))^2+|J(i)|}} \tag{4.42}$$

$$C_{ae}(i) = \frac{0.5}{1+\frac{1}{10^{-4}e^{(|J(i)|)}}} \tag{4.43}$$

The fuzzy membership functions of FABFA for input and output are depiced in Figure 4.25(a) and Figure 4.25(b) respectively. The fuzzy rules formulated as:

$$\begin{array}{lll} R_1 : & \text{IF } |J(i)| \text{ is ES THEN } C_{af}(i) \text{ is ES} & (1) \\ R_2 : & \text{IF } |J(i)| \text{ is VS THEN } C_{af}(i) \text{ is S} & (1) \\ R_3 : & \text{IF } |J(i)| \text{ is S THEN } C_{af}(i) \text{ is VB} & (1) \\ R_4 : & \text{IF } |J(i)| \text{ is M THEN } C_{af}(i) \text{ is EB} & (1) \\ R_5 : & \text{IF } |J(i)| \text{ is B THEN } C_{af}(i) \text{ is EB} & (1) \\ R_6 : & \text{IF } |J(i)| \text{ is VB THEN } C_{af}(i) \text{ is EB} & (1) \\ R_7 : & \text{IF } |J(i)| \text{ is EB THEN } C_{af}(i) \text{ is EB} & (1) \end{array} \tag{4.44}$$

result in correlation between input and output in the form of fuzzy surface depicted in Figure 4.25(c).

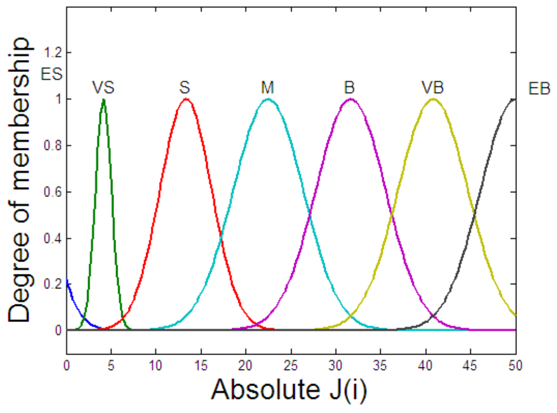

(a) Input: $|J(i)|$

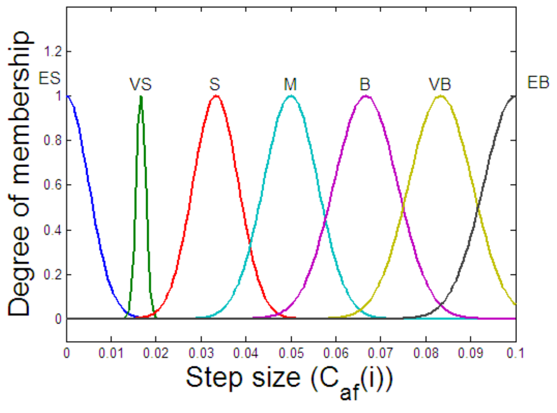

(b) Output: $C_{af}(i)$

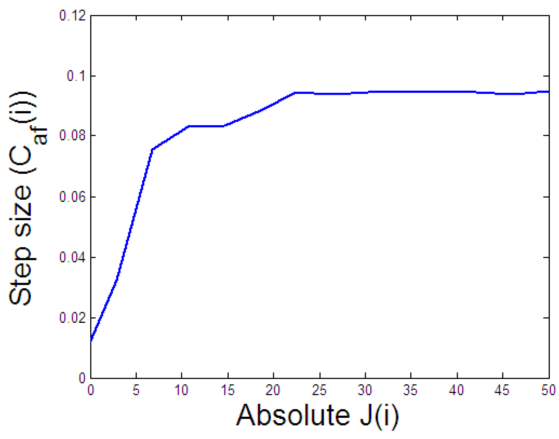

(c) Fuzzy surface

Figure 4.25: Fuzzy membership functions and surface of FABFA for two-dimension Schwefel's function 1.2 test function

The fuzzy surface show that the fuzzy adaptable chemotactic step size remains high, e.g. around 0.09 when the nutrient value $J(i)$ is considered high and then decreases dramatically when the nutrient value $J(i)$ is small. The numerical results in Table 4.7 show that all the four proposed algorithms were able to achieve better optimum J value than SBFA. LABFA and QABFA were able to hit the global minimum point (J equal to zero), while EABFA and FABFA achieved the best mean of optimum J (6.6280×10^{-7}) and the best standard deviation of optimum J (1.4404×10^{-6}) respectively.

Table 4.7 Numerical simulation results with two-dimension Schwefel's function 1.2

Algorithm	**The best optimum $\boldsymbol{J}$**	$\bar{J}$	σ_J	$C(i)$ **range**	**Convergence (steps)**
SBFA	4.0258×10^{-6}	110.9400×10^{-7}	7.7461×10^{-6}	0.009	83
LABFA	$\mathbf{0}$	53.0291×10^{-7}	8.7673×10^{-6}	[0, 0.2]	45
QABFA	$\mathbf{0}$	23.1800×10^{-7}	2.9087×10^{-6}	$[1.1902 \times 10^{-34}, 0.2]$	71
EABFA	4.3237×10^{-12}	$\mathbf{6.6280 \times 10^{-7}}$	1.9741×10^{-6}	$[4.9995 \times 10^{-5}, 0.5]$	80
FABFA	9.0323×10^{-8}	16.6932×10^{-7}	$\mathbf{1.4404 \times 10^{-6}}$	[0.0055, 0.95]	**43**

The convergence plots depicted in Figure 4.26(a) show that all the four proposed algorithms were able to converge faster than SBFA with FABFA as the fastest among them (converged in 43 steps). The SBFA converged in 83 steps. A comparison of the best optimum J for the algorithms is depicted in Figure 4.26(b). The bar chart shows that all the proposed algorithms result in significantly better optimum J than SBFA.

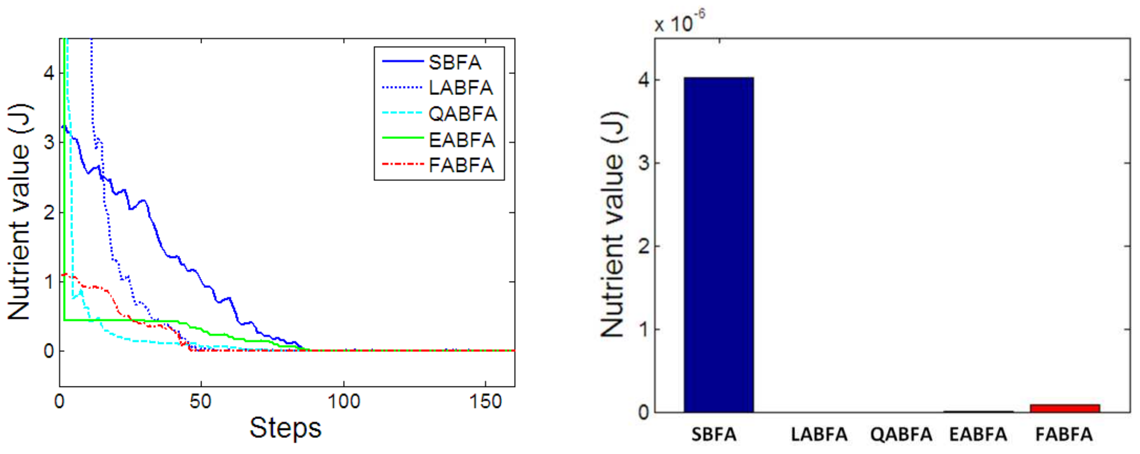

(a) Convergence plots (b) The best optimum J

Figure 4.26: Simulation results of all algorithms for Schwefel function 1.2

4.4.8 Comparison

The investigations above show that all the four proposed algorithms have achieved better best value, mean and standard deviation of optimum J with faster convergence for all benchmark functions. Since SBFA and all the four proposed algorithms used the same general parameters, the difference on their optimum J achieved and convergence speed must have resulted by the use of adaptable chemotactic step size. Also, because initial positions of bacteria were selected randomly in the nutrient media, although bacteria of SBFA fell in location near the global minimum, by using bigger chemotactic step size, all four proposed algorithms were able to converge faster than SBFA.

4.5. Summary

Four novel approaches for adaptable chemotactic step size of BFA have been presented and discussed. The adaptation schemes based on three functions, namely linear, quadratic, and exponential and based on FL have been investigated. It has been demonstrated with seven commonly used benchmark test functions that ABFAs have faster convergence to global optimum and are able to achieve better performance as compared to SBFA. Based on the results presented above, all of the four proposed algorithms may potentially be used in applications to replace the constant chemotactic step size in SBFA. The next chapter, Chapter 5, will discuss the application of BFA in linear modelling of flexible manipulator system.

CHAPTER 5
USING PARAMETRIC MODELLING OF FLEXIBLE MANIPULATOR WITH BACTERIAL FORAGING ALGORITHMS

5.1. Introduction

Linear parametric modelling is a linear system identification technique which formulates the model of the plant as a mathematical function relating the input to the output, usually in the form of differential/difference equation or transfer function. It can be noted from the literature that linear parametric modelling approaches have been used in broad areas such as the work by Sowell (1992) who used an autoregressive integrated moving average (ARIMA) model for modelling the long-run behaviour of a time series. Han and Yuan (1998) used autoregressive (AR), moving average (MA) and autoregressive moving average (ARMA) models for modelling and estimating of ultra wide band (UWB) radar echoes, Sakkalis et al. (2008) proposed ARMA model for modelling and analysis of electroencephalogram (EEG) activity, Li and Kareem (1993) used ARMA model for modelling of stochastic wave effects on offshore platforms, Mat Darus and Tokhi (2004) used autoregressive moving average with exogenous input (ARMAX) model for modelling two-dimensional flexible structure and etc.

This chapter presents the application of ABFAs proposed in Chapter 4 in modelling of flexible manipulator systems in the linear parametric form. The objective of the work is to develop a single-link flexible manipulator model based on ABFAs. Previous related works on modelling of flexible manipulator system have been addressed in Chapter 3. It can be noted from the literature that the use of BFA for modelling flexible manipulators has not been reported yet. Approaches for the modelling of a single-link flexible manipulator with ABFAs using real-world data collected from an experimental rig are presented in this chapter. The single-link flexible manipulator system considered in this work is a single-input multiple-output (SIMO) system, with one input, the torque of the motor, and three outputs, namely hub-angle, hub velocity and end-point acceleration. Three single-input single-output (SISO) models are developed representing the system behaviour from input torque to hub-angle, hub velocity and end-point acceleration outputs. The performances of the adaptive BFAs (ABFAs) are compared to that of standard BFA (SBFA). The comparison is made based on the convergence to optimum value, the optimum value achieved, and time-domain and frequency domain responses of the developed models.

5.2. Preliminary experimentation

The experimental input-output data needed for the modelling processes were gathered from a laboratory scale single-link flexible manipulator rig. A random signal of $\pm$ 0.3 Nm amplitude was applied as input to excite the flexible manipulator system and three outputs from sensors, namely: hub-angle, hub-velocity and end-point acceleration were measured. The input-output data thus gathered were presented in Chapter 3.

5.3. Model structure formulation

It is noted from the literature that there are various types of model structure that can potentially be used in a system identification process. These include AR, autoregressive with exogenous input (ARX), ARMA and ARMAX (Ljung, 1999). Among them, several model structures have been reported in the modelling of flexible manipulator systems, i.e. ARMAX (Shaheed and Tokhi, 2002) and ARMA (Alam and Tokhi, 2007; Md Zain et al., 2009a, b, c). Considering the simplicity, performance and computation costs, here the ARX structure, also called as equation error model structure, is chosen to model the flexible manipulator system. The general ARX model structure can be formulated as (Ljung, 1999):

$$\hat{y}(k) = -\sum_{i=1}^{N} a_i \times y(k-i) + \sum_{j=0}^{M} b_j \times u(k-j) + \eta(k) \tag{5.1}$$

where $a_i, (i = 1,2,3, \dots, N)$, $b_j, (j = 0,1,2, \dots, M)$, are the output and input coefficients, $N \geq M$ represents the order of the model and $\eta(k)$ is the disturbance or uncorrelated noise. If the model is "good enough" to represent the system and only depend on actual input-output, the noise term of the general ARX model can be neglected (Alam and Tokhi, 2007). Thus, the modelling process using ARX model is determining the numerical values of coefficients a_i and b_j which result in minimum error between measured and estimated outputs, y and $\hat{y}$. Then, the general ARX structure above can be expressed as discrete transfer function as:

$$H(z) = \frac{Y(z)}{U(z)} = \frac{b_0 z^M + b_1 z^{M-1} + \cdots + b_{M-1} z^1 + b_M}{z^N + a_1 z^{N-1} + \cdots + a_{N-1} z^1 + a_N} \tag{5.2}$$

Thus, the stability of the resulted model can be evaluated from the poles that can be calculated from the denominator of the discrete transfer function.

5.4. ABFA-based modelling

In this work, the coefficient values of ARX model, a_i and b_j, are determined using ABFAs. A block diagram of the optimisation mechanism is depicted in Figure 5.1.

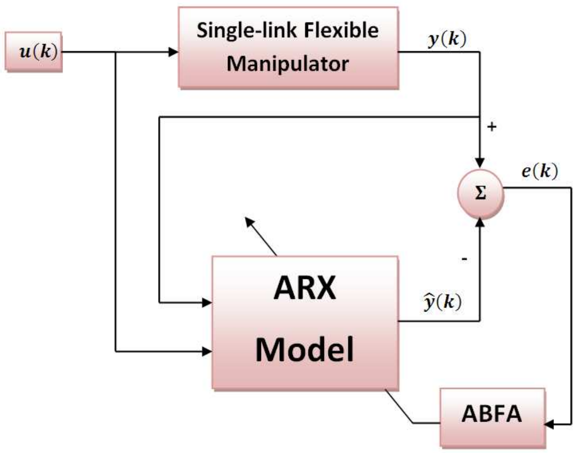

Figure 5.1: ABFA-based ARX model structure for flexible manipulator modelling

where $u(k)$ is the actual input, $y(k)$ is the actual output, $\hat{y}(k)$ is the predicted output and $e(k)$ is the prediction error;

$$e(k) = y(k) - \hat{y}(k) \tag{5.3}$$

The model prediction error is used to set up the cost function which will act as nutrient media to be optimised by ABFAs. In the optimisation process, bacteria will try to find optimum or minimum cost function value by using random walk for whole bacteria's lifetime determined by the total number of steps calculated as $N_c \times N_{re} \times N_{ed}$. The result of optimisation process will be optimised parameters of ARX model, a_i and b_j. The steps of computation of ABFA-based modelling of flexible are shown in the flowchart in Figure 5.2.

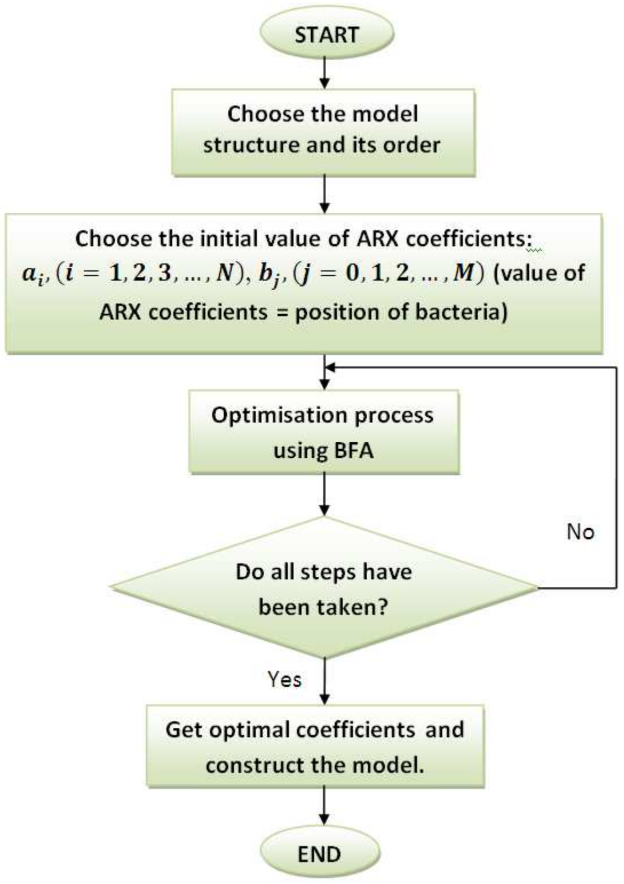
START
Choose the model structure and its order
Choose the initial value of ARX coefficients: $a_i, (i = 1, 2, 3, \dots, N), b_j, (j = 0, 1, 2, \dots, M)$ (value of ARX coefficients = position of bacteria)
Optimisation process using BFA
Do all steps have been taken?
No
Yes
Get optimal coefficients and construct the model.
END

Figure 5.2: ARX modelling process using BFA

5.5. Model Validation

To evaluate whether the developed models are adequate, validations are carried out in three steps as:

a. Firstly, stability check is conducted to check whether the resulted models are stable or not. The stability of models can be tested by using pole-zero plots.
b. The 6400 input-output experimental data pairs are split into two sets: the first 3400 data pairs are used for modelling phase and the remaining 3000 data pairs are used for validation phase.
c. Finally, correlation tests (Billings and Voon, 1986) described in equation (3.2) are performed on the developed models. Since the developed models are linear time-invariant models, the first two correlation tests of equation (3.2) are applicable (Billings and Voon, 1986).

The overall modelling process is outlined in Figure 5.3.

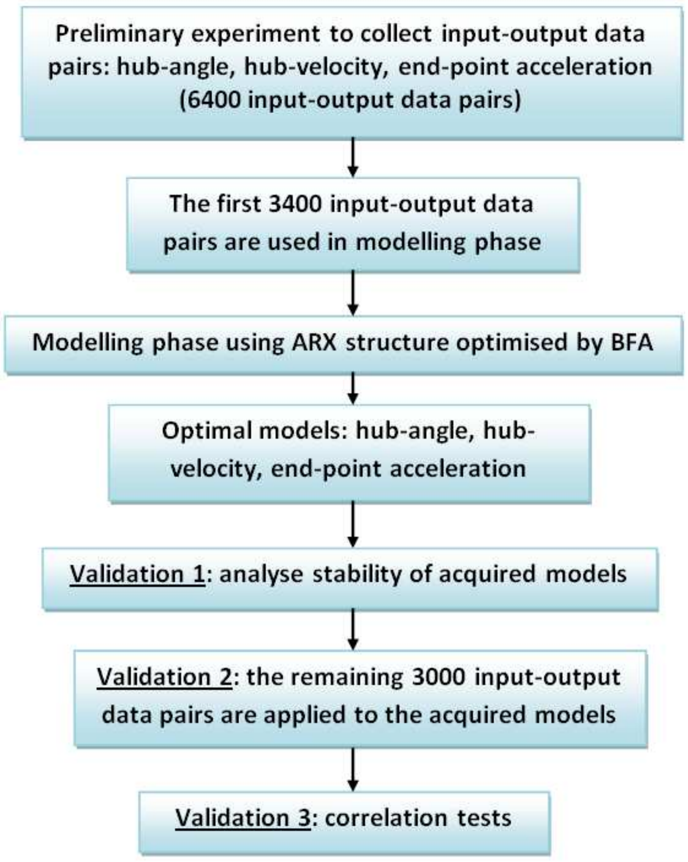
Preliminary experiment to collect input-output data pairs: hub-angle, hub-velocity, end-point acceleration (6400 input-output data pairs)
The first 3400 input-output data pairs are used in modelling phase
Modelling phase using ARX structure optimised by BFA
Optimal models: hub-angle, hub-velocity, end-point acceleration
Validation 1: analyse stability of acquired models
Validation 2: the remaining 3000 input-output data pairs are applied to the acquired models
Validation 3: correlation tests

Figure 5.3: Overall modelling sequence

5.6. Results and Discussion

There are three SISO models to model flexible manipulator, i.e. hub-angle, hub-velocity and end-point acceleration models. All models were developed based on the four proposed ABFAs developed and discussed in Chapter 4, i.e. LABFA, QABFA, EABFA and FABFA and then compared to the models developed based on SBFA. The scenario of the modelling computations is as:

1. All parameters of BFAs are used in the modelling process, except dimension of the search space p which was selected according to the order of the model structure, were selected by considering that bacteria should have enough lifetime (total number of steps), enough reproduction steps (N_{re}) so that bacteria can refine the nutrient value achieved and enough elimination and dispersal events (N_{ed}) so that bacteria were able to search most parts of the nutrient media to find locations closest to the global minimum but with minimum computation load.
2. As a preliminary simulation, several cost function formulas developed and used by researchers in various applications found in the literature are evaluated by using them in the modelling of hub-angle based on SBFA. The performances of

SBFA using several cost functions are evaluated based on their error of time-domain responses. The cost function which gives the best performance is used as cost function for the rest the modelling process.

3. For every modelling process, i.e. hub-angle, hub-velocity and end-point acceleration models, the performances of the proposed algorithms are compared to that of SBFA based on the best optimum cost function value achieved, convergence and time-domain response error.
4. Validation steps are performed for all developed models.

5.6.1. Preliminary simulation: empirical comparison of cost functions

There are three cost function alternatives considered as the nutrient media of BFAs, sum of absolute error (SAE), mean of absolute error (MAE) and mean squared error (MSE). These are formulated as:

$$J_{SAE} = \sum_{k=1}^{n} |e(k)| \tag{5.4}$$

$$J_{MAE} = \frac{1}{n}\sum_{k=1}^{n} |e(k)| \tag{5.5}$$

$$J_{MSE} = \frac{1}{n}\sum_{k=1}^{n} \left(e(k)\right)^2 \tag{5.6}$$

where n represents the number of data points, and $e(k)$ is the model prediction error. SAE measures the total absolute error of all data points while MAE measures the mean of absolute difference between actual and predicted output of each data point. These cost functions have the same units as the actual output. For example if the actual output is in degrees then the SAE or MAE will also be in degree. It can be noticed from literature that SAE has been used in various applications such as 3-D point set matching (Calafiore, 2008), block motion estimation (Yu et al., 2002) and fast output sampling control for blood perfusion uncertainity in hyperthermia (Auxilia and Sundaravadivelu, 2011). MAE has been used in various applications such as 3-D point set matching (Calafiore, 2008), estimation of generalised stack filter (Lin and Coyle, 1990) and gray-scale signals filtering (Dougherty, 1994). MSE measures the mean of squared predicted error of every data point. The unit of this cost function is squared of actual output unit, for example if the units of actual input are degrees then the units of MSE will be $degree^2$. MSE has been used in various applications such as block motion estimation (Yu et al., 2002), stock market indices prediction using bacterial foraging optimisation (BFO) (Majhi et al., 2009) and modelling and control of flexible manipulator systems

(Md Zain and Tokhi, 2009a; Md Zain et al, 2009b, c). The advantage of using MSE is that, since the error is squared, it can be used to remove large predicted error.

In this preliminary simulation, those three cost functions are used in the modelling of hub-angle using SBFA. For hub-angle modelling, a 6th order ($N = M = 6$) ARX model which consists of 13 coefficients ($a_1,...,a_6$ and $b_0,...,b_6$) was selected, following investigations with various model orders for best results. However, if the model is only depending on the previous input then the coefficient $b_0 = 0$ so that the total coefficients now become 12 ($a_1,...,a_6$ and $b_1,...,b_6$). Thus, there are 12 parameters to optimise which means the nutrient media or cost function is a 12-dimension search space. The initial values of SBFA parameters were selected as follow:

❖ $p = 12$	❖ $N_c = 30$	❖ $N_{re} = 5$	❖ $N_{ed} = 3$
❖ $S = 6$	❖ $N_s = 4$	❖ $S_r = S/2$	❖ $p_{ed} = 0.25$

Initial positions of bacteria were selected randomly across the cost function. Various chemotactic step size values $C(i)$ were used in the simulation and the best optimum J for the cost functions formulated in equations (5.4), (5.5) and (5.6) achieved was 0.0035. The time-domain responses and error in modelling phase depicted in Figure 5.4 show that using those three cost functions, the output of SBFA-based models could follow the actual output very well with MSE providing the closest predicted output to the actual output (smallest predicted error).

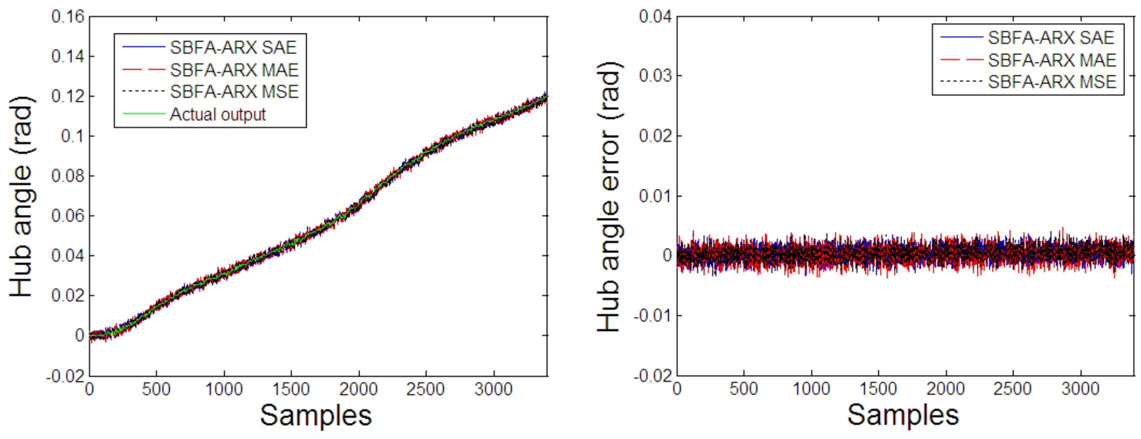

(a) Time-domain responses (b) Error

Figure 5.4: Simulation results of SBFA-ARX based models using all cost function in modelling phase

The numerical results presented in Table 5.1 confirm that SBFA-based model using MSE had the lowest optimum J (1.4323×10^{-6}) and predicted error range $[e_{min}, e_{max}]$, i.e[-0.0033, 0.0035] compared to using SAE and MAE.

Table 5.1: Numerical results of the cost functions in the modelling phase

Algorithm	**Optimum J**	**Range of error ($e(k)$)**	
		Minimum	**Maximum**
SBFA-ARX SAE	$J_{SAE} = 5.0112$	-0.1246	0.0436
SBFA-ARX MAE	$J_{MAE} = 0.0012$	-0.0037	0.0048
SBFA-ARX MSE	$J_{MSE} = 1.4323\times10^{-6}$	-0.0033	0.0035

Validation was performed by testing (validating) the developed models with the remaining 3000 input-output data points. The time-domain responses and error depicted in Figure 5.5 show that the hub-angle model using MSE had the closest predicted output to the actual output in comparison with using SAE and MAE. The numerical results outlined in Table 5.2 show that the SBFA-based model using MSE had the lowest optimum J (1.2637×10^{-5}) and smallest predicted range, e.g. [-0.0027, 0.1200] compared to using SAE and MAE.

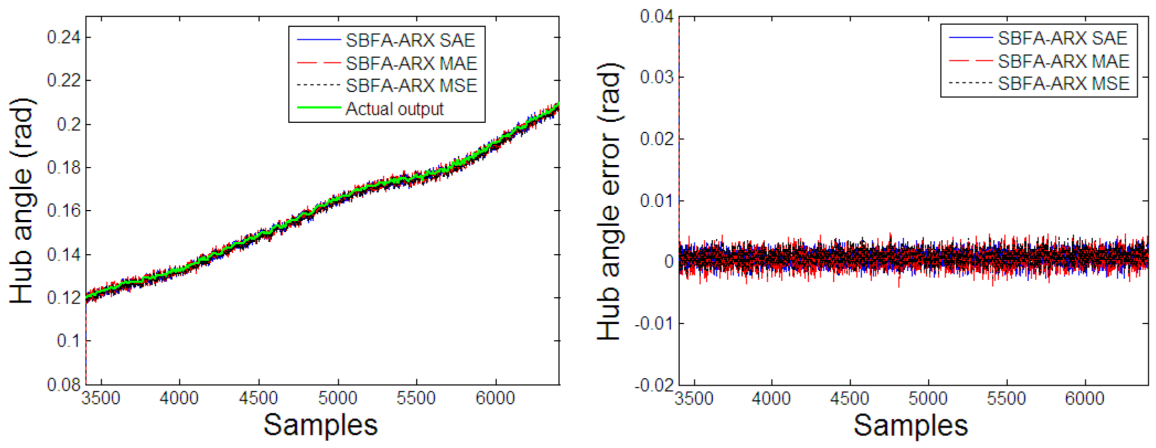

(a) Hub-angle response (b) Error of hub-angle response

Figure 5.5: Time-domain hub-angle response of SBFA-ARX based models using different cost functions in the validation phase

Table 5.2: Numerical results of the cost functions in the validation phase

Algorithm	**Optimum J**	**Range of error ($e(k)$)**	
		Minimum	**Maximum**
SBFA-ARX SAE	$J_{SAE} = 3.5651$	-0.0031	0.1205
SBFA-ARX MAE	$J_{MAE} = 0.0013$	-0.0040	0.1205
SBFA-ARX MSE	$J_{MSE} = 1.2637 \times 10^{-5}$	-0.0027	0.1200

The preliminary results suggest that MSE is suitable for the modelling process of the models, i.e. hub-angle, hub-velocity and end-point acceleration because it can remove large prediction error.

5.6.2. Hub-angle model

A. Modelling phase of hub-angle model

For hub-angle modelling, a 6th order ARX structure model with $b_0 = 0$ was selected, following investigations with various model orders for best results. Thus there are 12 parameters to optimise using BFAs. The initial values of BFA parameters were set up as follow:

❖ $p = 12$	❖ $N_c = 30$	❖ $N_{re} = 5$	❖ $N_{ed} = 3$
❖ $S = 6$	❖ $N_s = 4$	❖ $S_r = {}^{S}/_{2}$	❖ $p_{ed} = 0.25$

The initial positions of bacteria were selected randomly across the search space and MSE was used as the cost function. For SBFA, various chemotactic step size values were apllied in the optimisation process and the best optimum J of 14.323×10^{-7}, was achieved when the chemotactic step size $C(i)$ was equal to 0.0035. For LABFA, QABFA and EABFA, all parameters, i.e. c_{max}, b, d and g, were selected by trial and error and the best performance was achieved when the adaptable chemotactic step size values were as formulated for LABFA, QABFA and EABFA as:

$$C_{al}(i) = \frac{0.02}{1+\frac{1}{0.0245|J(i)|}} \tag{5.7}$$

$$C_{aq}(i) = \frac{0.02}{1+\frac{1}{10^{-3}\left((0.3J(i))^2+0.3|J(i)|\right)}} \tag{5.8}$$

$$C_{ae}(i) = \frac{0.02}{1+\frac{1}{0.03e^{10^{-3}|J(i)|}}} \tag{5.9}$$

These allow the chemotactic step size change adaptively in the range [0, 0.02]. For FABFA, seven-Gaussian fuzzy membership functions were used both in input and output and these are depicted in Figures 5.6(a) and 5.6(b) respectively. All parameters, i.e. m and σ were also selected by trial and error. Fuzzy rules, relating input to output in the form of fuzzy surface depicted in Figure 5.6(c), were formulated as:

$$\begin{array}{llll} R_1 & : & \text{IF } |J(i)| \text{ is ES THEN } C_{af}(i) \text{ is ES} & (1) \\ R_2 & : & \text{IF } |J(i)| \text{ is VS THEN } C_{af}(i) \text{ is VS} & (0.5) \\ R_3 & : & \text{IF } |J(i)| \text{ is S THEN } C_{af}(i) \text{ is S} & (0.6) \\ R_4 & : & \text{IF } |J(i)| \text{ is M THEN } C_{af}(i) \text{ is M} & (1) \\ R_5 & : & \text{IF } |J(i)| \text{ is B THEN } C_{af}(i) \text{ is B} & (1) \\ R_6 & : & \text{IF } |J(i)| \text{ is VB THEN } C_{af}(i) \text{ is VB} & (1) \\ R_7 & : & \text{IF } |J(i)| \text{ is EB THEN } C_{af}(i) \text{ is EB} & (1) \end{array} \quad (5.10)$$

The fuzzy surface shows that the fuzzy adaptable chemotactic step size for every bacterium $C_{af}(i)$ is in relation to the value of $|J(i)|$.

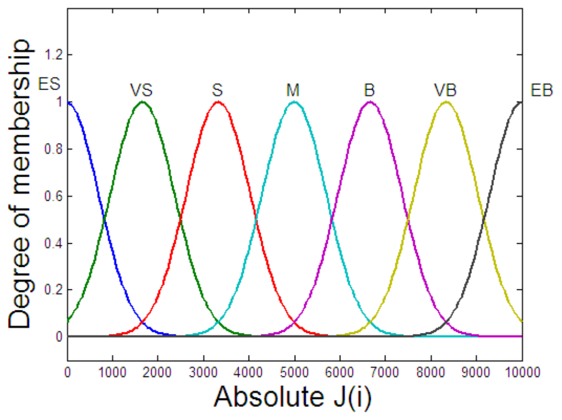

(a) Input: $|J(i)|$

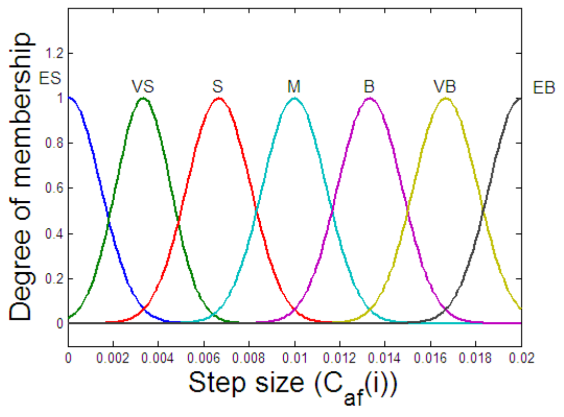

(b) Output: $C_{af}(i)$

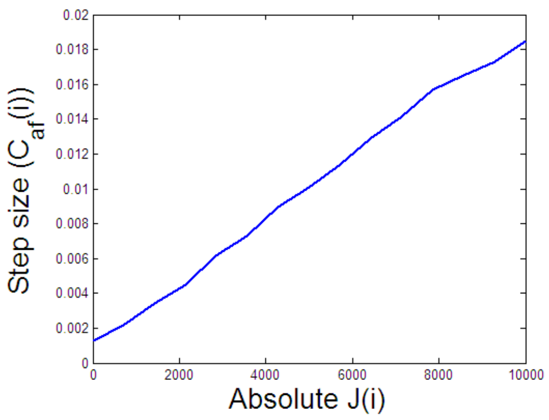

(c) Fuzzy surface

Figure 5.6: Fuzzy membership function and surface of FABFA for hub-angle model in the modelling phase

The numerical results presented in Table 5.3 show that all four proposed algorithms were able to achieve better step size with EABFA achieving has the best optimum J, i.e. 1.1807×10^{-7}, and also the smallest error range, e.g. [-0.0011, 0.0014]. Also all four proposed algorithms had faster convergence speed (able to converge in 178 steps) compared to SBFA, which converged in 327 steps.

Table 5.3: Numerical results of hub-angle models for the algorithms in modelling phase

Algorithm	$C(i)$ **range**	**Convergence (steps)**	**Optimum J**	**Range of error ($e(k)$)**	
				Minimum	**Maximum**
SBFA-ARX	0.0035	327	14.323×10^{-7}	-0.0033	0.0035
LABFA-ARX	[0.0012, 0.02]	178	3.5950×10^{-7}	-0.0017	0.0018
QABFA-ARX	[2.8232×10^{-6}, 0.02]	178	4.1589×10^{-7}	-0.0017	0.0023
EABFA-ARX	[5.8276×10^{-4}, 0.02]	178	$\mathbf{1.1807 \times 10^{-7}}$	**-0.0011**	**0.0014**
FABFA-ARX	[0.0013, 0.0182]	178	3.6375×10^{-7}	-0.0019	0.0021

The convergence plots and optimum J bar chart of all algorithms are depicted in Figure 5.7(a) and Figure 5.7(b) respectively. The time-domain hub-angle responses and error depicted in Figure 5.7(c) and Figure 5.7(d) respectively show that the hub-angle response of all models resulted by BFAs were able to mimic the actual output. However, SBFA-based model had the biggest error range.

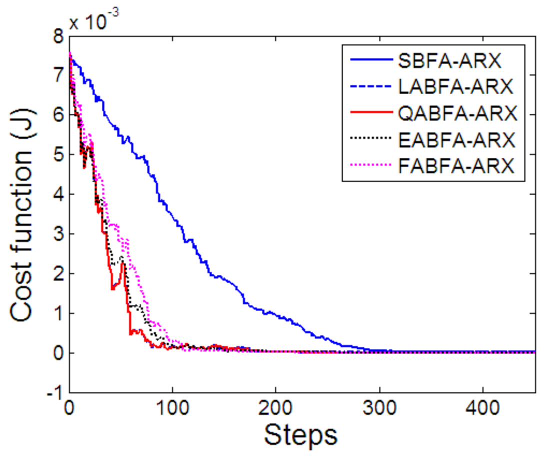

(a) Convergence plots

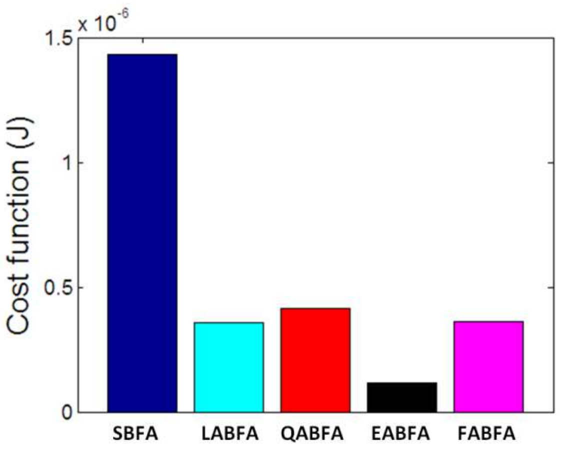

(b) Optimum J

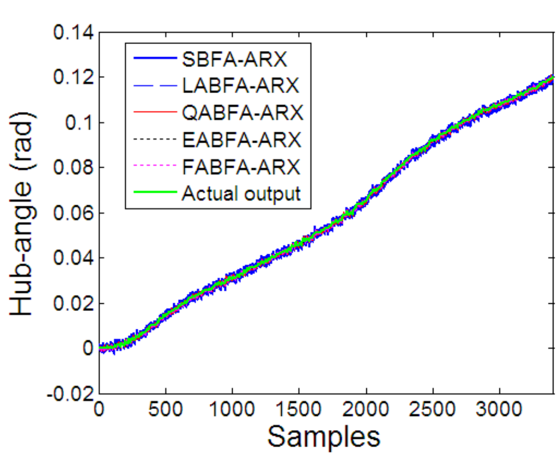

(c) Time-domain response

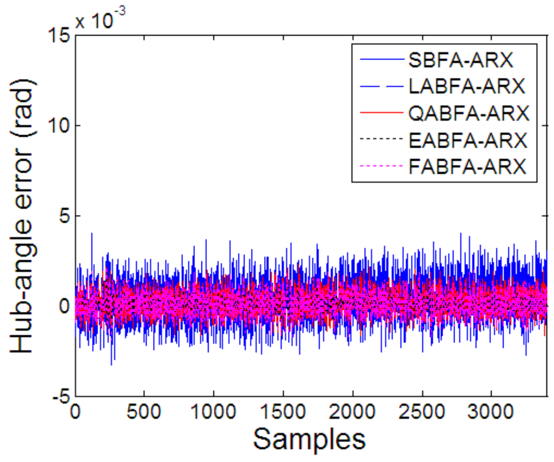

(d) Error

Figure 5.7: Simulation results for hub-angle model in the modelling phase

The discrete transfer functions constructed from the optimal parameters resulted with the algorithms with a sampling time of 0.001 seconds are given as:

$$H(z)_{SBFA} = \frac{-0.0028z^5+0.0000135z^4-0.003z^3-0.0017z^2+0.0046z+0.0011}{z^6-0.2281z^5-0.2285z^4-0.0739z^3-0.1651z^2-0.1654z-0.1347} \tag{5.11}$$

$$H(z)_{LABFA} = \frac{-0.000137z^5+0.0028z^4+0.000237z^3+0.000152z^2+0.000595z+0.000924}{z^6-0.1322z^5-0.2964z^4-0.0265z^3-0.3079z^2-0.1400z-0.0965} \tag{5.12}$$

$$H(z)_{QABFA} = \frac{0.0000124z^5-0.0020z^4+0.0015z^3+0.000364z^2-0.0002098z-0.0015}{z^6-0.1810z^5-0.2307z^4-0.2065z^3-0.1336z^2-0.1569z-0.0901} \tag{5.13}$$

$$H(z)_{EABFA} = \frac{-0.000316z^5+0.000553z^4-0.000202z^3+0.000342z^2+0.000529z+0.000357}{z^6-0.1843z^5-0.1628z^4-0.1137z^3-0.362z^2-0.1444z-0.0326} \tag{5.14}$$

$$H(z)_{FABFA} = \frac{-0.016z^5-0.000871437z^4-0.00029026z^3-0.0008816z^2+0.0022z+0.0005856}{z^6-0.1725z^5-0.0949z^4-0.0789z^3-0.3678z^2-0.2092z-0.0769} \tag{5.15}$$

B. Validation phase of hub-angle model

The hub-angle models were validated using the remaining 3000 pairs of input-output data. It was noticed from the numerical results presented in Table 5.4 that the cost function values for hub-angle validating process achieved were 8.2637×10^{-5}, 1.2273×10^{-5}, 1.1292×10^{-5}, 1.1836×10^{-5} and 1.13572×10^{-5} for SBFA-ARX, LABFA-ARX, QABFA-ARX, EABFA-ARX and FABFA-ARX models respectively. These cost function values suggest that ABFA-based models achieved better validating results than SBFA-based model with QABFA-ARX achieving the best optimum J value and EABFA-ARX with the smallest prediction error range, e.g. [-0.0012, 0.1200].

Table 5.4: Numerical results of hub-angle models for the algorithms in the validation phase

Algorithm	**Optimum J**	**Range of error ($\boldsymbol{e(k)}$)**	
		Minimum	**Maximum**
SBFA-ARX	8.2637×10^{-5}	-0.0027	0.1200
LABFA-ARX	1.2273×10^{-5}	-0.0017	0.1200
QABFA-ARX	$\mathbf{1.1292 \times 10^{-5}}$	-0.0019	0.1200
EABFA-ARX	1.1836×10^{-5}	**-0.0012**	**0.1200**
FABFA-ARX	1.13572×10^{-5}	-0.0022	0.1202

The optimum J of the algorithms in the validation phase is depicted in Figure 5.8(a). The time-domain hub-angle responses and error for the validating phase depicted in Figure 5.8(b) and Figure 5.8(c) show that all the models were able to mimic the measured output well but SBFA-based model had the largest prediction error range. The pole-zero diagram and correlation tests are depicted in Figures 5.9-5.13 for SBFA, LABFA, QABFA, EABFA and FABFA-based models respectively. It is noticed that all the models were stable, all poles of the transfer function were inside the unit circle, and the correlation functions were within the 95 % confidence interval. One or more zeros were outside the unit circle indicating non-minimum phase behaviour.

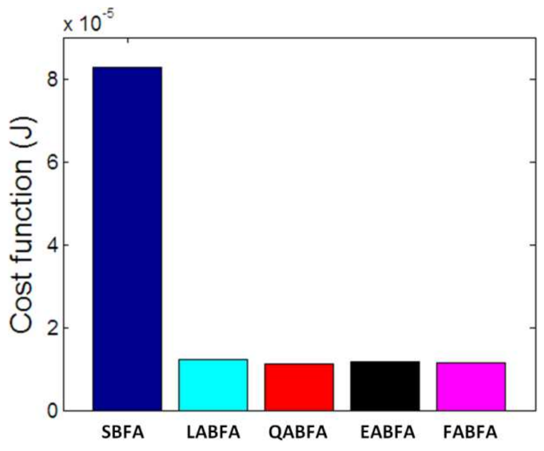

(a) Optimum cost function

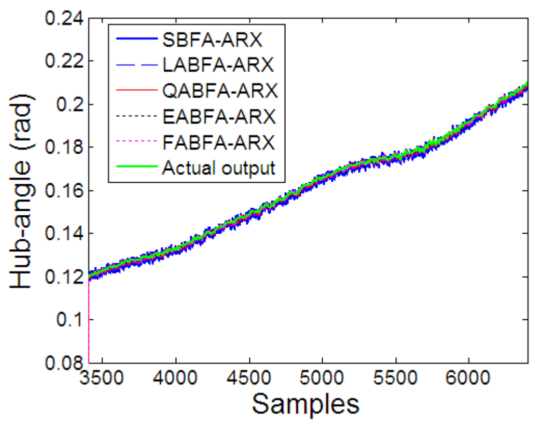

(b) Time-domain response

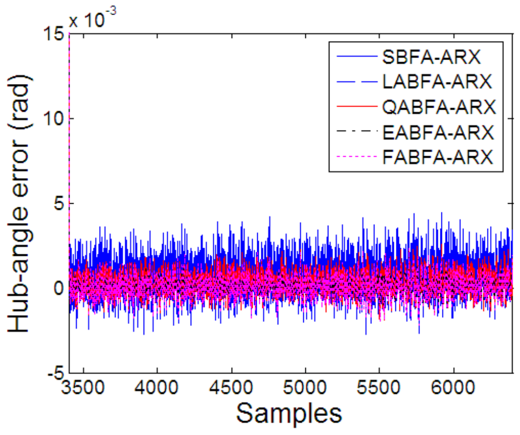

(c) Error

Figure 5.8: Simulation results of the algorithms for hub-angle model in the validation phase

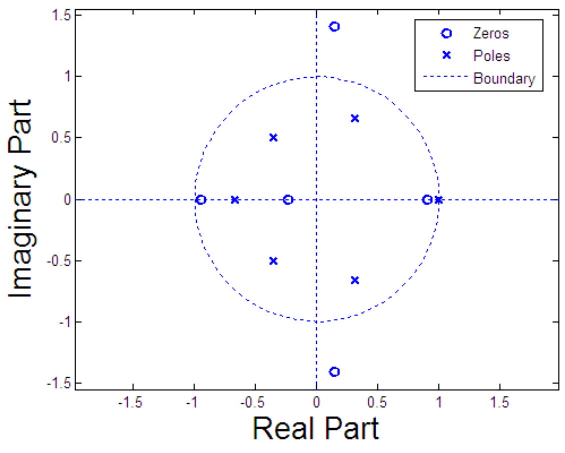

(a) Pole-zero diagram

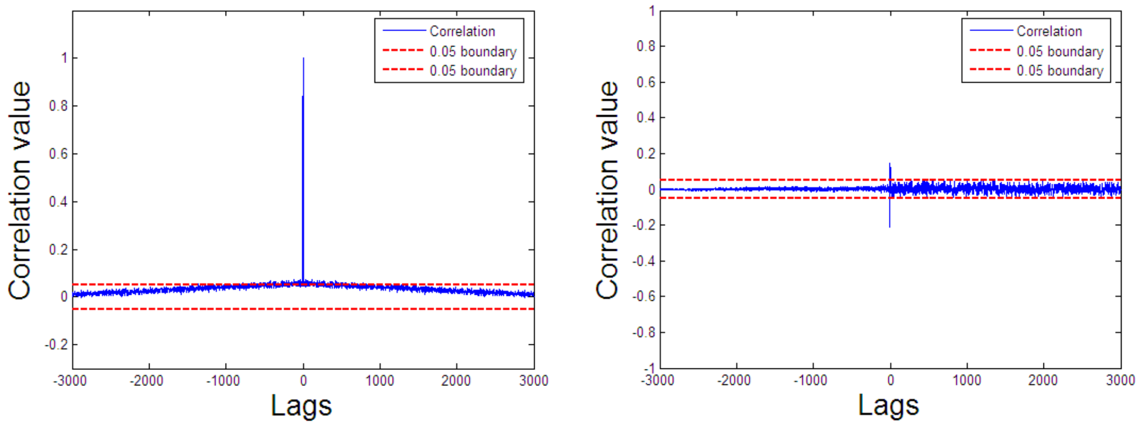

(b) $\phi_{\varepsilon\varepsilon}(\tau)$ (c) $\phi_{u\varepsilon}(\tau)$

Figure 5.9: Validation test for SBFA-ARX for hub-angle model

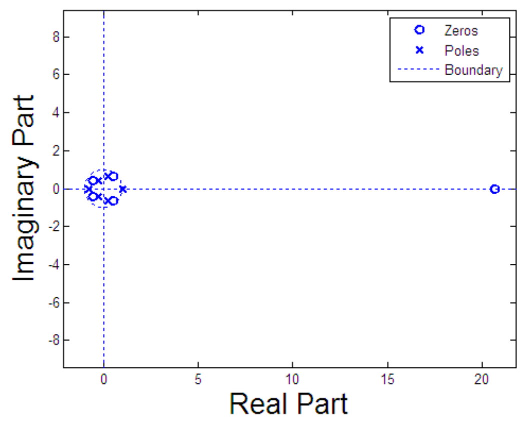

(a) Pole-zero diagram

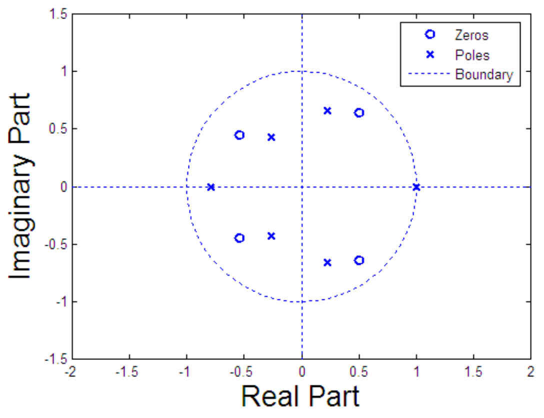

(b) Pole-zero diagram (zoomed)

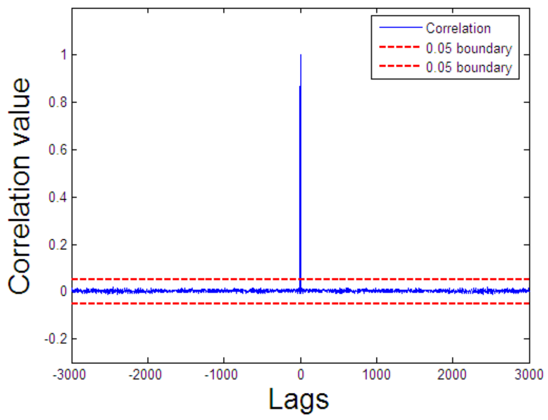

(c) $\phi_{\varepsilon\varepsilon}(\tau)$

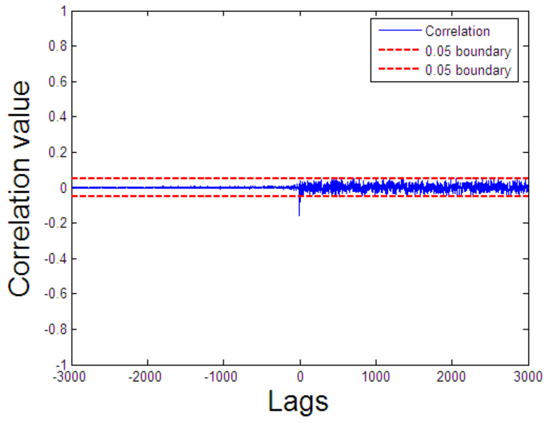

(d) $\phi_{u\varepsilon}(\tau)$

Figure 5.10: Validation test for LABFA-ARX for hub-angle model

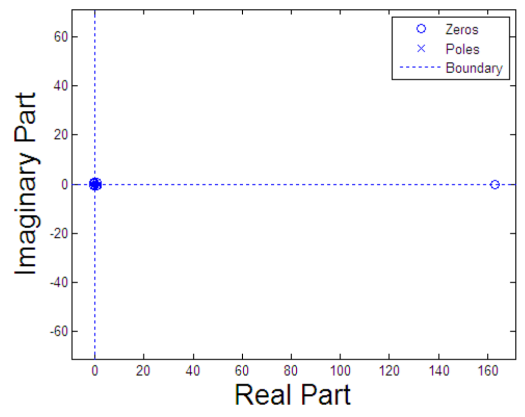

(a) Pole-zero diagram

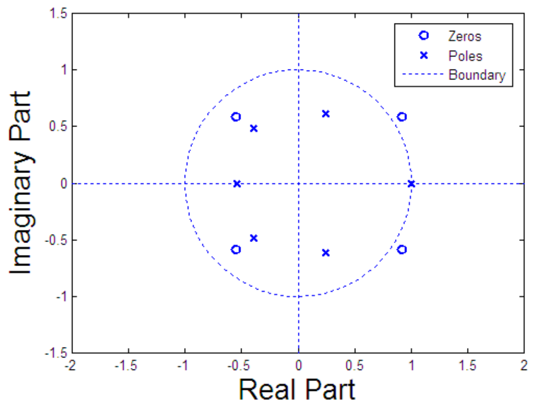

(b) Pole-zero diagram (zoomed)

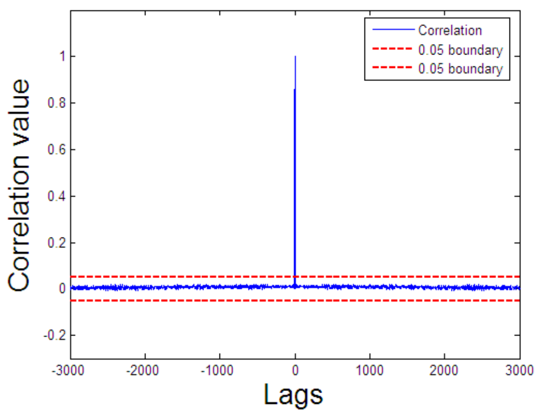

(c) $\phi_{\varepsilon\varepsilon}(\tau)$

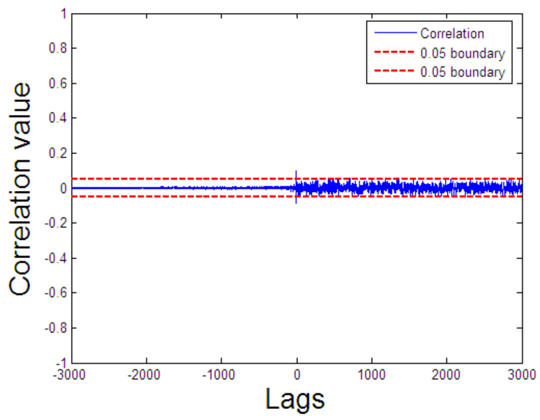

(d) $\phi_{u\varepsilon}(\tau)$

Figure 5.11: Validation test for QABFA-ARX for hub-angle model

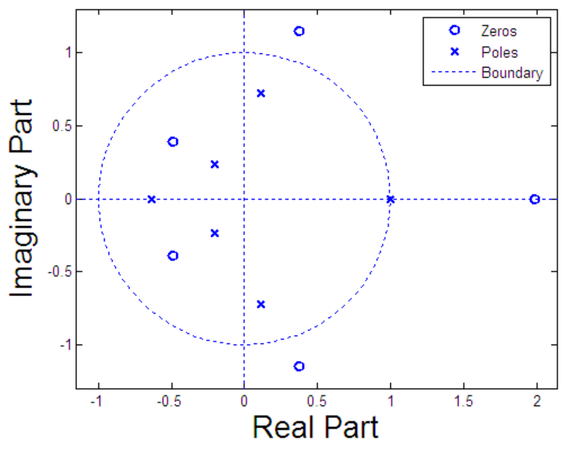

(a) Pole-zero diagram

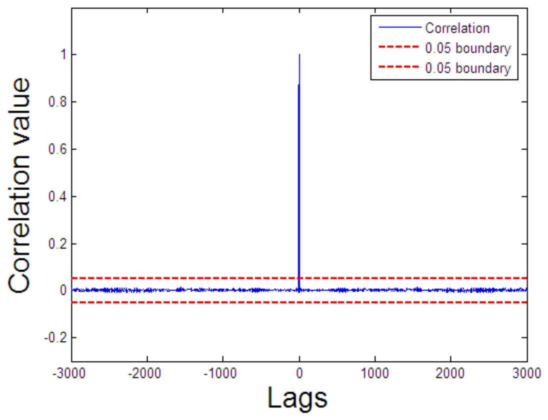

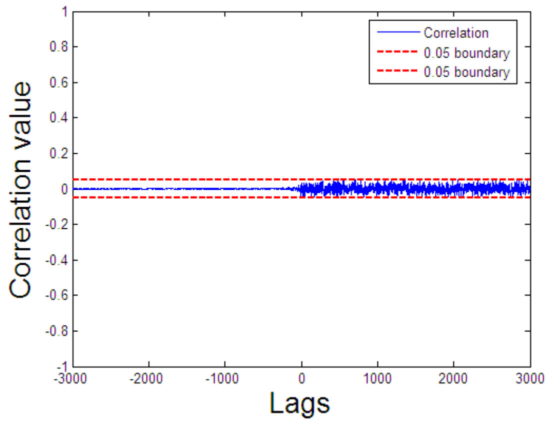

(b) $\phi_{\varepsilon\varepsilon}(\tau)$ (c) $\phi_{u\varepsilon}(\tau)$

Figure 5.12: Validation test for EABFA-ARX for hub-angle model

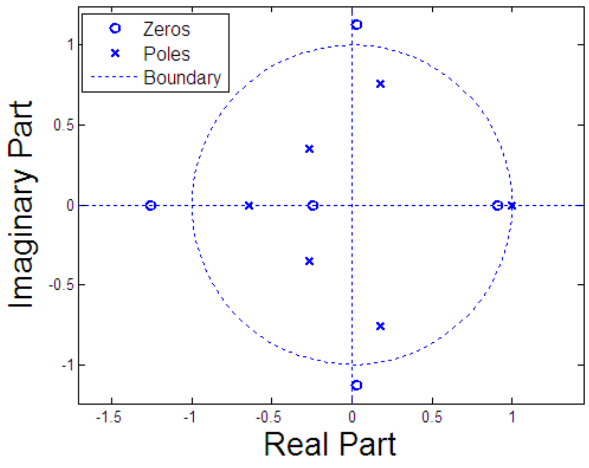

(a) Pole-zero

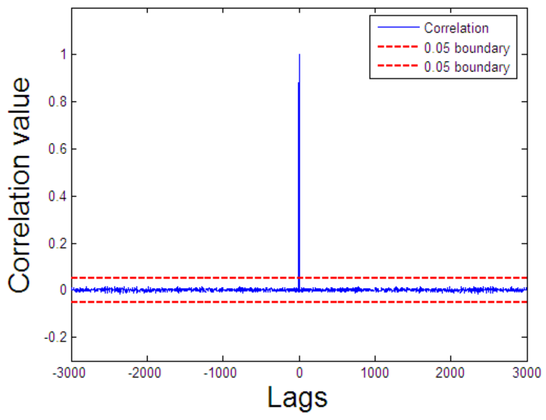

(b) $\phi_{\varepsilon\varepsilon}(\tau)$

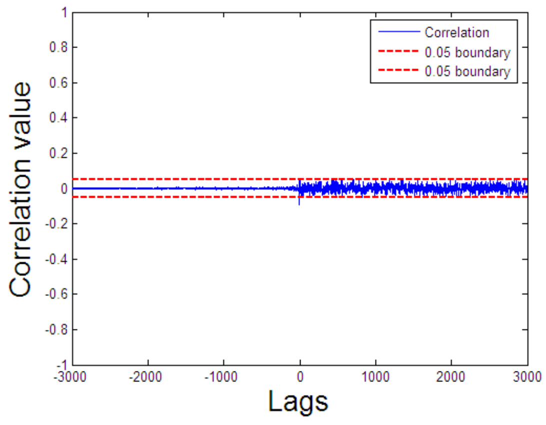

(c) $\phi_{u\varepsilon}(\tau)$

Figure 5.13: Validation test of FABFA-ARX for hub-angle model

5.6.3. Hub-velocity modelling

A. Hub-velocity model in modelling phase

Hub-velocity is the first differential of the hub-angle. Because in this work hub-angle was modelled using 6th order model, here for hub-velocity modelling, a 5th order ($N = M = 5$) ARX model was used. With coefficient $b_0 = 0$, thus, there are ten parameters to optimise using BFAs:

- Five coefficients for previous actual output samples: $a_1, \dots, a_5$
- Five coefficients for previous input samples: $b_1, \dots, b_5$

The initial value of BFAs were selected as:

❖ $p = 10$	❖ $N_c = 20$	❖ $N_{re} = 3$	❖ $N_{ed} = 3$
❖ $S = 6$	❖ $N_s = 3$	❖ $S_r = S/2$	❖ $p_{ed} = 0.25$

The initial positions of bacteria were selected randomly and the MSE was used as the cost function. Various chemotactic step size values were used in the simulations for SBFA. However, the best cost function value J of 0.04191, was achieved when the chemotactic step size was equal to 0.011. For LABFA, QABFA and FABFA, the parameters and settings for c_{max}, b, d and g were chosen by trial and error and the optimum cost function value J was achieved with the adaptable chemotactic step sizes:

$$C_{al}(i) = \frac{0.2}{1+\frac{1}{0.1|J(i)|}} \tag{5.16}$$

$$C_{aq}(i) = \frac{0.1}{1+\frac{1}{0.1\left(\left(J(i)\right)^2+|J(i)|\right)}} \tag{5.17}$$

$$C_{ae}(i) = \frac{0.1}{1+\frac{1}{0.1e^{(|J(i)|)}}} \tag{5.18}$$

For FABFA, seven Gaussian membership functions were used for input and output with the parameters m and σ selected by trial and error. The fuzzy membership functions for input and output are depicted in Figure 5.14(a) and Figure 5.14(b) respectively. Fuzzy rules, relating the input and output in the form of fuzzy surface depicted in Figure 5.14(c), were formulated as:

R_1	:	IF $\lvert J(i)\rvert$ is ES THEN $C_{af}(i)$ is ES	(1)	
R_2	:	IF $\lvert J(i)\rvert$ is VS THEN $C_{af}(i)$ is VS	(0.1)	
R_3	:	IF $\lvert J(i)\rvert$ is S THEN $C_{af}(i)$ is S	(0.4)	
R_4	:	IF $\lvert J(i)\rvert$ is M THEN $C_{af}(i)$ is M	(1)	(5.19)
R_5	:	IF $\lvert J(i)\rvert$ is B THEN $C_{af}(i)$ is B	(1)	
R_6	:	IF $\lvert J(i)\rvert$ is VB THEN $C_{af}(i)$ is VB	(1)	
R_7	:	IF $\lvert J(i)\rvert$ is EB THEN $C_{af}(i)$ is EB	(1)	

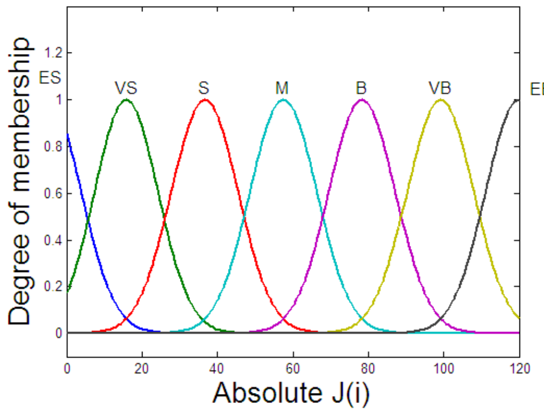

(a) Input: $|J(i)|$

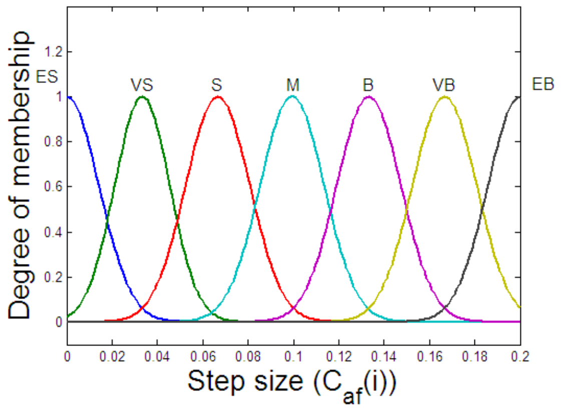

(b) Output: $C_{af}(i)$

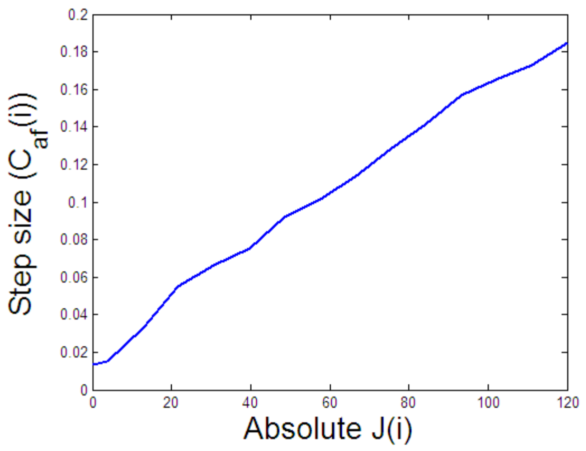

(c) Fuzzy surface

Figure 5.14: Fuzzy membership functions and surface of FABFA for hub-velocity model in modelling phase

The numerical results presented in Table 5.5 show that optimum cost function values for the hub-velocity modelling achieved were 0.04191, 0.0105, 0.0152, 0.0099 and 0.0142 for SBFA–ARX, LABFA–ARX, QABFA–ARX, EABFA–ARX and FABFA–ARX respectively. It can be noticed that all proposed algorithms were able to achieve better cost function values with EABFA achieving the best J value. Also, all proposed algorithms had smaller prediction error range than SBFA.

Table 5.5: Numerical results of hub-velocity models for the algorithms in modelling phase

Algorithm	$C(i)$ **range**	**Convergence (steps)**	**Optimum J**	**Range of error ($e(k)$)**	
				Minimum	**Maximum**
SBFA-ARX	0.011	80	0.04191	-3.0802	0.1157
LABFA-ARX	$[2.1044\times10^{-4}$, 0.2]	3	0.0105	-3.3814	0.1228
QABFA-ARX	$[1.5448\times10^{-4}$, 0.1]	3	0.0152	-3.7806	0.1652
EABFA-ARX	[0.0092, 0.1]	3	**0.0099**	-2.8620	0.2443
FABFA-ARX	[0.0123,]	5	0.0142	-2.7681	0.3142

The optimum J values achieved by the algorithms are depicted in Figure 5.15(a). The convergence plots depicted in Figure 5.15(b) show that ABFA-ARX models were able to converge to optimum value faster (3 and 5 steps) than SBFA-ARX (80 steps). The actual and predicted hub velocity responses and prediction error are depicted in Figure 5.15(c) and Figure 5.15(d) respectively. The transfer functions of the hub-velocity models formulated with a sampling period of 0.001 seconds are as follows:

$$H(z)_{SBFA} = \frac{0.0582z^4+0.1696z^3+0.0202z^2-0.1312z+0.15}{z^5-0.5446z^4-0.0931z^3-0.1818z^2-0.2230z+0.0446} \tag{5.20}$$

$$H(z)_{LABFA} = \frac{0.2008z^4+0.0139z^3-0.1166z^2-0.1158z+0.0191}{z^5-0.5483z^4+0.0649z^3-0.3726z^2+0.0534z-0.1974} \tag{5.21}$$

$$H(z)_{QABFA} = \frac{-0.0505z^4+0.1813z^3-0.1258z^2-0.09z+0.2246}{z^5-0.2896z^4-0.2817z^3-0.0062z^2-0.1829z-0.2398} \tag{5.22}$$

$$H(z)_{EABFA} = \frac{0.2606z^4+0.12z^3+0.0327z^2+0.2736z+0.2665}{z^5-0.649z^4-0.4783z^3+0.0057z^2+0.0366z+0.0862} \tag{5.23}$$

$$H(z)_{FABFA} = \frac{-0.0061z^4+0.0366z^3+0.1527z^2-0.0175z-0.1595}{z^5-0.7587z^4-0.6782z^3+0.2250z^2+0.2401z-0.0258} \tag{5.24}$$

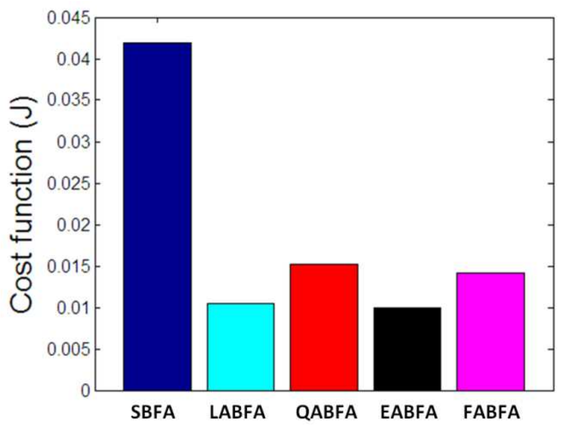

(a) Optimum *J*

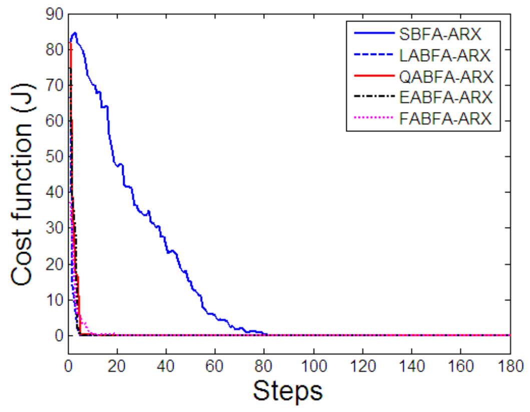

(b) Convergence plots

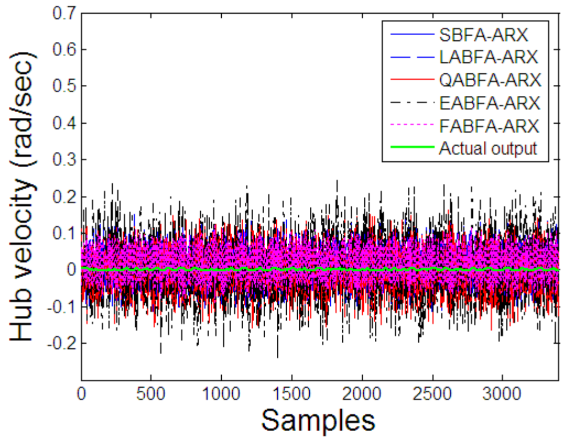

(c) Time-domain response

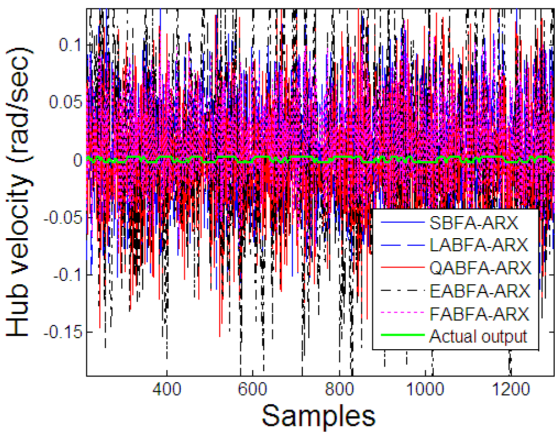

(d) Time-domain response (zoomed)

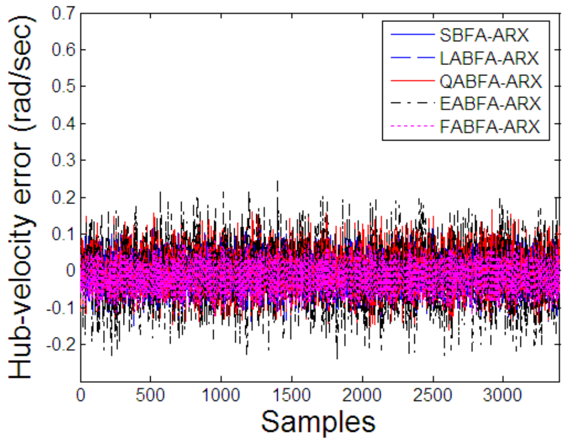

(e) Time-domain error

Figure 5.15: Simulation results of the algorithms for hub-velocity model in modelling phase

B. Hub-velocity model in validation phase

The numerical results presented in Table 5.6 show that cost function values achieved for hub-velocity model in the validating phase were 0.0485, 0.0311, 0.0340, 0.0291 and 0.0266 for SBFA-ARX, LABFA-ARX, QABFA-ARX, EABFA-ARX and FABFA-ARX models respectively. It is noticed that all models developed based on the proposed ABFA-ARX models were able to achieve better optimum J values than SBFA-ARX with FABFA-ARX achieving the best optimum J value.

Table 5.6: Numerical results of hub-velocity models for the algorithms in validation phase

Algorithm	**Optimum J**	**Range of error ($e(k)$)**	
		Minimum	**Maximum**
SBFA-ARX	0.0485	-0.5574	0.3598
LABFA-ARX	0.0311	-0.5468	0.1285
QABFA-ARX	0.0340	-0.5655	0.1711
EABFA-ARX	0.0291	-0.5424	0.12204
FABFA-ARX	0.0266	-0.5622	0.13166

A comparison of the optimum J values achieved by the algorithms in the validation phase can be seen in the graphical illustration depicted in Figure 5.16(a). Both actual and predicted time-domain responses and error achieved in the validating phase are depicted in Figure 5.16(b) and Figure 5.16(c). Pole-zero plots and correlation test results for SBFA-ARX, LABFA-ARX, QABFA-ARX and FABFA-ARX are depicted in Figure 5.17-Figure 5.21 respectively. These figures show that all the models were stable because all poles lie inside the unit circle and the models exhibit non-minimum phase behaviour since one or more zeros are outside the unit circle. The validation test results using correlation functions show that all models are acceptable.

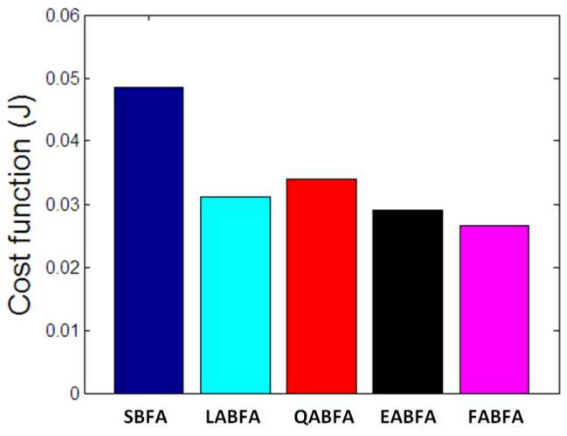

(a) Optimum *J*

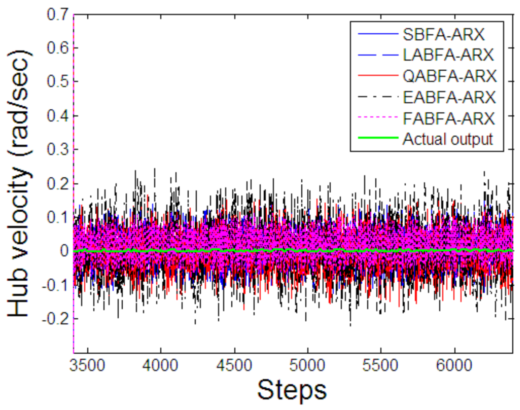

(b) Time-domain responses

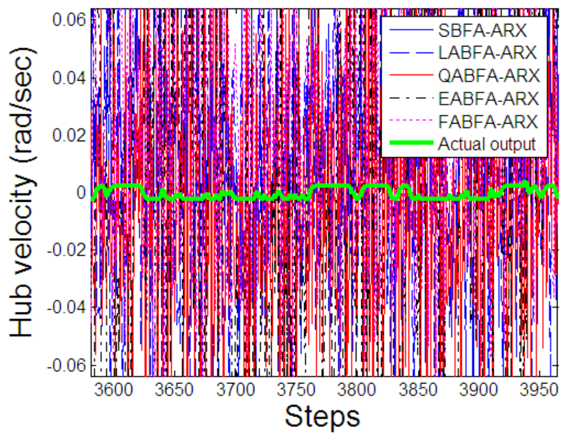

(c) Time-domain responses (zoomed)

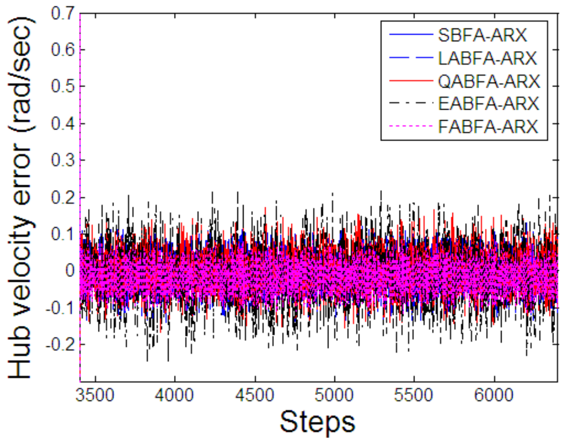

(d) Time-domain error

Figure 5.16: Simulation results of the algorithms for hub-velocity model in validation phase

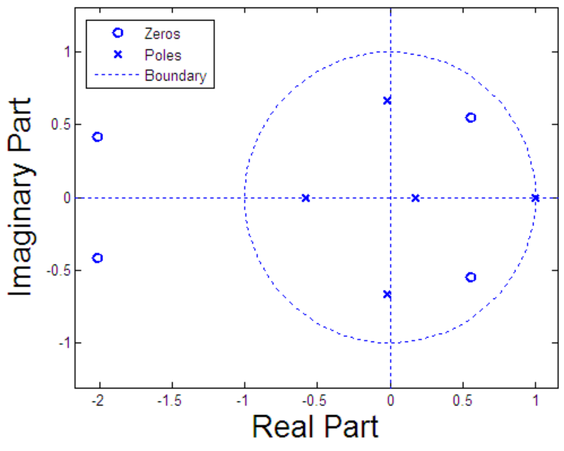

(a) Pole-zero diagram

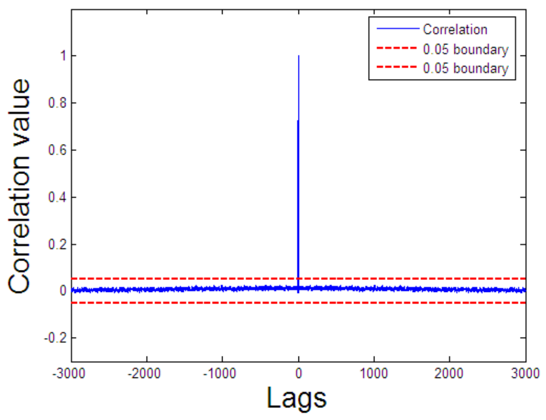

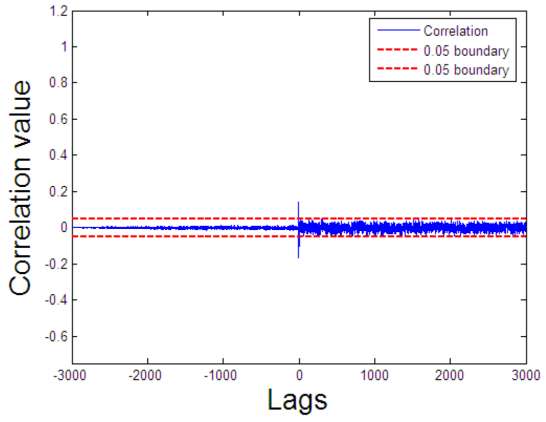

(b) $\phi_{\varepsilon\varepsilon}(\tau)$ (c) $\phi_{u\varepsilon}(\tau)$

Figure 5.17: Validation test for SBFA-ARX for hub-velocity modelling

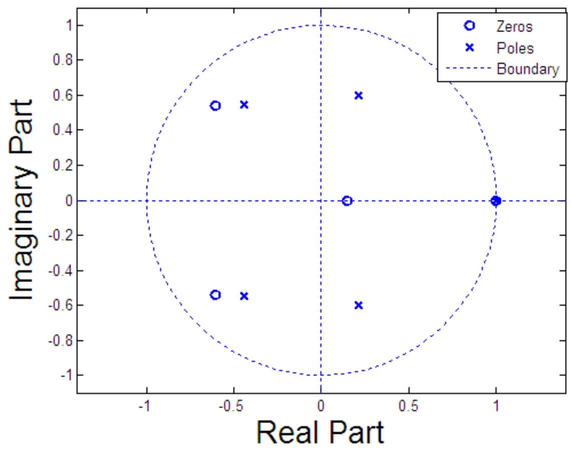

(a) Pole-zero diagram

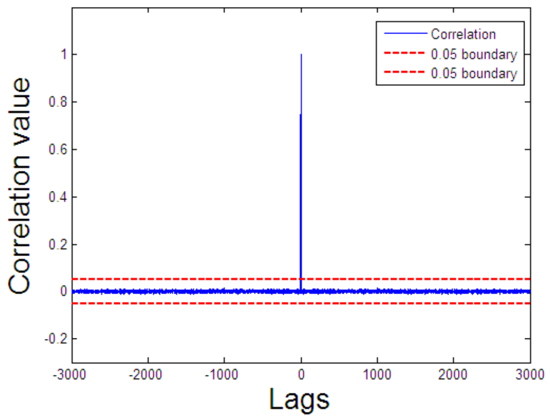

(b) $\phi_{\varepsilon\varepsilon}(\tau)$

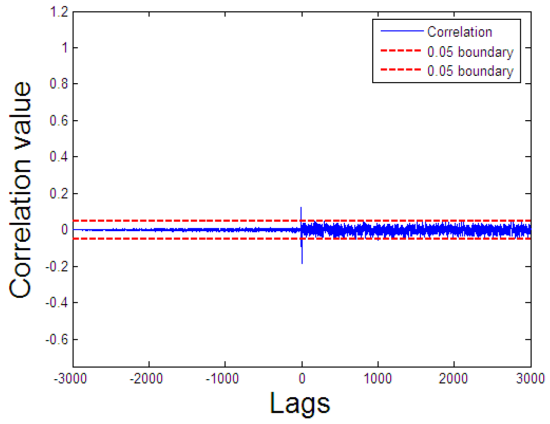

(c) $\phi_{u\varepsilon}(\tau)$

Figure 5.18: Validation test for LABFA-ARX for hub-velocity modelling

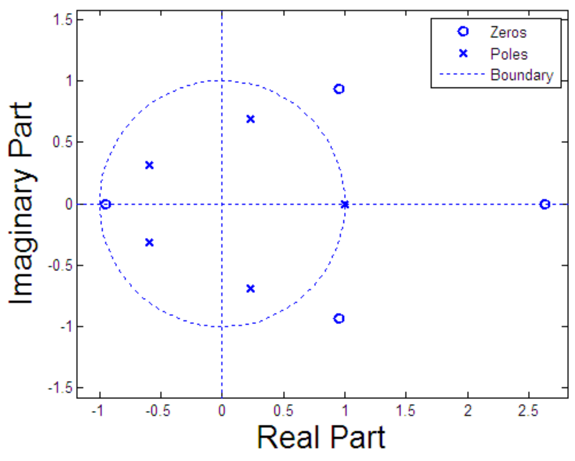

(a) Pole-zero diagram

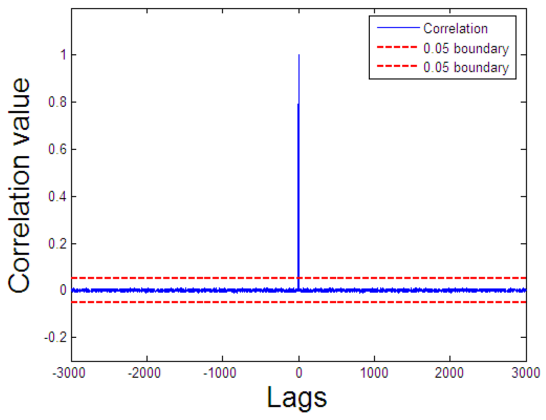

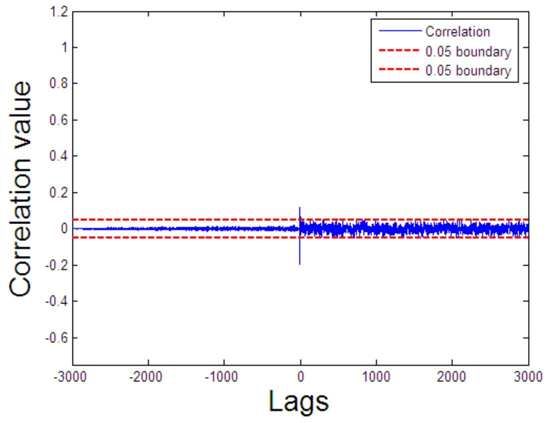

(b) $\phi_{\varepsilon\varepsilon}(\tau)$ (c) $\phi_{u\varepsilon}(\tau)$

Figure 5.19: Validation test for QABFA-ARX for hub-velocity modelling

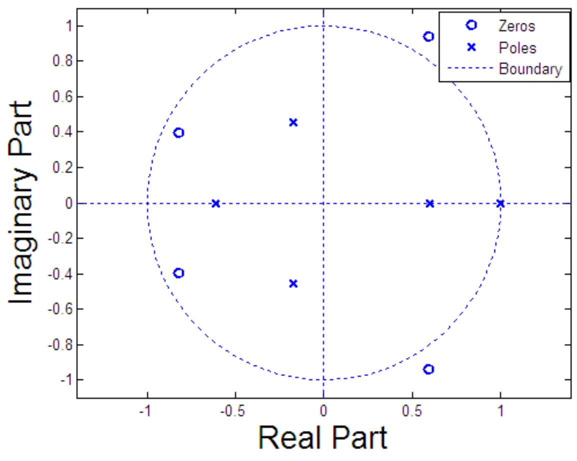

(a) Pole-zero diagram

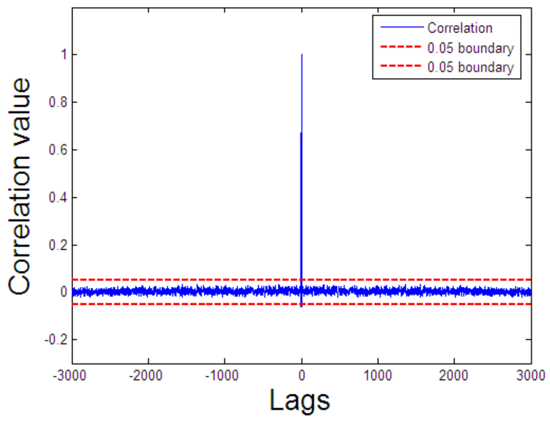

(b) $\phi_{\varepsilon\varepsilon}(\tau)$

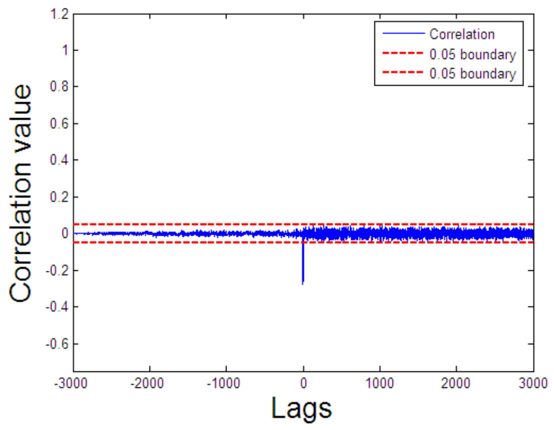

(c) $\phi_{u\varepsilon}(\tau)$

Figure 5.20: Validation test for EABFA-ARX for hub-velocity modelling

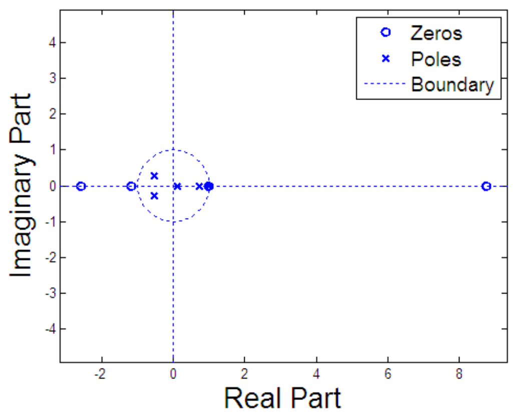

(a) Pole-zero diagram

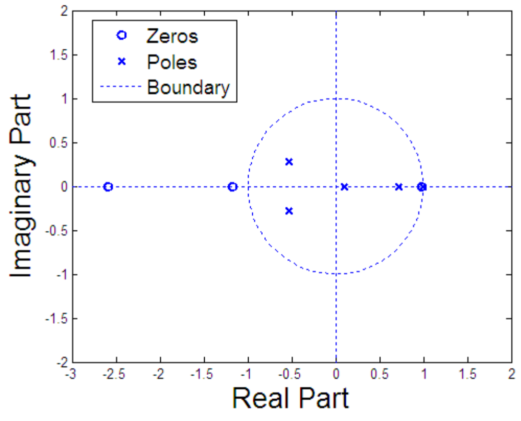

(b) Pole-zero diagram (zoomed)

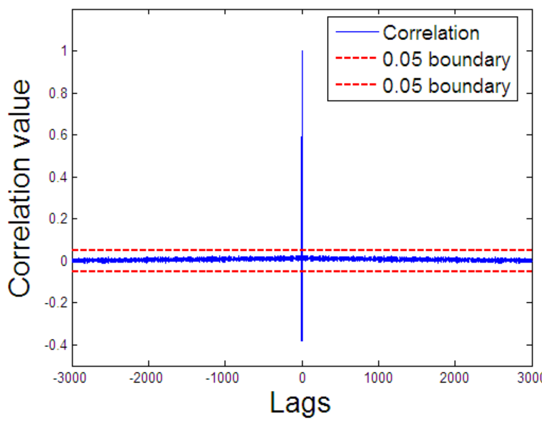

(c) $\phi_{\varepsilon\varepsilon}(\tau)$

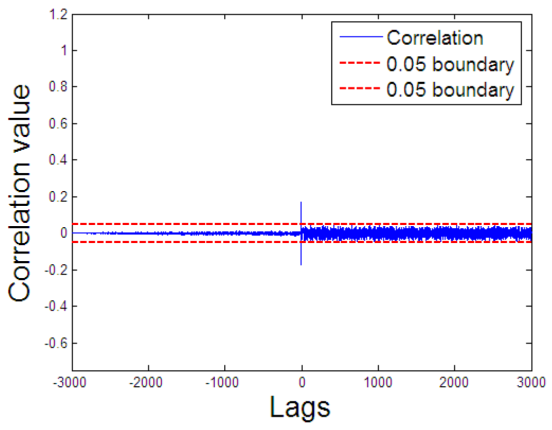

(d) $\phi_{u\varepsilon}(\tau)$

Figure 5.21: Validation test for FABFA-ARX for hub-velocity modelling

5.6.4. End-point acceleration

A. End-point acceleration model in modelling phase

Because of the nature of the flexible manipulator, vibration will occur when the manipulator is moved. Each frequency resonance mode of vibration is represented by a pair of complex conjugate poles. In the current work, the first three resonance modes are investigated, thus three pairs of complex conjugate poles are needed. Hence, a 6th order structure model is needed to cover three pairs of complex conjugate poles. Moreover, the system contains rigid body dynamics. Accordingly, an 8th order ($N = M = 8$) ARX model was used to represent the end-point acceleration model. With coefficient $b_0 = 0$, thus there are 16 parameters to optimise:

- Eight parameters for previous actual output samples: $a_1, \dots, a_8$
- Eight parameters for previous input samples: $b_1, \dots, b_8$

The initial parameters of BFA are selected as follows:

❖ $p = 16$	❖ $N_c = 30$	❖ $N_{re} = 3$	❖ $N_{ed} = 3$
❖ $S = 6$	❖ $N_s = 3$	❖ $S_r = {}^{S}/_{2}$	❖ $p_{ed} = 0.25$

The initial positions of bacteria were selected randomly in the nutrient media. After testing various chemotactic step size values for SBFA, the best cost function value J was achieved when the chemotactic step size was equal to 0.03. For LABFA, QABFA and EABFA, the parameters c_{max}, b, d and g were chosen by trial and error and the best optimum J values were achieved with adaptable chemotactic step sizes set up as:

$$C_{al}(i) = \frac{1.4}{1+\frac{1}{|J(i)|}} \tag{5.25}$$

$$C_{aq}(i) = \frac{1.4}{1+\frac{1}{0.95\left((J(i))^2+|J(i)|\right)}} \tag{5.26}$$

$$C_{ae}(i) = \frac{0.1}{1+\frac{1}{0.45e^{40|J(i)|}}} \tag{5.27}$$

For FABFA, seven-Gaussian membership function were used for input and output with the parameters m and σ chosen by trial and error. The fuzzy membership functions used in the investigation for input and output are depicted in Figure 5.22(a) and Figure 5.22(b) respectively. Fuzzy rules were formulated as:

$$\begin{array}{llll}
R_1 & : & \text{IF } |J(i)| \text{ is ES THEN } C_{af}(i) \text{ is ES} & (1) \\
R_2 & : & \text{IF } |J(i)| \text{ is VS THEN } C_{af}(i) \text{ is VS} & (0.1) \\
R_3 & : & \text{IF } |J(i)| \text{ is S THEN } C_{af}(i) \text{ is S} & (0.8) \\
R_4 & : & \text{IF } |J(i)| \text{ is M THEN } C_{af}(i) \text{ is M} & (1) \\
R_5 & : & \text{IF } |J(i)| \text{ is B THEN } C_{af}(i) \text{ is B} & (1) \\
R_6 & : & \text{IF } |J(i)| \text{ is VB THEN } C_{af}(i) \text{ is VB} & (1) \\
R_7 & : & \text{IF } |J(i)| \text{ is EB THEN } C_{af}(i) \text{ is EB} & (1)
\end{array} \tag{5.28}$$

The rules thus formulated resulted the fuzzy surface depicted in Figure 5.22(c). The fuzzy surface reveals that fuzzy chemotactic step size for every bacterium $C_{af}(i)$ changes depending on the absolute cost function value $|J(i)|$.

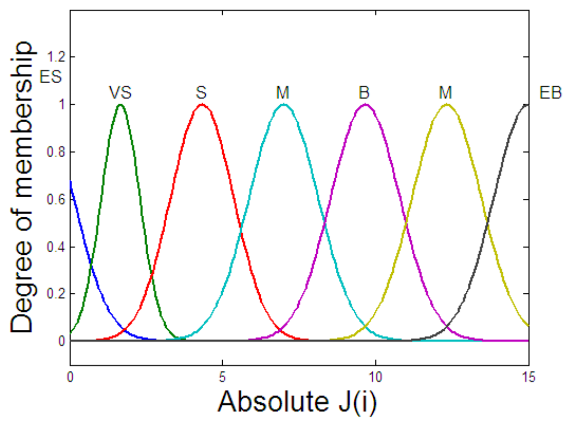

(a) Input: $|J(i)|$

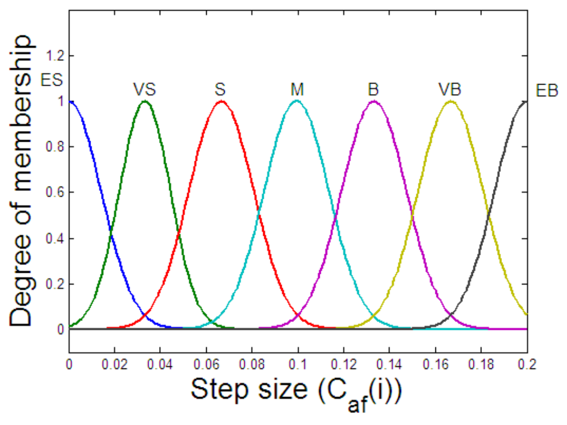

(b) Output: $C_{af}(i)$

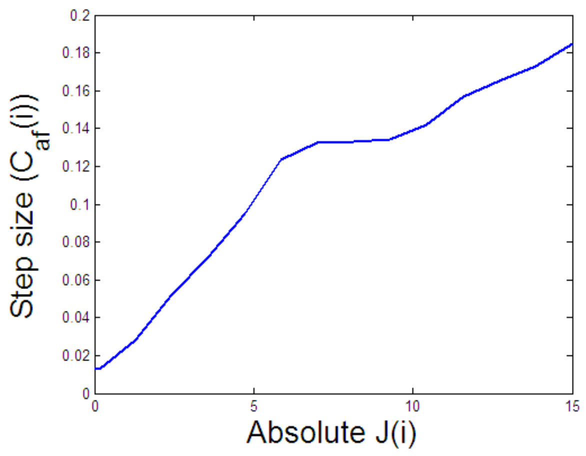

(c) Fuzzy surface

Figure 5.22: Fuzzy membership function and surface of FABFA for end-point acceleration models for the algorithms in modelling phase

Numerical results outlined in Table 5.7 reveal that optimum values of the cost function achieved in the modelling phase were 0.00744, 0.0025, 0.0025, 0.0032 and 0.00142 for SBFA-ARX, LABFA-ARX, QABFA-ARX, EABFA-ARX and FABFA-ARX respectively. These cost function values indicate that ABFA-ARX models were able to result in better optimum J than SBFA-ARX with the best optimum J achieved by FABFA-ARX.

Table 5.7: Numerical results of end-point acceleration models for the algorithms in modelling phase

Algorithm	$C(i)$ **range**	**Convergence (steps)**	**Optimum** J	**Range of error ($e(k)$)**	
				Minimum	**Maximum**
SBFA-ARX	0.03	260	0.00744	-0.3302	0.3485
LABFA-ARX	[0.0039, 1.4]	190	0.0025	-0.3137	0.3485
QABFA-ARX	[0.0036, 1.4]	190	0.0025	-0.3119	0.3449
EABFA-ARX	[0.0350, 0.1]	230	0.0032	**-0.3159**	**0.2391**
FABFA-ARX	[0.0136, 0.185]	190	**0.00142**	-0.3145	0.2816

A comparison of these optimum J values is depicted in Figure 5.23(a). The convergence plots depicted in Figure 5.23(b) show that ABFA-ARX models were able to converge to the optimum value faster (190 and 230 steps) than SBFA-ARX (260 steps). The actual and predicted time-domain end-point acceleration and error depicted in Figure 5.23(c) and Figure 5.23(d) show that in general all models were able to mimic the actual output but SBFA-ARX resulted the largest prediction error range [-0.3302, 0.3485] among them. The corresponding power spectral density (PSD) depicted in Figure 5.23(e) show that the first three resonance frequencies of the system found in these modelling were 11.67 Hz, 36.96 Hz and 64.22 Hz for the 1st mode, 2nd mode and 3rd mode respectively. The transfer functions of the models formulated with a sampling period of 0.001 seconds are as follows:

$$H(z)_{SBFA} = \frac{-0.0448z^7+0.0011z^6+0.0835z^5-0.0131z^4+0.0626z^3+0.0745z^2-0.0061z+0.0395}{z^8-1.1208z^7-0.1264z^6+0.0470z^5+0.4877z^4-0.0549z^3-0.1263z^2+0.1034z-0.1305} \quad (5.29)$$

$$H(z)_{LABFA} = \frac{0.0532z^7+0.0111z^6-0.0156z^5-0.0497z^4-0.0243z^3-0.0043z^2-0.0197z+0.0077}{z^8-1.1125z^7-0.4903z^6+0.6728z^5+0.2052z^4+0.2170z^3-0.0855z^2-0.7243z+0.4867} \quad (5.30)$$

$$H(z)_{QABFA} = \frac{0.0639z^7+0.0043z^6-0.0245z^5-0.0522z^4-0.034z^3-0.0206z^2-0.0251z+0.0159}{z^8-1.1370z^7-0.4776z^6+0.7115z^5+0.1954z^4+0.2074z^3-0.1306z^2-0.6827z+0.4857} \quad (5.31)$$

$$H(z)_{EABFA} = \frac{-0.0787z^7-0.1229z^6-0.0258z^5-0.0191z^4+0.0205z^3-0.0725z^2-0.0084z+0.0802}{z^8-1.5258z^7+0.3594z^6+0.1576z^5+0.186z^4+0.3114z^3-0.6779z^2+0.47z-0.2181} \quad (5.32)$$

$$H(z)_{FABFA} = \frac{-0.0109z^7+0.0110z^6+0.0096z^5+0.0031z^4-0.0307z^3+0.0286z^2+0.0186z-0.0152}{z^8-1.329z^7-0.4773z^6+1.5231z^5-0.5004z^4-0.2164z^3+0.2666z^2-0.3264z+0.1844} \quad (5.33)$$

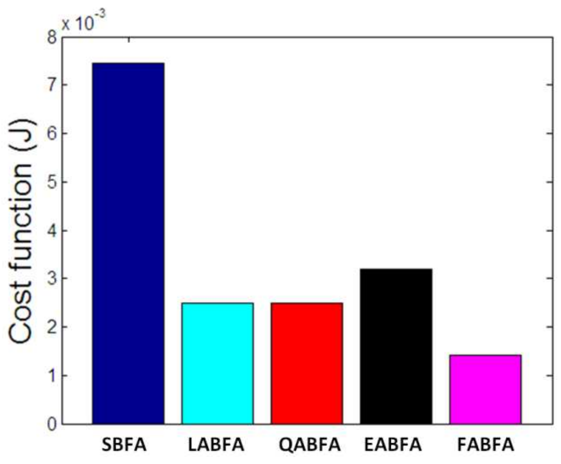

(a) Optimum *J*

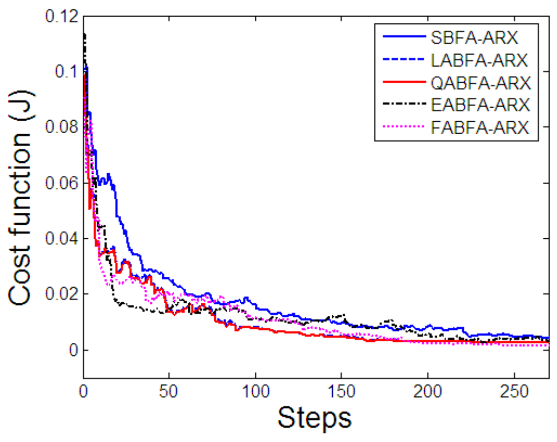

(b) Convergence plots

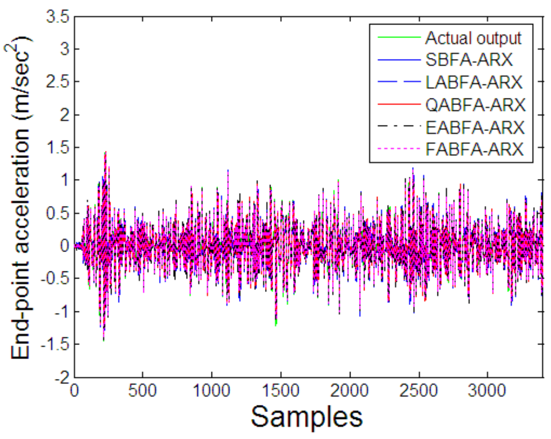

(c) Time-domain responses

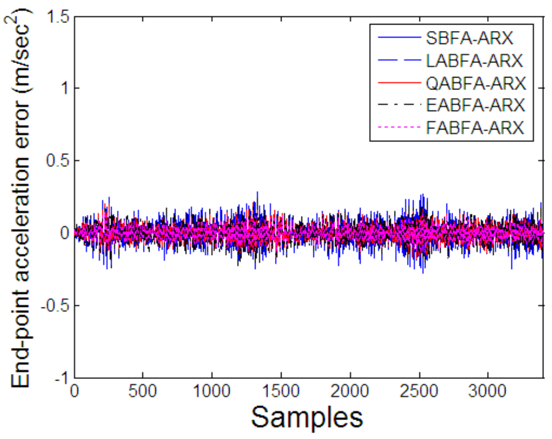

(d) Error

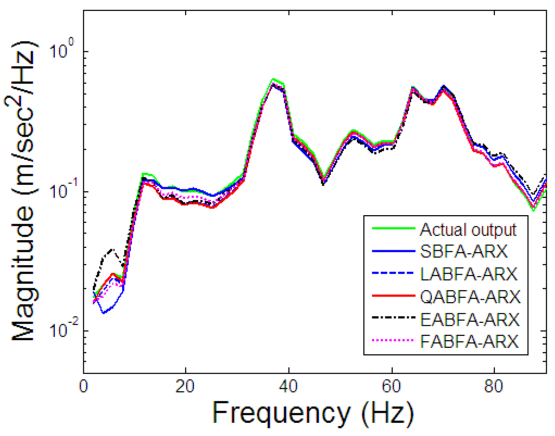

(e) Spectral density

Figure 5.23: Simulation results of end-point acceleration model for the algorithms in modelling phase

B. End-point acceleration model in validation phase

Numerical results presented in Table 5.8 show that the cost function values achieved for end-point acceleration models in the validating phase were 0.0091, 0.0047, 0.0046, 0.0058 and 0.00127 for SBFA-ARX, LABFA-ARX, QABFA-ARX, EABFA-ARX and FABFA-ARX models respectively. Again, these results show that end-point acceleration models based on ABFA-ARX models achieved better optimum J value than SBFA-ARX in the validation phase with FABFA-ARX as the best among them.

Table 5.8: Numerical results of end-point acceleration models for the algorithms in validation phase

Algorithm	**Optimum J**	**Range of error ($\boldsymbol{e(k)}$)**	
		Minimum	**Maximum**
SBFA-ARX	0.0091	-0.3260	0.3545
LABFA-ARX	0.0047	-0.2353	0.3507
QABFA-ARX	0.0046	-0.2355	0.3515
EABFA-ARX	0.0058	-0.2762	0.3420
FABFA-ARX	0.00127	-0.2966	0.3430

A comparison of these optimum J values is illustrated in the bar chart depicted in Figure 5.24(a). The actual and predicted time-domain responses and error in validating phase are depicted in Figure 5.24(b) and Figure 5.24(c) respectively, showing that all the models were able to mimic the actual output but SBFA-ARX model had the largest prediction error range, e.g. [-0.3260, 0.3545]. It is noticed from the PSD depicted in Figure 5.24(e) that the first three resonance frequencies for all the models matched one another; these were at 11.67 Hz, 36.96 Hz and 64.22 Hz for the 1st, 2nd and 3rd modes respectively.

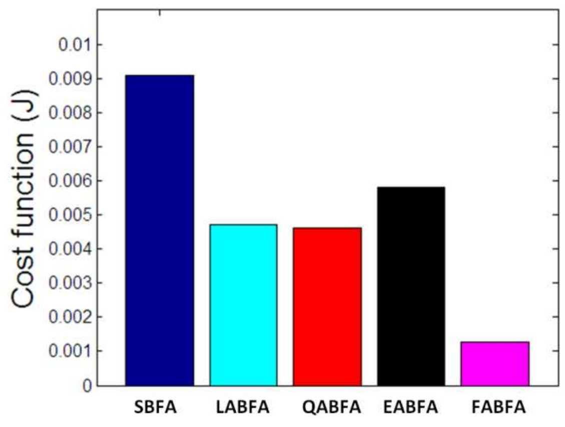

(a) Optimum *J*

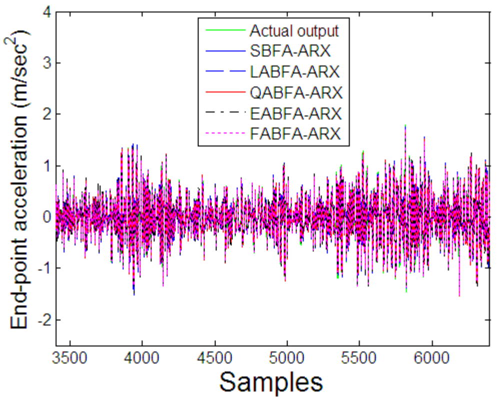

(b) Time-domain responses

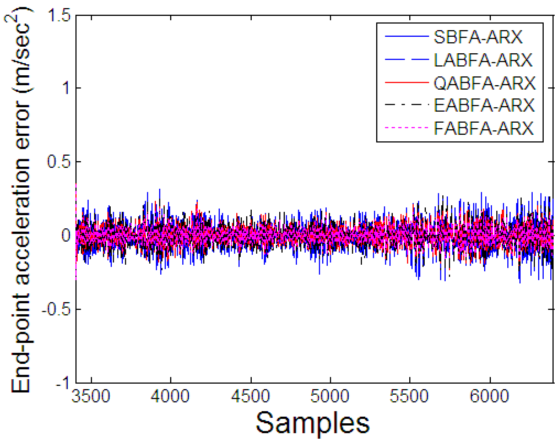

(c) Error

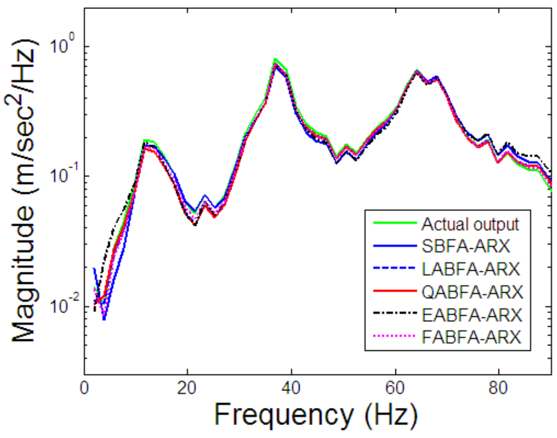

(d) Power spectral density

Figure 5.24: Simulation results of end-point acceleration model for the algorithms in validation phase

The pole-zero diagrams and correlation tests for SBFA-ARX, LABFA-ARX, QABFA-ARX, EABFA-ARX and FABFA-ARX are depicted in Figure 5.25-Figure 5.29 respectively, indicating that all models were stable with non-minimum phase behaviour. The correlation test functions results confirm that the models are acceptable.

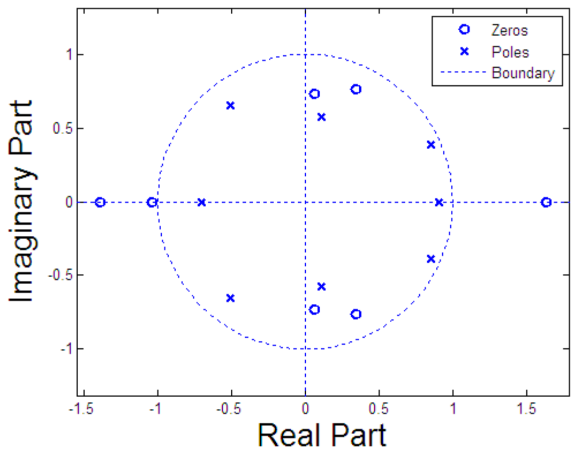

(a) Pole-zero diagram

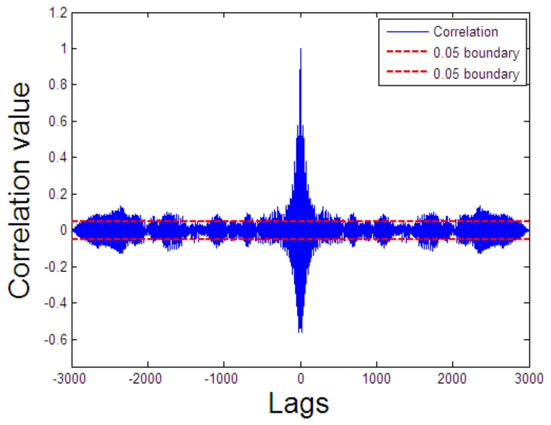

(b) $\phi_{\varepsilon\varepsilon}(\tau)$

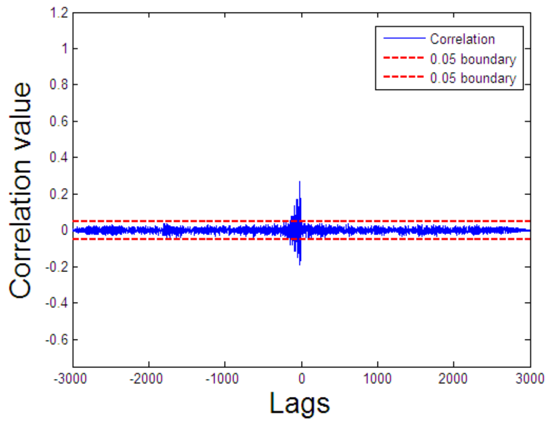

(c) $\phi_{u\varepsilon}(\tau)$

Figure 5.25: Validation test for SBFA-ARX for end-point acceleration model

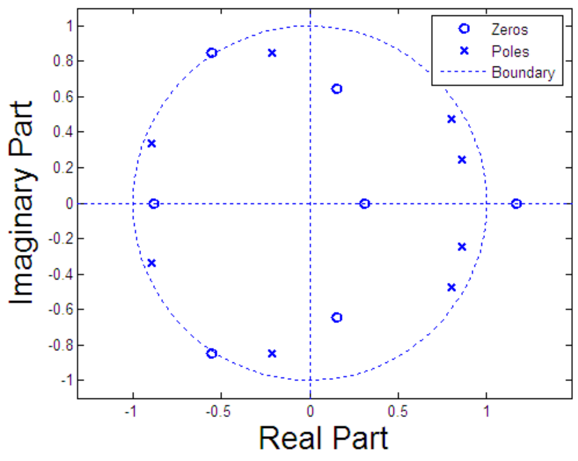

(a) Pole-zero diagram

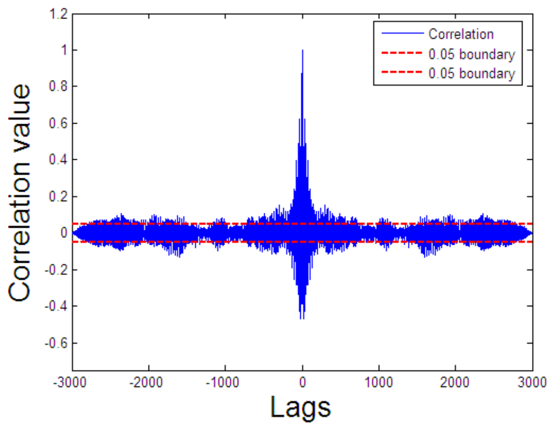

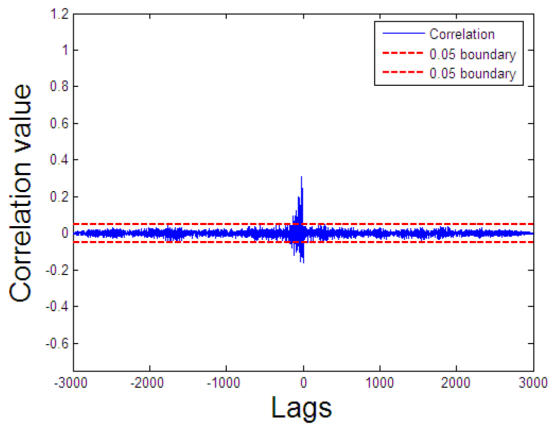

(b) $\phi_{\varepsilon\varepsilon}(\tau)$ (c) $\phi_{u\varepsilon}(\tau)$

Figure 5.26: Validation test for LABFA-ARX for end-point acceleration model

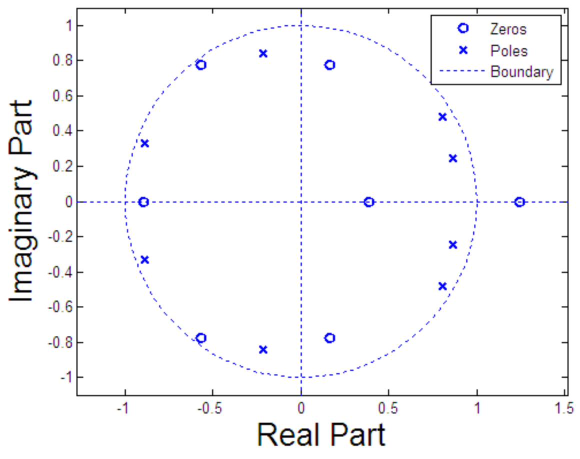

(a) Pole-zero diagram

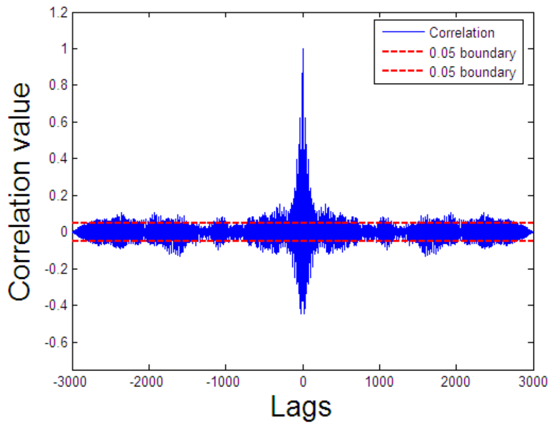

(b) $\phi_{\varepsilon\varepsilon}(\tau)$

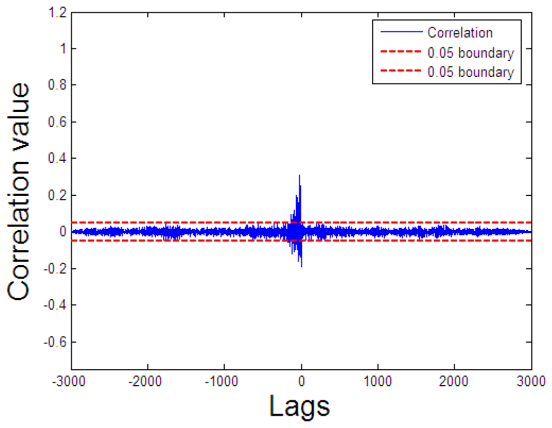

(c) $\phi_{u\varepsilon}(\tau)$

Figure 5.27: Validation test for QABFA-ARX for end-point acceleration model

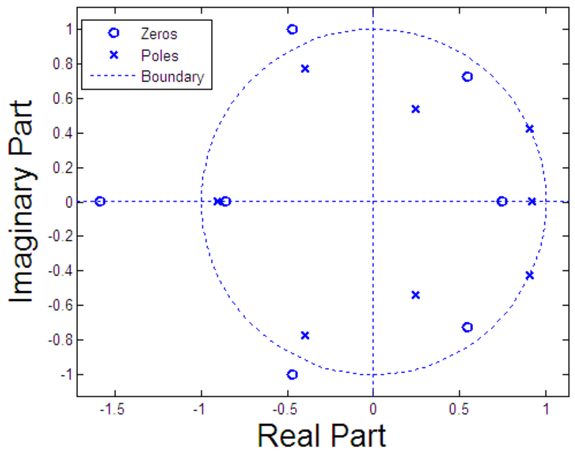

(a) Pole-zero diagram

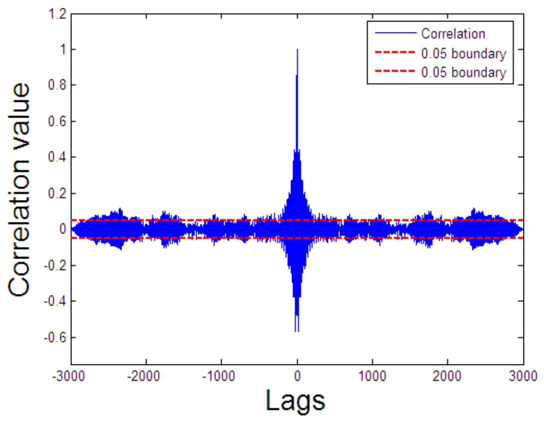

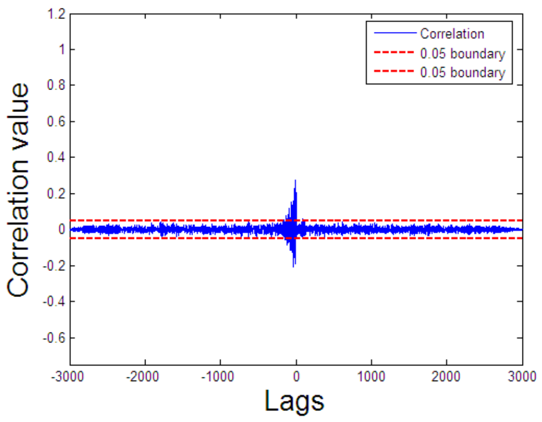

(b) $\phi_{\varepsilon\varepsilon}(\tau)$ (c) $\phi_{u\varepsilon}(\tau)$

Figure 5.28: Validation test for EABFA-ARX for end-point acceleration model

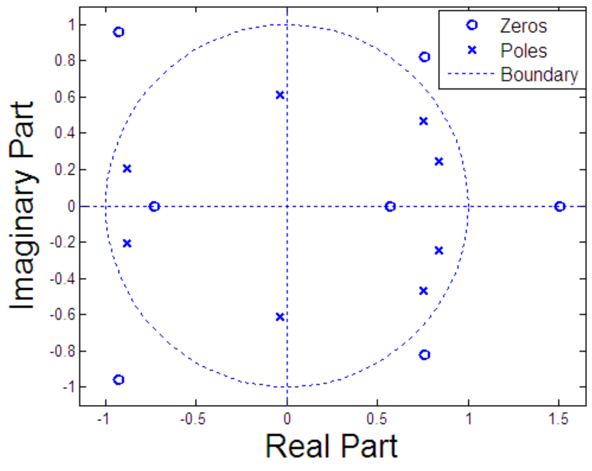

(a) Pole-zero plot

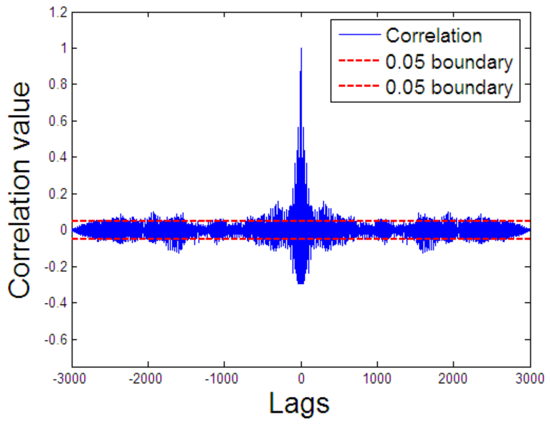

(b) $\phi_{\varepsilon\varepsilon}(\tau)$

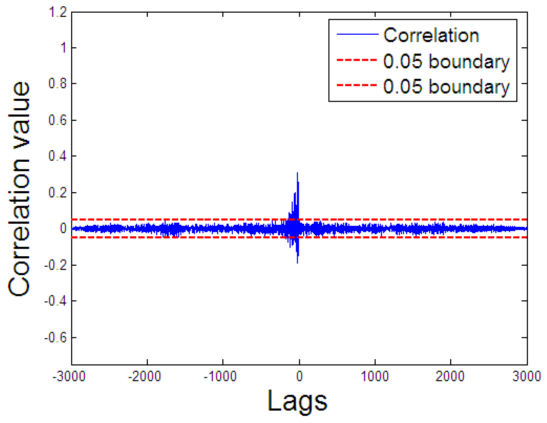

(c) $\phi_{u\varepsilon}(\tau)$

Figure 5.29: Validation test for FABFA-ARX model for end-point acceleration

5.7. Summary

In this work, BFAs with adaptable chemotactic step size have been adopted for modelling a single-link flexible manipulator system. Input-output data pairs have been collected from an experimental single-link flexible manipulator rig and used in developing linear models of the system from input torque to hub-angle, hub-velocity and end-point acceleration. The performances of ABFA-ARX models have been assessed in comparison to SBFA-ARX based on the optimum cost function achieved, convergence speed, time-domain and frequency-domain response. It has been demonstrated that the ABFA-ARX models converge faster and achieve better optimum value, and thus provide better model than SBFA-ARX. Since in the tests presented, SBFA and all proposed ABFA used the same general parameters and the initial positions bacteria were selected randomly in the search space, the better performance ABFA demonstrated must be due to the adaptable chemotactic step size. Further work on modelling will consider combination of BFAs and other intelligent methods such as NN and FL for nonlinear modelling of flexible manipulator systems, and this is presented in Chapters 6.

CHAPTER 6
MODELLING OF FLEXIBLE MANIPULATOR USING NEURAL NETWORKS AND FUZZY LOGIC OPTIMISED BY BACTERIAL FORAGING ALGORITHM

6.1. Introduction

Artificial neural network (ANN) or simply neural network (NN) is a computational method which mimics a biological neural network in the human brain (Hagan et al., 1996). The method involves non-linear processing elements arranged and interconnected in a special structure. NN has several advantages such as massive parallelism, distributed representation and computation, generalisation ability, adaptability, inherent contextual information processing and learning capability (Jain and Mohiuddin, 1996).

The above advantages have inspired researchers to apply NNs wide range of applications such as in modelling durations of syllables (Sreenivasa Rao and Yegnanarayana, 2007), analysing properties of oil shale (Nazzal et al., 2008), estimating sediment in a river (Haghizadeh et al., 2010), selecting vendor supplier (Golmohammadi et al., 2009), forecasting rainfall (Hung et al., 2009), stock performance modelling (Refenes et al., 1993), modelling complex process dynamics (Parlos et al., 1994), crane collision modelling (Garcia-Fernandez et al., 2004), control of flexible manipulators (Sharma et al., 2003; Jnifene and Andrews, 2005), dynamic modelling of a twin rotor system (Aldebrez et al., 2004), modelling and control of flexible structures (Mat Darus and Tokhi, 2005) and adaptive control of robots (Zalzala and Morris, 1991). For application in the areas of flexible manipulator, Talebi et al. (1998) used recurrent NN for modelling flexible manipulators for space applications. Also, multilayer perceptron (MLP) NN with backpropagation learning algorithm and radial basis function (RBF) NN have been utilised for modelling single-link flexible manipulators (Shaheed and Tokhi, 2002).

It can be noted from the literature that the potential drawbacks of these learning algorithms are they potentially getting trapped in the local minima. To overcome being trapped at local minima, researchers have proposed to utilise intelligent approaches, such as genetic algorithm (GA) optimisation, as NN's learning algorithm. Sharma et al. (2003) utilised GA to optimise NN: network architecture, weights, biases and slope parameters of activation function of NN to control flexible manipulators. Ben Omrane and Chatti (2010) used GA to train NN for modelling and controlling a nonlinear system of water level regulation.

It can be noted from the literature that BFA has been used to optimise a NN. Ulagammai et al. (2007) used SBFA for optimising weights and biases of neural network for load forecasting of power systems. Ying et al. (2008) used SBFA for optimising NN for image compression applications. The application of NN optimised by BFA for modelling single-link flexible manipulator system has not been reported yet.

The fuzzy logic (FL) concept was first introduced by Lotfi Zadeh (Zadeh, 1965, 1968, 1973) to model human reasoning from imprecise and incomplete information in the form of rule base. FL maps input to output by using human-like reasoning in the form of rule base which are constructed from a set of IF-THEN operations. Since its introduction, FL has been widely applied in various control application by researchers including in the area of flexible manipulators such as control of a non-linear multivariable chemical processes (Mahfouf et al., 2002), control of a single-link flexible manipulator (Alam and Tokhi, 2007; Jnifene and Andrews, 2005; Siddique, 2002; Siddique and Tokhi, 2006;), control of flexible-link robot (Moudgal et al., 1994), control of robotic system (Sun and Er, 2004) and suppression of vibration of a cantilever beam (Kwak and Sciulli, 1996).

In the area of modelling, FL has been used in a broad range of applications, to mention a few, such as modelling and prediction of maximum daily temperature (Tatli and Sen, 1999), modelling of headgear appliance types for orthodontic patients (Akcam and Takada, 2002), modelling of powder snow avalanches (Barpi, 2004), modelling and control of the air system of a diesel engine (Simani and Bonfe, 2009) and modelling of tumorous cerebral tissues on MRI images (Dou et al., 2005). It is noted from the literature that several works have been carried out on optimising FL using BFA. Alavandar et al. (2010) proposed a hybrid between PSO and BFA and applied it to optimising FL for controlling a two-link rigid-flexible manipulator. Jain and et al. (2009) proposed a hybrid algorithm combining GA, PSO and BFA and then utilised this for optimising PD-like fuzzy pre-compensated control for a two-link rigid-flexible manipulator. Moreover SBFA has been used for optimising membership function parameter of fuzzy model for recognition of handwritten Hindi numerals (Hanmandlu et al., 2007). The literature shows that FL has not been used for modelling of flexible manipulator systems.

In this work, NN and FL optimised by ABFA are proposed and used for modelling a single-link flexible manipulator system. For NN, as a learning algorithm, improved bacterial foraging algorithms are used to optimise neural network's parameters, i.e. weights, biases and slope parameters of activation function. For FL-based, ABFA are used for optimising the weights of every fuzzy rule. Three SISO NN-based and FL-based models are developed to characterise hub-angle, hub-velocity and end-point acceleration responses of flexible manipulators. The objective of the work is to assess the performance of ABFAs in the NN-based and FL-based modelling task in comparison to SBFA. The assessment is based on the optimum cost function value achieved, convergence speed and time-domain response.

6.2. Brief fundamentals of neural network

There are various NN structures proposed, developed and used by researchers (Hagan et. al., 1996) such as multilayer perceptron (MLP), radial basis function (RBF), Hopfield, cellular and adaptive resonance theory (ART). Among them, MLP is one of the most popular structures and used in applications such as pattern recognition, function approximation, system identification, prediction and control, speech and natural language processing (Leondes, 1998; Shaheed, 2000). Thus, in this work MLP is used for modelling single-link flexible manipulator systems.

The general structure of MLP is depicted in Figure 6.1 (Dunne, 2007). The MLP network is constructed from processing units (here represented by circles) called perceptron (neuron) which are fully connected with each other. The neurons in the same layer are not connected to one another. In general there are three layers in MLP: the layer where data are inputted to MLP network is called input layer, the layer from where data are taken from MLP network is called output layer and all layers between input layer and output layers are called hidden layers.

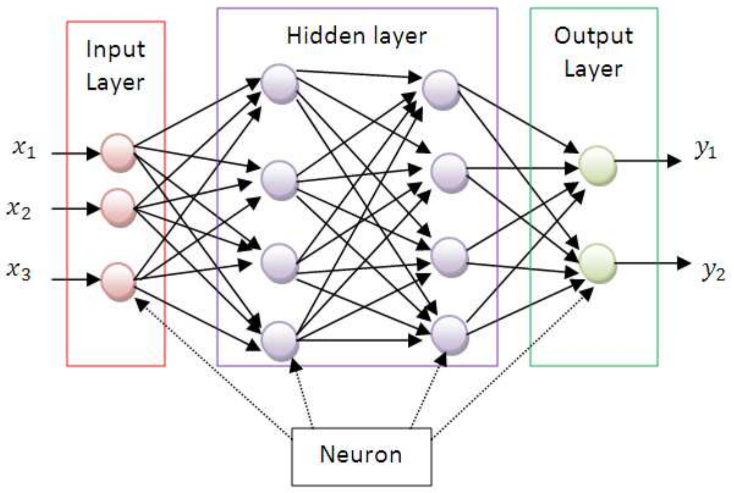

Figure 6.1: General structure of MLP: three input in input layer, 2 hidden layers and two output in output layer

Every neuron in an NN will receive weighted signal and produce output signal by using an activation function. The general structure of a single neuron of NN is depicted in Figure 6.2 (Dunne, 2007), Where $i_1, i_2, \dots, i_n$ are inputs, $w_1, w_2, \dots, w_n$ are weights for every input, b is the threshold (bias) value and $f(x)$ is the activation function.

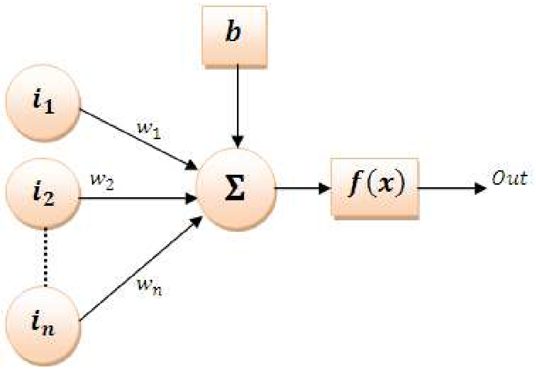

Figure 6.2: A single neuron in NN

The general working mechanism of every neuron can be explained as follow. Firstly, all the inputs are summed up as:

$$x = b + \sum_{v=1}^{v=n} i_v w_v \tag{6.1}$$

Then, the value of x is mapped into output value by using activation function of the neuron. There are various activation function alternatives applicable for NN such as hard limit, symmetric hard limit, linear, log sigmoid, bipolar sigmoid, hyperbolic tangent sigmoid, etc. Compared to other cost functions, hyperbolic tangent sigmoid activation function is able to representi nonlinearity, giving faster learning process and resulting better accuracy while linear activation function offers simplicity and ability to produce output linearly related to the input (Karlik and Olgac, 2010; Negnevitsky, 2005). In general, hyperbolic tangent sigmoid function can be formulated as:

$$f(x) = \frac{e^{ax} - e^{-ax}}{e^{ax} + e^{-ax}} \tag{6.2}$$

where a is parameter that defines the output shape of the function. The shape of hyperbolic tangent sigmoid function for different a values is depicted in Figure 6.3(a). The general formula for linear activation function is given as:

$$f(x) = cx \tag{6.3}$$

where c is parameter that defines the slope of the linear function. The shape of the linear activation function for different c values is depicted in Figure 6.3(b).

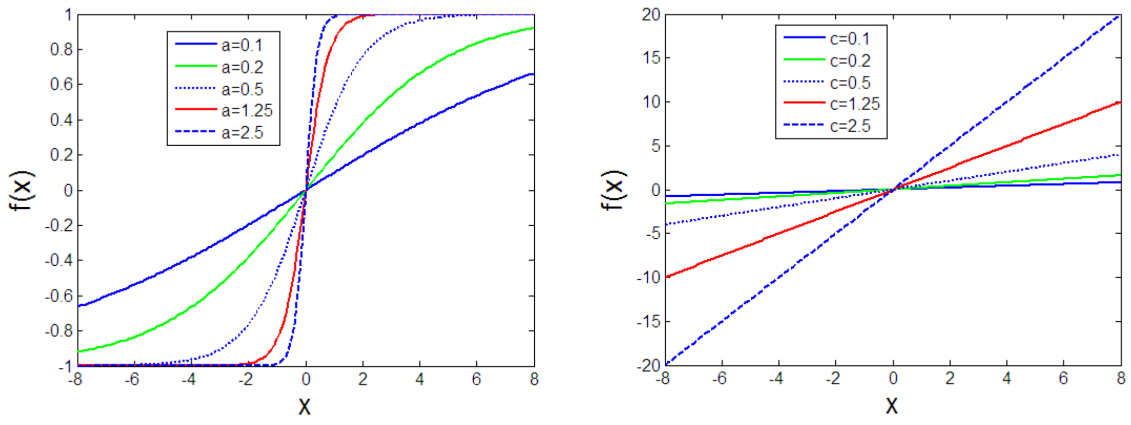

(a) Sigmoid function for various a values (b) Linear function for various c values

Figure 6.3: Activation functions used by NN

Parameters of NN, i.e. weights (w), biases (b) and activation function parameters, need to be tuned to produce satisfactory results using a learning algorithm or training algorithm. There are three main categories of learning algorithm (Hagan et al., 1996): supervised learning, reinforcement learning and unsupervised learning.

a. Supervised learning

In supervised learning, the NN parameters are modified based on given input and correct (actual) output. Thus the availability of input-output data pairs is very essential for the learning algorithm. For every input applied to NN, the predicted output is compared to the actual output. The difference between the predicted output and actual output is referred to as prediction error. All NN parameters are adjusted during the learning process to produce predicted output closer and closer to the actual output.

b. Reinforcement learning

In general, reinforcement learning is almost the same as supervised learning. The difference is that in the reinforcement learning, the predicted output of NN is not compared to the actual output but is given a grade or a score. The grade or score is a measurement of the NN performance over some input sequence. Then, NN parameters are modified based on the score.

c. Unsupervised learning

In unsupervised learning, all NN parameters are modified only based on the inputs and the correct output as a target is not available.

In this work, because the actual input-output data pairs are available, supervised learning technique was chosen to be used in the investigations. ABFAs, proposed in Chapter 4, are used as the training algorithms for the NN.

6.3. NN-based modelling computation

6.3.1. Model structure formulation

There are several modelling techniques that can be used with NNs to identify non-linear system dynamics. These include state-output model, recurrent state model and Non-linear Auto-Regressive Moving Average with eXogeneous input (NARMAX) model. The literature reveals that if the actual input and output data pairs of the plant are available, the NARMAX model is a suitable choice for modelling nonlinear systems. General NARMAX model can be formulated as (Luo and Unbehauen, 1997):

$$\hat{y}(t) = f\begin{bmatrix} y(t-1), y(t-2), \dots, y(t-n_y), \\ u(t), u(t-1), \dots, u(t-n_u), \\ \eta(t-1), \eta(t-2), \dots, \eta(t-n_\eta) \end{bmatrix} + \eta(t) \qquad (6.4)$$

where $\hat{y}(t)$ is the predicted output, $y(t)$ is the actual output, $u(t)$ is the input, $\eta(t)$ is the noise, n_y, n_u and n_η are the maximum lags number of actual output, input and noise respectively and $f[\cdot]$ is a non-linear function mapping. If the model is good enough to identify the system without incorporating the noise term, the model can be represented in a NARX form as (Sze, 1995; Luo and Unbehauen, 1997):

$$\hat{y}(t) = f\left[y(t-1), y(t-2), \dots, y\left(t-n_y\right), u(t), u(t-1), \dots, u(t-n_u)\right] \tag{6.5}$$

6.3.2. Computation steps of NN-based model

In this work, NN trained by ABFAs, referred to as ABFA-NN, is used as the non-linear function that maps the input to output. ABFA optimises NN's parameters such as weights, biases and parameters of activation function based on the cost function formulated from the predicted error. Thus, the general block diagram of training mechanism of NN with NARX model is represented in Figure 6.4.

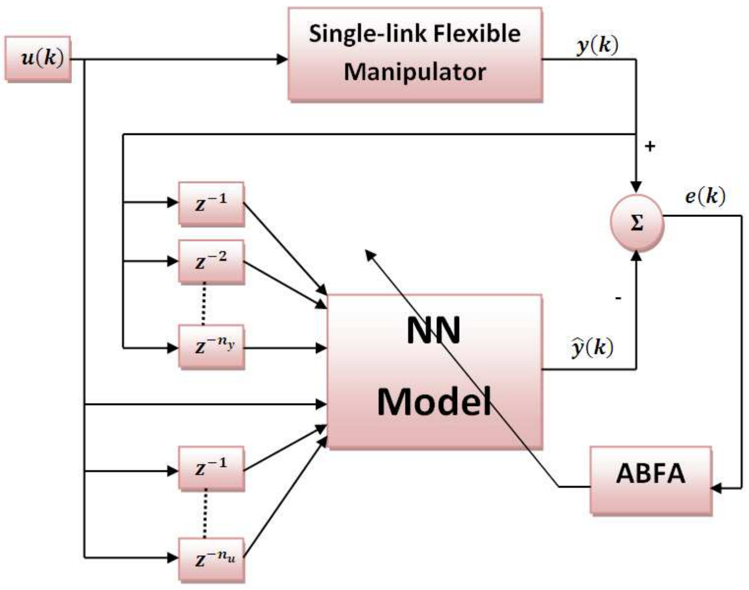

Figure 6.4: Basic diagram of NARX model identification with NN-ABFA

where $u(k)$ is the actual input, $y(k)$ is the actual output, $\hat{y}(k)$ is the predicted output and $e(k)$ is the prediction error;

$$e(k) = y(k) - \hat{y}(k) \tag{6.6}$$

In the modelling process, parameters that will be optimised by ABFAs for every neuron of NN are weights of every input (w), threshold values or biases (b) and activation function parameters a and c. In the optimisation process, bacteria will try to find optimum or minimum cost function value by using random walk for whole bacteria's lifetime determined by the total number of steps, calculated as $N_c \times N_{re} \times N_{ed}$. The cost function developed is based on the predicted error $e(k)$ formulated in equation (6.6), and used as the nutrient media in which bacteria will find optimum position. Since the global minimum of $e(k)$ is equal to zero, when the predicted output is exactly the same as actual output, thus the global minimum value of cost function is also equal to zero. From the BFAs optimisation point of view, the lowest cost function value means the place with the highest nutrient level. The details of ABFA computation steps were discussed in Chapter 4. The optimisation process will result in NNs with optimal parameters, representing hub-angle, hub-velocity and end-point acceleration models. The general NN optimisation sequence for modelling of single-link flexible manipulator system is depicted in Figure 6.5.

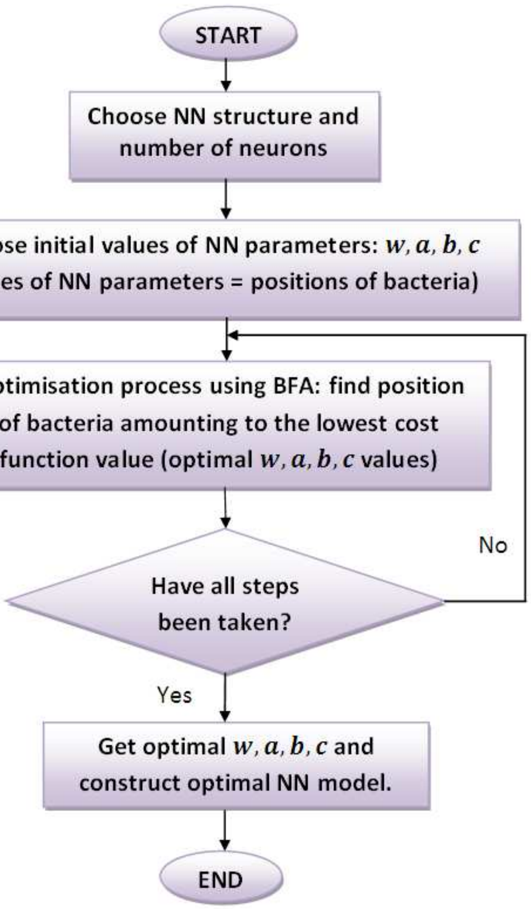
START
Choose NN structure and number of neurons
Choose initial values of NN parameters: w, a, b, c (values of NN parameters = positions of bacteria)
Optimisation process using BFA: find position of bacteria amounting to the lowest cost function value (optimal w, a, b, c values)
No
Have all steps been taken?
Yes
Get optimal w, a, b, c and construct optimal NN model.
END

Figure 6.5: Optimisation process of NN with BFA

6.3.3. Model validation for BFA-NN models

After the models have been developed, validations are carried out as follows:

a. The 6400 input-output experimental data pairs are split into two sets: the first 3400 data pairs are used for modelling phase and the remaining 3000 data pairs are used for validation phase.
b. Correlation tests (Billings and Voon, 1986) described in equation (3.2) are performed on the developed models.

The overall modelling process using NN-ABFA is depicted in Figure 6.6.

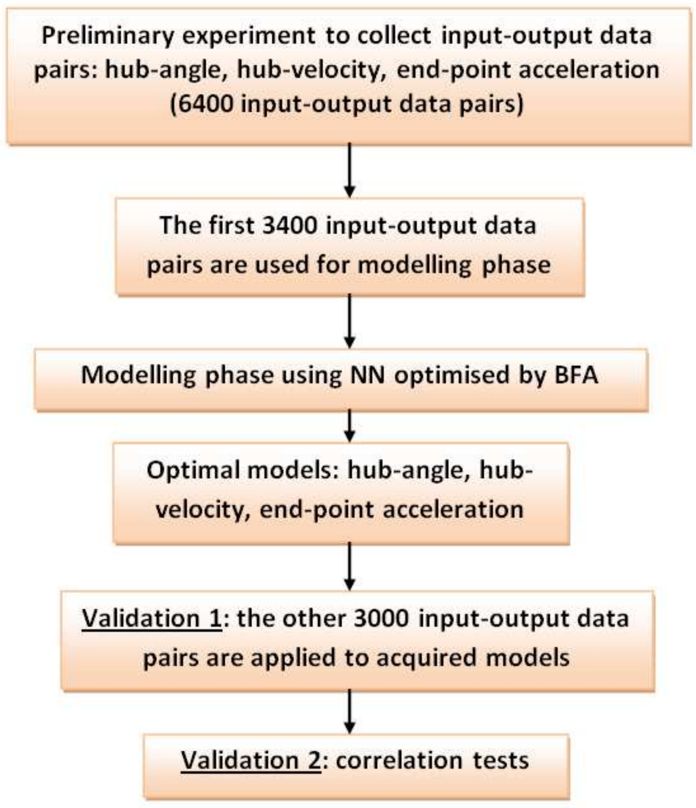
Preliminary experiment to collect input-output data pairs: hub-angle, hub-velocity, end-point acceleration (6400 input-output data pairs)
The first 3400 input-output data pairs are used for modelling phase
Modelling phase using NN optimised by BFA
Optimal models: hub-angle, hub-velocity, end-point acceleration
Validation 1: the other 3000 input-output data pairs are applied to acquired models
Validation 2: correlation tests

Figure 6.6: Flowchart of overall modelling sequence for NN-based modelling

6.4. FL-based modelling computation

6.4.1. Model structure formulation

A brief description of fundamentals of FL was presented in Chapter 4. If measured input-output data pairs available, a plant can be modelled by using an approach which only depends on the actual input-output data pairs. Black box modelling is an approach that represents transfer of input to output without any knowledge of internal working or mechanism of a plant under study.

In this work, a black-box modelling approach based on FL is used for modelling a single-link flexible manipulator system. In order to simplify the computation complexity and load, the FL structure considered in this investigation contains two fuzzy inputs (previous actual input ($u(k-1)$) and previous actual output ($y(k-1)$)) with one fuzzy output (predicted output ($\hat{y}(k)$)). More fuzzy input will provide more input for FL model, however will also rise the computation complexity and loads. In order to produce more accurate model, tuneable scaling factors K_1, K_2 and K_3 are used for previous actual input ($u(k-1)$), previous actual output ($y(k-1)$) and predicted output ($\hat{y}(k)$) respectively. For each input, the predicted output $\hat{y}(k)$ of FL-based model is compared to the actual output y(k) and the difference between the predicted output $\hat{y}(k)$ and actual output $y(k)$ formed giving predicted error $e(k)$. Then, ABFA optimise the FL-based model and the three scaling factors based on the cost function developed based on the predicted error $e(k)$ level. Thus, the general block diagram describing modelling of flexible manipulator system based on ABFA-optimised FL, here indicated as ABFA – FL, is shown in Figure 6.7, where $u(k)$ is the actual input, $y(k)$ is the actual output, $\hat{y}(k)$ is the predicted output and $e(k)$ is the error.

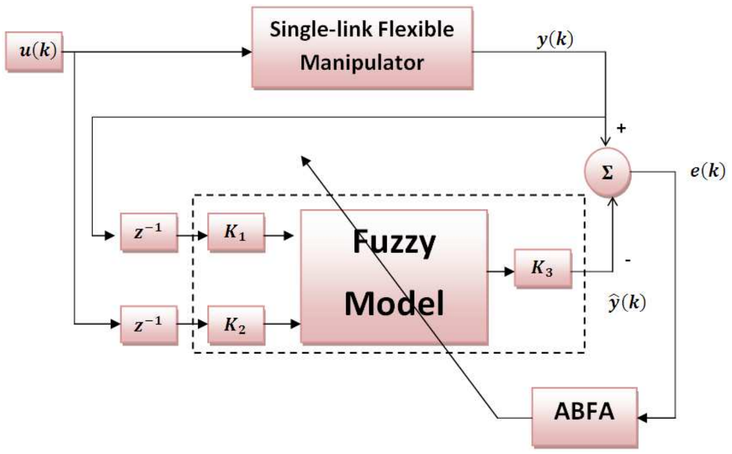

Figure 6.7: Basic diagram of modelling of single-link flexible manipulator system using ABFA-FL: K_1, K_2 and K_3 are scaling factors for input and output

In this investigation, Gaussian membership functions were chosen because they are able to represent uncertainty in measurements most adequately (Kreinovich et al., 1992). Various number of membership functions for input and output were considered in the simulation. However, five-membership function FL structure for both inputs and output gave good result with acceptable computation time. More membership functions will result more fuzzy rules and will consume more computational time. The fuzzy inputs and output with five Gaussian membership functions is depicted, in general terms, in Figure 6.8.

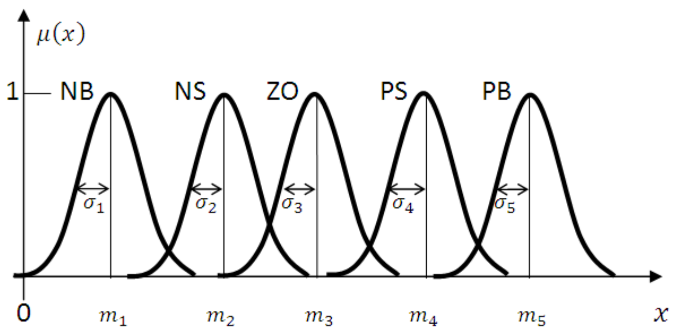

Figure 6.8: Fuzzy input with five Gaussian membership functions: NB is negative big, NS is negative small, ZO is zero, PS is positive small and PB is positive big

6.4.2. Computation steps of BFA-FL

Mamdani type FL (Mamdani and Assilian, 1974) with centroid of area (COA) defuzzification is used in this work. The general form of fuzzy rule of Mamdani type FL can be formulated as:

IF $u(k-1)$ is A and $y(k-1)$ is B THEN $\hat{y}(k)$ is C $\quad (w)$

where w is weighting factor of the rule. So that the output of consequence part of every fuzzy rule is $C \times w$. In order to fit with the nature of problem the weight of every rule can be changed in the range [0, 1], weight equal to zero means the output value is zero and weight equal to one means the output is in full scale (100 %). Hence, the parameters to be optimised in ABFA-FL based flexible manipulator system model are parameters of Gaussian membership functions ($m_1, \dots, m_5$ and $\sigma_1, \dots, \sigma_2$), weight of every rule (w) and scaling factors (K_1, K_2 and K_3).

It is noticed in the literature that, in various applications, tuning the scaling factors or tuning membership functions can lead to the same result (Chen and Linkens, 1998; Siddique and Tokhi, 2006). Tuning the scaling factors is simpler because only fewer parameters are there to tune than tuning membership functions. In this work for both input and output, all parameters of Gaussian membership functions ($m_1, \dots, m_5$ and $\sigma_1, \dots, \sigma_5$) were selected manually by trial and error. Thus, the investigation here focuses on optimising weights (w) of every fuzzy rule and the scaling factors (K_1, K_2 and K_3) using BFAs.

In the optimisation process, a cost function formulated from the predicted error ($e(k)$) is used as the nutrient media in which bacteria will find optimum value. Since the minimum value of predicted error ($e(k)$) is equal to zero, at which point the predicted output is exactly the same as actual output, the global minimum value of J is also equal to zero. From the BFAs optimisation point of view, the lowest cost function value means the place with the highest nutrient level. Bacteria will try to find closest location to the global minimum point by applying biased random walk until their lifetime which is determined by number of steps calculated as $N_c \times N_{re} \times N_{ed}$. The general computation steps for modelling of flexible manipulator system based on BFA-FL is depicted in Figure 6.9.

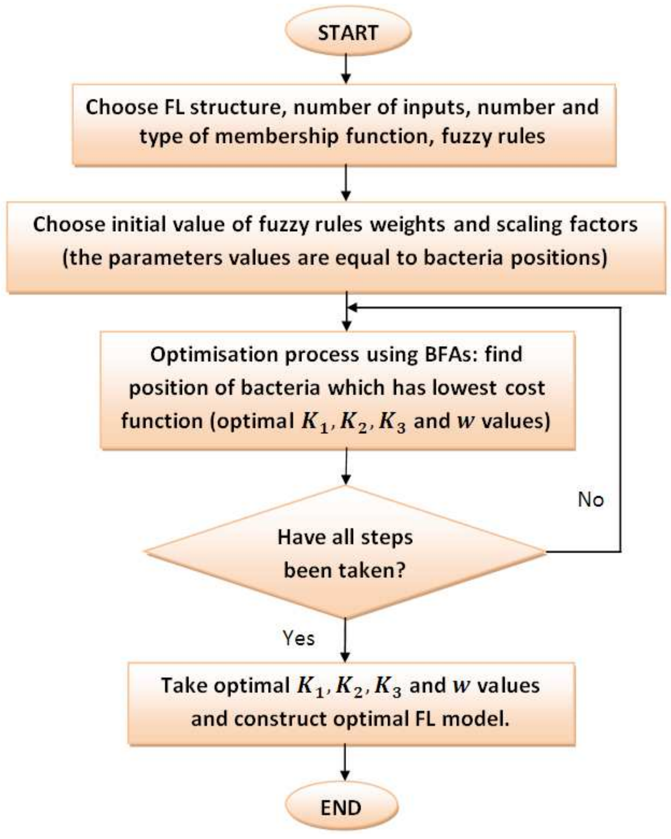
START
Choose FL structure, number of inputs, number and type of membership function, fuzzy rules
Choose initial value of fuzzy rules weights and scaling factors (the parameters values are equal to bacteria positions)
Optimisation process using BFAs: find position of bacteria which has lowest cost function (optimal K_1, K_2, K_3 and w values)
Have all steps been taken?
No
Yes
Take optimal K_1, K_2, K_3 and w values and construct optimal FL model.
END
Figure 6.9: BFA-FL computation steps flowchart

6.4.3. Model validation for BFA-FL models

Here, the validation of developed model is carried out in two steps:

c. The 6400 input-output experimental data pairs are split into two sets: the first 3400 data pairs are used for modelling phase and then all 6400 data pairs are used for validation phase. To validate the models, the entire 6400 data pairs are applied to the resulted models.

d. Finally, correlation tests (Billings and Voon, 1986) described in equation (3.2) are performed on the developed models.

The overall sequence of steps of modelling of the single-link flexible manipulator system using BFA-FL is depicted in Figure 6.10.

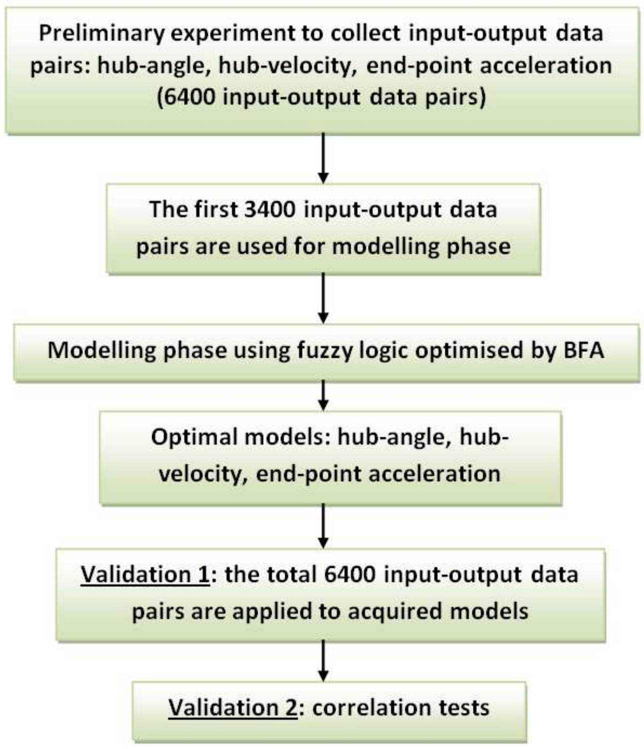
Preliminary experiment to collect input-output data pairs: hub-angle, hub-velocity, end-point acceleration (6400 input-output data pairs)
The first 3400 input-output data pairs are used for modelling phase
Modelling phase using fuzzy logic optimised by BFA
Optimal models: hub-angle, hub-velocity, end-point acceleration
Validation 1: the total 6400 input-output data pairs are applied to acquired models
Validation 2: correlation tests

Figure 6.10: Flowchart of overall modelling sequence for FL-based modelling

6.5. Protocol and preliminary computation

6.5.1. Protocol computation

Three SISO ABFA-NN and BFA-FL models, representing hub-angle, hub-velocity and end-point acceleration are developed. The computation scenarios used in models development are:

a. All parameters of BFAs used in the modelling process, dimension of the search space p (selected according to the order of the model structure), are selected heuristically. The parameters are selected by considering that BFA should have enough number of bacteria (S), bacteria should have enough lifetime (total number of steps), enough reproduction steps (N_{re}) so that bacteria can refine the nutrient value achieved and enough elimination and dispersal events (N_{ed}) so that bacteria are able to search most parts of nutrient media to find location closest to the global minimum but with minimum computation loads.

b. As a preliminary simulation, several cost function developed and used by researchers in various applications found in the literature are evaluated empirically by using them in the modelling of hub-angle based on SBFA-based model. The performances of SBFA-based model using several cost functions are evaluated based on their error of time-domain responses. The cost function which gives the best performance is used as cost function for the rest of the modelling process.

c. For every modelling process, i.e. hub-angle, hub-velocity and end-point acceleration models, several runs of all BFAs-NN and BFA-FL are performed to find the best optimum cost function value. Then, the performances of the proposed algorithms are compared to that of SBFA-based model on the best optimum cost function value achieved, convergence and time-domain response error.
d. Validation steps are performed for all developed models.

6.5.2. Preliminary simulation: empirical comparison of cost functions

There are four cost function alternatives considered as the nutrient media of BFA. These are sum of absolute error (SAE), mean of absolute error (MAE), mean squared error (MSE) and root mean square error (RMSE), formulated as:

$$J_{SAE} = \sum_{k=1}^{n} |e(k)| \tag{6.7}$$

$$J_{MAE} = \frac{1}{n}\sum_{k=1}^{n} |e(k)| \tag{6.8}$$

$$J_{MSE} = \frac{1}{n}\sum_{k=1}^{n} \big(e(k)\big)^2 \tag{6.9}$$

$$J_{RMSE} = \sqrt[2]{\frac{1}{n}\sum_{k=1}^{k=n} \big(e(k)\big)^2} \tag{6.10}$$

where n represents the number of data points, and $e(k)$ is the prediction error. The first three cost functions have been discussed and also used in the preliminary simulations in Chapter 5. RMSE is developed by taking roots of MSE. The advantage of using RMSE is that it will remove big prediction error and the unit of RMSE is the same as the actual and predicted output. In the preliminary simulation, these four cost function alternatives are used in the modelling of hub-angle using SBFA-NN. Then the cost function which gives the best result, measured by how close the predicted output is to the actual, is used throughout the work.

Various number of previous actual output samples (n_y) and previous actual input samples (n_u) were used in the modelling process. Also various alternatives of NN structures were considered and used. It was noticed from the simulation results that, by considering the optimum cost function value achieved and computational complexity, a three-layer NN containing input layer, one eight-neuron hidden layer and output layer, with eight previous actual input-output samples ($n_y = n_u = 8$) was chosen. Also, it can be noted that the more hidden layers used, the slower the convergence of BFA will be. Thus, in total there were 154 parameters to be optimised;

- 128 parameters for weights of signals from inputs (actual previous input and actual previous output) enter neurons in the hidden layer.
- 8 parameters for biases of eight neurons in the hidden layer.
- 8 parameters for hyperbolic tangent sigmoid activation functions parameter of eight neurons in the hidden layer.
- 8 parameters for weights of signal from hidden layer to output layer
- 1 parameter for bias of one neuron in the output layer
- 1 parameter for linear activation function parameter of one neuron in the output layer

In the simulation, SBFA used the same general parameters as:

❖ $p = 154$	❖ $N_c = 110$	❖ $S_r = S/2$	❖ $N_{ed} = 5$
❖ $S = 8$	❖ $N_s = 4$	❖ $N_{re} = 6$	❖ $p_{ed} = 0.25$

The initial positions of bacteria were selected randomly across the nutrient media. Various chemotactic step sizes $C(i)$, were used in the modelling process and the best cost function value was achieved when $C(i)$ was equal to 0.006. The time-domain responses depicted in Figure 6.11(a) show that, in general, using all those four cost function values, the predicted output followed the actual output but the closest predicted output was achieved when SBFA used RMSE as the cost function. Error of time-domain responses depicted in Figure 6.11(b) show that all models had their own prediction error range. The numerical results presented Table 6.1 show that the smallest prediction error range, [-0.0032, 0.0041], was achieved when model was developed based on RMSE.

Table 6.1: Numerical results of hub-angle BFA-NN model using different cost functions in the training phase

Algorithm	**Optimum** J	**Range of error** $(e(k))$	
		Minimum	**Maximum**
SBFA-NN SAE	J_{SAE} = 2.8084	-0.0039	0.0041
SBFA-NN MAE	J_{MAE} = 8.2600e-004	-0.0039	0.0041
SBFA-NN MSE	J_{MSE} = 2.2472e-006	-0.0035	0.0089
SBFA-NN RMSE	J_{RMSE} = 0.0012	-0.0032	0.0041

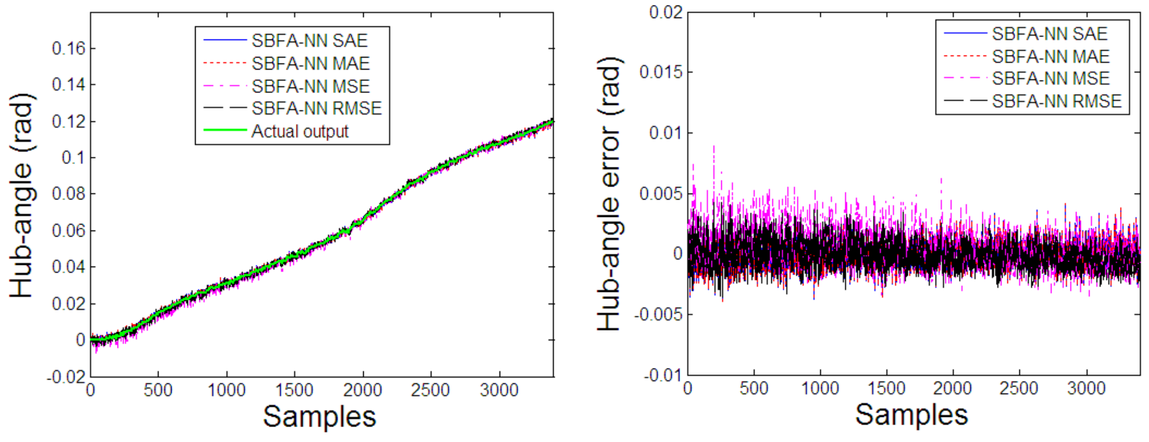

(a) Time-domain responses (b) Error

Figure 6.11: Simulation results of hub-angle model using different cost functions in the training phase

The time-domain responses and error in validation phase presented in Figure 6.12(a) and Figure 6.12(b) respectively show that the predicted output using the cost functions followed the actual output with different ranges of closeness. The numerical results presented in Table 6.2 show that the model developed based on RMSE as cost function had the smallest prediction error range, [-0.0090, 0.1193], compared to other models. Based on these empirical comparative results, RMSE was selected as cost function throughout the work in this chapter.

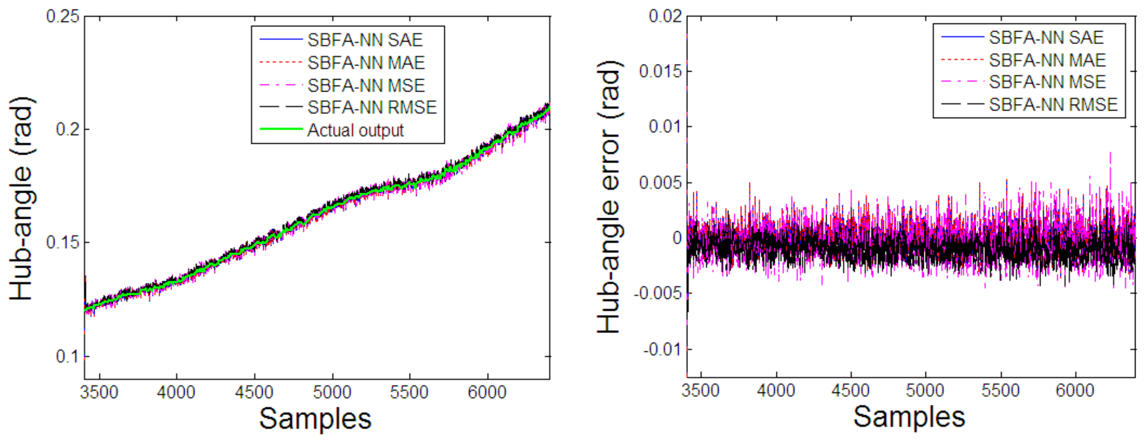

(a) Time-domain responses (b) Error

Figure 6.12: Simulation results of hub-angle models using different cost functions in validation phase

Table 6.2: Numerical result of hub-angle models using different cost functions in the validation phase

Algorithm	**Optimum J**	**Range of error ($e(k)$)**	
		Minimum	**Maximum**
SBFA-NN SAE	$J_{SAE} = 3.4960$	-0.0153	0.1198
SBFA-NN MAE	$J_{MAE} = 0.0012$	-0.0153	0.1198
SBFA-NN MSE	$J_{MSE} = 0.000018456$	-0.0092	0.1209
SBFA-NN RMSE	$J_{RMSE} = 0.0051$	-0.0090	0.1193

6.6. Results and discussions: BFA-NN models

6.6.1. Hub-angle model

A. Hub-angle model in the training phase

Based on the results in preliminary simulation, in modelling the hub-angle, an NN was set up with $n_u = n_y = 8$, one hidden layer with 8 neurons and one output layer with one neuron. Thus, in total, there were 154 parameters to optimise. In the simulation, all ABFAs and SBFA used the same general parameters as

❖ $p = 154$	❖ $N_c = 110$	❖ $S_r = S/2$	❖ $N_{ed} = 5$
❖ $S = 8$	❖ $N_s = 4$	❖ $N_{re} = 6$	❖ $p_{ed} = 0.25$

The initial positions of bacteria were selected randomly across the nutrient media and RMSE was used as the cost function. As indicated in the preliminary simulation, for

SBFA, the best optimum cost function value was achieved with chemotactic step size equal to 0.006. For LABFA, QABFA and EABFA, all the parameters and settings, i.e. c_{max}, b, d and g were chosen manually by trial and error. The best cost function results were achieved when the adaptable chemotactic step size for every bacterium of LABFA, QABFA and EABFA, i.e. $C_{al}(i), C_{aq}(i)$ and $C_{ae}(i)$ respectively, were as:

$$C_{al}(i) = \frac{0.05}{1+\frac{1}{0.002|J(i)|}} \tag{6.11}$$

$$C_{aq}(i) = \frac{0.05}{1+\frac{1}{3\times10^{-5}\left((J(i))^2+|J(i)|\right)}} \tag{6.12}$$

$$C_{ae}(i) = \frac{0.05}{1+\frac{1}{0.0175e^{0.01|J(i)|}}} \tag{6.13}$$

For FABFA, one-input one-output fuzzy structure was used, the input was absolute cost function value of every bacterium ($|J(i)|$) and the output as fuzzy adaptable chemotactic step size for every bacterium ($C_{af}(i)$). Seven Gaussian membership functions were used for input and output. The parameters m and σ of the Gaussian membership functions, were chosen manually by trial and error. The fuzzy membership functions for input and output of FABFA are depicted in Figure 6.13(a) and Figure 6.13(b). The fuzzy surface depicted in Figure 6.13(c) determines relationship between input and output based on the fuzzy rules formulated as:

R_1	:	IF $|J(i)|$ is ES THEN $C_{af}(i)$ is ES	(1)	
R_2	:	IF $|J(i)|$ is VS THEN $C_{af}(i)$ is S	(0.2)	
R_3	:	IF $|J(i)|$ is S THEN $C_{af}(i)$ is M	(1)	
R_4	:	IF $|J(i)|$ is M THEN $C_{af}(i)$ is B	(1)	(6.14)
R_5	:	IF $|J(i)|$ is B THEN $C_{af}(i)$ is VB	(1)	
R_6	:	IF $|J(i)|$ is VB THEN $C_{af}(i)$ is VB	(1)	
R_7	:	IF $|J(i)|$ is EB THEN $C_{af}(i)$ is EB	(1)	

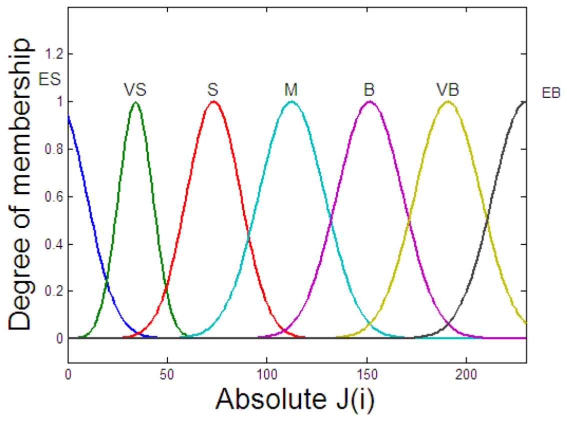

(a) Input: $|J(i)|$

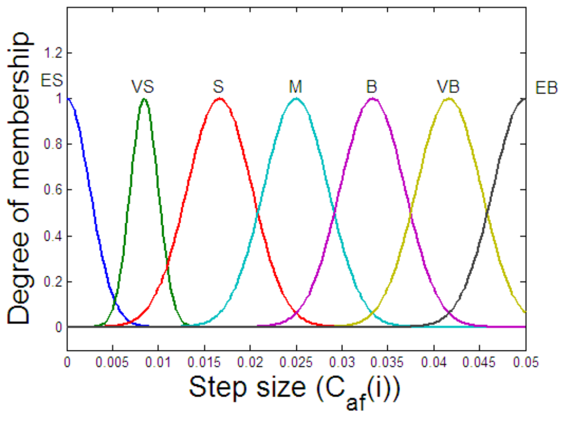

(b) Output: $C_{af}(i)$

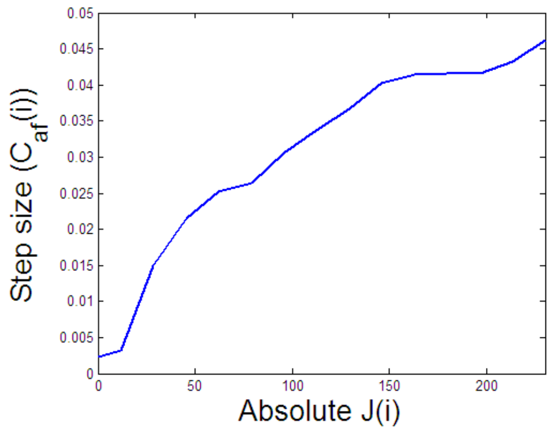

(c) Fuzzy surface

Figure 6.13: Fuzzy membership functions and surface of FABFA for hub-angle model in the training phase

A comparison of the optimum J values achieved by the all algorithms is depicted in Figure 6.14(a). The convergence plots depicted in Figure 6.14(b) show that all the ABFA-NN models were able to converge to the optimum value much faster, with QABFA-NN as the fatest among them; QABFA-NN converged in **1380** steps, and SBFA-NN converged in 2500 steps. The time-domain hub-angle responses in modelling phase depicted in Figure 6.14(c) and Figure 6.14(d) confirm that all predicted outputs followed the actual output, but models developed based on the proposed ABFA-NN models achieved smaller prediction error range than that based on SBFA-NN.

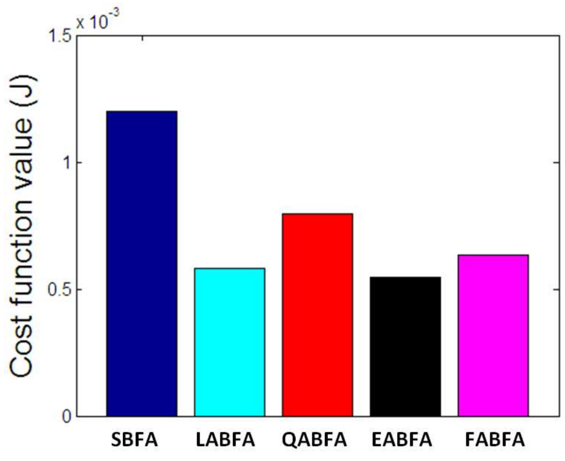

(a) Optimum J

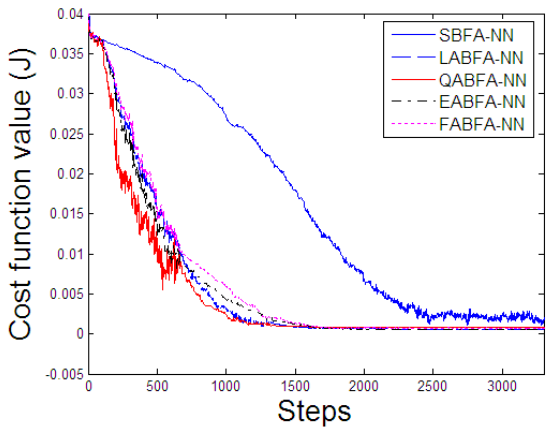

(b) Convergence plots

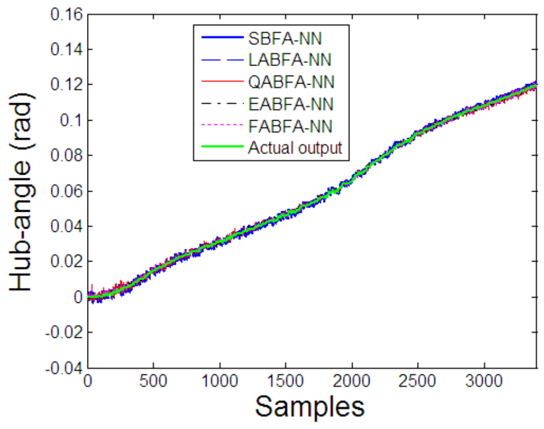

(c) Time-domain responses

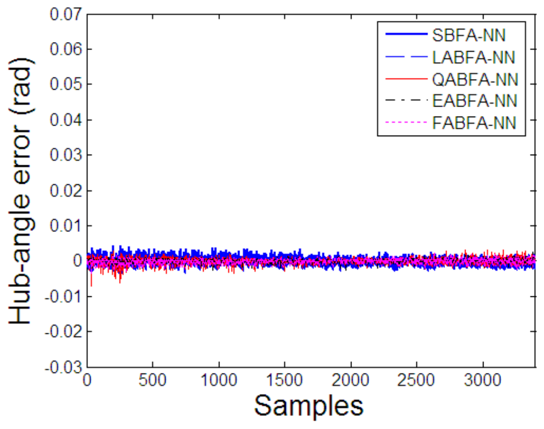

(d) Error

Figure 6.14: Simulation results of hub-angle BFA-NN models in the training phase

The numerical results presented in Table 6.3 show that the optimum values obtained by the algorithms were 12.001×10^{-4}, 5.8192×10^{-4}, 7.9804×10^{-4}, 5.4748×10^{-4} and 6.3428×10^{-4} for SBFA-NN, LABFA-NN, QABFA-NN, EABFA-NN and FABFA-NN respectively. All the four ABFA-NN models achieved smaller cost function values than SBFA-NN with EABFA-NN achieving the best optimum J value.

Table 6.3: Numerical results of hub-angle models for all algorithms in the training phase

Algorithm	$C(i)$ **range**	**Convergence (steps)**	**Optimum J**	**Range of error ($e(k)$)**	
				Minimum	**Maximum**
SBFA-NN	0.007	2500	12.001×10^{-4}	-0.0032	0.0041
LABFA-NN	$[6.0684 \times 10^{-4}, 0.05]$	1450	5.8192×10^{-4}	-0.0031	0.0021
QABFA-NN	$[1.0797 \times 10^{-4}, 0.05]$	**1380**	7.9804×10^{-4}	-0.0050	0.0031
EABFA-NN	$[9.1173 \times 10^{-4}, 0.05]$	1620	$\mathbf{5.4748 \times 10^{-4}}$	-0.0026	0.0024
FABFA-NN	[0.0019, 0.046]	1640	6.3428×10^{-4}	-0.0031	0.0021

B. Hub-angle model in the validation phase

Results of validating the models with unseen data presented in Table 6.4 show that the cost function values for the models in the validation phase were 0.0051, 0.0038, 0.0040, 0.0039 and 0.0037 for SBFA-NN, LABFA-NN, QABFA-NN, EABFA-NN and FABFA-NN respectively. It is noted that ABFA-NN models achieved smaller cost function value compared to SBFA-NN model and the best optimum J was achieved by FABFA-NN.

Table 6.4: Numerical results of hub-angle BFA-NN models in the validation phase

Algorithm	**Optimum J**	**Range of error ($e(k)$)**	
		Minimum	**Maximum**
SBFA-NN	0.0051	-0.0090	0.1193
LABFA-NN	0.0038	-0.0031	0.1190
QABFA-NN	0.0040	-0.0023	0.1193
EABFA-NN	0.0039	-0.0032	0.1192
FABFA-NN	0.0037	-0.0032	0.1191

A comparison of optimum J values achieved models in the validation phase is shown in Figure 6.15(a). Time-domain responses and error plots depicted in Figure 6.15(b) and Figure 6.15(c) respectively show that all models were able to mimic the actual output with the ABFA-based models achieving smaller prediction error range compared to SBFA-based model. The correlation tests of equation (3.2) for the models depicted in Figure 6.16 – Figure 6.20 show that all correlation values were within 95% confidence boundary indicating acceptable performance of the models.

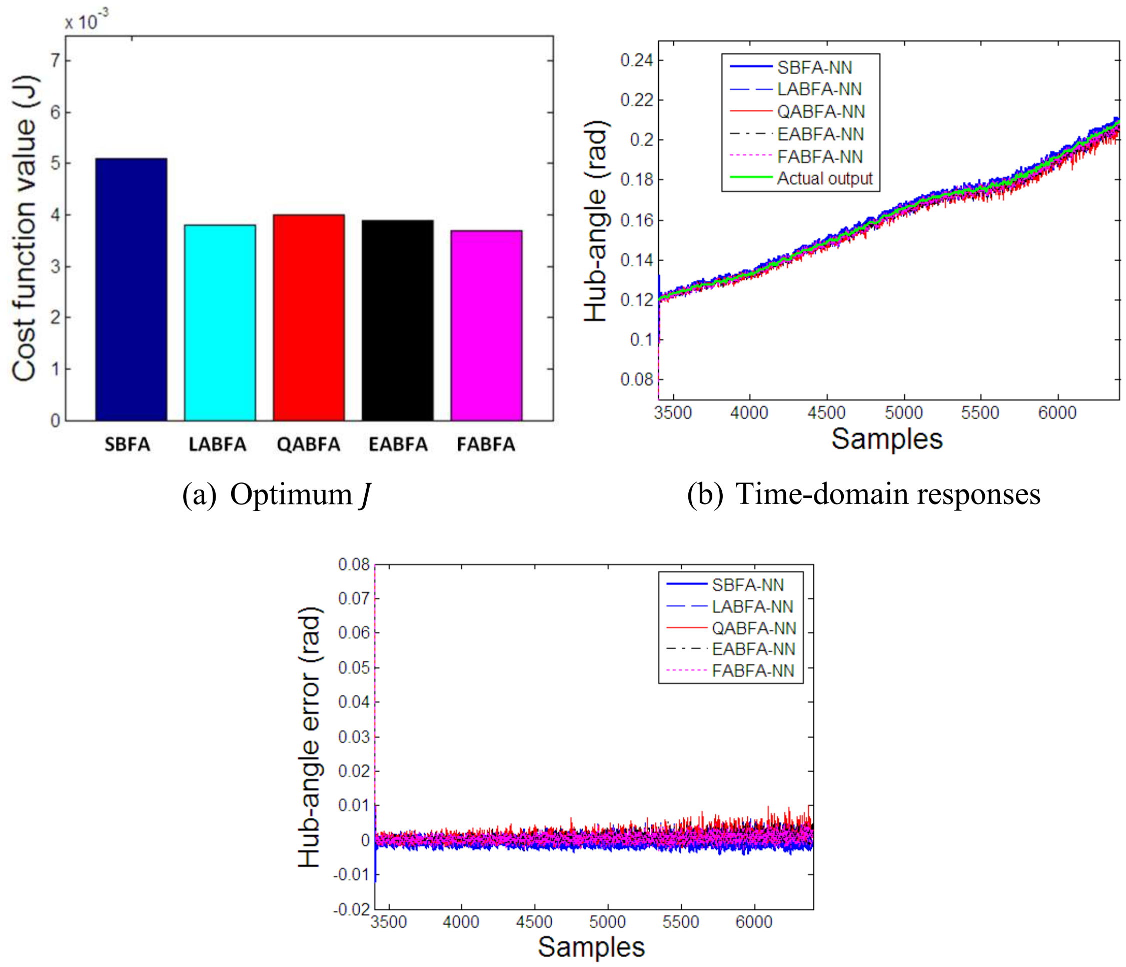

(a) Optimum J

(b) Time-domain responses

(c) Error

Figure 6.15: Simulation results of hub-angle BFA-NN models in the validation phase

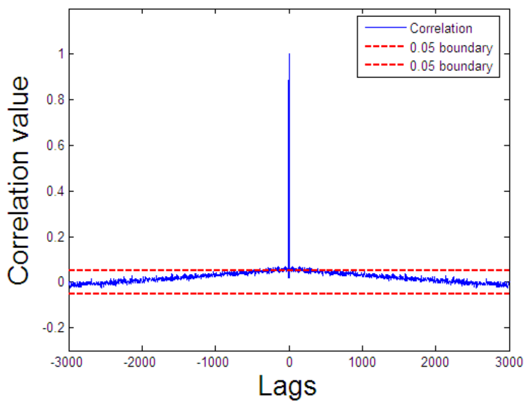

(a) $\phi_{\varepsilon\varepsilon}(\tau)$

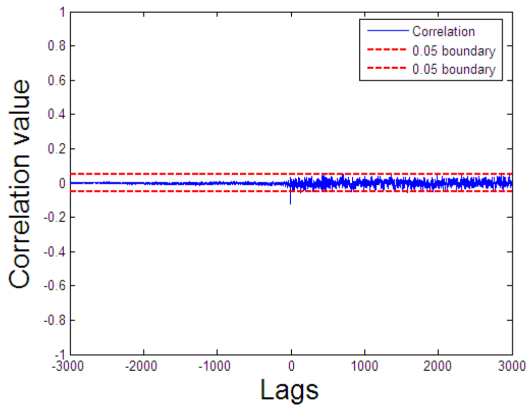

(b) $\phi_{u\varepsilon}(\tau)$

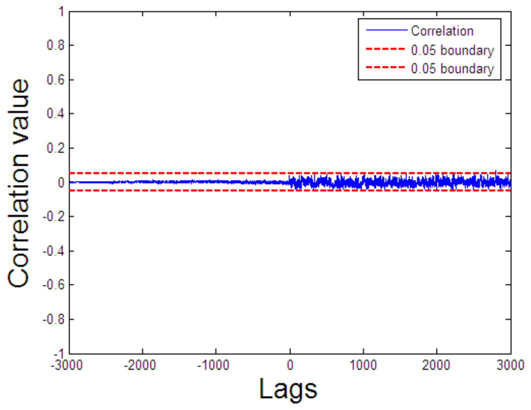

(c) $\phi_{u^2\varepsilon}(\tau)$

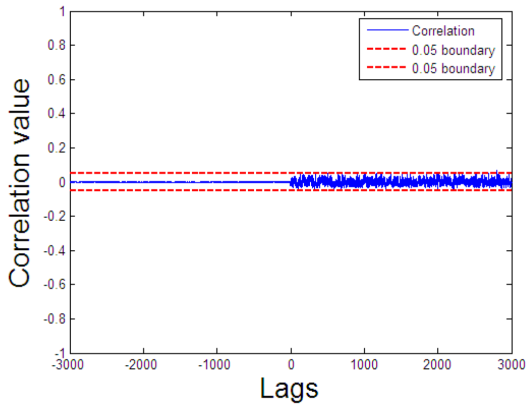

(d) $\phi_{u^2\varepsilon^2}(\tau)$

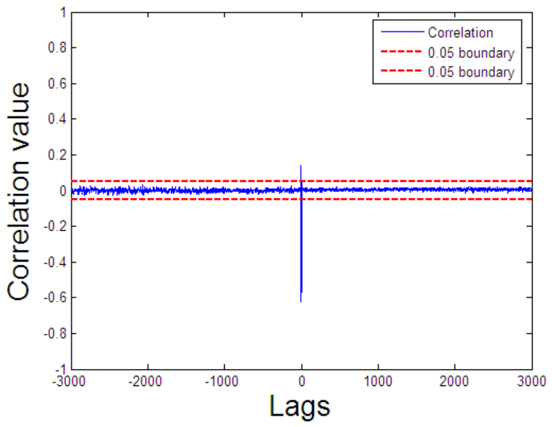

(e) $\phi_{\varepsilon(\varepsilon u)}(\tau)$

Figure 6.16: Correlation tests of hub-angle SBFA-NN model

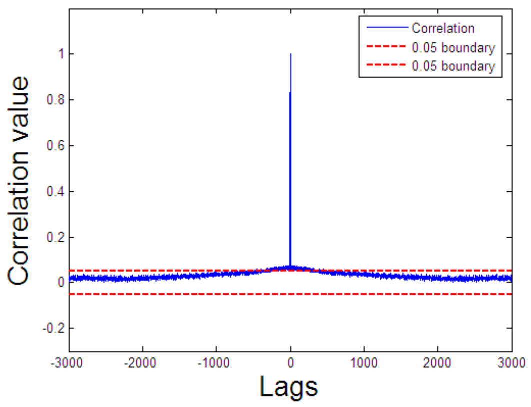

(a) $\phi_{\varepsilon\varepsilon}(\tau)$

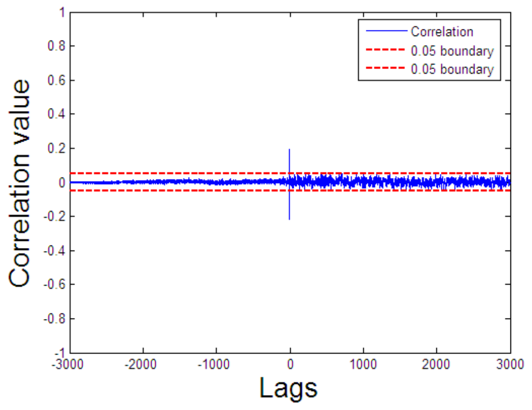

(b) $\phi_{u\varepsilon}(\tau)$

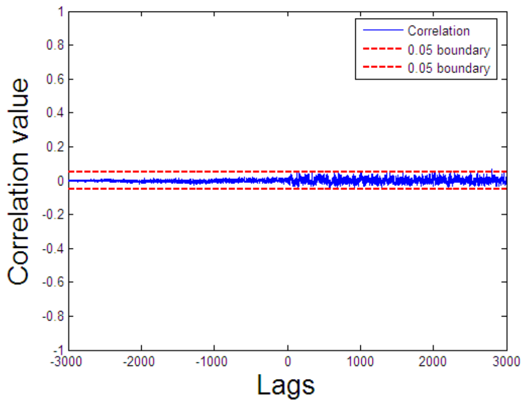

(c) $\phi_{u^2\varepsilon}(\tau)$

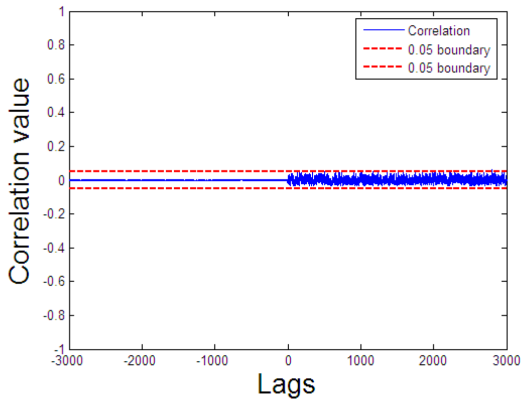

(d) $\phi_{u^2\varepsilon^2}(\tau)$

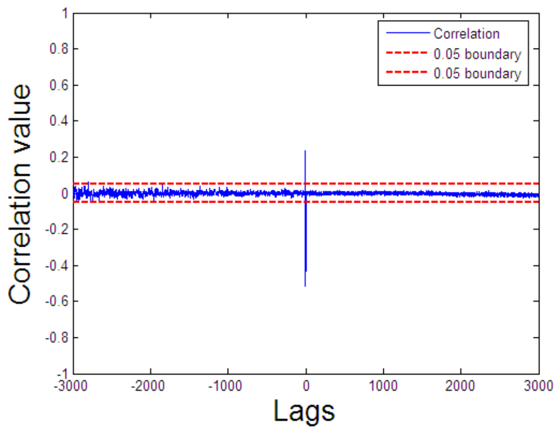

(e) $\phi_{\varepsilon(\varepsilon u)}(\tau)$

Figure 6.17: Correlation tests of hub-angle LABFA-NN model

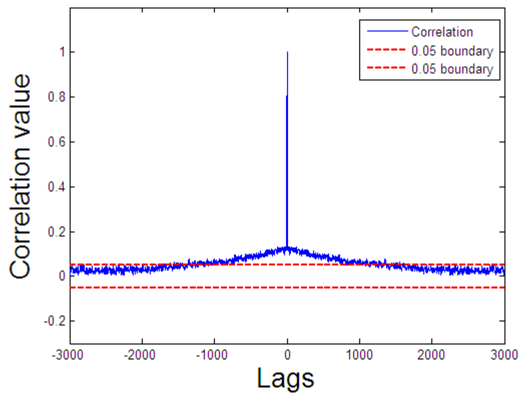

(a) $\phi_{\varepsilon\varepsilon}(\tau)$

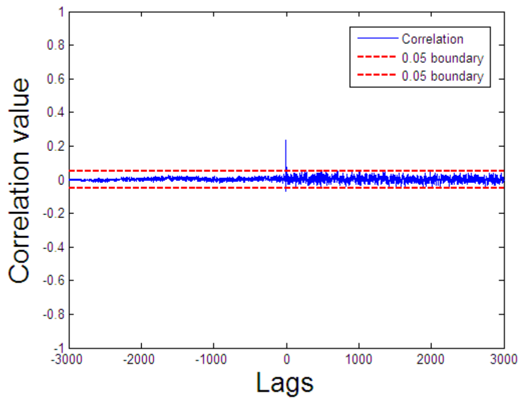

(b) $\phi_{u\varepsilon}(\tau)$

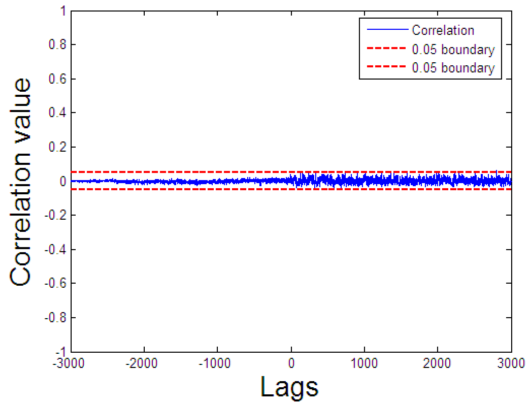

(c) $\phi_{u^2\varepsilon}(\tau)$

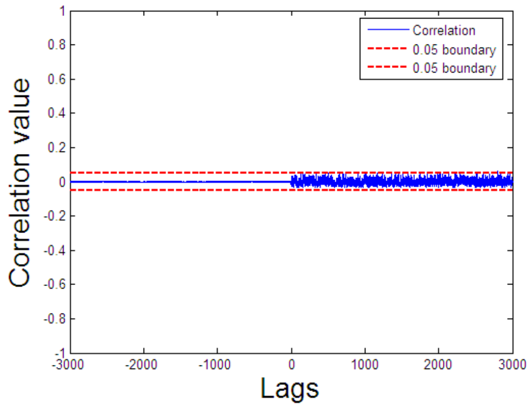

(d) $\phi_{u^2\varepsilon^2}(\tau)$

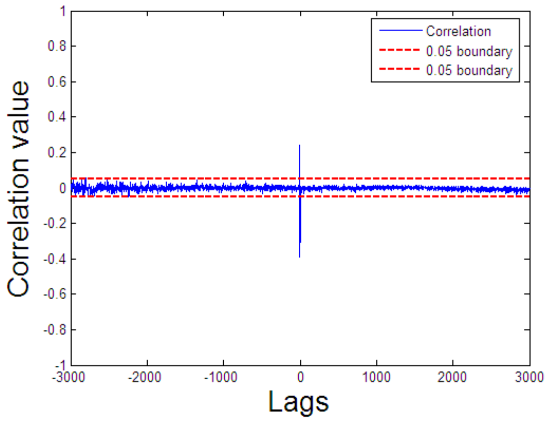

(e) $\phi_{\varepsilon(\varepsilon u)}(\tau)$

Figure 6.18: Correlation tests of hub-angle QABFA-NN model

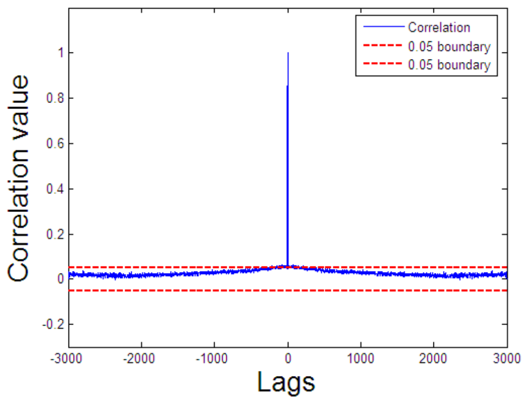

(a) $\phi_{\varepsilon\varepsilon}(\tau)$

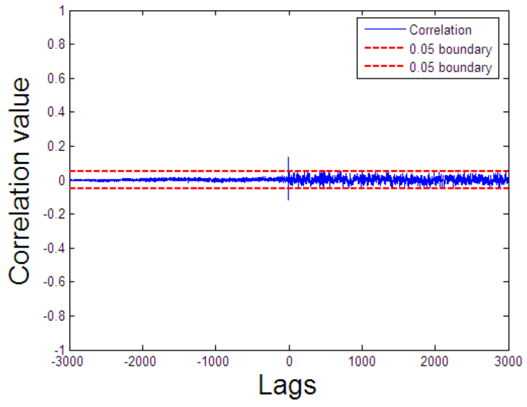

(b) $\phi_{u\varepsilon}(\tau)$

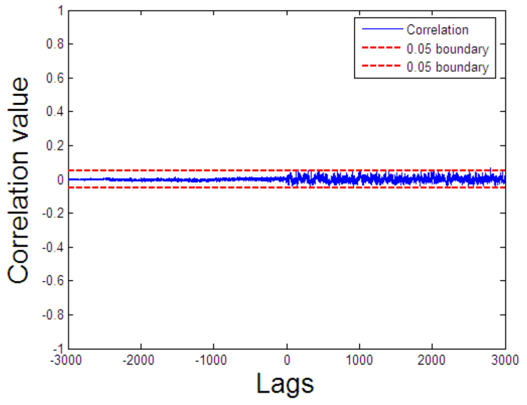

(c) $\phi_{u^2\varepsilon}(\tau)$

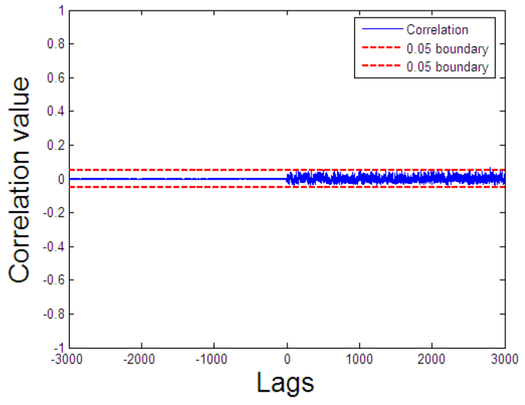

(d) $\phi_{u^2\varepsilon^2}(\tau)$

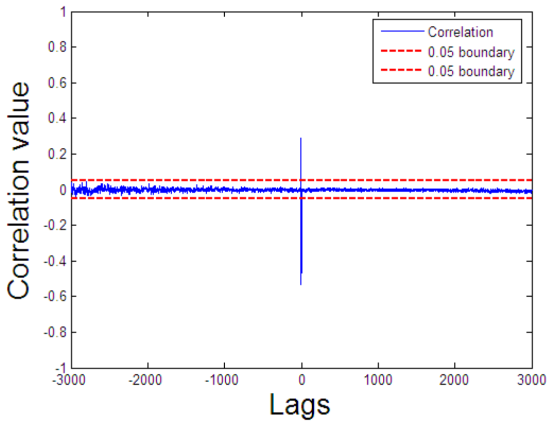

(e) $\phi_{\varepsilon(\varepsilon u)}(\tau)$

Figure 6.19: Correlation tests of hub-angle EABFA-NN model

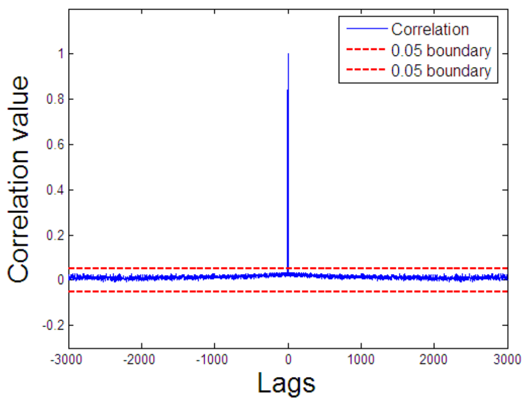

(a) $\phi_{\varepsilon\varepsilon}(\tau)$

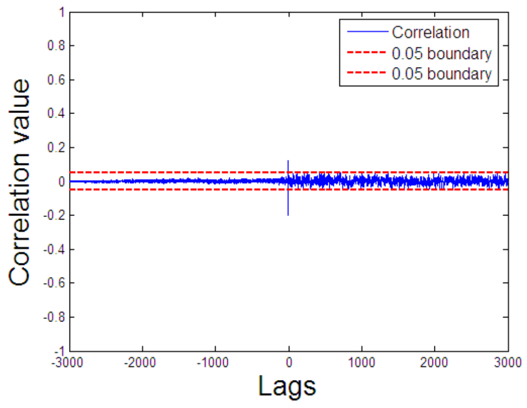

(b) $\phi_{u\varepsilon}(\tau)$

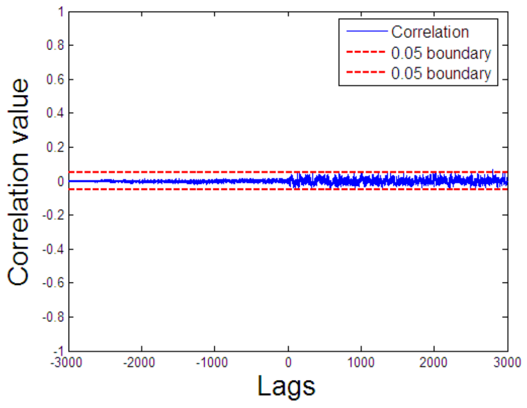

(c) $\phi_{u^2\varepsilon}(\tau)$

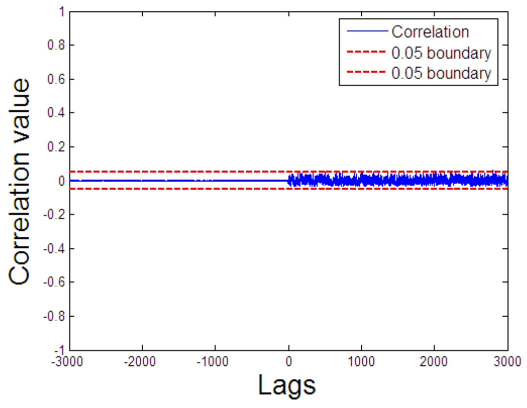

(d) $\phi_{u^2\varepsilon^2}(\tau)$

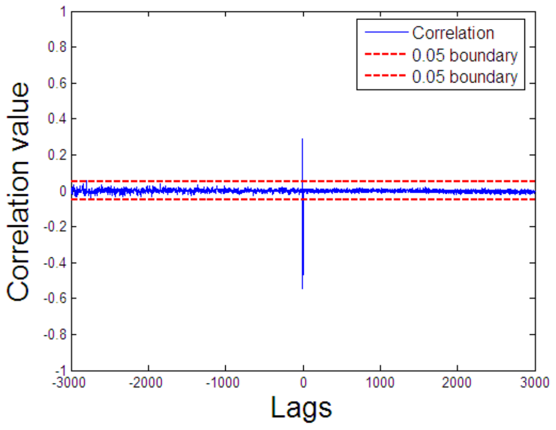

(e) $\phi_{\varepsilon(\varepsilon u)}(\tau)$

Figure 6.20: Correlation tests of hub-angle FABFA-NN model

6.6.2. Hub-velocity model

A. Hub-velocity model in the training phase

In the modelling process of hub-velocity, an NN was set up with $n_u = n_y = 8$, a hidden layer with 8 neurons and one output layer with one neuron. Thus, in total, there were 154 parameters to optimise. All of ABFAs and SBFA used the same general parameters as:

❖ $p = 154$	❖ $N_c = 110$	❖ $S_r = S/2$	❖ $N_{ed} = 2$
❖ $S = 8$	❖ $N_s = 4$	❖ $N_{re} = 6$	❖ $p_{ed} = 0.25$

Initial positions of bacteria were selected randomly across the nutrient media and RMSE was used as the cost function. After trying various chemotactic step sizes ($C(i)$), the best optimum J for SBFA was achieved when $C(i)$ was equal to 0.015. All parameters of LABFA, QABFA and EABFA were chosen by trial and error and the best optimum J values for ABFAs were achieved when adaptable chemotactic step sizes were set up as:

$$C_{al}(i) = \frac{0.2}{1+\frac{1}{0.008|J(i)|}} \tag{6.15}$$

$$C_{aq}(i) = \frac{0.2}{1+\frac{1}{0.002\left((0.9J(i))^2+0.9|J(i)|\right)}} \tag{6.16}$$

$$C_{ae}(i) = \frac{0.2}{1+\frac{1}{0.008e^{0.1|J(i)|}}} \tag{6.17}$$

For FABFA, parameters of Gaussian membership functions for input and output were also selected manually by trial and error. Fuzzy rules forming relationship between input and output in the form of fuzzy surface were formulated as:

$$\begin{array}{lll l}
R_1 : & \text{IF } |J(i)| \text{ is ES THEN } C_{af}(i) \text{ is ES} & (1) & \\
R_2 : & \text{IF } |J(i)| \text{ is VS THEN } C_{af}(i) \text{ is VS} & (0.2) & \\
R_3 : & \text{IF } |J(i)| \text{ is S THEN } C_{af}(i) \text{ is M} & (1) & \\
R_4 : & \text{IF } |J(i)| \text{ is M THEN } C_{af}(i) \text{ is B} & (1) & (6.18) \\
R_5 : & \text{IF } |J(i)| \text{ is B THEN } C_{af}(i) \text{ is VB} & (1) & \\
R_6 : & \text{IF } |J(i)| \text{ is VB THEN } C_{af}(i) \text{ is VB} & (1) & \\
R_7 : & \text{IF } |J(i)| \text{ is EB THEN } C_{af}(i) \text{ is EB} & (1) &
\end{array}$$

The weight of rule R_2 was chosen equal to 0.2 to ensure $C_{af}(i)$ was not too big for the corresponding cost function value and make $C_{af}(i)$ as small as possible so that bacteria are able to achieve nearest position to global minimum point. The fuzzy membership functions for input and output and fuzzy surface are depicted in Figure 6.21.

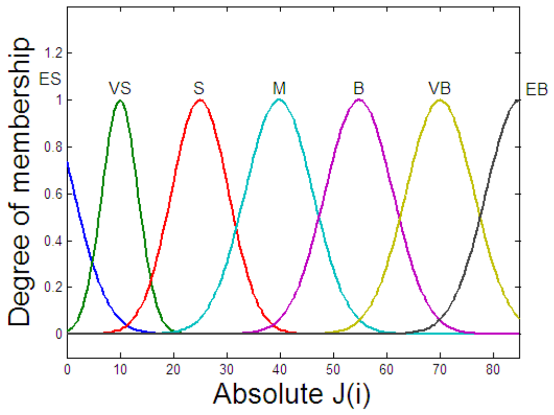

(a) Input: $|J(i)|$

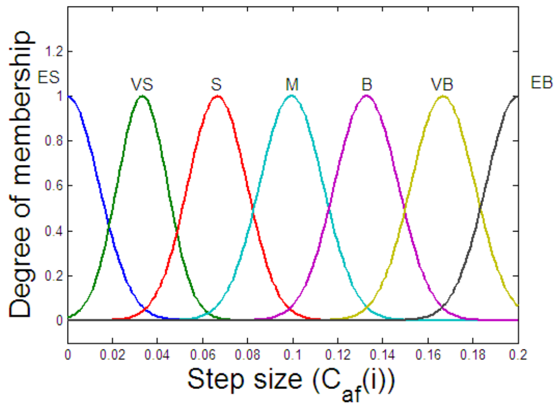

(b) Output: $C_{af}(i)$

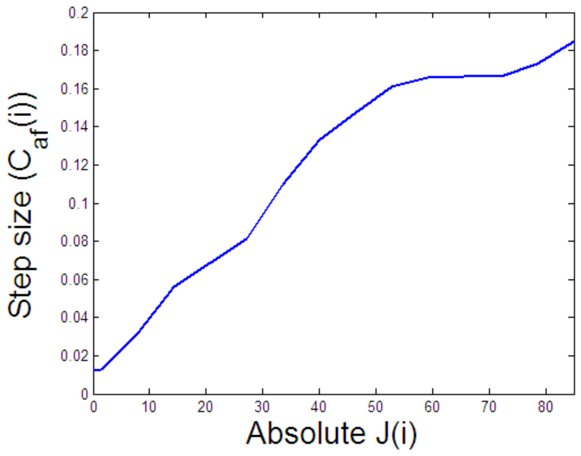

(c) Fuzzy surface

Figure 6.21: Fuzzy membership function and surface of FABFA for hub-velocity model in the training phase

The numerical results presented in Table 6.5 show that the cost function values achieved at hub-velocity modelling were 0.1010, 0.0880, 0.0549, 0.0416 and 0.0156 for SBFA-NN, LABFA-NN, QABFA-NN, EABFA-NN and FABFA-NN models respectively. These results show that all ABFA-NN models achieved smaller const function value than SBFA-NN model with FABFA-NN achieving the best optimum J value. A comparison of optimum J values achieved by the algorithms is shown outlined in Figure 6.22(a). The convergence plots depicted in Figure 6.22(b) show that all the ABFA-NN were able to converge to the optimum value faster (between 185-195 steps) than SBFA-NN which converged in 890 steps. The time-domain responses and error depicted in Figure 6.22(c) and Figure 6.22(d) respectively show that although predicted outputs of all models followed actual output, all the ABFA-NN models had smaller prediction error range compared to that of SBFA-NN model.

Table 6.5: Numerical results of hub-velocity BFA-NN models in the training phase

Algorithm	$C(i)$ range	Convergence (steps)	Optimum J	Range of error ($e(k)$)	
				Minimum	Maximum
SBFA-NN	0.015	890	0.1010	-0.0381	0.0263
LABFA-NN	[0.0014, 0.2]	195	0.0880	-0.0372	0.0257
QABFA-NN	[0.00029689, 0.2]	185	0.0549	-0.0231	0.0214
EABFA-NN	[0.0017, 0.2]	190	0.0416	-0.0196	0.0183
FABFA-NN	[0.0120, 0.185]	185	0.0156	-0.0189	0.0175

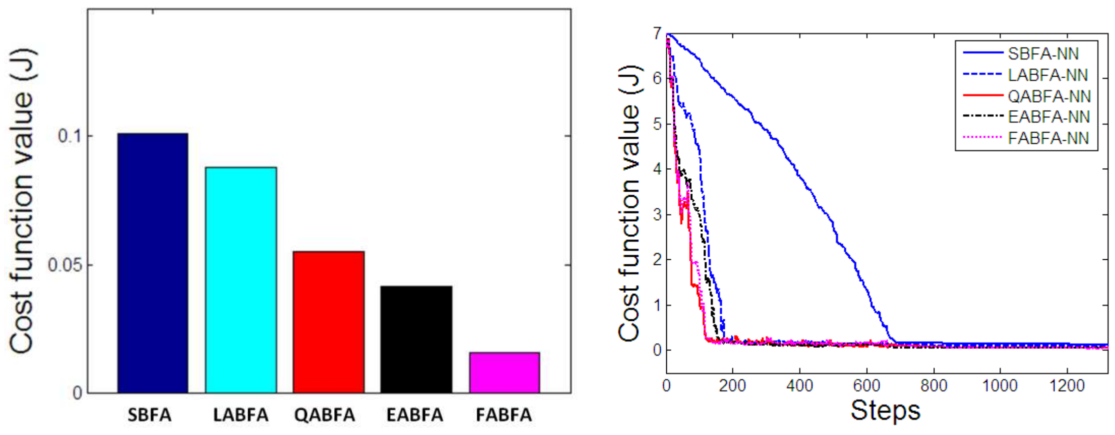

(a) Optimum J (b) Convergence plots

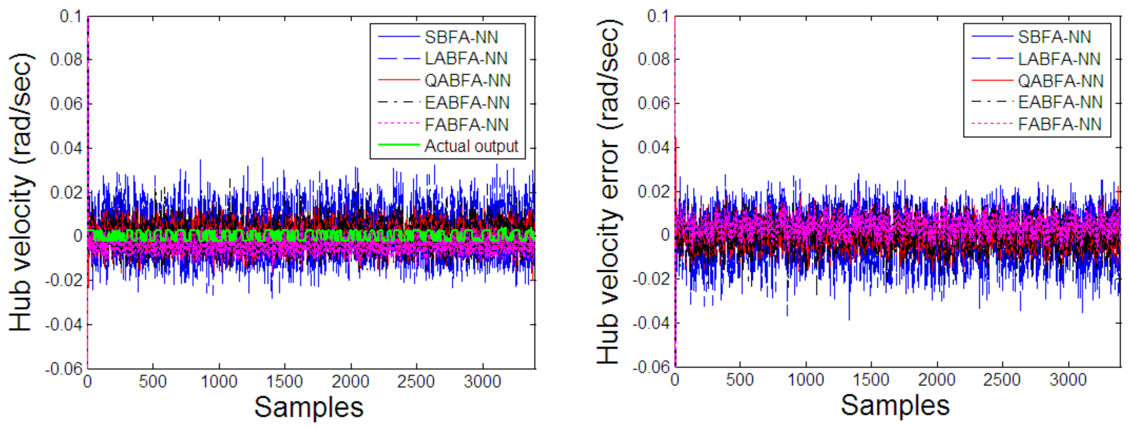

(c) Time-domain responses (d) Error

Figure 6.22: Simulation results of hub-velocity BFA-NN models in the training phase

B. Hub-velocity model in the validation phase

The numerical results of hub-velocity models in validation phase presented in Table 6.6 show that the cost function values achieved were 0.1079, 0.0939, 0.0589, 0.0445, and 0.0203 for SBFA-NN, LABFA-NN, QABFA-NN, EABFA-NN and FABFA-NN models respectively. It can be noticed from the results that all ABFA-NN models achieved smaller cost function values than SBFA-NN model with the best optimum J value achieved by FABFA-NN.

Table 6.6: Numerical result of hub-velocity BFA-NN models in the validation phase

Algorithm	**Optimum** $C(i)$	**Range of error** $(\boldsymbol{e}(\boldsymbol{k}))$	
		Minimum	**Maximum**
SBFA-NN	0.1079	-0.0364	0.0222
LABFA-NN	0.0939	-0.0365	0.0226
QABFA-NN	0.0589	-0.0237	0.0211
EABFA-NN	0.0445	-0.0193	0.0189
FABFA-NN	0.0203	-0.0185	0.0179

The bar chart depicted in Figure 6.23(a) show a comparison of the optimum J values achieved by the algorithms. The time-domain responses and error depicted in Figure 6.23(b) and Figure 6.23(c) respectively show that in general all the models were able to mimic the actual output, however, the ABFA-NN models had smaller prediction error range. The correlation tests of equation (3.2) for the models depicted in Figure 6.24-Figure 6.28 show that all correlation values were within 95% confidence boundary indicating acceptable performance of the models.

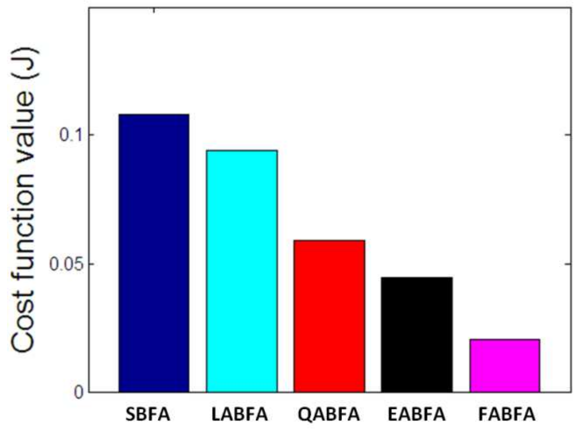

(a) Optimum J

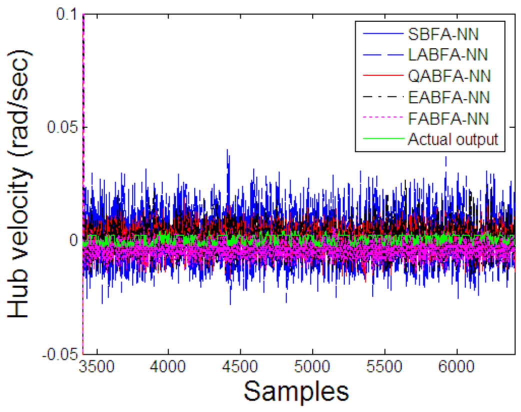

(b) Time-domain responses

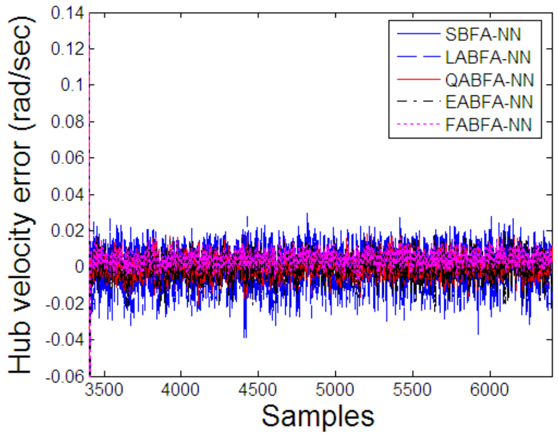

(c) Error

Figure 6.23: Simulation results of hub-velocity BFA-NN models in the validation phase

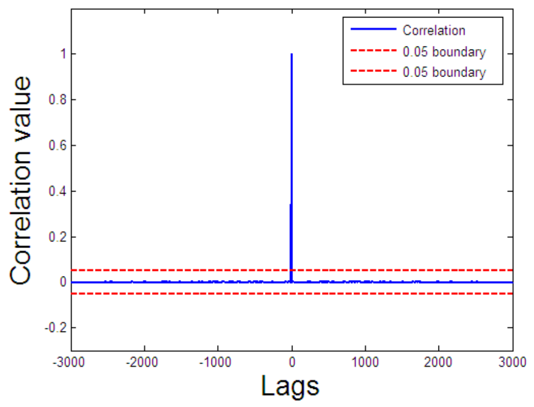

(a) $\phi_{\varepsilon\varepsilon}(\tau)$

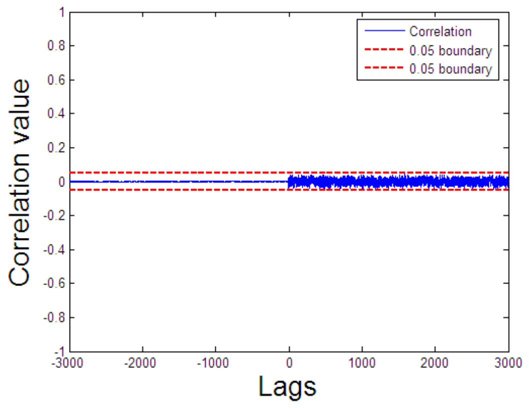

(b) $\phi_{u\varepsilon}(\tau)$

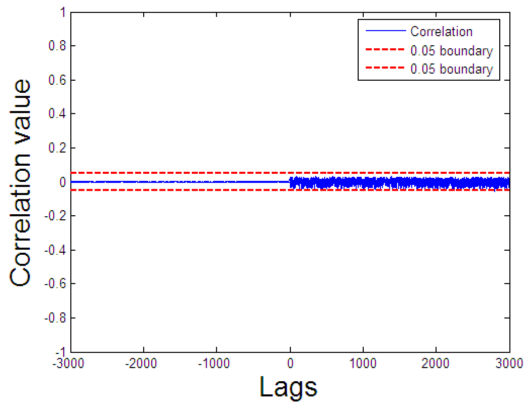

(c) $\phi_{u^2\varepsilon}(\tau)$

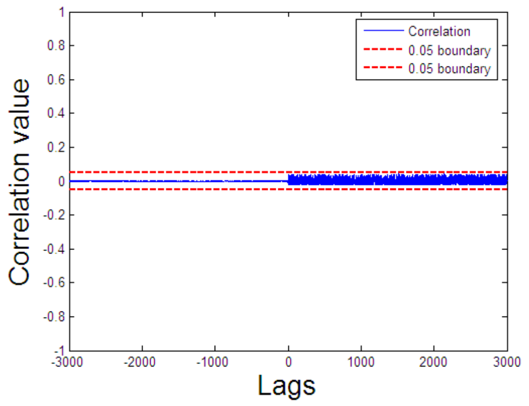

(d) $\phi_{u^2\varepsilon^2}(\tau)$

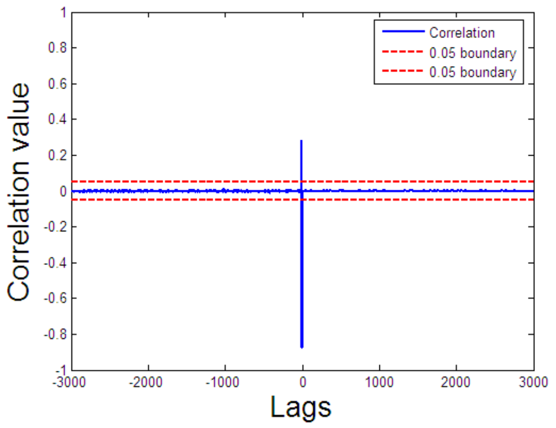

(e) $\phi_{\varepsilon(\varepsilon u)}(\tau)$

Figure 6.24: Correlation tests of hub-velocity SBFA-NN model

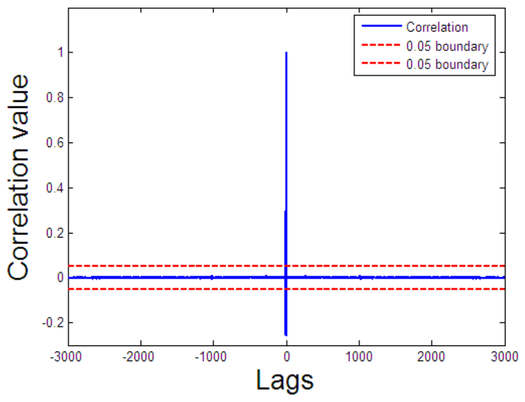

(a) $\phi_{\varepsilon\varepsilon}(\tau)$

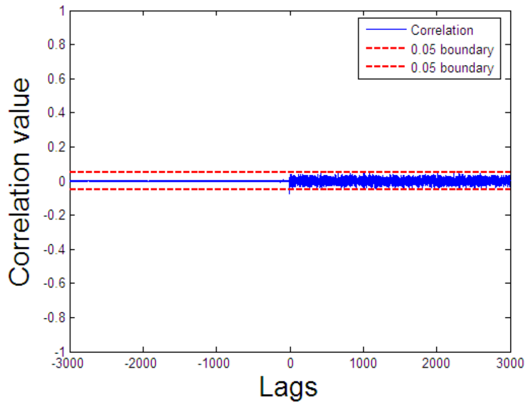

(b) $\phi_{u\varepsilon}(\tau)$

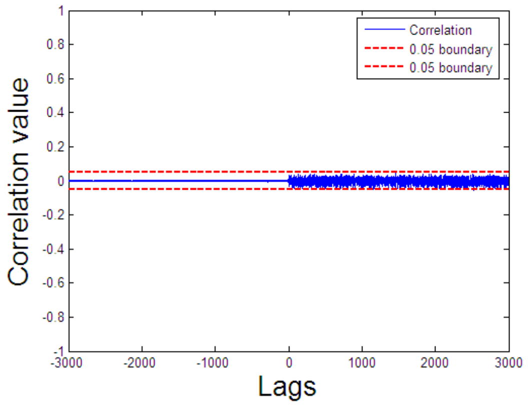

(c) $\phi_{u^2\varepsilon}(\tau)$

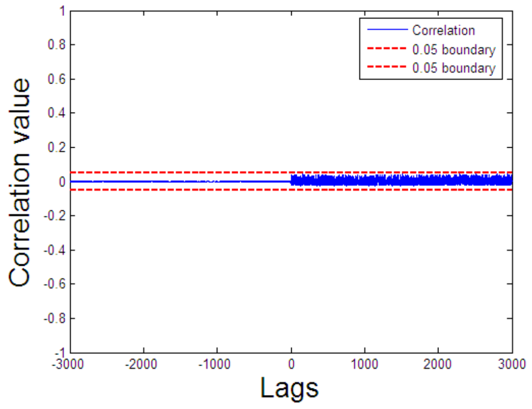

(d) $\phi_{u^2\varepsilon^2}(\tau)$

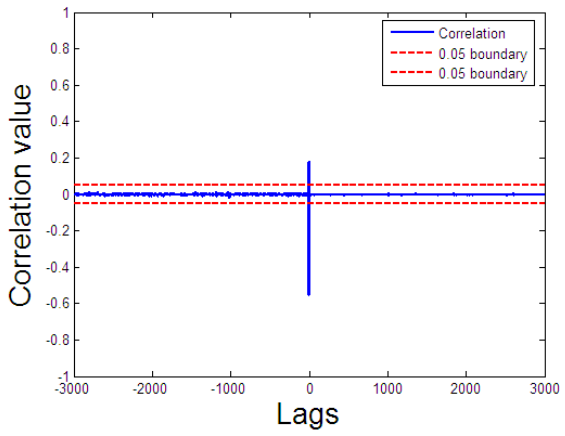

(e) $\phi_{\varepsilon(\varepsilon u)}(\tau)$

Figure 6.25: Correlation tests of hub-velocity LABFA-NN model

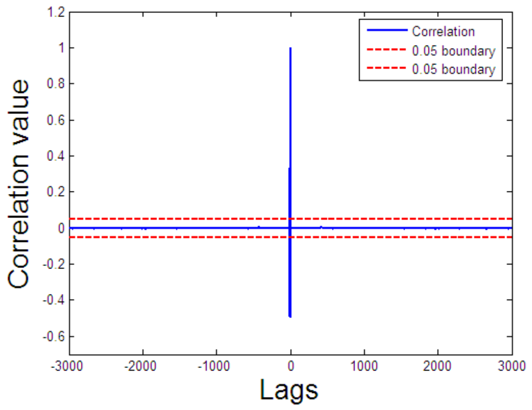

(a) $\phi_{\varepsilon\varepsilon}(\tau)$

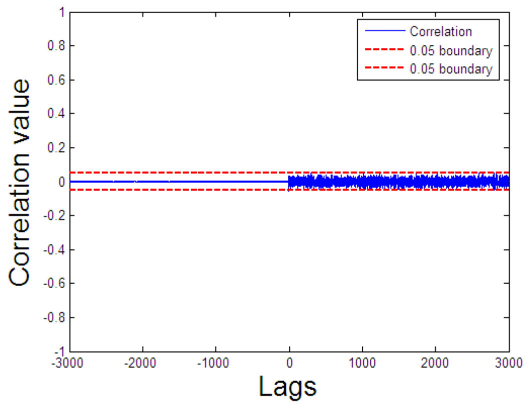

(b) $\phi_{u\varepsilon}(\tau)$

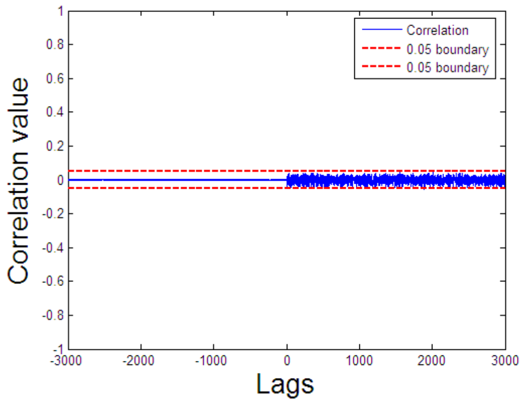

(c) $\phi_{u^2\varepsilon}(\tau)$

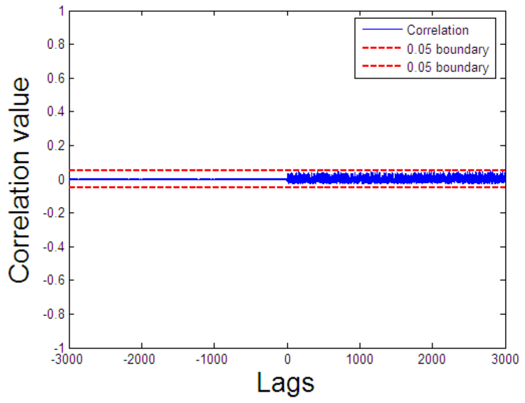

(d) $\phi_{u^2\varepsilon^2}(\tau)$

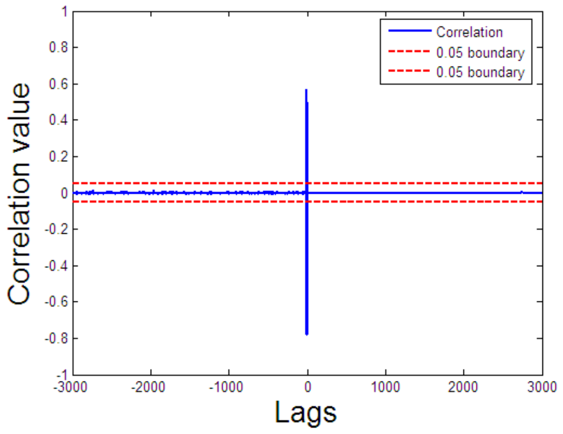

(e) $\phi_{\varepsilon(\varepsilon u)}(\tau)$

Figure 6.26: Correlation tests of hub-velocity QABFA-NN model

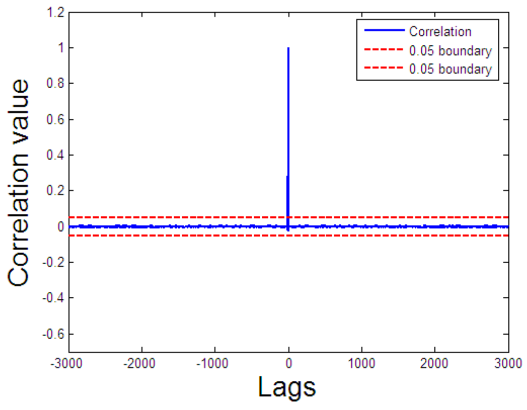

(a) $\phi_{\varepsilon\varepsilon}(\tau)$

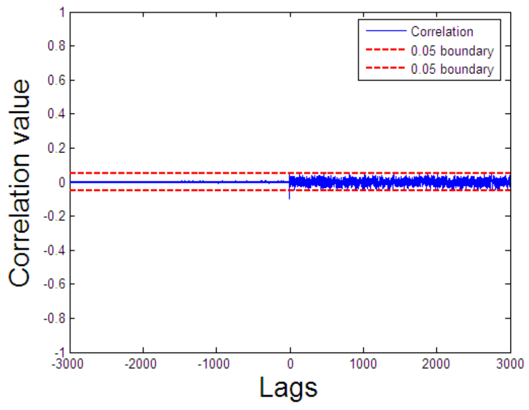

(b) $\phi_{u\varepsilon}(\tau)$

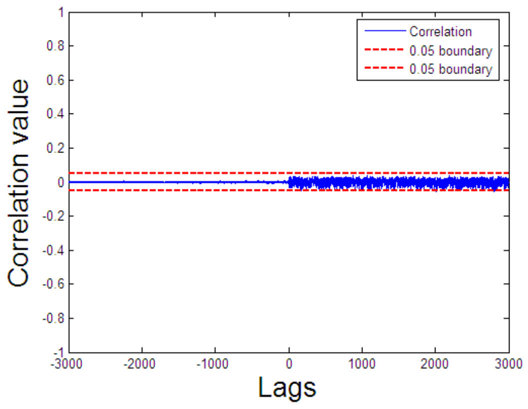

(c) $\phi_{u^2\varepsilon}(\tau)$

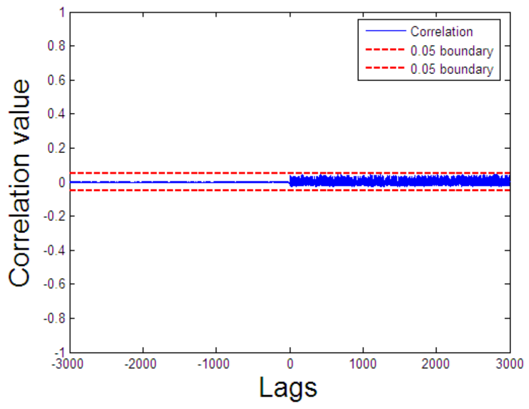

(d) $\phi_{u^2\varepsilon^2}(\tau)$

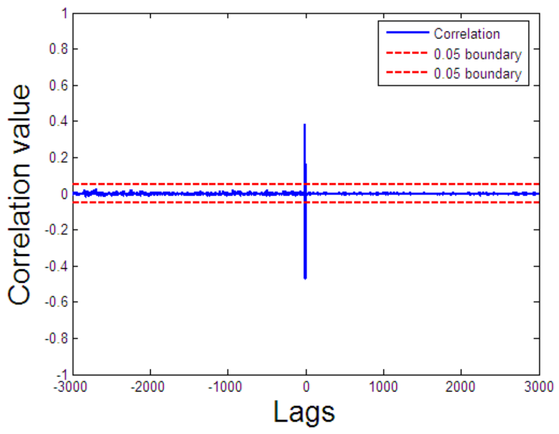

(e) $\phi_{\varepsilon(\varepsilon u)}(\tau)$

Figure 6.27: Correlation tests of hub-velocity EABFA-NN model

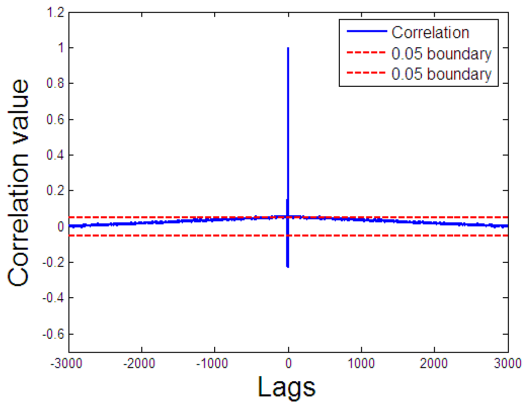

(a) $\phi_{\varepsilon\varepsilon}(\tau)$

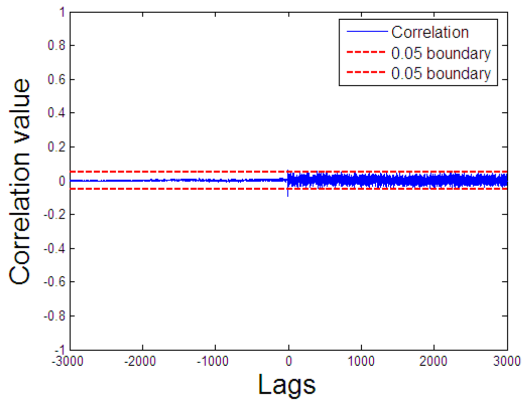

(b) $\phi_{u\varepsilon}(\tau)$

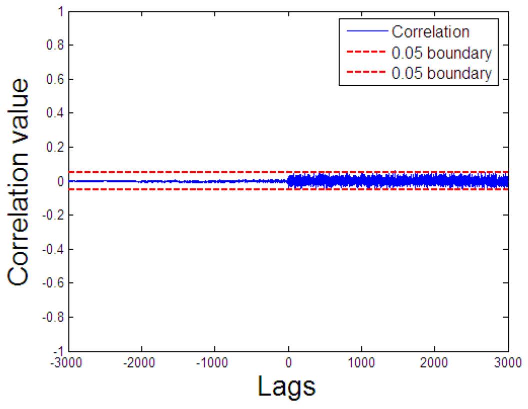

(c) $\phi_{u^2\varepsilon}(\tau)$

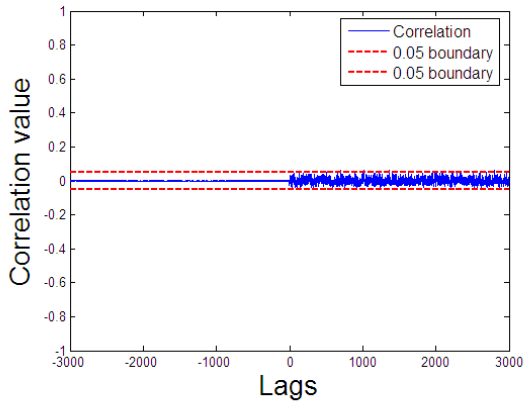

(d) $\phi_{u^2\varepsilon^2}(\tau)$

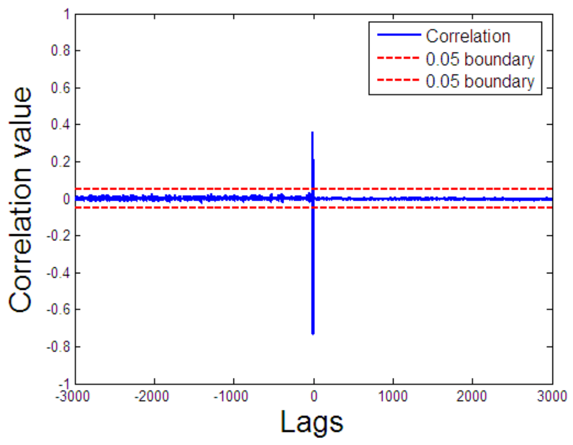

(e) $\phi_{\varepsilon(\varepsilon u)}(\tau)$

Figure 6.28: Correlation tests of hub-velocity FABFA-NN model

6.6.3. End-point acceleration model

A. End-point acceleration model in the training phase

In the modelling process of end-point acceleration an NN was set up with $n_u = n_y = 8$, one hidden layer with eight neurons and one output layer with one neuron. Thus, in total, there were 154 parameters to optimise. All the ABFA and SBFA used the same general parameters as:

❖ $p = 154$	❖ $N_c = 110$	❖ $S_r = S/2$	❖ $N_{ed} = 5$
❖ $S = 8$	❖ $N_s = 4$	❖ $N_{re} = 6$	❖ $p_{ed} = 0.25$

Initial positions of bacteria were selected randomly across the nutrient media and RMSE was used as the cost function. It was noticed in the investigations that the best optimum J of SBFA was achieved when the chemotactic step size $C(i)$ was equal to 0.022. For ABFAs, all parameters of $C_{al}(i), C_{aq}(i)$ and $C_{ae}(i)$ were selected manually by trial and error and the best results were achieved with adaptable chemotactic step sizes set up as:

$$C_{al}(i) = \frac{0.25}{1+\frac{1}{0.015|J(i)|}} \tag{6.19}$$

$$C_{aq}(i) = \frac{0.25}{1+\frac{1}{0.0025\left(\left(0.6J(i)\right)^2+0.6|J(i)|\right)}} \tag{6.20}$$

$$C_{ae}(i) = \frac{0.25}{1+\frac{1}{0.04e^{0.1|J(i)|}}} \tag{6.21}$$

For FABFA, parameters of seven Gaussian membership functions for input and output were chosen by trial and error. The fuzzy input, $|J(i)|$, was related to fuzzy output, $C_{af}(i)$, using fuzzy rules formulated as:

R_1	:	IF $|J(i)|$ is ES THEN $C_{af}(i)$ is ES	(1)	
R_2	:	IF $|J(i)|$ is VS THEN $C_{af}(i)$ is ES	(0.1)	
R_3	:	IF $|J(i)|$ is S THEN $C_{af}(i)$ is S	(0.1)	
R_4	:	IF $|J(i)|$ is M THEN $C_{af}(i)$ is M	(0.2)	(6.22)
R_5	:	IF $|J(i)|$ is B THEN $C_{af}(i)$ is B	(1)	
R_6	:	IF $|J(i)|$ is VB THEN $C_{af}(i)$ is VB	(1)	
R_7	:	IF $|J(i)|$ is EB THEN $C_{af}(i)$ is EB	(1)	

The Gaussian membership functions for input and output and fuzzy surface of FABFA are depicted in Figure 6.29.

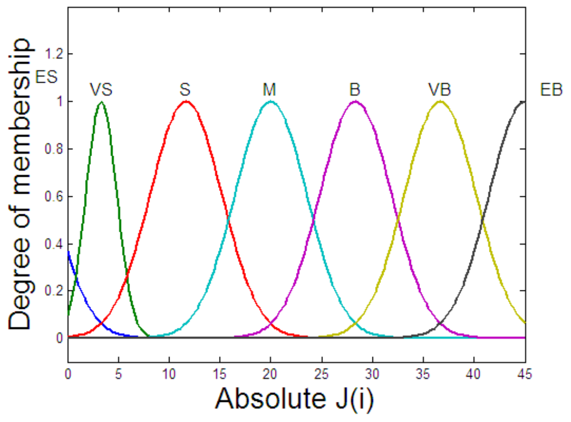

(a) Input: $|J(i)|$

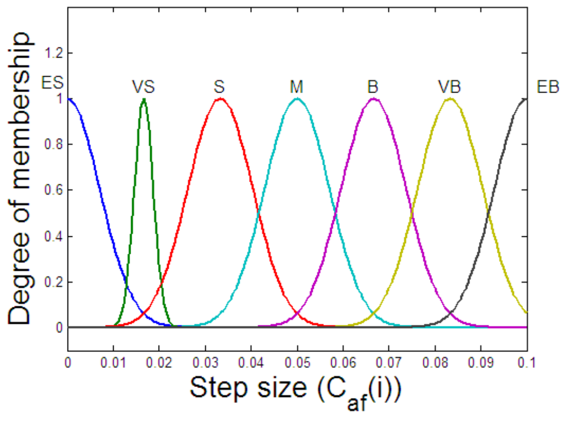

(b) Output: $C_{af}(i)$

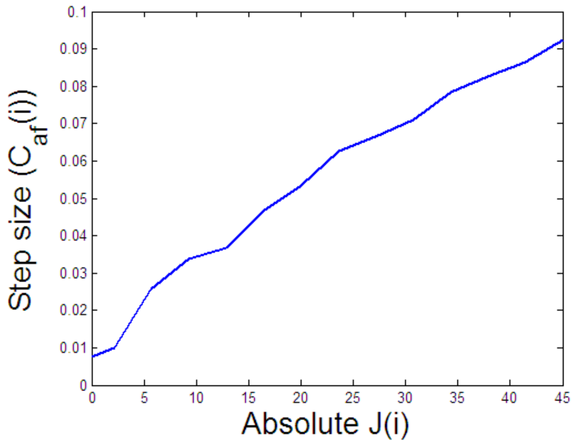

(c) Fuzzy surface

Figure 6.29: Fuzzy membership function and surface of FABFA for end-point acceleration models in the training phase

The numerical results of end-point acceleration in modelling phase for the algorithms presented in Table 6.7 show that the cost function values achieved were 0.0449, 0.0337, 0.0364, 0.0366 and 0.0338 for SBFA-NN, LABFA-NN, QABFA-NN, EABFA-NN and FABFA-NN model respectively. These results show that all ABFA-NN models achieved better optimum J values than SBFA-NN with the best optimum J achieved by LABFA-NN.

Table 6.7: Numerical results of end-point acceleration BFA-NN models in the training phase

Algorithm	$C(i)$ **range**	**Convergence (steps)**	**Optimum** J	**Range of error (**$\boldsymbol{e(k)}$**)**	
				Minimum	**Maximum**
SBFA-NN	0.022	1780	0.0449	-0.1554	0.2511
LABFA-NN	[0.0139, 0.25]	1500	**0.0337**	-0.1483	0.1235
QABFA-NN	[0.0069, 0.25]	1500	0.0364	-0.1494	0.1794
EABFA-NN	[0.0146, 0.25]	1500	0.0366	-0.1554	0.2029
FABFA-NN	[0.0135, 0.093]	1500	0.0338	-0.1554	0.1222

The bar chart depicted in Figure 6.30(a) show a comparison of the optimum J values. The convergence plots depicted in Figure 6.30(b) show that all ABFA-NN models were faster in convergence and able to find lower cost function values than SBFA-NN. The time-domain responses and error depicted in Figure 6.30(c) and Figure 6.30(d) respectively show that, although the predicted outputs all followed actual output, ABFA-NN models had smaller prediction error range than SBFA-NN model. From the PSD plots of end-point acceleration depicted in Figure 6.30(e), it can be noticed that all models exhibit the same resonance frequencies as the actual output. The frequency resonance frequencies were 11.67 Hz, 36.96 Hz and 64.22 Hz for the 1st, 2nd and 3rd mode respectively.

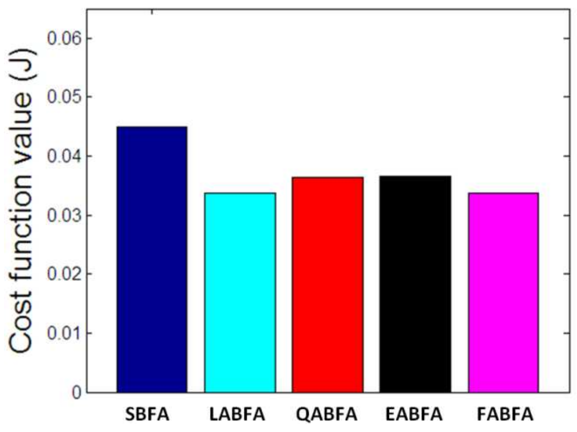

(a) Optimum *J*

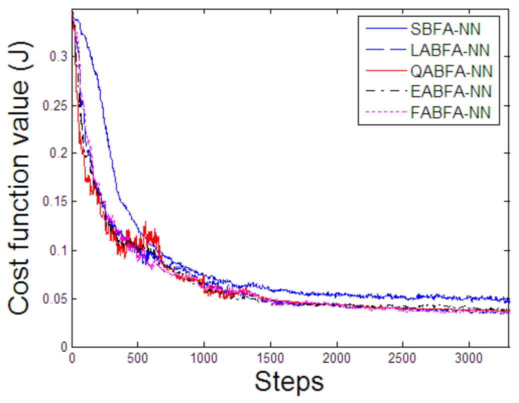

(b) Convergence plots

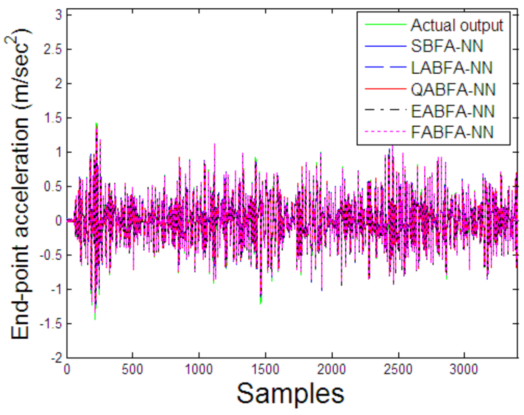

(c) Time-domain responses

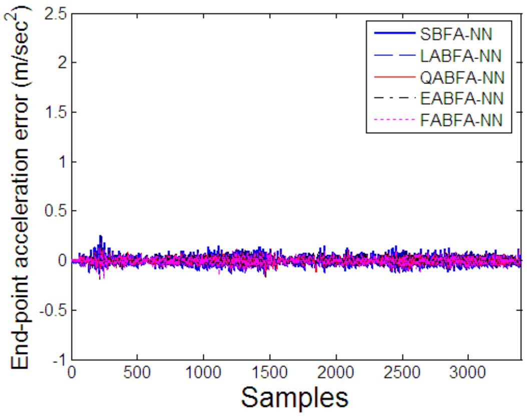

(d) error

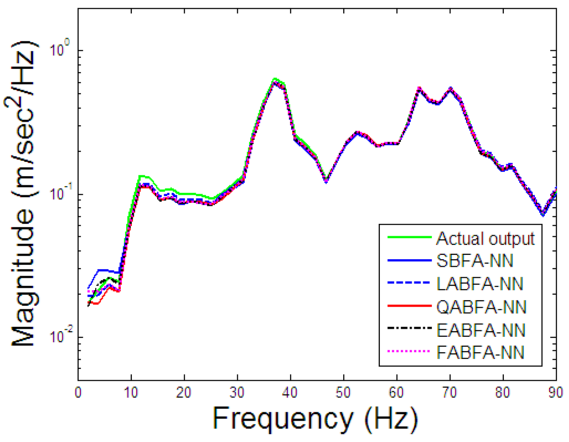

(e) PSD

Figure 6.30: Simulation results of end-point acceleration BFA-NN model in the training phase

B. End-point acceleration model in the validation phase

Numerical results presented in Table 6.8 show that the cost function values achieved in the validating phase were 0.0593, 0.0427, 0.0459, 0.0473 and 0.0437 for SBFA-NN, LABFA-NN, QABFA-NN, EABFA-NN and FABFA-NN models respectively. These results show that ABFA-NN models achieved lower cost function values than SBFA-NN with the lowest optimum J achieved by LABFA-NN.

Table 6.8: Numerical results of end-point acceleration BFA-NN models in the validation phase

Algorithm	**Optimum** J	**Range of error ($e(k)$)**	
		Minimum	**Maximum**
SBFA-NN	0.0593	-0.2011	0.4414
LABFA-NN	**0.0427**	-0.2010	0.3463
QABFA-NN	0.0459	-0.2010	0.3499
EABFA-NN	0.0473	-0.2008	0.3455
FABFA-NN	0.0437	-0.2003	0.3506

A comparison of optimum J values achieved by the algorithms is shown in the bar chart depicted in Figure 6.31(a). Time domain responses and prediction error depicted in Figure 6.31(b) and Figure 6.31(c) show that in general all models were able to predict the actual output very well, however, ABFA-NN models had smaller prediction error range which means closer to the actual output than SBFA-NN. The PSD plots of end-point acceleration depicted in Figure 6.31(d) show that all predicted outputs had the same resonance frequencies as with the actual output. The resonance frequencies for the first three modes were 11.67 Hz, 36.96 Hz and 64.22 Hz. The correlation tests of equation (3.2) for the models depicted in Figure 6.32-Figure 6.36 show that all correlation values were within 95% confidence boundary indicating the acceptability of the models.

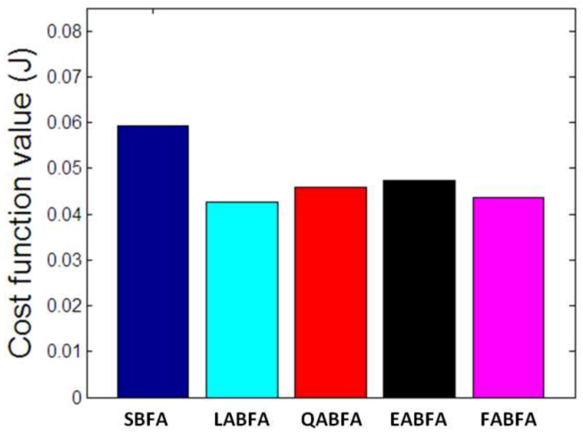

(a) Optimum *J*

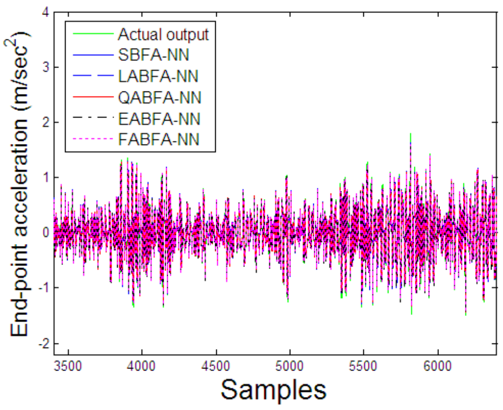

(b) Time-domain response

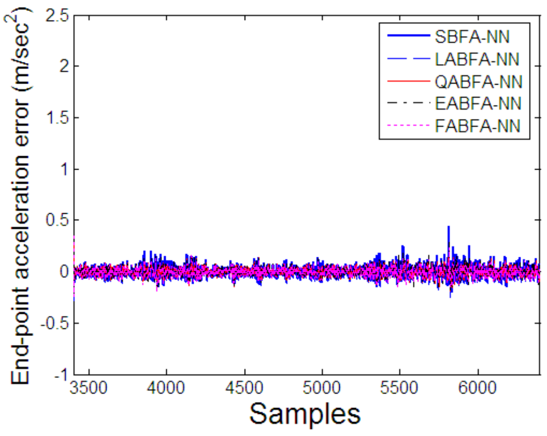

(c) Error

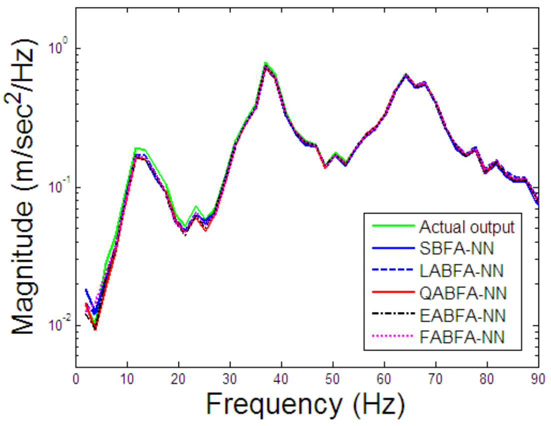

(d) PSD

Figure 6.31: Simulation results of end-point acceleration BFA-NN model in the validation phase

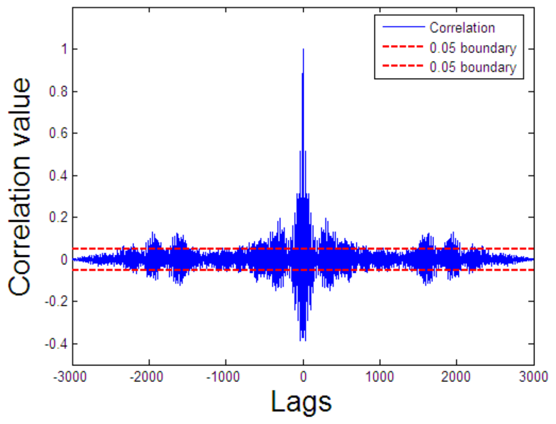

(a) $\phi_{\varepsilon\varepsilon}(\tau)$

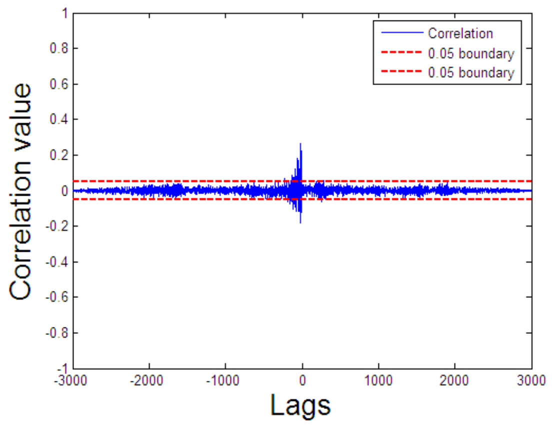

(b) $\phi_{u\varepsilon}(\tau)$

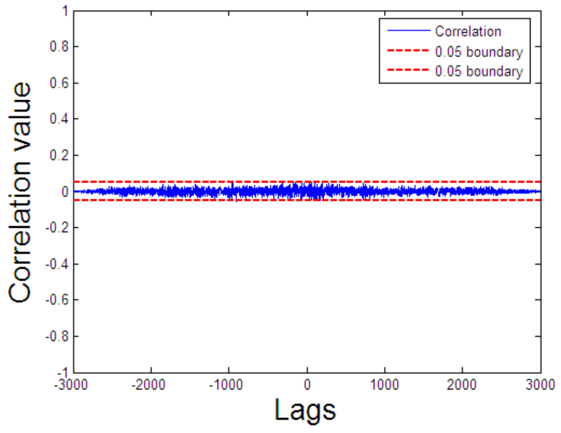

(c) $\phi_{u^2\varepsilon}(\tau)$

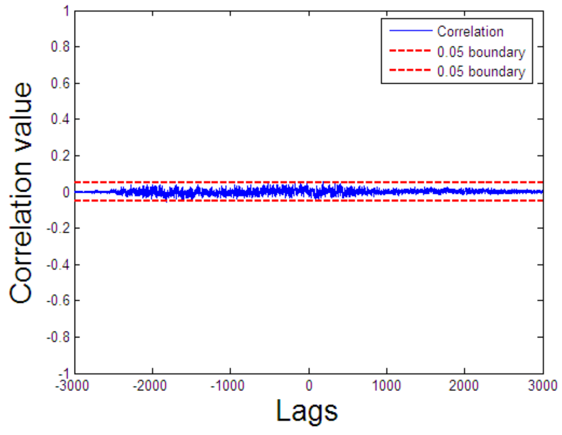

(d) $\phi_{u^2\varepsilon^2}(\tau)$

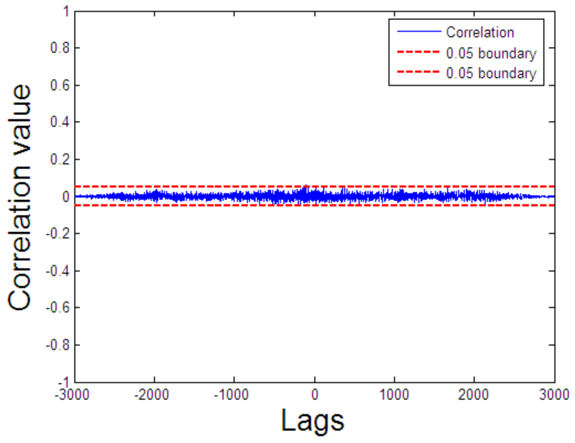

(e) $\phi_{\varepsilon(\varepsilon u)}(\tau)$

Figure 6.32: Correlation tests of end-point acceleration SBFA-NN model

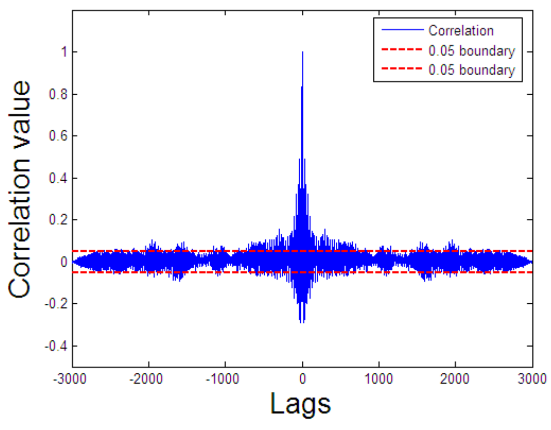

(a) $\phi_{\varepsilon\varepsilon}(\tau)$

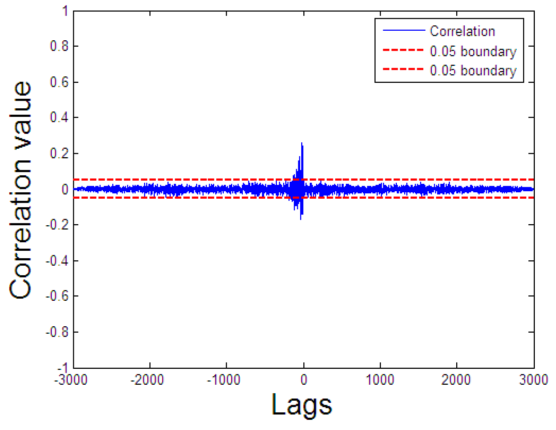

(b) $\phi_{u\varepsilon}(\tau)$

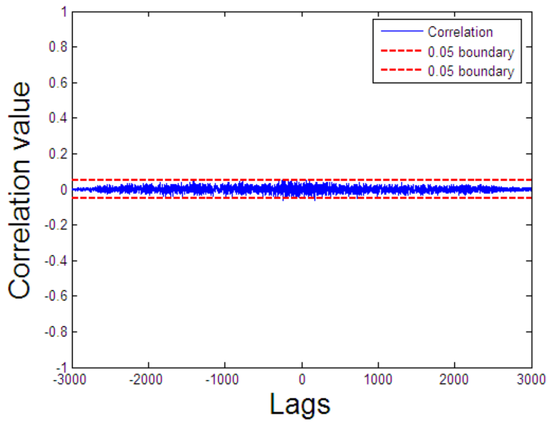

(c) $\phi_{u^2\varepsilon}(\tau)$

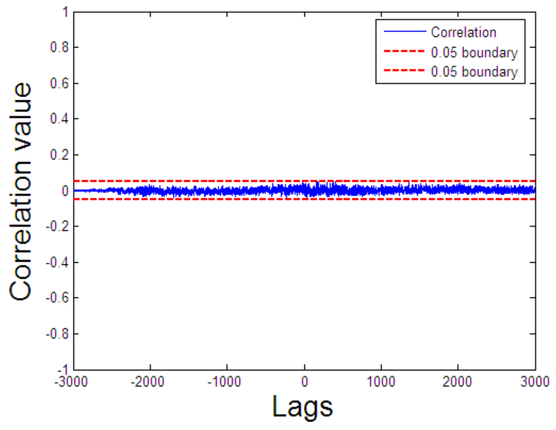

(d) $\phi_{u^2\varepsilon^2}(\tau)$

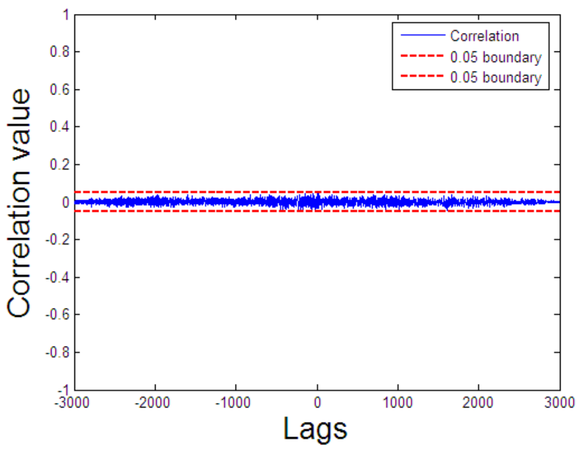

(e) $\phi_{\varepsilon(\varepsilon u)}(\tau)$

Figure 6.33: Correlation tests of end-point acceleration LABFA-NN model

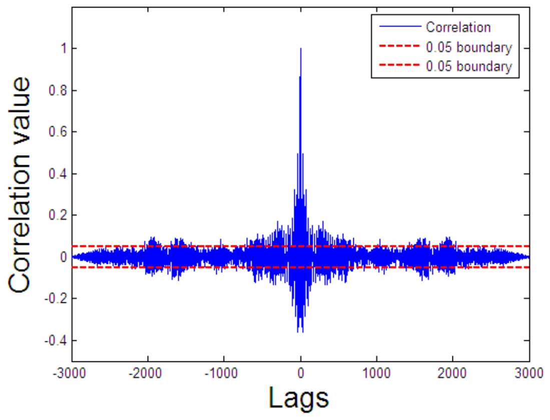

(a) $\phi_{\varepsilon\varepsilon}(\tau)$

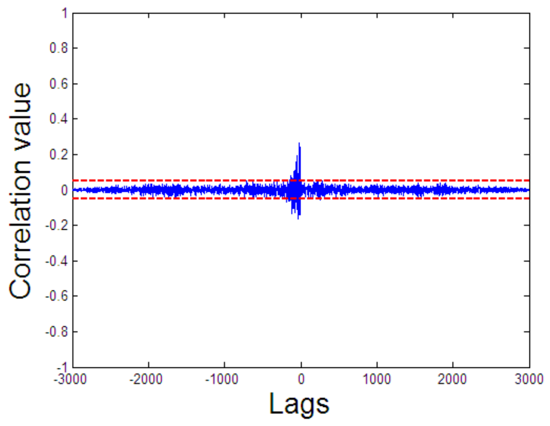

(b) $\phi_{u\varepsilon}(\tau)$

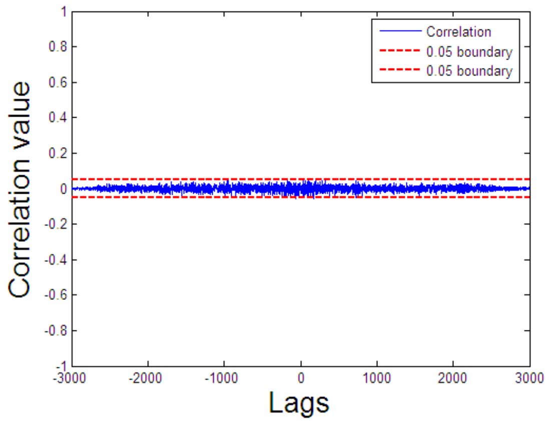

(c) $\phi_{u^2\varepsilon}(\tau)$

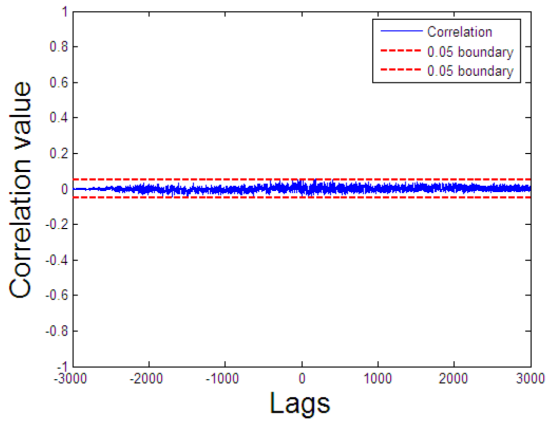

(d) $\phi_{u^2\varepsilon^2}(\tau)$

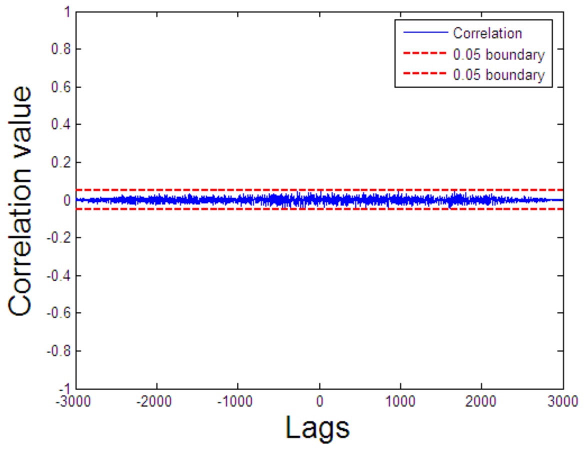

(e) $\phi_{\varepsilon(\varepsilon u)}(\tau)$

Figure 6.34: Correlation tests of end-point acceleration QABFA-NN model

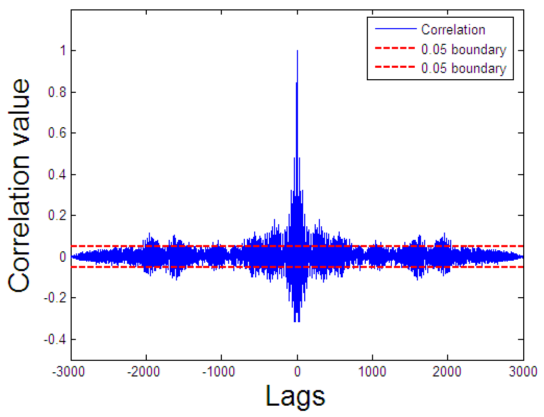

(a) $\phi_{\varepsilon\varepsilon}(\tau)$

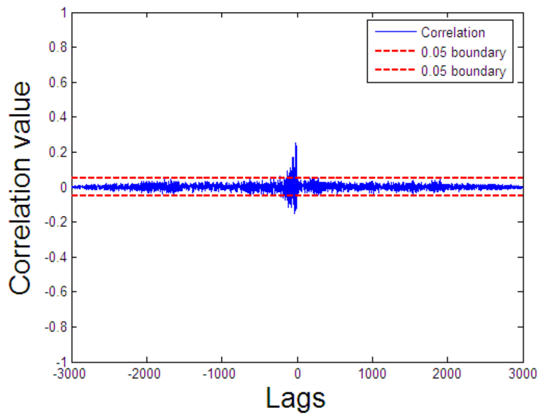

(b) $\phi_{u\varepsilon}(\tau)$

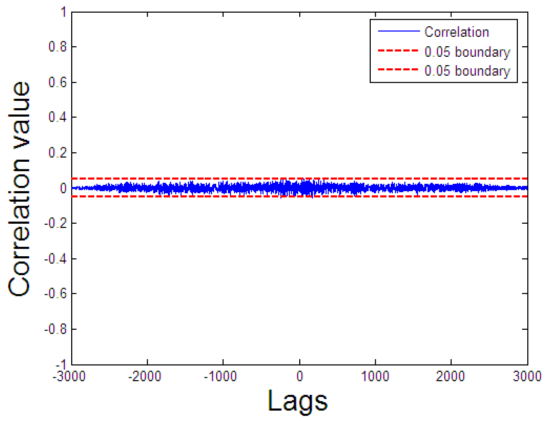

(c) $\phi_{u^2\varepsilon}(\tau)$

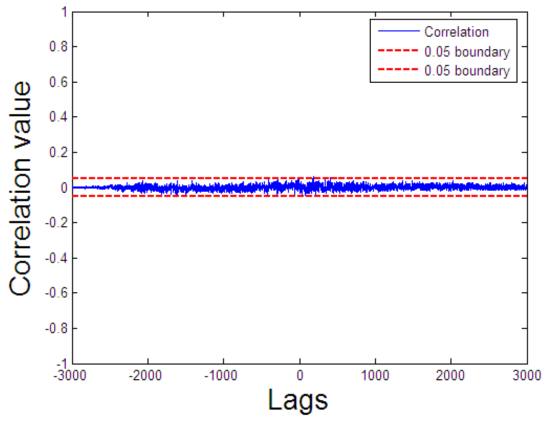

(d) $\phi_{u^2\varepsilon^2}(\tau)$

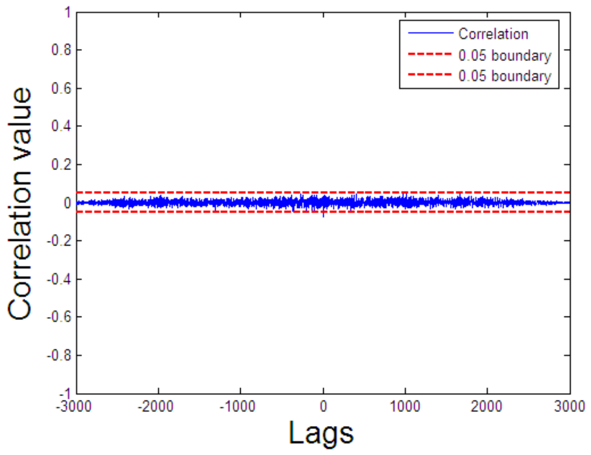

(e) $\phi_{\varepsilon(\varepsilon u)}(\tau)$

Figure 6.35: Correlation tests of end-point acceleration EABFA-NN model

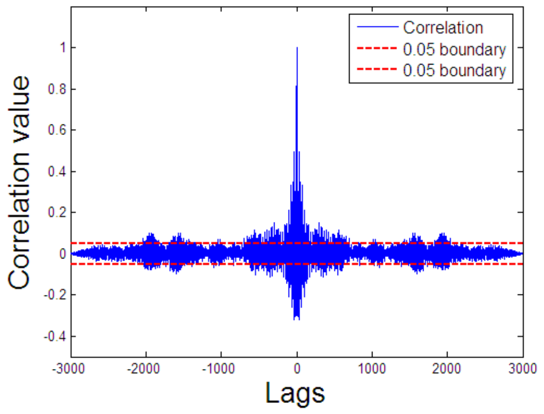

(a) $\phi_{\varepsilon\varepsilon}(\tau)$

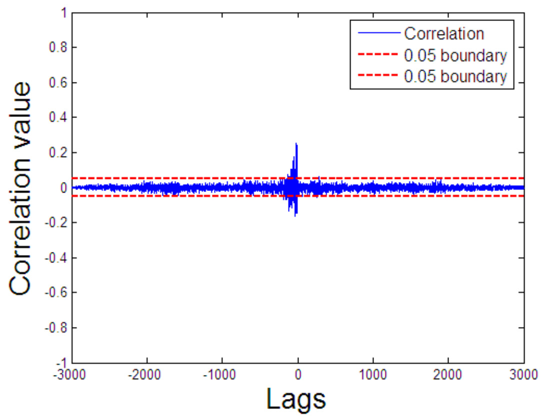

(b) $\phi_{u\varepsilon}(\tau)$

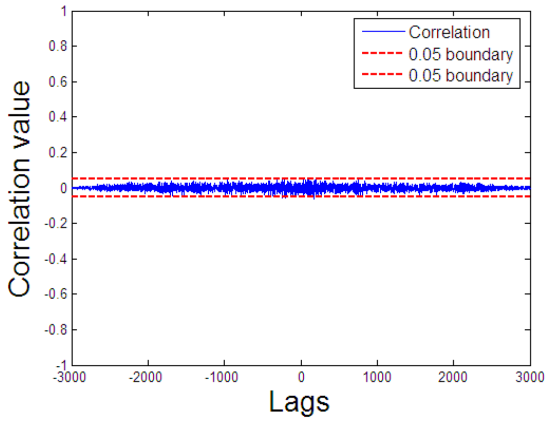

(c) $\phi_{u^2\varepsilon}(\tau)$

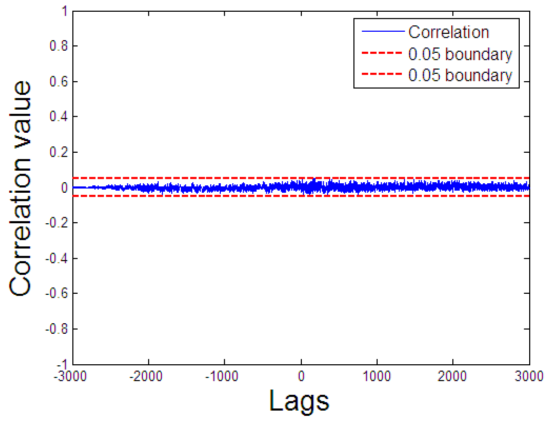

(d) $\phi_{u^2\varepsilon^2}(\tau)$

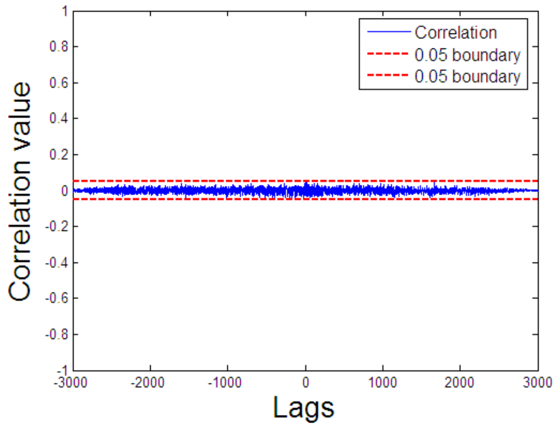

(e) $\phi_{\varepsilon(\varepsilon u)}(\tau)$

Figure 6.36: Correlation tests of end-point acceleration FABFA-NN model

6.7. Results and discussion: BFA-FL models

6.7.1. Hub-angle model

A. Hub-angle model in the training phase

It was noticed through simulations that, in this investigation, the best cost function value was achieved with $K_2 = K_3 = 1$. Thus, in the hub-angle modelling, there are 26 parameters to be optimised. These comprise:

- 25 parameters for weights of each rule. There are 25 fuzzy rules in total resulting from two inputs with five Gaussian membership functions each.
- 1 parameter for scaling factor K_1

In this work all BFAs used the same general parameters as:

❖ $p = 26$	❖ $N_c = 30$	❖ $S_r = S/2$	❖ $N_{ed} = 2$
❖ $S = 8$	❖ $N_s = 3$	❖ $N_{re} = 6$	❖ $p_{ed} = 0.25$

The initial positions of bacteria were selected randomly across the nutrient media. Various chemotactic step size values were tested with SBFA ($C(i)$) and it was noticed that the best optimum cost function J was achieved when $C(i)$ was equal to 0.0125. For ABFA, the parameters of adaptable chemotactic step size were chosen manually by trial and error and the best optimum J was achieved when adaptable chemotactic step sizes were formulated as:

$$C_{al}(i) = \frac{0.4}{1+\frac{1}{0.007|J(i)|}} \tag{6.23}$$

$$C_{aq}(i) = \frac{0.4}{1+\frac{1}{0.075\left(\left(0.06J(i)\right)^2+0.06|J(i)|\right)}} \tag{624}$$

$$C_{ae}(i) = \frac{0.4}{1+\frac{1}{0.0175e^{(0.075|J(i)|)}}} \tag{6.25}$$

As indicated earlier, the construction of FL consists of two inputs, i.e. $u(k-1)$ in the range of [-0.3, 0.3] and $y(k-1)$ in the range of [0, 0.25], and one output, i.e. $\hat{y}(k)$ in the range of [-0.01, 0.275]. All Gaussian membership function parameters were set manually by trial and error. The membership functions of inputs and output are depicted in Figure 6.37. The fuzzy rules which determine the relation between input and output were determined by trial and error based on experience and experimental input-output data pairs, and these are shown in Table 6.9.

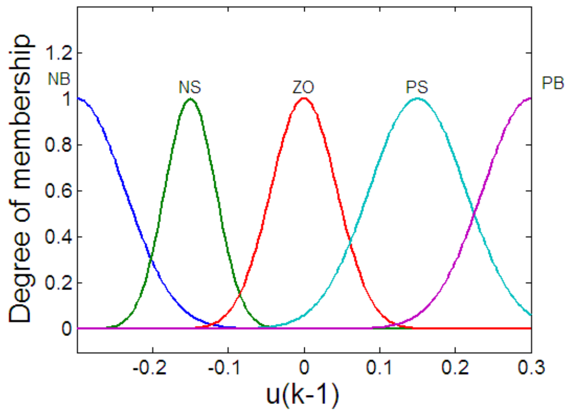

(a) Input 1: $u(k-1)$

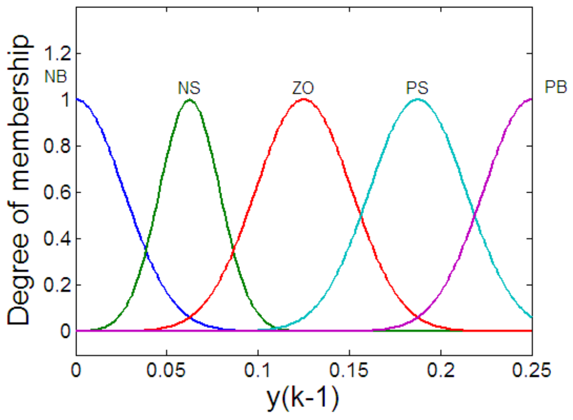

(b) Input 2: $y(k-1)$

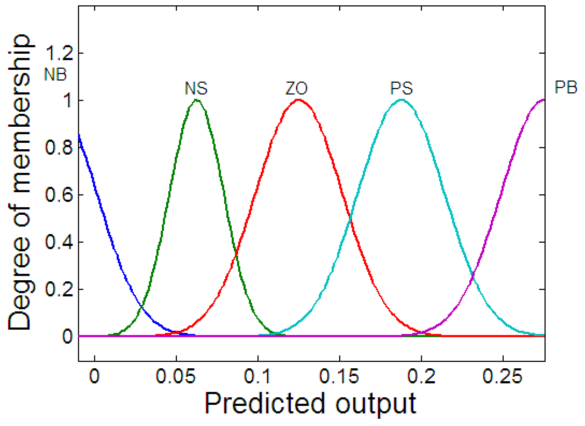

(c) Output: predicted output ($\hat{y}(k)$)

Figure 6.37: Fuzzy membership functions of BFA-FL for hub-angle model

Table 6.9: Fuzzy rules for hub-angle model

Input 1:	**Input 2: $y(k-1)$**				
$u(k-1)$	**NB**	**NS**	**ZO**	**PS**	**PB**
NB	NB (w_{r1})	NS (w_{r6})	ZO (w_{r11})	PS (w_{r16})	PB (w_{r21})
NS	NB (w_{r2})	NS (w_{r7})	ZO (w_{r12})	PS (w_{r17})	PB (w_{r22})
ZO	NB (w_{r3})	NS (w_{r8})	ZO (w_{r13})	PS (w_{r18})	PB (w_{r23})
PS	NB (w_{r4})	NS (w_{r9})	ZO (w_{r14})	PS (w_{r19})	PB (w_{r24})
PB	NB (w_{r5})	NS (w_{r10})	PS (w_{r15})	PB (w_{r20})	PB (w_{r25})

Numerical results presented in Table 6.10 show that, by using formula in equation (7.3)-(7.5), adaptable step size values of ABFAs were in the range [0.0119, 0.4], [0.0094, 0.4] and [0.0096, 0.4] for LABFA, QABFA and EABFA respectively. By using these adaptable chemotactic step sizes, the optimum J values achieved were

0.0043, 0.0042 and 0.0045 for LABFA, QABFA and EABFA respectively lower than 0.0056 of SBFA.

Table 6.10: Numerical results of hub-angle BFA-FL models in the training phase

Algorithm	$C(i)$ **range**	**Convergence (steps)**	**Optimum** J	**Range of error** $(e(k))$	
				Minimum	**Maximum**
SBFA-FL	0.0125	180	0.0056	-0.0075	0.0084
LABFA-FL	[0.0119, 0.4]	150	0.0043	-0.0075	0.0081
QABFA-FL	[0.0094, 0.4]	150	**0.0042**	-0.0074	0.0082
EABFA-FL	[0.0096, 0.4]	150	0.0045	-0.0074	0.0083

A comparison of the optimum J values achieved by the algorithms is shown in the bar chart in Figure 6.38(a). The convergence plots of the algorithms are depicted in Figure 6.38(b). It can be noted that all ABFA-FL converged to optimum value faster than SBFA-FL which converged in 180 steps. The time-domain responses and error for the models are depicted in Figure 6.38(c) and Figure 6.38(d) respectively. The fuzzy surfaces of the models are presented in Figure 6.39.

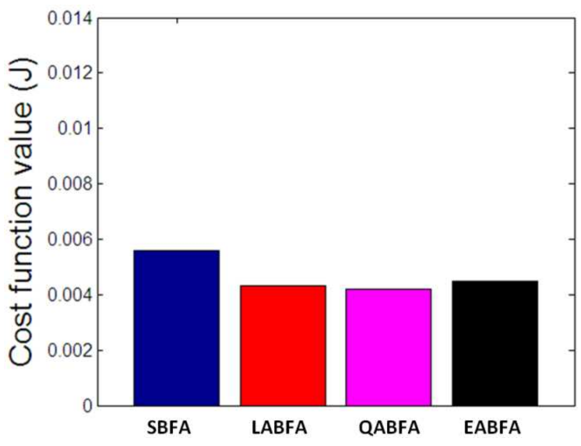

(a) Optimum J

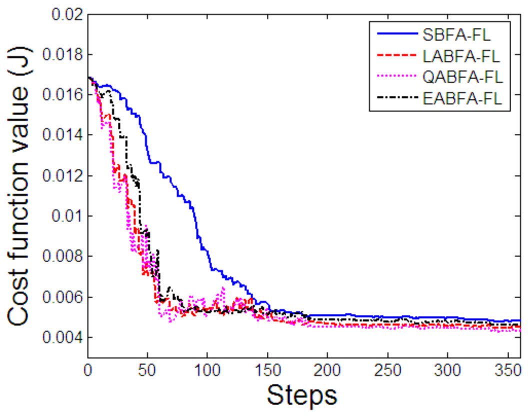

(b) Convergence plots

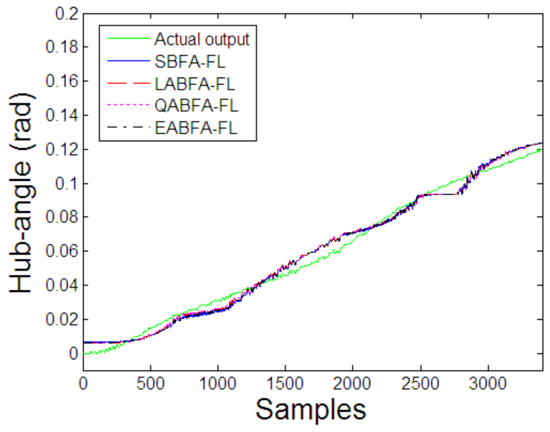

(c) Time-domain responses

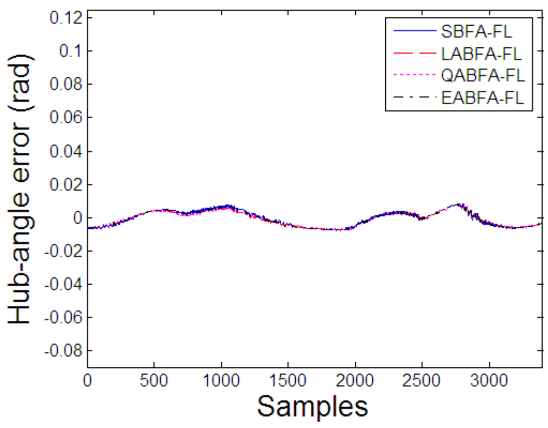

(d) Error

Figure 6.38: Simulation results of hub-angle BFA-FL models in modelling phase

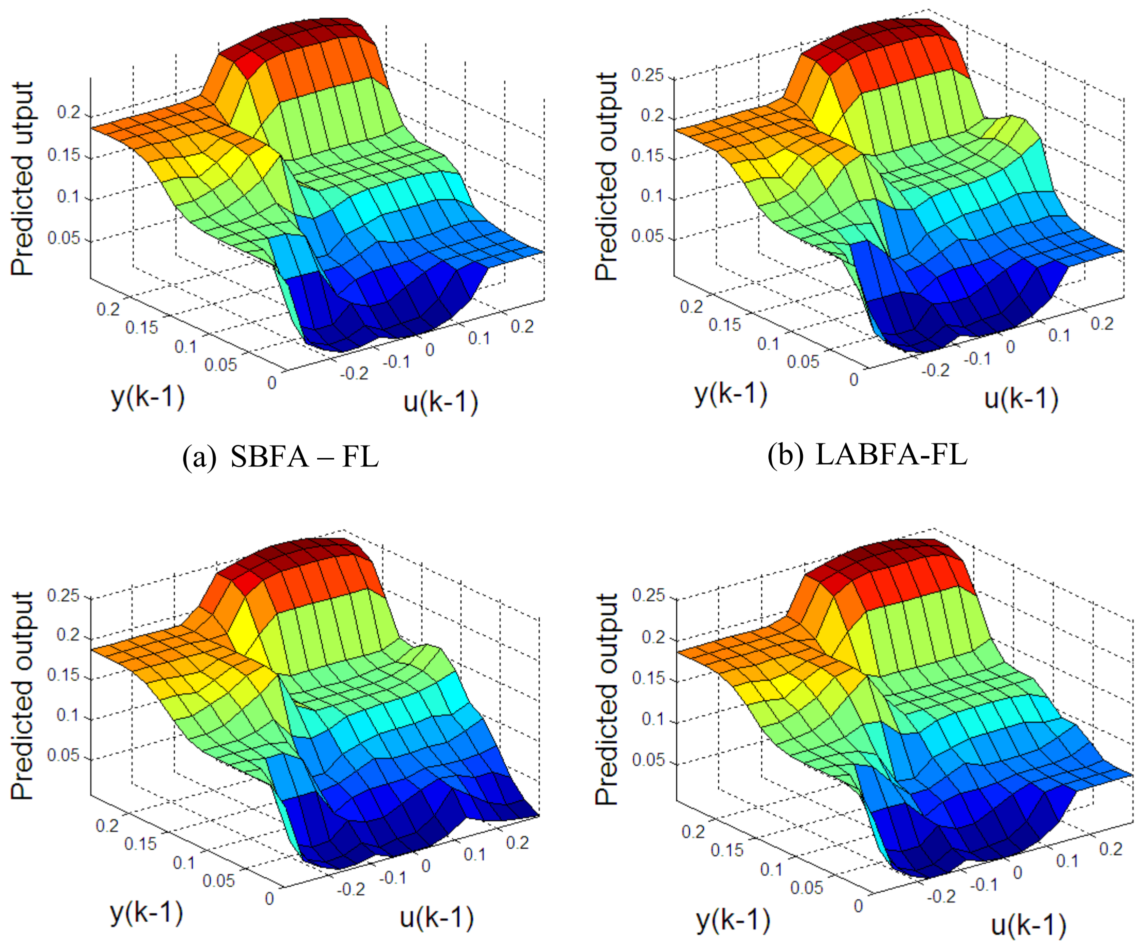

(a) SBFA – FL (b) LABFA-FL

(c) QABFA-FL (d) EABFA-FL

Figure 6.39: Fuzzy surfaces of hub-angle BFA-FL models

B. Hub-angle model in the validation phase

Numerical results outlined in Table 6.11 show that the cost function values achieved in the validation phase were 0.0194, 0.0162, 0.0162 and 0.0157 for SBFA-FL, LABFA-FL, QABFA-FL and EABFA-FL respectively. These results show that all ABFAs-FL based models achieved better optimum J values than SBFA-FL with the best optimum J achieved by EABFA-FL. A comparison of optimum J values for the algorithms in the validating phase is depicted in Figure 6.40(a). The hub-angle responses and error in the validation phase plotted in Figure 6.40(b) and Figure 6.40(c) respectively show that the predicted outputs of ABFA-FL based models were closer to the actual output than that of SBFA-FL based model. Correlation tests depicted in Figure 6.41-Figure 6.44 show that all models were acceptable because the correlation values were within 95% confidence boundary (stated as 0.05 boundary).

Table 6.11: Numerical results of hub-angle BFA-FL models in the validation phase

Algorithm	**Optimum J**	**Range of error $(e(k))$**	
		Minimum	**Maximum**
SBFA-FL	0.0194	-0.0075	0.0418
LABFA-FL	0.0162	-0.0102	0.0360
QABFA-FL	0.0162	-0.0102	0.0361
EABFA-FL	0.0157	-0.0110	0.0353

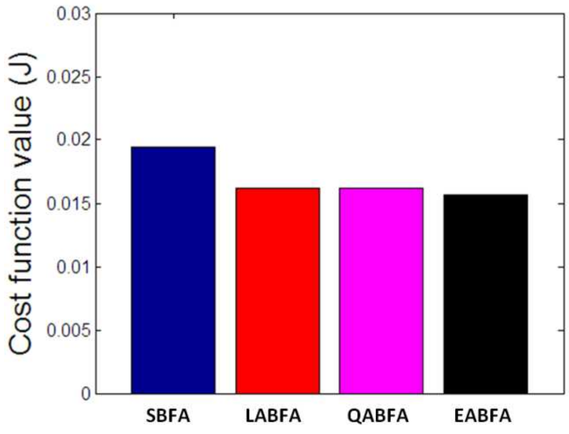

(a) Optimum J

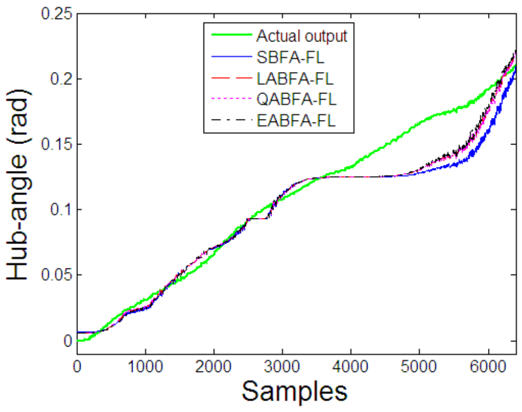

(b) Time-domain responses

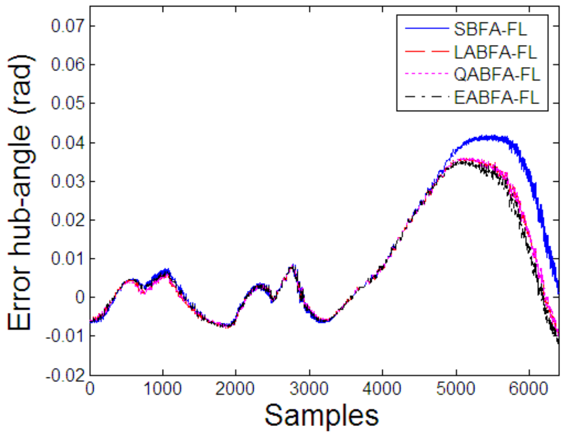

(c) Error

Figure 6.40: Simulation results of hub-angle BFA-FL models in the validation phase

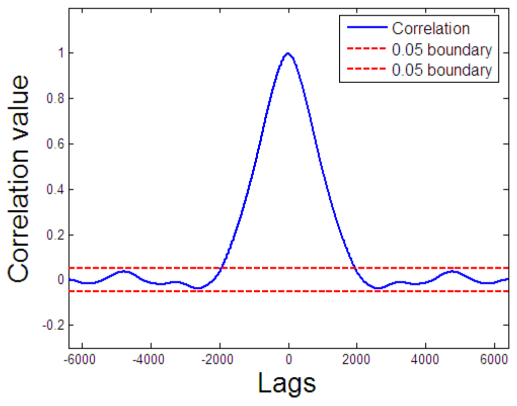

(a) $\phi_{\varepsilon\varepsilon}(\tau)$

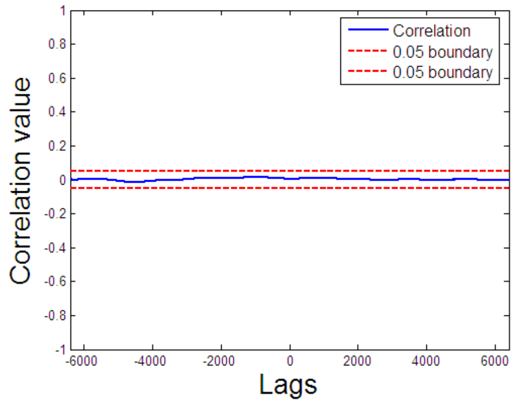

(b) $\phi_{u\varepsilon}(\tau)$

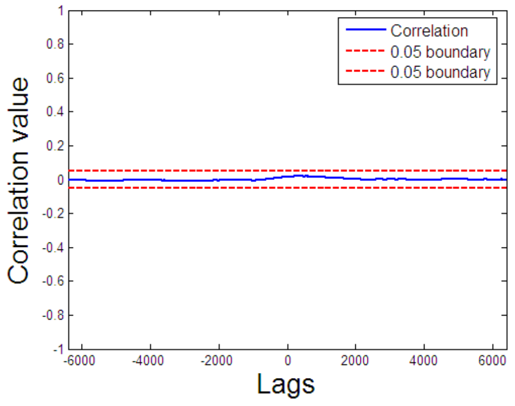

(c) $\phi_{u^2\varepsilon}(\tau)$

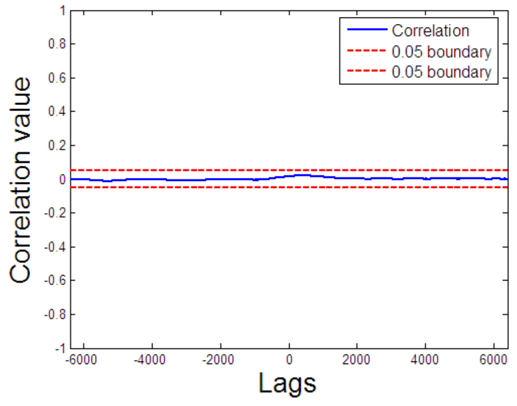

(d) $\phi_{u^2\varepsilon^2}(\tau)$

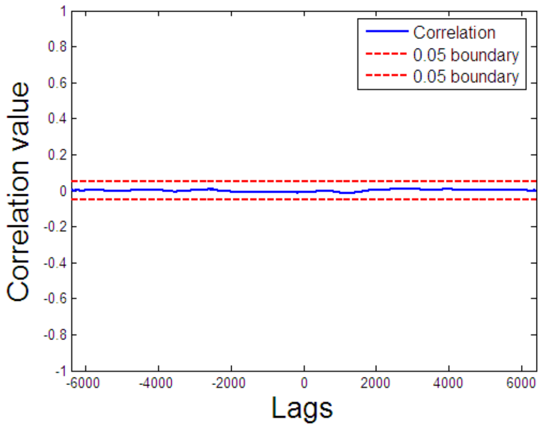

(e) $\phi_{\varepsilon(\varepsilon u)}(\tau)$

Figure 6.41: Correlation tests of hub-angle SBFA-FL model

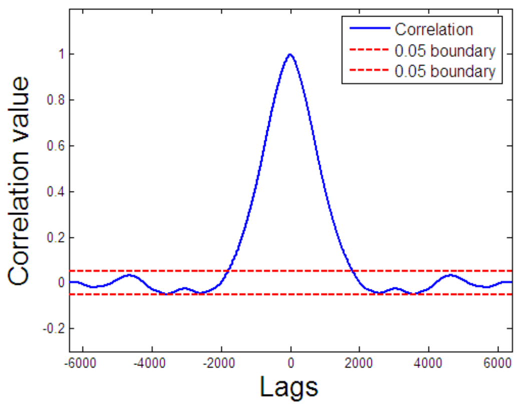

(a) $\phi_{\varepsilon\varepsilon}(\tau)$

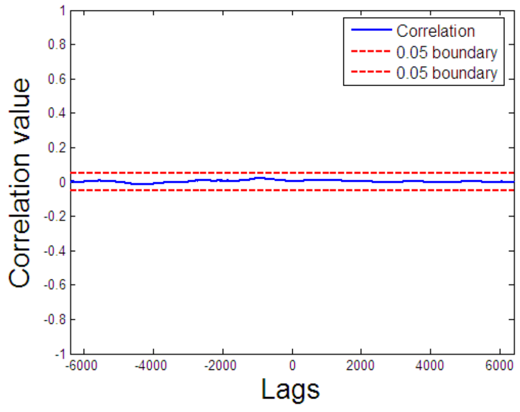

(b) $\phi_{u\varepsilon}(\tau)$

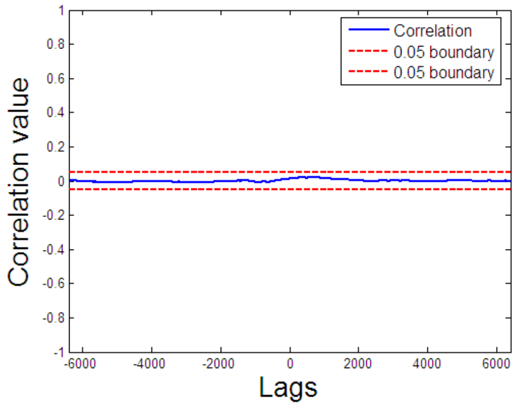

(c) $\phi_{u^2\varepsilon}(\tau)$

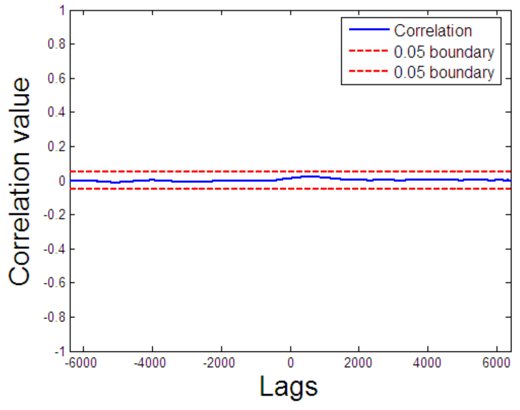

(d) $\phi_{u^2\varepsilon^2}(\tau)$

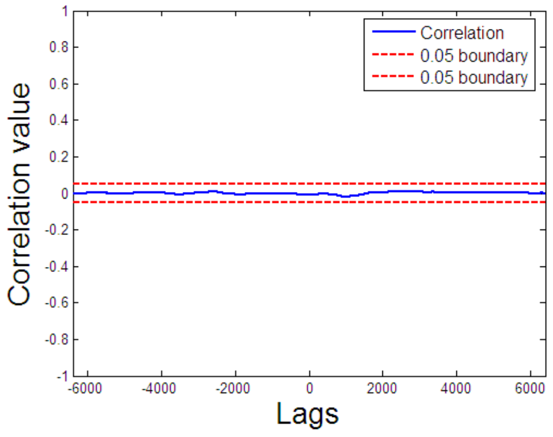

(e) $\phi_{\varepsilon(\varepsilon u)}(\tau)$

Figure 6.42: Correlation tests of hub-angle LABFA-FL model

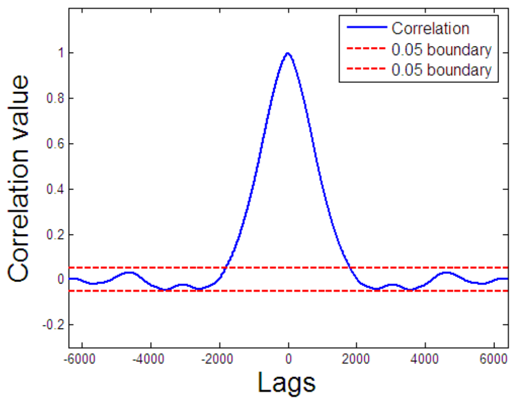

(a) $\phi_{\varepsilon\varepsilon}(\tau)$

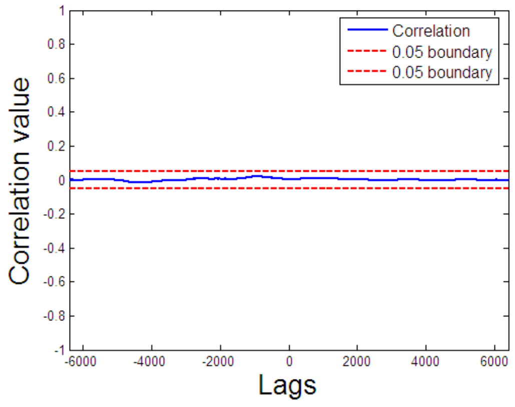

(b) $\phi_{u\varepsilon}(\tau)$

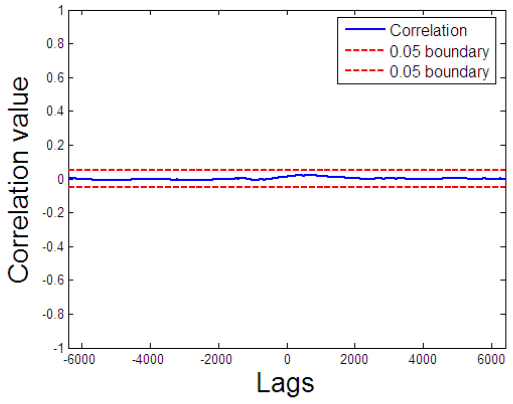

(c) $\phi_{u^2\varepsilon}(\tau)$

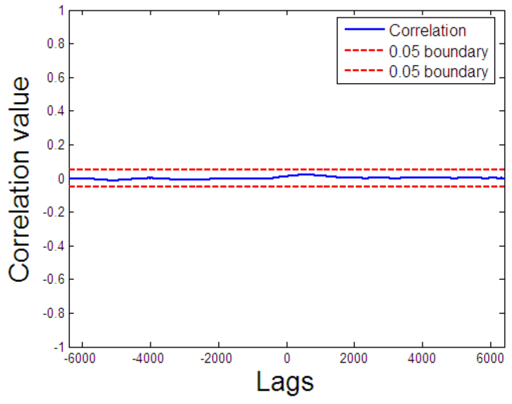

(d) $\phi_{u^2\varepsilon^2}(\tau)$

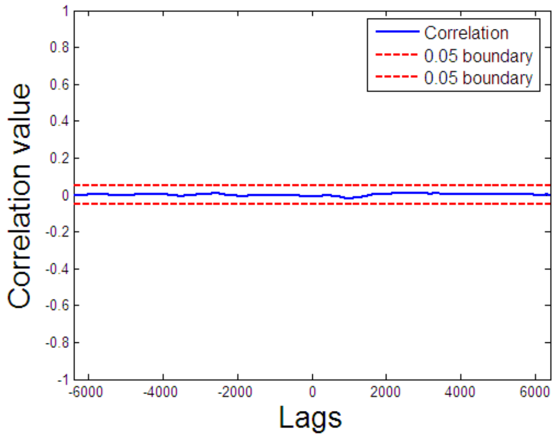

(e) $\phi_{\varepsilon(\varepsilon u)}(\tau)$

Figure 6.43: Correlation tests of hub-angle QABFA-FL model

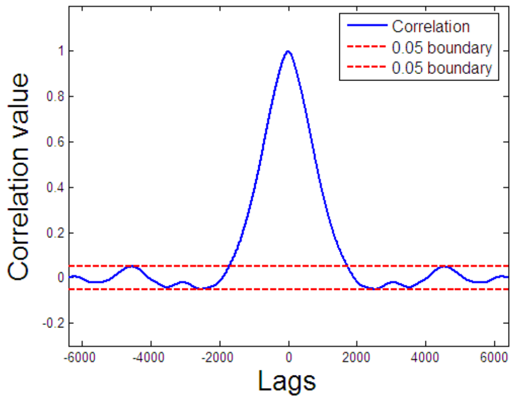

(a) $\phi_{\varepsilon\varepsilon}(\tau)$

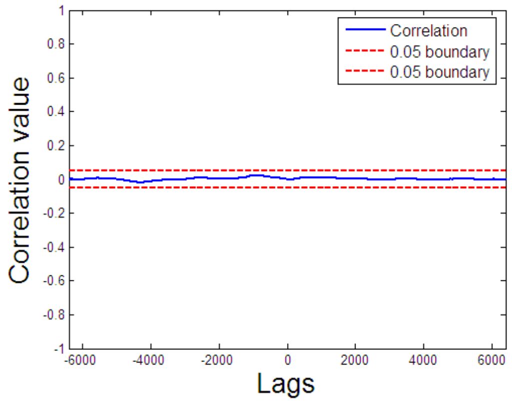

(b) $\phi_{u\varepsilon}(\tau)$

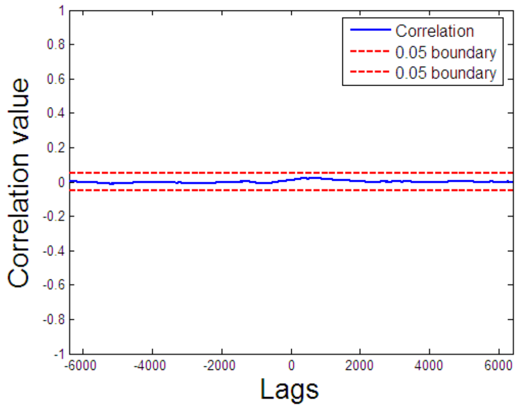

(c) $\phi_{u^2\varepsilon}(\tau)$

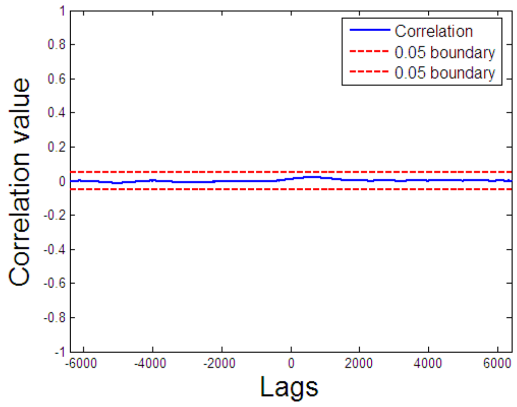

(d) $\phi_{u^2\varepsilon^2}(\tau)$

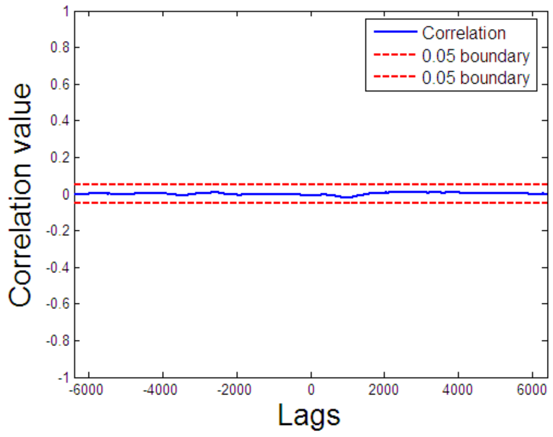

(e) $\phi_{\varepsilon(\varepsilon u)}(\tau)$

Figure 6.44: Correlation tests of hub-angle EABFA-FL model

6.7.2. Hub-velocity model

A. Hub-velocity in the training phase

Through the modelling work it was noticed that the same FL structure as for hub-angle produce the best result for hub-velocity modelling. The total number of parameters to be optimised was 26: 25 weights of fuzzy rules ($w_{r1}, \dots, w_{r25}$) plus one scaling factor in the input 1 path (K_1) while K_2 and K_3 were set to unity. Thus, for hub velocity modelling, all ABFAs and SBFA used the same general parameters as:

❖ $p = 26$	❖ $N_c = 30$	❖ $S_r = S/2$	❖ $N_{ed} = 2$
❖ $S = 8$	❖ $N_s = 3$	❖ $N_{re} = 6$	❖ $p_{ed} = 0.25$

The initial positions of bacteria were selected randomly across the nutrient media. Several step size values were used in the simulation using SBFA and the best optimum value was achieved when the step size value was equal to 0.01. All parameters of LABFA, QABFA and EABFA were selected manually by trial and error and the best optimum J was achieved when the adaptable chemotactic step sizes were formulated as:

$$C_{al}(i) = \frac{0.2}{1+\frac{1}{0.009|J(i)|}} \tag{6.26}$$

$$C_{aq}(i) = \frac{0.2}{1+\frac{1}{0.06\left(\left(0.1J(i)\right)^2+0.1|J(i)|\right)}} \tag{6.27}$$

$$C_{ae}(i) = \frac{0.2}{1+\frac{1}{0.015e^{0.2|J(i)|}}} \tag{6.28}$$

Five Gaussian membership functions were used for fuzzy logic construction with the Gaussian membership function parameters set manually by trial and error. There were two fuzzy inputs: $u(k-1)$ with range [-0.3, 0.3] and $y(k-1)$ with range [-0.0025, 0.004], and one fuzzy output, i.e. $\hat{y}(k)$ with the range [-0.0035, 0.0055]. These values were chosen based on experience by considering experimental input-output data pairs. The fuzzy membership functions for inputs and outputs are depicted in Figure 6.45. The relation between inputs and output were addressed in the fuzzy rules presented in Table 6.12.

Table 6.12: Fuzzy rules of hub-velocity BFA-FL model

Input 1: $u(k-1)$	**Input 2: $y(k-1)$**				
	NB	**NS**	**ZO**	**PS**	**PB**
NB	NB (w_{r1})	NB (w_{r6})	NS (w_{r11})	ZO (w_{r16})	PS (w_{r21})
NS	NB (w_{r2})	NB (w_{r7})	NS (w_{r12})	ZO (w_{r17})	PS (w_{r22})
ZO	NB (w_{r3})	NB (w_{r8})	ZO (w_{r13})	ZO (w_{r18})	PB (w_{r23})
PS	NB (w_{r4})	NS (w_{r9})	ZO (w_{r14})	PS (w_{r19})	PB (w_{r24})
PB	NB (w_{r5})	NS (w_{r10})	ZO (w_{r15})	PS (w_{r20})	PB (w_{r25})

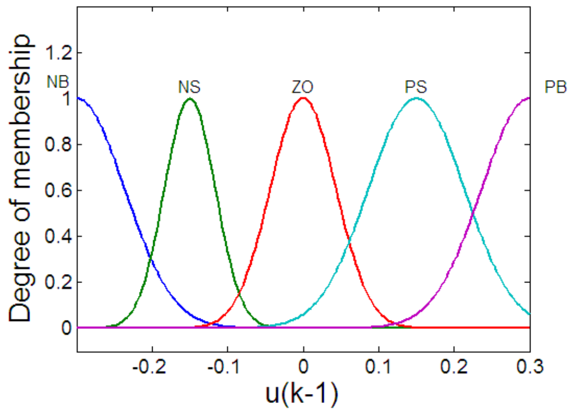

(a) Input 1: $u(k-1)$

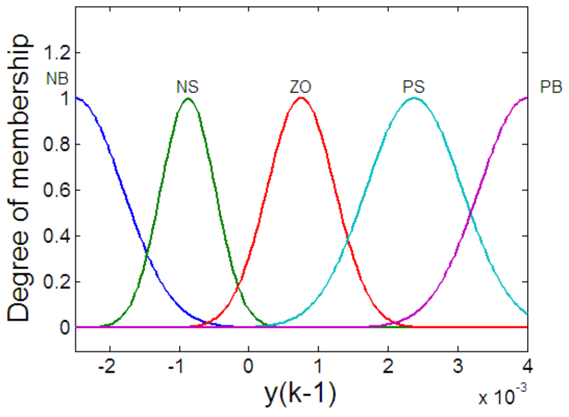

(b) Input 2: $y(k-1)$

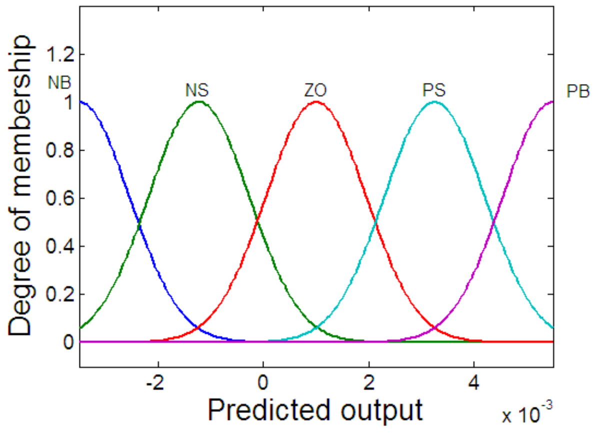

(c) Output: $\hat{y}(k)$

Figure 6.45: Fuzzy membership functions of hub-velocity BFA-FL model

It can be noted from the numerical results presented in Table 6.13 that the step size of ABFA were the ranges of [0.0084, 0.2], [0.0084, 0.2] and [0.0077, 0.2] for LABFA-FL, QABFA-FL and EABFA-FL respectively. The optimum cost function J values achieved were 0.00049, 0.00048, 0.00048 and 0.00048 for SBFA-FL, LABFA-FL, QABFA-FL and EABFA-FL respectively. These results show that all ABFA-FL models achieved lower optimum J value compared to SBFA-FL. In addition, all the BFA-FL models achieved lower optimum J values than 0.00096 of not-optimised fuzzy model. The bar chart plotted in Figure 6.46(a) shows a comparison of the optimum J values achieved by the algorithms. Because of the nature of cost function, either heavily multimodal or rather flat, the convergence plots depicted in Figure 6.46(b) show that all the algorithms had almost the same speed of convergence. The time-domain responses and error depicted in Figure 6.46(c) and Figure 6.46(d) respectively show that all optimised fuzzy models were able to match the actual output. The surfaces of fuzzy logic of hub velocity model are plotted in Figure 6.47.

Table 6.13: Numerical results of hub-velocity BFA-FL models in the training phase

Algorithm	$C(i)$ **range**	**Convergence speed (steps)**	**Optimum *J***	**Range of error ($e(k)$)**	
				Minimum	**Maximum**
SBFA-FL	0.01	282	0.00049	-0.0020	0.0025
LABFA-FL	[0.0084, 0.2]	241	0.00048	-0.0020	0.0025
QABFA-FL	[0.0084, 0.2]	240	0.00048	-0.0020	0.0025
EABFA-FL	[0.0077, 0.2]	234	0.00048	-0.0020	0.0025

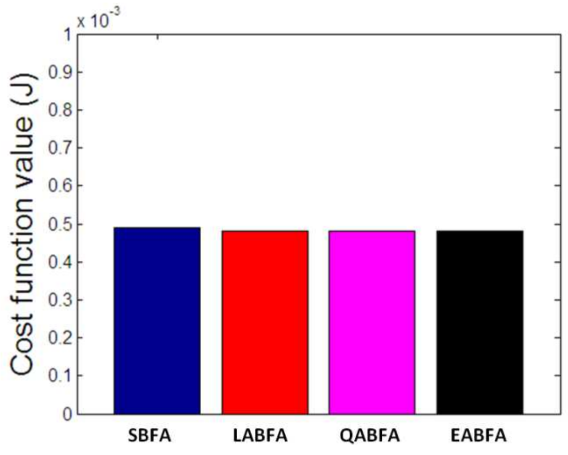

(a) Optimum J

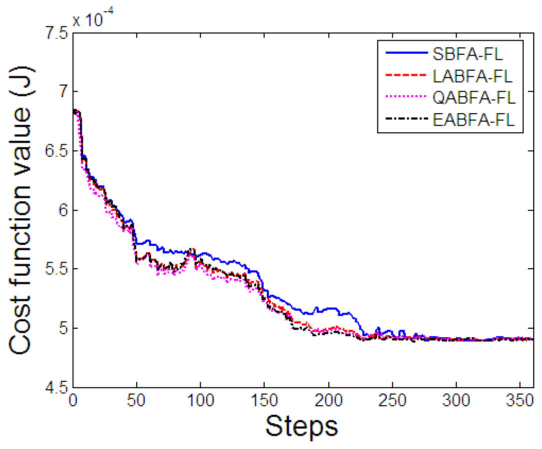

(b) Convergence plots

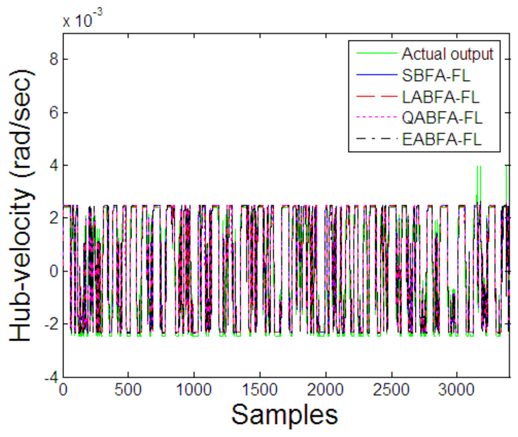

(c) Time-domain responses

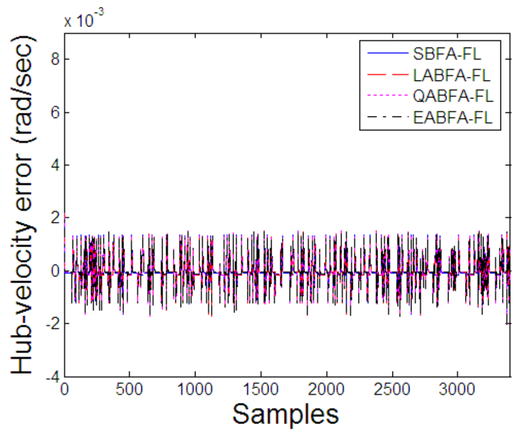

(d) Error

Figure 6.46: Simulation results of hub-velocity BFA-FL models in the training phase

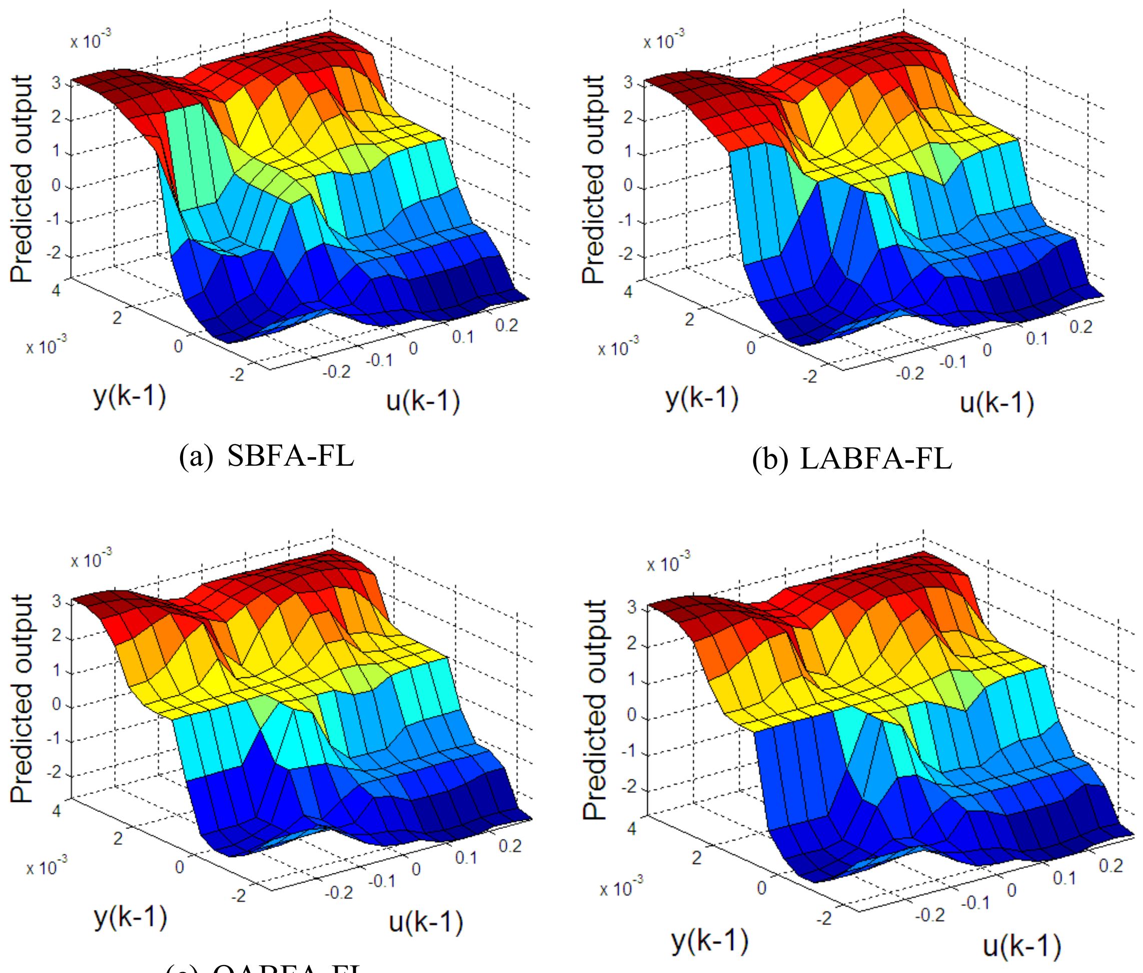

(a) SBFA-FL

(b) LABFA-FL

(c) QABFA-FL

(d) EABFA-FL

Figure 6.47: Fuzzy surfaces of hub-velocity BFA-FL models

B. Hub-velocity model in the validation phase

Numerical results in validation phase outlined in Table 6.14 show that the cost function values for validation phase were 0.00055, 0.00055, 0.00055 and 0.00055 for SBFA-FL, LABFA-FL, QABFA-FL and EABFA-FL models respectively. All models achieved the same optimum J value. A comparison of optimum J values achieved by the algorithms is depicted in Figure 6.48(a). The time-domain responses and error in validation phase plotted in Figure 6.48(b) and Figure 6.48(c) confirm that all models' responses matched the actual output well. Correlation test results depicted in Figure 6.49-Figure 6.52 show that all models were acceptable since all the correlation values were within the 95% confidence levels.

Table 6.14: Numerical results of hub-velocity BFA-FL models in the validation phase

Algorithm	**Optimum J**	**Range of error $(e(k))$**	
		Minimum	**Maximum**
SBFA-FL	0.00055	-0.0020	0.0025
LABFA-FL	0.00055	-0.0020	0.0025
QABFA-FL	0.00055	-0.0020	0.0025
EABFA-FL	0.00055	-0.0020	0.0025

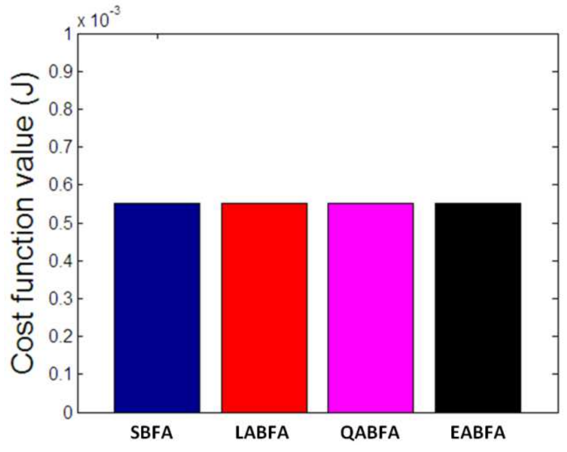

(a) Optimum J

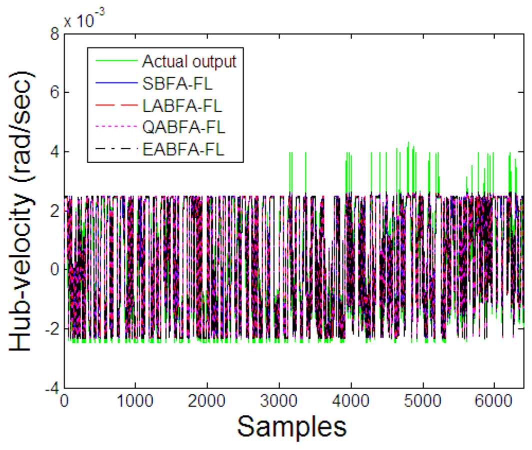

(b) Time-domain responses

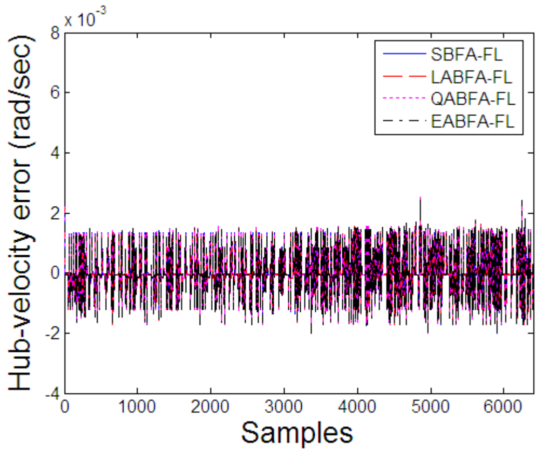

(c) Error

Figure 6.48: Simulation results of for hub-velocity BFA-FL models in the validation phase

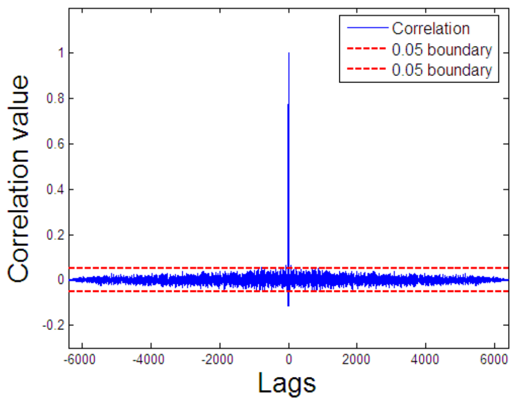

(a) $\phi_{\varepsilon\varepsilon}(\tau)$

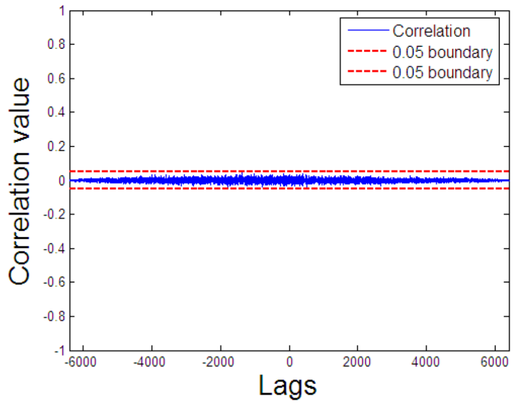

(b) $\phi_{u\varepsilon}(\tau)$

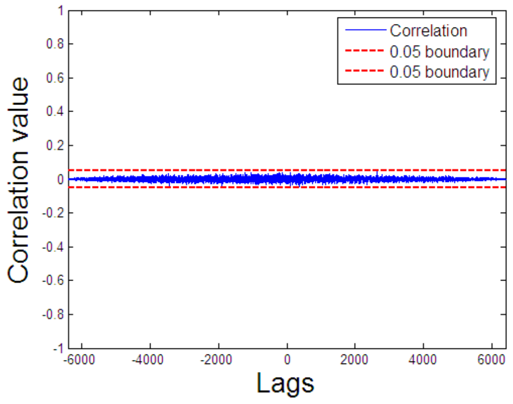

(c) $\phi_{u^2\varepsilon}(\tau)$

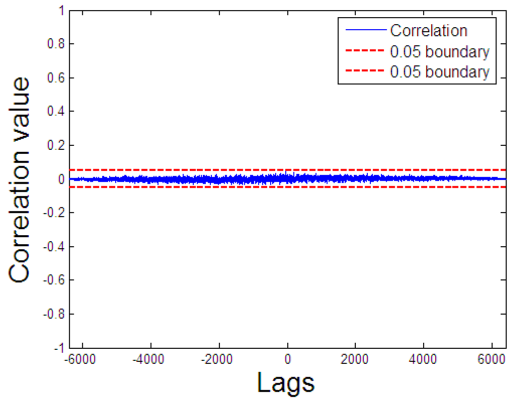

(d) $\phi_{u^2\varepsilon^2}(\tau)$

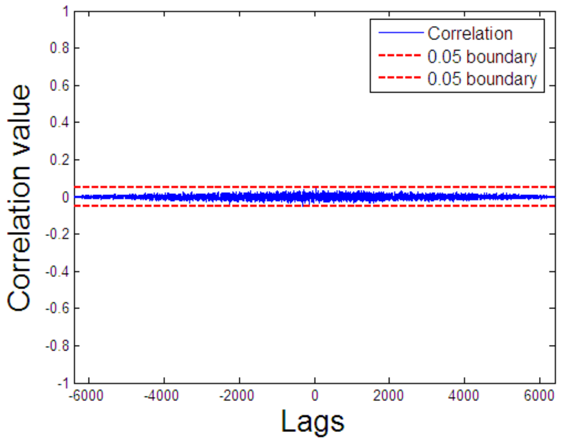

(e) $\phi_{\varepsilon(\varepsilon u)}(\tau)$

Figure 6.49: Correlation tests of hub-velocity SBFA-FL model

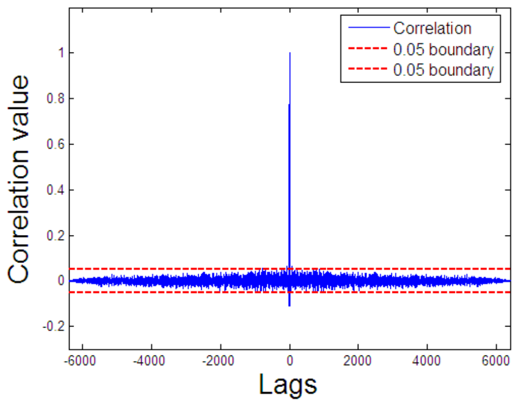

(a) $\phi_{\varepsilon\varepsilon}(\tau)$

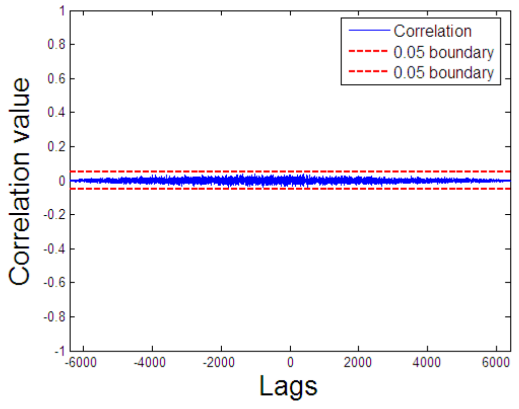

(b) $\phi_{u\varepsilon}(\tau)$

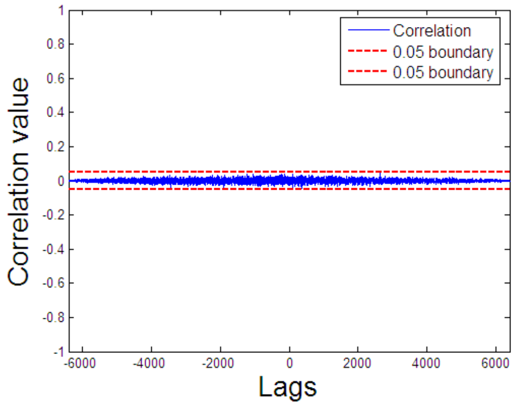

(c) $\phi_{u^2\varepsilon}(\tau)$

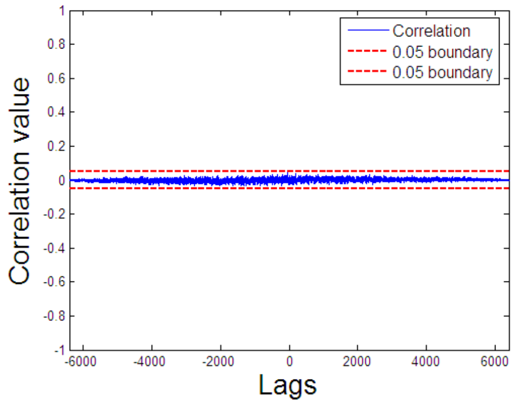

(d) $\phi_{u^2\varepsilon^2}(\tau)$

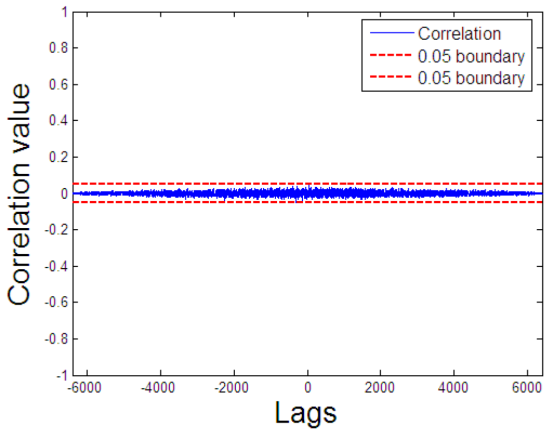

(e) $\phi_{\varepsilon(\varepsilon u)}(\tau)$

Figure 6.50: Correlation tests of hub-velocity LABFA-FL model

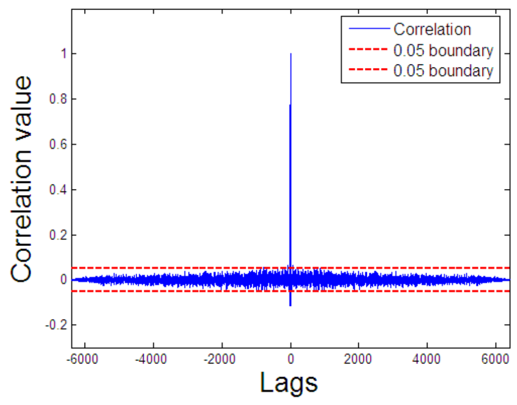

(a) $\phi_{\varepsilon\varepsilon}(\tau)$

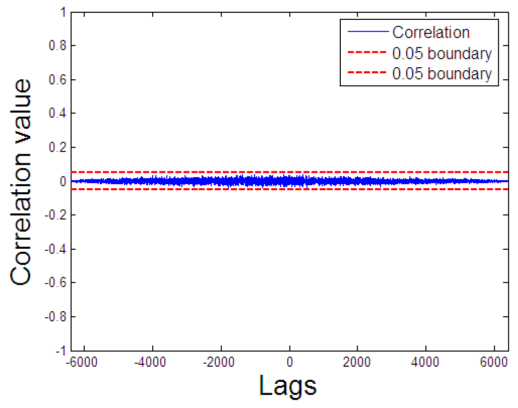

(b) $\phi_{u\varepsilon}(\tau)$

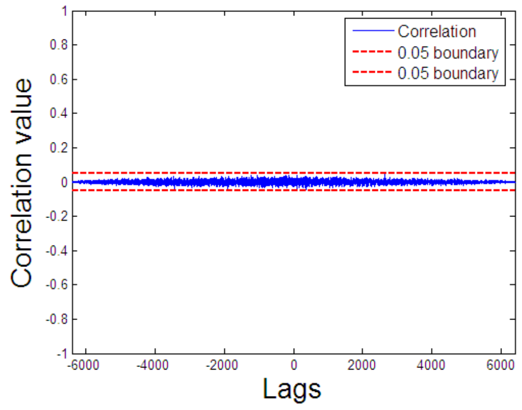

(c) $\phi_{u^2\varepsilon}(\tau)$

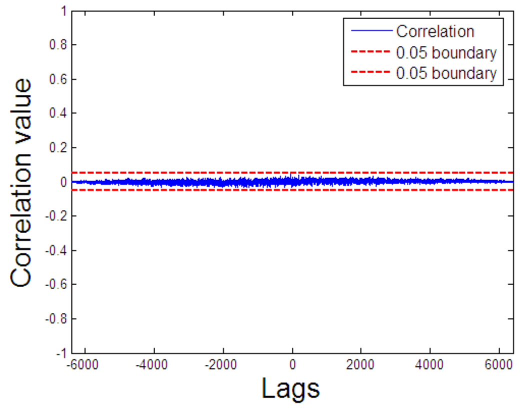

(d) $\phi_{u^2\varepsilon^2}(\tau)$

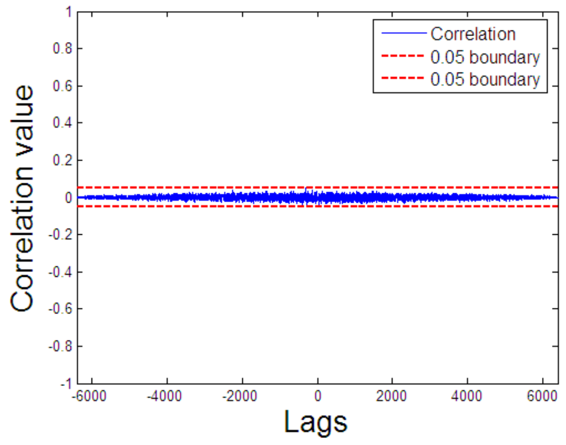

(e) $\phi_{\varepsilon(\varepsilon u)}(\tau)$

Figure 6.51: Correlation tests of hub-velocity QABFA-FL model

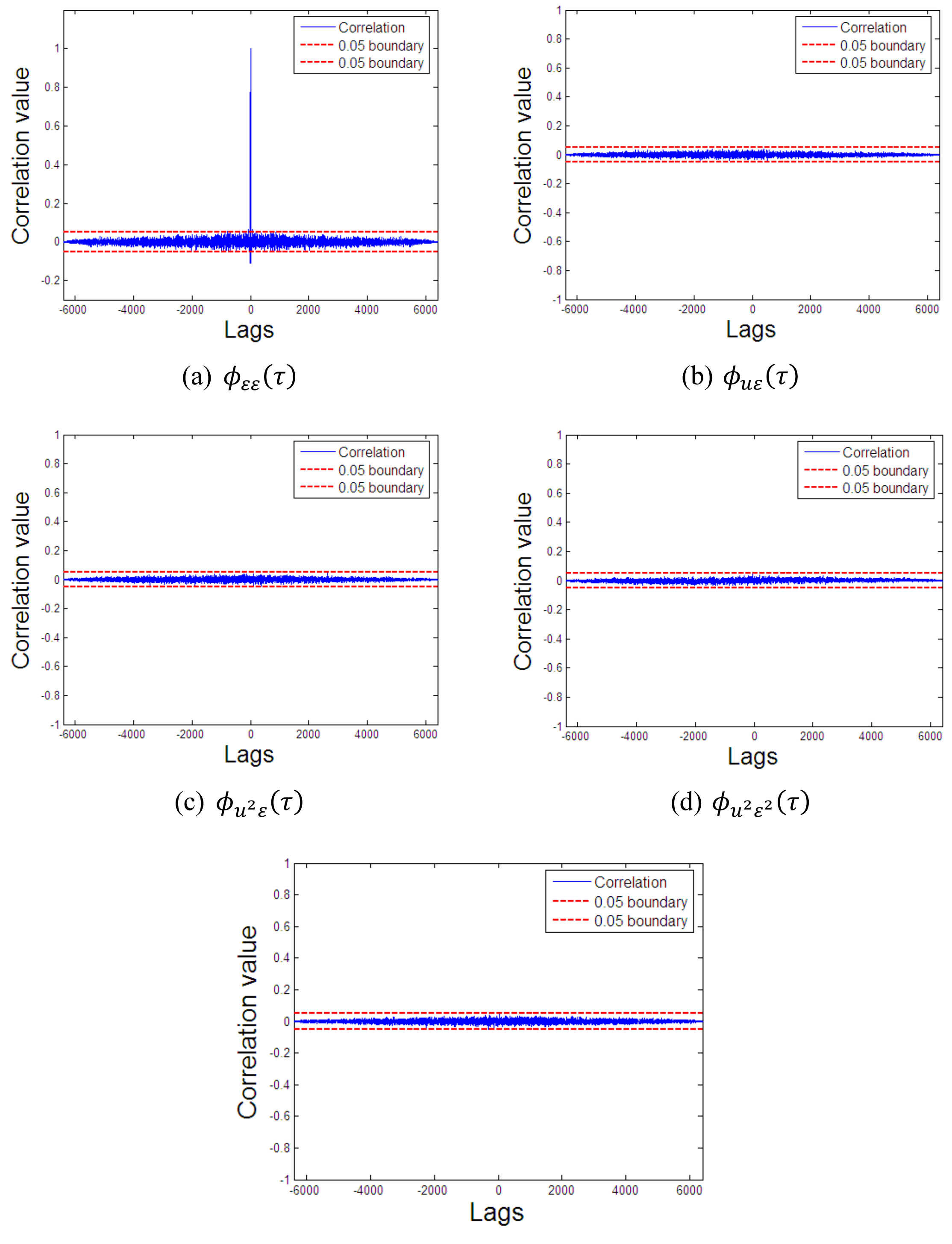

(a) $\phi_{\varepsilon\varepsilon}(\tau)$ (b) $\phi_{u\varepsilon}(\tau)$

(c) $\phi_{u^2\varepsilon}(\tau)$ (d) $\phi_{u^2\varepsilon^2}(\tau)$

(e) $\phi_{\varepsilon(\varepsilon u)}(\tau)$

Figure 6.52: Correlation tests of hub-velocity EABFA-FL model

6.7.3. End-point acceleration model

A. End-point acceleration in the training phase

In contrast to hub-angle and hub-velocity models, in the end-point acceleration modelling an FL structure with scaling factors set to unity ($K_1 = K_2 = K_3 = 1$) proved to be suitable. Thus, the total number of parameters to be optimised were 25, e.g. weights of fuzzy rules ($w_{r1}, \dots, w_{r25}$). In the modelling process, all BFAs used the same general parameters as:

❖ $p = 25$	❖ $N_c = 30$	❖ $S_r = {}^{S}/_{2}$	❖ $N_{ed} = 2$
❖ $S = 8$	❖ $N_s = 3$	❖ $N_{re} = 3$	❖ $p_{ed} = 0.25$

The initial positions of bacteria were selected randomly across the nutrient media and RMSE was used as nutrient value. After trying various values, in the optimisation process the step size value for SBFA was set to 0.013. All parameters of LABFA, QABFA and EABFA were selected manually by trial and error and the best settings of adaptable chemotactic step sizes were:

$$C_{al}(i) = \frac{0.2}{1+\frac{1}{0.0027|J(i)|}} \tag{6.29}$$

$$C_{aq}(i) = \frac{0.2}{1+\frac{1}{0.01\left(\left(0.1J(1)\right)^2+0.1|J(i)|\right)}} \tag{6.30}$$

$$C_{ae}(i) = \frac{0.2}{1+\frac{1}{0.01e^{0.08|J(i)|}}} \tag{6.31}$$

Five Gaussian membership functions were used for fuzzy logic construction with all Gaussian membership function parameters set manually. The FL structure consisted of two inputs: $u(k-1)$ with range [-0.3, 0.3] and $y(k-1)$ with range [-1.55, 1.9], and one output, i.e. $\hat{y}(k)$ with the range [-1.8, 2.3]. The fuzzy membership functions for inputs and output are depicted in Figure 6.53. The fuzzy rules which describe the relation between two inputs and output are presented in Table 6.15.

Table 6.15: Fuzzy rules for end-point acceleration model

Input 1: $u(k-1)$	**Input 2: $y(k-1)$**				
	NB	**NS**	**ZO**	**PS**	**PB**
NB	NB (w_{r1})	NB (w_{r6})	NS (w_{r11})	ZO (w_{r16})	PS (w_{r21})
NS	NB (w_{r2})	NS (w_{r7})	NS (w_{r12})	ZO (w_{r17})	PS (w_{r22})
ZO	NB (w_{r3})	NS (w_{r8})	ZO (w_{r13})	ZO (w_{r18})	PS (w_{r23})
PS	NB (w_{r4})	NS (w_{r9})	ZO (w_{r14})	PS (w_{r19})	PB (w_{r24})
PB	NB (w_{r5})	NS (w_{r10})	ZO (w_{r15})	PS (w_{r20})	PB (w_{r25})

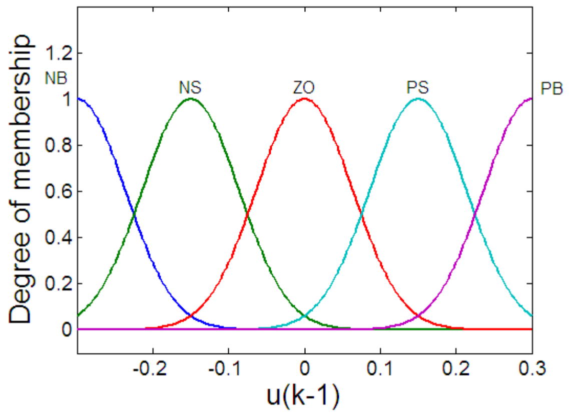

(a) Input 1: $u(k-1)$

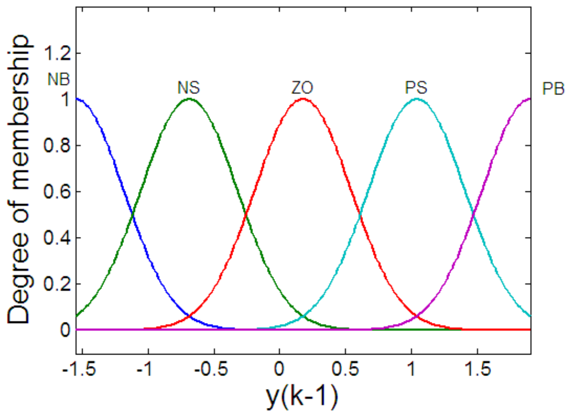

(b) Input 2: $y(k-1)$

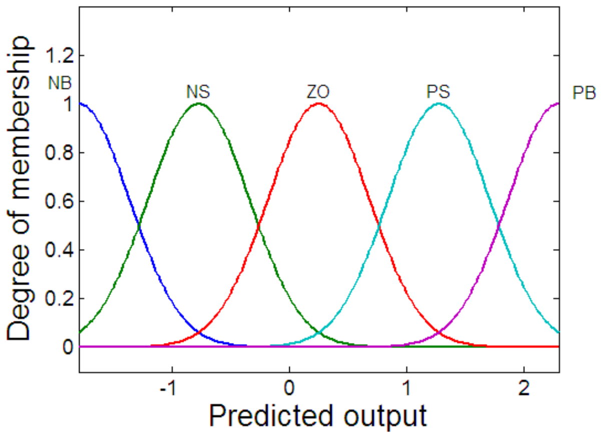

(c) Output: $\hat{y}(k)$

Figure 6.53: Fuzzy membership function of BFA-FL for end-point acceleration models

By using the formulae in equation (7.9)-equation (7.11), the step sizes of ABFA were adaptable based on the cost function value in the range [0.0110, 0.2], [0.0124, 0.2] and [0.0098, 0.2] for LABFA, QABFA and EABFA respectively. It can be noticed from the numerical results presented in Table 6.16 that optimum values achieved were 0.1890, 0.1865, 0.1845 and 0.1848 for SBFA-FL, LABFA-FL, QABFA-FL and EABFA-FL models respectively.

Table 6.16: Numerical results of end-point acceleration BFA-FL models in the training phase

Algorithm	$C(i)$ **range**	**Convergence (steps)**	**Optimum J**	**Range of error ($e(k)$)**	
				Minimum	**Maximum**
SBFA-FL	0.013	140	0.1890	-0.7038	0.8652
LABFA-FL	[0.011, 0.2]	135	0.1865	-0.7038	0.8652
QABFA-FL	[0.0124, 0.2]	139	0.1845	-0.7030	0.8635
EABFA-FL	[0.0098, 0.2]	139	0.1848	-0.7033	0.8620

The optimum J results are plotted in the bar chart depicted in Figure 6.54(a). Because of the cost function landscape, either flat or highly multimodal, the convergence plots depicted in Figure 6.54(b) show that all ABFA-FL models were able to converge to optimum value slightly faster than SBFA-FL. Time-domain responses and error of end-point acceleration depicted in Figure 6.54(c) and Figure 6.54(d) show that all the optimised fuzzy models were able to match the actual output while the response of not-optimised fuzzy model had large error. The power spectral density plots in Figure 6.54(e) show that responses of all models matched the actual output, with the first resonance frequency is slightly shifted. Resonance frequencies of the system were 11.67 Hz, 36.96 Hz and 64.22 for the 1st, 2nd and 3rd modes respectively. Surfaces of fuzzy structure for end-point acceleration models are plotted in Figure 6.55.

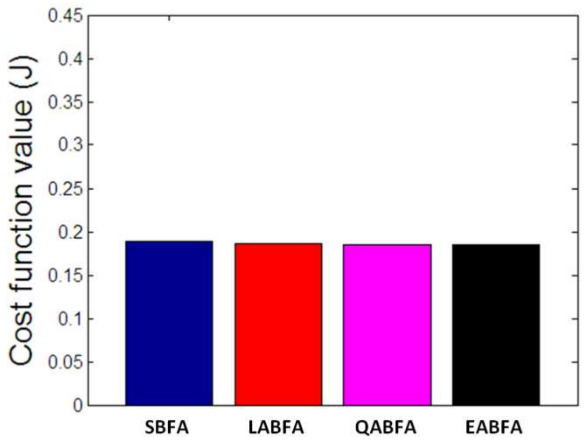

(a) Optimum J

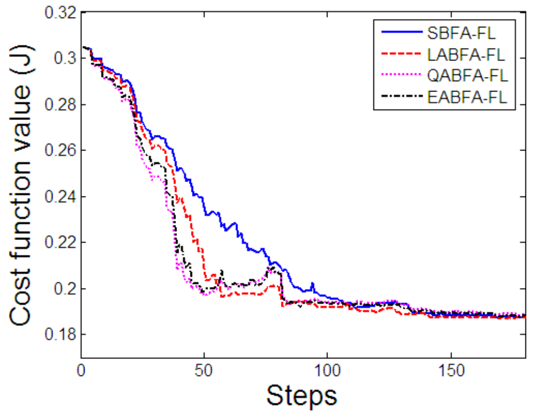

(b) Convergence plots

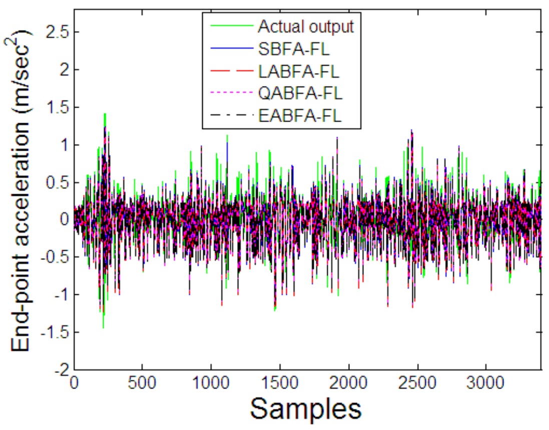

(c) Time-domain responses

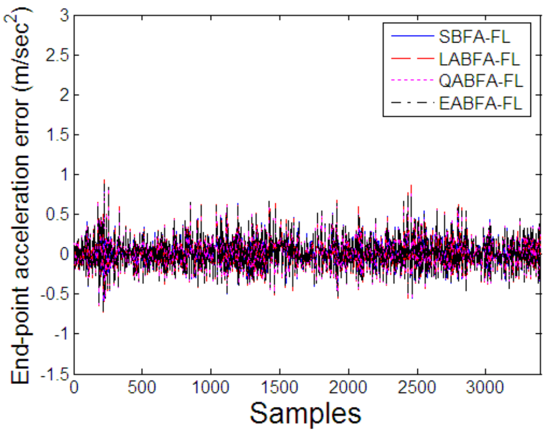

(d) Error

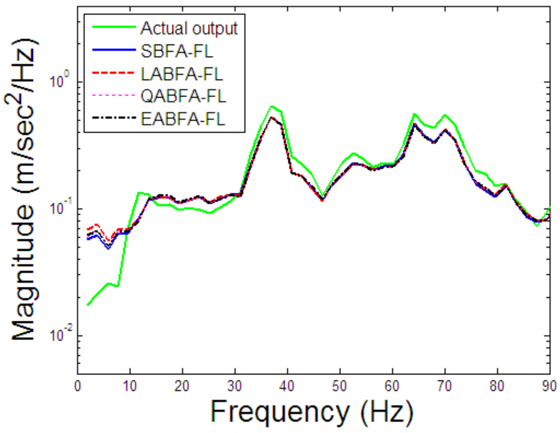

(e) PSD of end-point acceleration

Figure 6.54: Simulation results of end-point acceleration BFA-FL models in the training phase

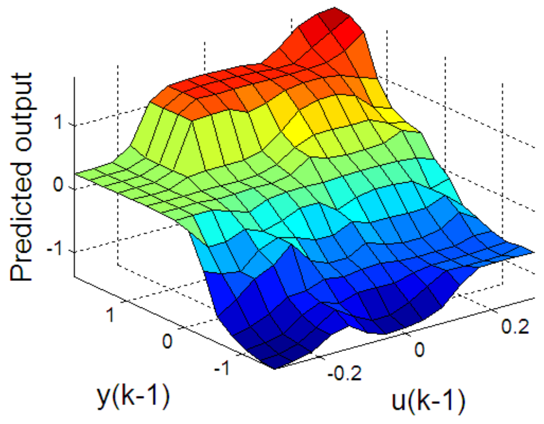

(a) SBFA-FL

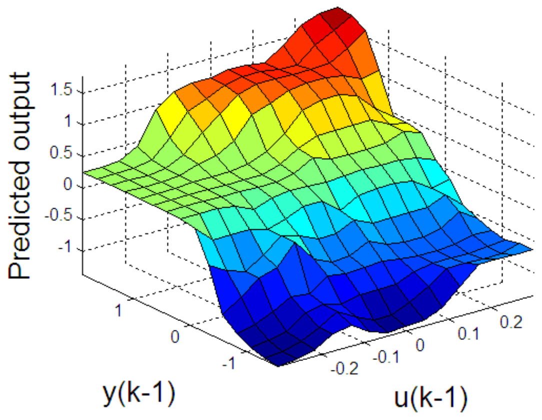

(b) LABFA-FL

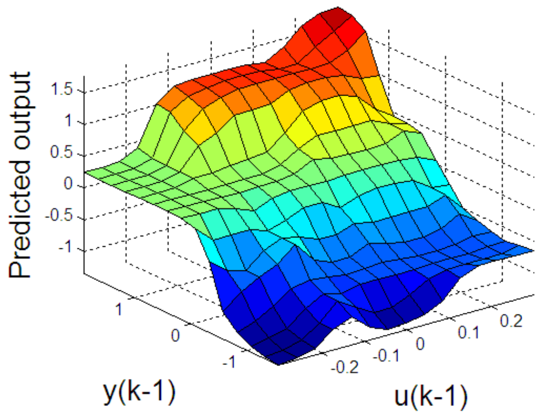

(c) QABFA-FL

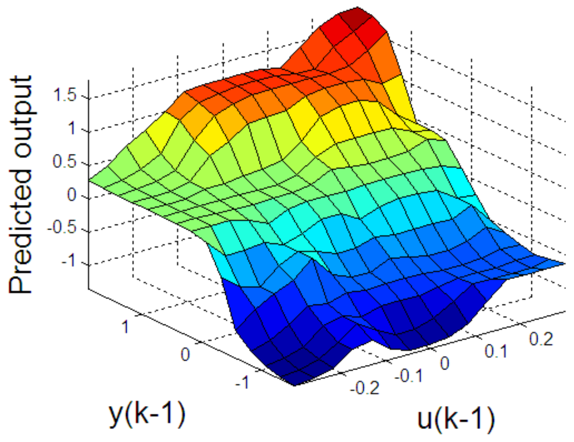

(d) EABFA-FL

Figure 6.55: Surfaces of fuzzy models for end-point acceleration models

B. End-point acceleration in the validation phase

Numerical results outlined in Table 6.17 show that the optimum *J* values of the models in the validation phase were 0.2096, 0.2078, 0.2063 and 0.2058 for SBFA-FL, LABFA-FL, QABFA-FL and EABFA-FL respectively. A comparison of these results is outlined in the bar chart depicted in Figure 6.56(a). The time domain end-point acceleration responses, error and their power spectral densities depicted in Figure 6.56(b), Figure 6.56(c) and Figure 6.56(d) respectively show that all models were able to match the actual output. Correlation tests results plotted in Figure 6.57-Figure 6.60 confirm that all models were acceptable.

Table 6.17: Numerical results of end-point acceleration BFA-FL models in the validation phase

Algorithm	**Optimum** J	**Range of error** $(e(k))$	
		Minimum	**Maximum**
SBFA-FL	0.2096	-0.7047	1.3822
LABFA-FL	0.2078	-0.7045	1.3794
QABFA-FL	0.2063	-0.7046	1.3429
EABFA-FL	0.2058	-0.7045	1.2414

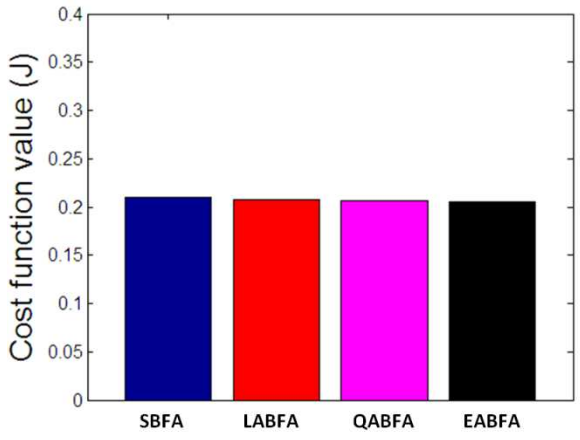

(a) Optimum J

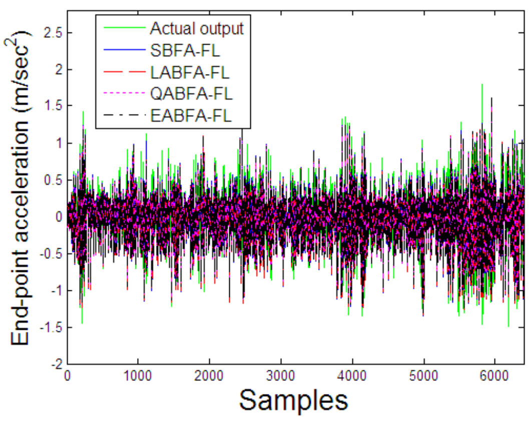

(b) Time-domain responses

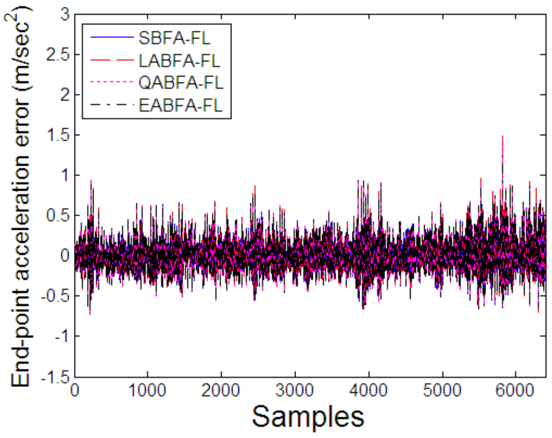

(c) Error

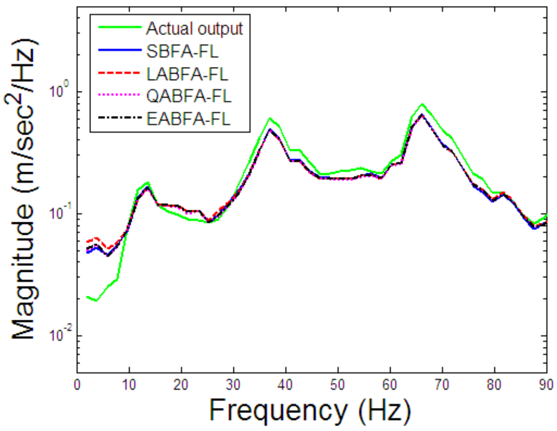

(d) PSD of end-point acceleration

Figure 6.56: Simulation results of end-point acceleration BFA-FL models in the validation phase

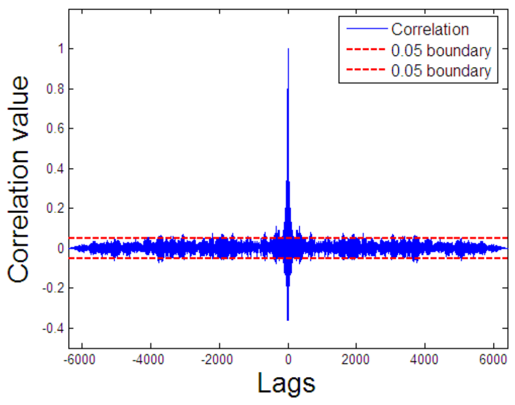

(a) $\phi_{\varepsilon\varepsilon}(\tau)$

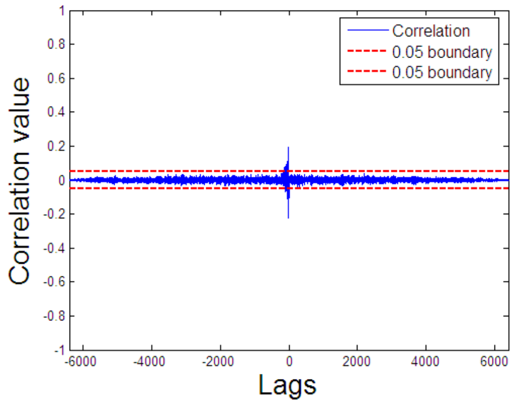

(b) $\phi_{u\varepsilon}(\tau)$

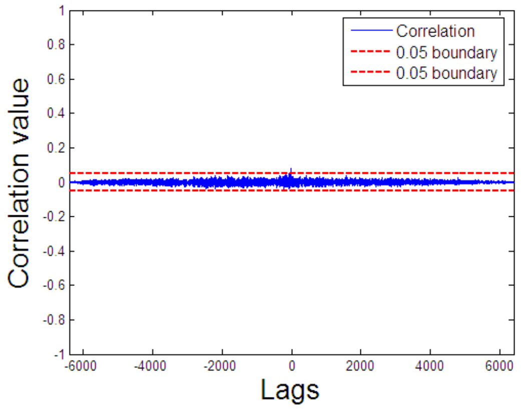

(c) $\phi_{u^2\varepsilon}(\tau)$

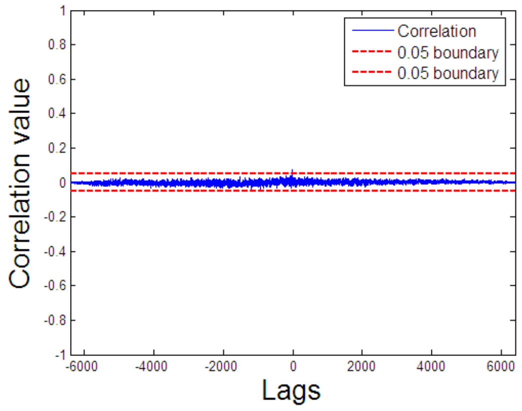

(d) $\phi_{u^2\varepsilon^2}(\tau)$

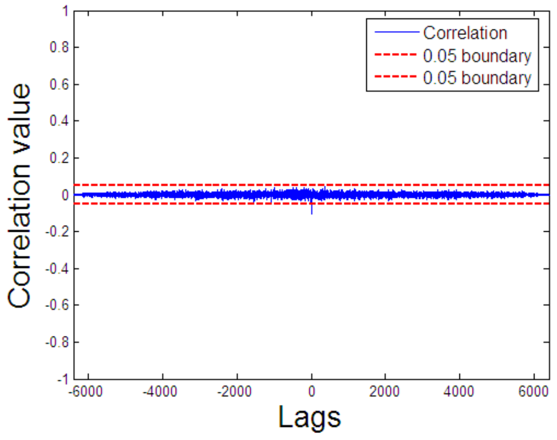

(e) $\phi_{\varepsilon(\varepsilon u)}(\tau)$

Figure 6.57: Correlation tests of end-point acceleration SBFA-FL model

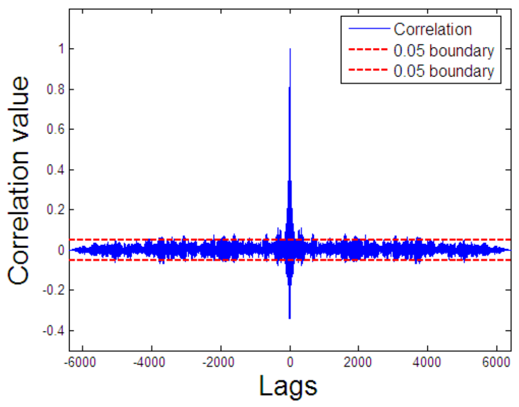

(a) $\phi_{\varepsilon\varepsilon}(\tau)$

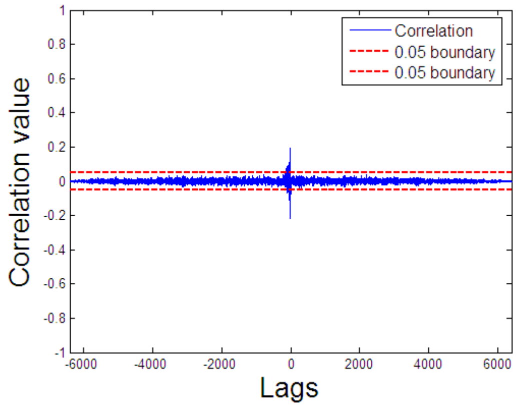

(b) $\phi_{u\varepsilon}(\tau)$

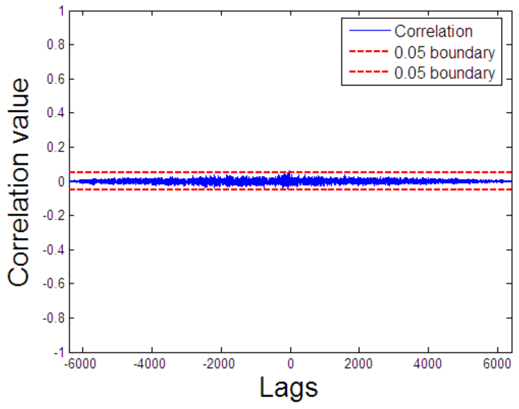

(c) $\phi_{u^2\varepsilon}(\tau)$

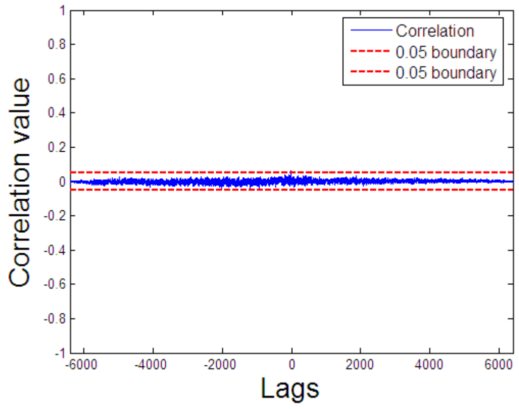

(d) $\phi_{u^2\varepsilon^2}(\tau)$

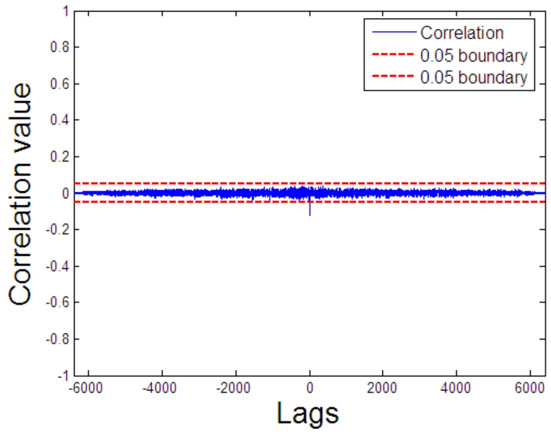

(e) $\phi_{\varepsilon(\varepsilon u)}(\tau)$

Figure 6.58: Correlation tests of end-point acceleration LABFA-FL model

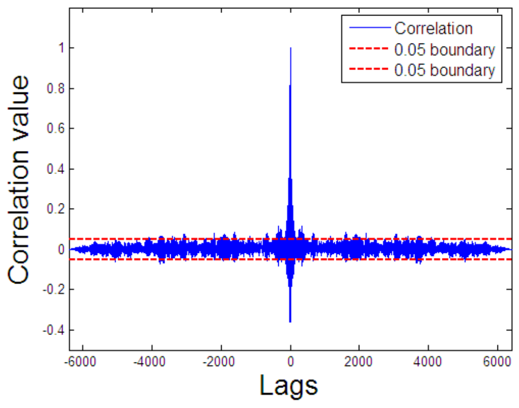

(a) $\phi_{\varepsilon\varepsilon}(\tau)$

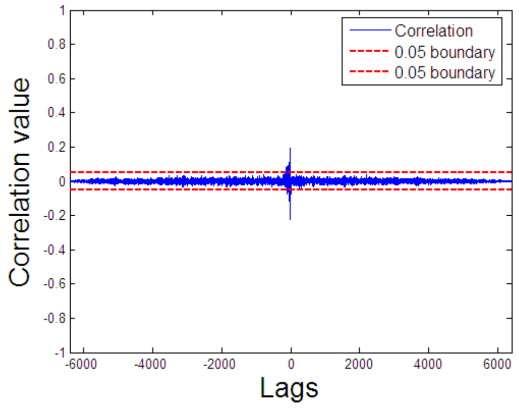

(b) $\phi_{u\varepsilon}(\tau)$

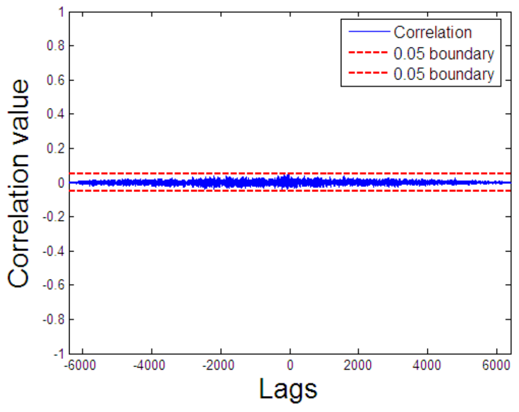

(c) $\phi_{u^2\varepsilon}(\tau)$

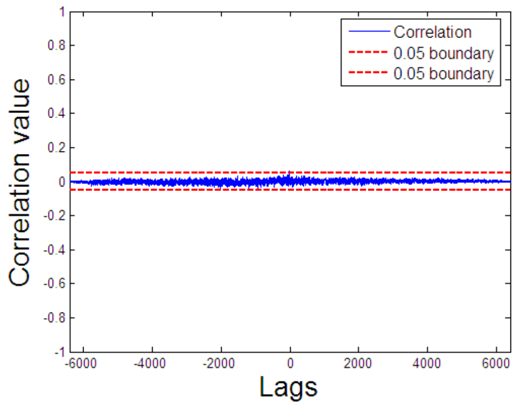

(d) $\phi_{u^2\varepsilon^2}(\tau)$

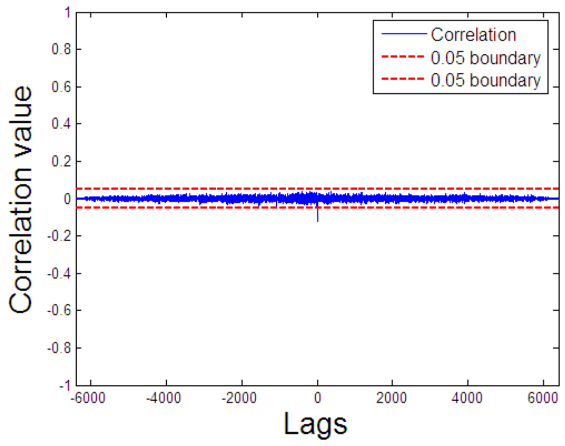

(e) $\phi_{\varepsilon(\varepsilon u)}(\tau)$

Figure 6.59: Correlation tests of end-point acceleration QABFA-FL model

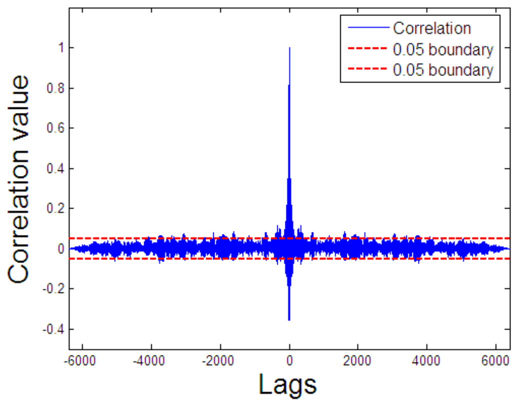

(a) $\phi_{\varepsilon\varepsilon}(\tau)$

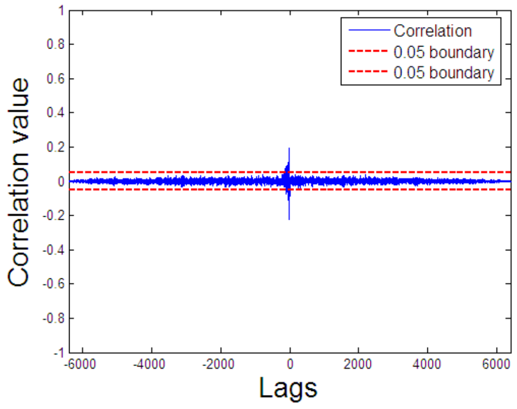

(b) $\phi_{u\varepsilon}(\tau)$

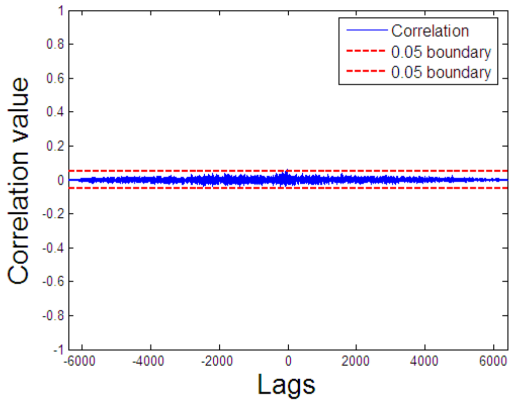

(c) $\phi_{u^2\varepsilon}(\tau)$

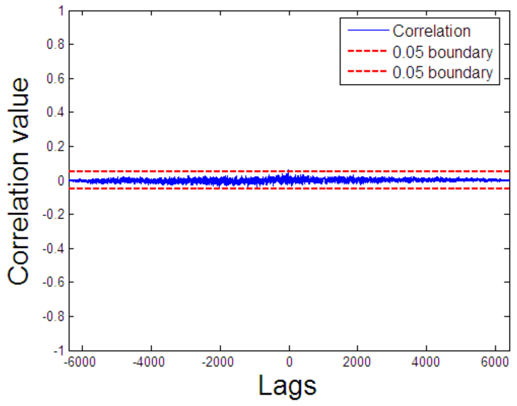

(d) $\phi_{u^2\varepsilon^2}(\tau)$

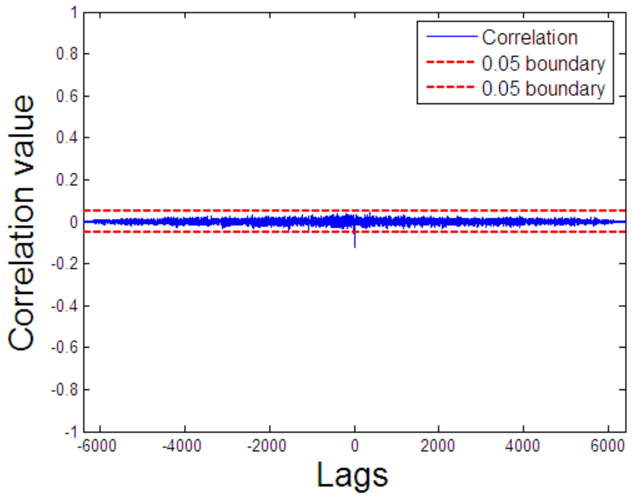

(e) $\phi_{\varepsilon(\varepsilon u)}(\tau)$

Figure 6.60: Correlation tests of end-point acceleration EABFA-FL model

6.8. Summary

A laboratory-scale single-link flexible manipulator has been modelled with NNs trained by ABFA and FL optimised by ABFA. Three SISO models have been constructed to represent the single-link flexible manipulator from torque input to hub-angle, hub velocity and end-point acceleration. Input-output data pairs obtained from the experimental rig were split into two parts: one part for modelling phase and another part for validating phase. Moreover, a set of correlation tests were carried out to validate all resulted models. The investigations have focused on in the performance of ABFAs to that of SBFA. The comparisons have been made based on the convergence speed, optimum cost function value achieved, time-domain and frequency-domain responses.

The results show that all ABFAs have faster convergence and are able to achieve lower cost function values than SBFA. Since all ABFA and SBFA used the same general parameters, and initial positions of bacteria were selected randomly across search space, the superior results of ABFAs can be attributed to the adaptable chemotactic step size.

All models were developed and validated based on the experimental input-output data pairs collected from a single-link flexible manipulator rig. In general, the optimisation results suggested that all ABFAs were able to achieve better optimum J values and have faster convergence speed than SBFA. Their time domain responses, error and PSD both in modelling and validation phases show that the predicted output of developed models followed the actual output well. The correlation tests show that all models are representative of the real systems. The application of ABFA for optimising controllers for controlling hub-angular displacement and vibration of end-point of flexible arm will be presented in Chapter 7.

CHAPTER 7
CONTROL OF FLEXIBLE MANIPULATOR SYSTEM USING BACTERIAL FORAGING ALGORITHMS

7.1. Introduction

The oscillatory behaviour of the flexible manipulator system impacts on both the notion trajectory of the hub and structural vibration of the flexible arm at the end-point of the flexible arm. In general, there are two control objectives with a single-link flexible manipulator: to control the hub-angular displacement and to suppress vibration at the end point.

It can be noted from the literature that previous works on hub-angular displacement controllers of a single-link flexible manipulator have been proposed by researchers. A proportional-derivative (PD)-like controller called joint-based collocated (JBC) control, here cited as JBC PD control, has been used (Azad, 1994; Md Zain, 2006; Md Zain et al., 2005; Poerwanto, 1998; Tokhi and Md Zain, 2006; Tokhi et al., 2004). There are only two parameters to tune in JBC PD, i.e. proportional gain in the feed forward path of hub-angle reference input and derivative gain in hub-velocity feedback path. Although only a simple controller, its time-domain performances show that JBC PD has arguably satisfying performance. The literature shows that various end-point acceleration feedback control types have been proposed in combination with JBC PD control to achieve reference tracking and vibration control. Among these are genetic algorithm (GA)-optimised iterative learning control (ILC) (Md Zain et al., 2005; Tokhi and Md Zain, 2006), ILC and PID (Tokhi et al., 2004) and strain feedback (Mohamed et al., 2005). These reports suggest that the addition of controller in the end-point acceleration feedback could damp the vibration of end-point of flexible arm.

In the JBC PD control applications above, the root locus approach has been used to design the controller. In the root locus approach, the two parameters of JBC PD are obtained by finding the poles of the closed loop transfer function of the plant graphically (Ogata, 2002). Thus, in order to get accurate controller, accurate model of the plant under study is needed. Another technique which can be utilised to find optimal parameters of JBC PD controller is to use an optimisation algorithm. Those reports referred to above show that controllers of end-point acceleration feedback have been mainly optimised using GA.

It can be noted from the literature that BFA has been used for tuning PD and PID controllers in various applications, for example as for tuning PID controller for suppression of power oscillation of load frequency control (Ali and Abd-Elazim; 2010), optimising PI controller for active power filter application (Mishra and Bhende, 2007), tuning PID controller for multivariable system (Kim and Cho, 2005), finding optimum PID controllers for different-order systems (Niu et al., 2006), optimising PID controller's parameters for various different order systems (Ali and Majhi, 2006) and tuning PD-PI controller (Jain and Nigam, 2008a, b). The application of BFA in the control single-link flexible manipulator has not been reported yet. However, a hybrid BFA and particle swarm optimisation (PSO) has been used for optimising a hybrid fuzzy pre-compensated PD controller in trajectory control of a two-link rigid flexible manipulator (Alavandar et al., 2010).

Motivated by the previous works, here, BFA with adaptable chemotactic step size, i.e. LABFA, QABFA, EABFA, and FABFA, as proposed and discussed in Chapter 4, are adopted for optimising JBC PD control for controlling the hub-angular displacement and for optimising controller of end-point acceleration feedback. Here, ABFA were chosen instead of root locus and heuristic methods because they have advantages as they do not need exact mathematical model of flexible manipulators, are not time consuming as a heuristic method, and are able to find optimal parameters as well as avoid being trapped in local minima. The objective of the investigation is to assess the performances of ABFA proposed and discussed in Chapter 4 in finding optimal solution of JBC PD control and controller with end-point acceleration feedback parameters for the flexible manipulator control application. The ABFA's performances are then compared to that of SBFA based on their speed of convergence, optimum value achieved and time-domain responses. Throughout this work, all the simulations are carried out using Matlab/Simulink software while experimentations are done using a single-link flexible manipulator system rig.

7.2. Brief overview of PID control

Proportional-integral-derivative (PID) control is very popular and more than half of industrial controllers are either PID or modified PID controllers (Ogata, 2002). PID controllers contain three parameters, i.e. proportional gain (K_p), integral gain (K_i) and derivative gain (K_d). In general, output signal of PID controller can be formulated as:

$$u(t) = K_p e(t) + K_i \int e(t)dt + K_d \frac{de(t)}{dt} \tag{7.1}$$

where $e(t)$ is the error, the difference between set point and actual output. This formula can also be presented in the form of Laplace transform as:

$$U(s) = \left(K_p + \frac{K_i}{s} + K_d s\right) E(s) \tag{7.2}$$

Each of the three PID control parameters has its own characteristics and impact on the time-domain of closed-loop actual output which can be summarised as in Table 7.1.

Table 7.1: Effects of each parameter of PID control

Parameter	Rise time	Maximum overshoot	Settling time	Steady-state error
K_p	Decreasing	Increasing	Small change	Decreasing
K_i	Decreasing	Increasing	Increasing	Eliminating
K_d	Small change	Decreasing	Decreasing	Small change

The performance of PID control is determined by the composition of the three parameters so that the value of each parameter needs to be chosen properly. The characteristics of PID control parameters presented in Table 7.1 can be used as a rough guide. In practice, there are two most popular tuning methods that can be used to find optimal PID parameters, i.e. manual or heuristic and Ziegler-Nichols followed by re-tune methods (Ogata, 2002). The manual or heuristic tuning method does not require detailed information of the system under control but needs experience of the operator. Ziegler-Nichols method also can be applied to the system where its mathematical model is not properly known. However, the tuning process might also need very extensive effort.

7.3. Single-link flexible manipulator model

Since it has been widely used in the control development by previous researchers such as Alam and Tokhi (2008), Md Zain and Tokhi (2009), Md Zain et al. (2009c) and Tokhi et al. (2004), the mathematical model representing a single-link flexible manipulator under study developed by Azad (1994) and then enhanced by Poerwanto (1998) is used in the simulations in this work.

7.4. Hub-angular reference tracking control

The serial tasks usually performed by robot manipulators in industrial applications include picking up a payload from initial location, move to a specified location or along pre-planned trajectory, and to place the payload in a desired location (Shaheed et al., 2004). One of the commonly used trajectories is the bang-bang pattern movement. Thus, in this investigation, JBC PD control optimised by BFAs is used as the input tracking controller of hub-angular movement.

7.4.1. ABFA-JBC PD control structure and computation

The output signal of JBC PD control for the flexible manipulator control can be formulated as:

$$u(t) = K_p e(t) - K_v \frac{d\theta(t)}{dt} \tag{7.3}$$

where $u(t)$ is the control command, K_p is proportional gain, K_v is the derivative gain, $e(t) = R - \theta(t)$ is the error (R is the reference of angular displacement), and $\theta(t)$ is the actual angular displacement. Here, ABFA are used to find the optimal value of JBC parameters as shown in the block diagram in Figure 7.1. The nutrient media which will be optimised by ABFA is the cost function which is formulated based on the hub-angle error. The details of ABFA computation was presented in Chapter 4. The computation steps of JBC PD-BFA are outlined in Figure 7.2.

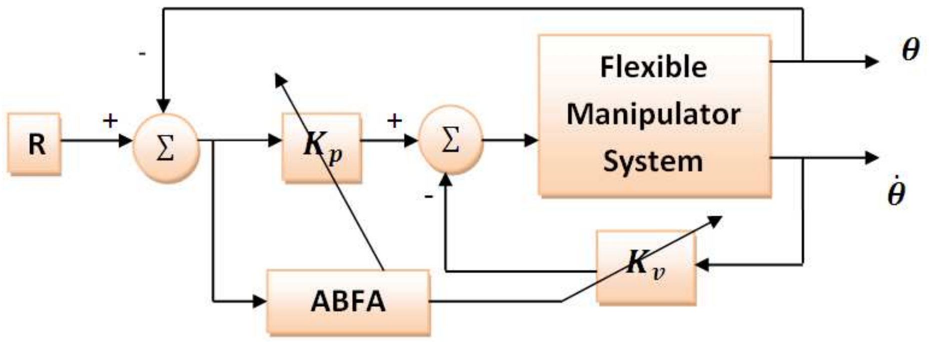

Figure 7.1: ABFA-tuned JBC PD control of flexible manipulator

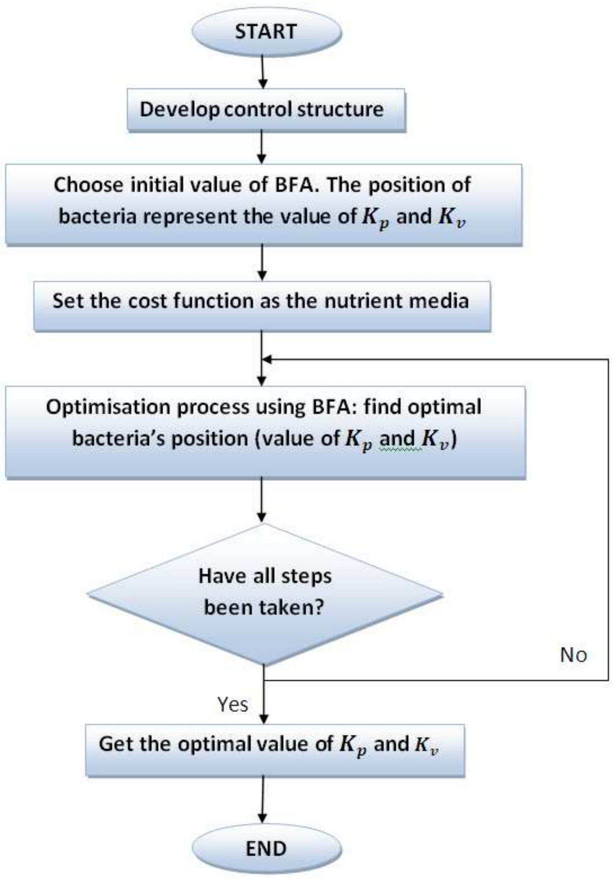
START
Develop control structure
Choose initial value of BFA. The position of bacteria represent the value of K_p and K_v
Set the cost function as the nutrient media
Optimisation process using BFA: find optimal bacteria's position (value of K_p and K_v)
Have all steps been taken?
No
Yes
Get the optimal value of K_p and K_v
END

Figure 7.2: Flowchart of JBC PD-BFA computation steps

7.4.2. Protocol of simulation and experimentation

The scenarios the simulations and experimentations are outlined as follows:

1. All parameters of BFAs used in the optimisation process, except dimension of the search space p, which is selected according to the parameters of the controller, are selected by trial and error. The parameters are selected by considering that bacteria should have enough lifetime (total number of steps), enough reproduction steps (N_{re}) so that bacteria can refine the nutrient value achieved and enough elimination and dispersal events (N_{ed}) so that bacteria are able to search most parts of the nutrient media to find closest optimum location to the global minimum but with minimum computation load.
2. The flexible manipulator model used in the simulation as considered has hub inertia and structural damping factor equal to 0.024.
3. Preliminary simulation to choose suitable cost function is performed. JBC PD is optimised by using SBFA only. Various chemotactic step size values are applied for each cost function and the best result is used in the comparison. For this

purpose, there are two input references used: step input with 75 degree to test the step response and bang-bang input with 75 degree magnitude, depicted in Figure 7.3. Bang-bang-type input is chosen because it reflects nature of the task performed by the manipulator, i.e. to accelerate from an initial position and then decelerate to a target location. Besides, the bang-bang signal is chosen because it consists of one positive pulse and one negative pulse and is considered adequate to study the control performance using this signal (Md Zain and Tokhi, 2009). The effect of the cost function considered is evaluated based on the time-domain responses.

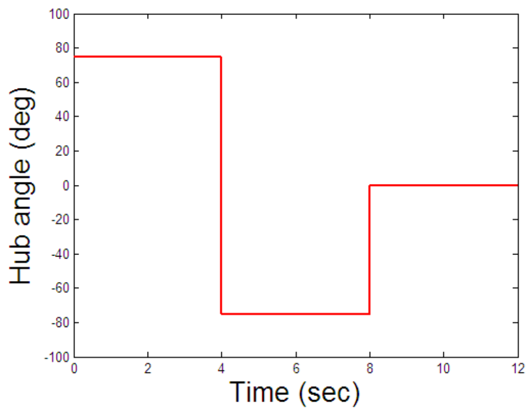

Figure 7.3: A bang-bang input with 75 degree magnitude for reference input

4. After comparison process, the most effective cost function is used in the rest of simulations and experiments with bang-bang signal used as the reference input. The performances of ABFAs are compared to that of SBFA based on the optimum cost function achieved, convergence speed (number of steps needed by algorithm to converge to the optimal) and time-domain responses.
5. The parameters of JBC PD controller obtained in the simulations are applied to actual flexible manipulator rig and their performances are compared based on the time-domain responses.
6. For the time-domain responses, following numerical measurements are made and used in the comparison:
   a. Rise time for positive pulse and step input (t_{ri}) is defined as the time required for the flexible manipulator to move from initial position (zero degree) until reach 90 % of maximum value of hub-angular set point.

b. Settling time for positive pulse and step input (t_{si}) is defined as the time required for the flexible manipulator to move from initial position (zero degree) until reach 98 % of maximum value of hub-angular set point.

c. Maximum overshoot for positive pulse and step input (σ_o) in per cent is formulated as:

$$\sigma_o = \frac{Max\ \theta - Max\ R}{Max\ R} \times 100 \tag{7.4}$$

where R is the hub-angle set point value and θ is the actual hub-angle movement.

d. Steady state error of positive pulse and step input (e_{ssi}) in per cent is formulated as:

$$e_{ssi} = \frac{Max\ R - \theta_{ss}}{Max\ R} \times 100 \tag{7.5}$$

where θ_{ss} is the actual hub-angle value in the steady state level.

e. Decreasing time for negative pulse (t_{rd}) is defined as the time needed by flexible manipulator to move from maximum hub-angle set point until reach 90 % of minimum hub-angle set point value.

f. Settling time for negative pulse (t_{sd}) is defined as the time needed by flexible manipulator to move from maximum hub-angle set point until reach 98 % of minimum hub-angle set point value.

g. Maximum undershoot for negative pulse (σ_u) in per cent is formulated as:

$$\sigma_u = \frac{Min\ \theta - Min\ R}{Min\ R} \times 100 \tag{7.6}$$

h. Steady state error for negative pulse (e_{ssd}) in per cent is formulated as:

$$e_{ssd} = \frac{Min\ R - Min\ \theta_{ss}}{Min\ R} \times 100 \tag{7.7}$$

where $Min\ \theta_{ss}$ is the actual hub-angle movement at steady state condition of negative pulse.

i. Maximum overshoot for the last stage of bang-bang input movement from negative pulse back to the initial position (σ_n) in per cent is formulated as:

$$\sigma_n = \frac{Max\ \theta_n}{Max\ R} \times 100 \tag{7.8}$$

where θ_n is the actual hub-angle output in last stage of bang-bang input.

j. Steady state error for the last stage of bang-bang input (e_{ssn}) in per cent is formulated as:

$$e_{ssn} = \frac{\theta_{ssn}}{Max\ R} \times 100 \tag{7.9}$$

where θ_{0ss} is the actual hub-angle movement at the steady state condition of the last stage of bang-bang input.

Thus, the overall simulation process is illustrated in Figure 7.4.

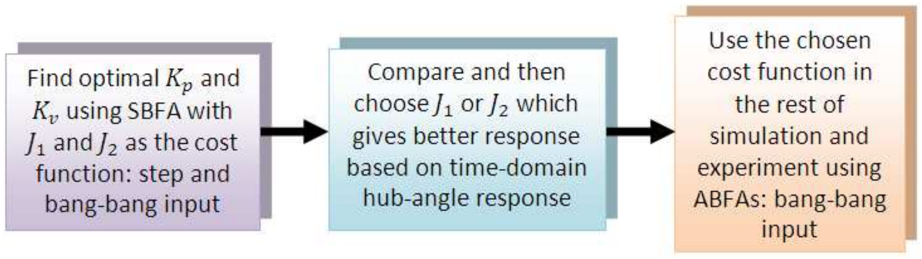
Find optimal K_p and K_v using SBFA with J_1 and J_2 as the cost function: step and bang-bang input
Compare and then choose J_1 or J_2 which gives better response based on time-domain hub-angle response
Use the chosen cost function in the rest of simulation and experiment using ABFAs: bang-bang input

Figure 7.4: Overall simulation and experiment sequence

7.4.3. Preliminary simulation: empirical cost function comparison

It can be noted from the literature that mean squared error (MSE) has been succesfully used in controller tuning of hub-angle control of flexible manipulator (Md Zain and Tokhi, 2009a; Md Zain et al., 2009c). This is formulated as:

$$J_1 = \frac{1}{N}\sum_{k=1}^{N}\left(e(k)\right)^2 \tag{7.10}$$

where $e(k) = R - \theta(k)$ is the angular displacement error and N is the total number of data points. An overshoot is usual phenomenon in the step response testing of controller. In the simulation using bang-bang input, overshot could happen in the positive pulse while undershoot may arise in the negative pulse. In order to suppress unwanted overshoot/undershoot, the cost function is modified by adding weighted absolute maximum overshoot/undershoot value as:

$$J_2 = \left(\frac{1}{N}\sum_{k=1}^{N}\left(e(k)\right)^2\right) + |\sigma_u| * \omega \tag{7.11}$$

where σ_u is maximum overshoot or undershoot, and ω is the weighting factors. Bigger ω value results in bigger suppression on overshoot and undershoot. Because the minimum value of $e(k)$ is equal to zero, in which case the hub-angular displacement output is exactly the same as the set point, the global minimum values for cost function J_1 and J_2 are also equal to zero. In terms of BFA computation, lower cost function value means higher nutrient level so that the highest nutrient level is when the cost function is equal to zero. Thus the main aim of optimisation in this work is to find minimum values of cost function J_1 and J_2. For the time-domain hub-angle output, the smallest cost function value means that the actual hub-angle output of the flexible manipulator is the closest to the reference input.

Because JBC PD controller has two parameters to optimise, the cost function becomes two-dimension search space. In the tuning process using SBFA, the following initial values were used

• $p = 2$	• $N_c = 16$	• $N_{re} = 3$	• $N_{ed} = 2$
• $S = 4$	• $N_s = 2$	• $S_r = {}^{S}/_{2}$	• $P_{ed} = 0.25$

Initial positions of bacteria were selected randomly across the nutrient media and after using various chemotactic step sizes $C(i)$, the best optimum cost function J value was achieved when $C(i)$ was equal to 0.02. Total number steps of computation the BFA were calculated as $N_c \times N_{re} \times N_{ed}$ and the cost function J value in every step refers to the position of bacterium that has the least cost function value.

A. Step input

In the investigation for step input, σ_u was the maximum overshoot. Various weighting factors ω were used and the most suitable value was equal to 50. Lower ω value than 50 always resulted overshoot while bigger value resulted slower response. Figure 7.5(a) shows the convergence of SBFA using J_1 and J_2. As noted the convergence speeds were the same with J_1 and J_2. The difference in position at the initial step was because bacteria were placed randomly; with optimisation using J_1, some bacteria were in locations near the optimum value. Time-domain responses of SBFA-JBC PD using J_1 and J_2 are depicted in Figure 7.5(b).

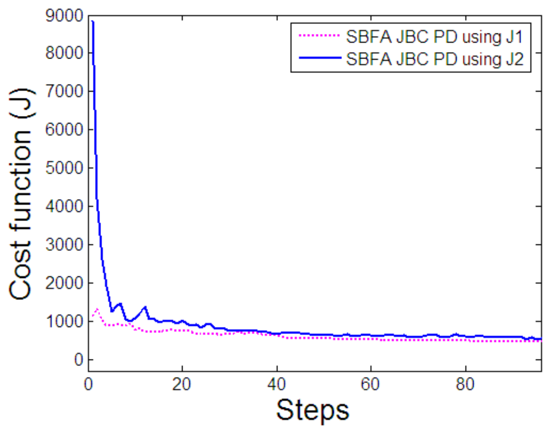

(a) Convergence plots

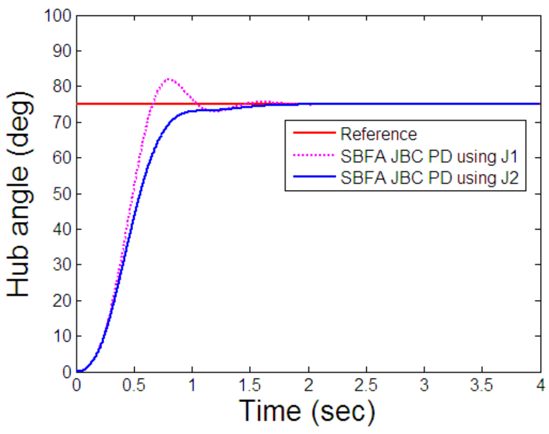

(b) Time-domain hub-angle

Figure 7.5: Simulation results with SBFA-JBC PD for step input using J_1 and J_2

The numerical results presented in Table 7.2 show that although using J_1 SBFA achieved lower optimum J and slightly faster rise and settling time, it resulted 9.071 % maximum overshoot in the response. On the contrary, by using J_2 the response overshoot was completely removed.

Table 7.2: Performance of controllers for step input using J_1 and J_2

Control	K_p	K_v	**Optimum** J	t_r **(s)**	t_s **(s)**	M_p **(%)**	e_{ss} **(%)**
Using J_1	1.7459	0.5687	470.4040	0.6001	1.3008	9.071	0
Using J_2	1.0655	0.5050	504.9843	0.7574	1.6623	0	0

B. Bang-bang input

In the investigation for bang-bang input, σ_u in equation (8.11) was the maximum undershoot of the negative pulse. Similar to the case of step input, the optimal ω value was equal to 50 for the bang-bang input. The convergence plots depicted in Figure 7.6(a) show that by using J_1 SBFA-JBC PD was able converged in 23 steps faster than using J_2 which converged in 55 steps. The time-domain responses depicted in Figure 7.6(b) show the comparison of all results.

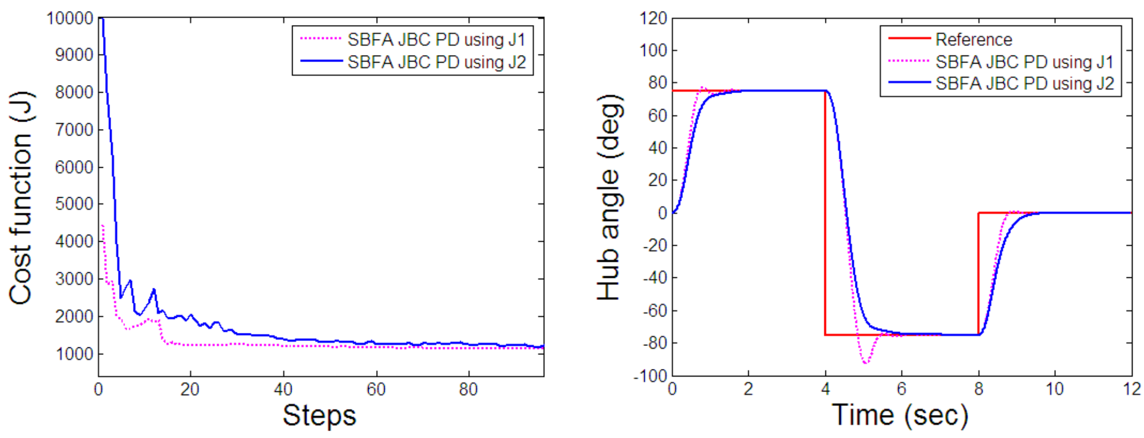

(a) Convergence plots (b) Time-domain hub-angle

Figure 7.6: Simulation results with bang-bang input using J_1 and J_2

From numerical results presented in Table 7.3 and Table 7.4 it can be noticed that using J_1 SBFA-JBC PD achieved better optimum J (1.1080×10^3) than using J_2 (1.1855×10^3) and slightly faster rise time and settling time for positive and negative pulses. However, using J_1 the overshoot in the positive pulse and undershoot in the negative pulse were 1.8714% and 17.5970% respectively, whereas with J_2 there was neither overshoot nor undershoot.

Table 7.3: Optimal results of SBFA-JBC PD using J_1 and J_2

Controller	Convergence (steps)	K_p	K_v	Optimum J
Using J_1	13	1.6795	0.6003	1.1080×10^3
Using J_2	55	0.9394	0.4887	1.1855×10^3

Table 7.4: Time-domain responses of SBFA-JBC PD using J_1 and J_2

Controller	t_{ri} (s)	t_{si} (s)	M_{pi} (%)	e_{ssi} (%)	t_{rd} (s)	t_{sd} (s)	M_{pd} (%)	e_{ssd} (%)
Using J_1	0.625	1.259	1.871	0	0.8195	1.5719	17.5970	0
Using J_2	0.843	1.437	0	0	1.1167	1.7290	0	0

The two investigations above show that cost function J_2 is suitable to be used throughout the work because it could remove overshoot and undershoot of hub-angle response.

7.4.4. Closed-loop simulation using J_2

A. Simulation results

Here, the hub-angular displacement is controlled using JBC PD optimised by SBFA and ABFA with cost function J_2, here only cited as J, as the nutrient media. Then their performances based on convergence speed, optimum value achieved and time-domain hub-angle output are compared to those of SBFA. In the simulation, SBFA and ABFA used the same initial parameters as:

• $p = 2$	• $N_c = 16$	• $N_{re} = 3$	• $N_{ed} = 2$
• $S = 4$	• $N_s = 2$	• $S_r = S/2$	• $P_{ed} = 0.25$

The initial positions of the bacteria were selected randomly across the search space. Chemotactic step size for SBFA is a constant value. In the convergence analysis, the nutrient value J is plotted against the total number of computation steps of BFA calculated as $N_c \times N_{re} \times N_{ed}$, which is equal to 96 steps. The nutrient value J in every step means the position of bacterium that has the smallest cost function value.

In the time-domain representation, the hub-angle output is plotted against time. In this work, the performance of the controller is assessed based on 10 parameters of the time-domain hub-angle output described in section 7.4.2 above. As noticed in the preliminary simulation, for SBFA, the best optimum solution was achieved when chemotactic step size $C(i)$ was equal to 0.02. For ABFA, the parameters of LABFA, QABFA and EABFA were selected manually by trial and error and the best optimum J was obtained when adaptable chemotactic step sizes were set up as:

$$C_{al}(i) = \frac{0.2}{1+\frac{1}{7.5\times10^{-5}|J(i)|}} \tag{7.12}$$

$$C_{aq}(i) = \frac{0.2}{1+\frac{1}{10^{-8}\left(\left(J(i)\right)^2+|J(i)|\right)}} \tag{7.13}$$

$$C_{ae}(i) = \frac{0.2}{1+\frac{1}{9\times10^{-8}e^{(0.01|J(i)|)}}} \tag{7.14}$$

For FABFA, the membership functions of input and output are plotted in Figure 7.7(a) and 7.7(b) respectively. The fuzzy rules connecting the input to output resulted in the fuzzy surface depicted in Figure 7.7(c). The fuzzy rules were formulated as:

R_1	:	IF $|J(i)|$ is ES THEN $C_{af}(i)$ is VS	(1)	
R_2	:	IF $|J(i)|$ is VS THEN $C_{af}(i)$ is S	(0.3)	
R_3	:	IF $|J(i)|$ is S THEN $C_{af}(i)$ is B	(1)	
R_4	:	IF $|J(i)|$ is M THEN $C_{af}(i)$ is EB	(1)	(7.15)
R_5	:	IF $|J(i)|$ is B THEN $C_{af}(i)$ is EB	(1)	
R_6	:	IF $|J(i)|$ is VB THEN $C_{af}(i)$ is EB	(1)	
R_7	:	IF $|J(i)|$ is EB THEN $C_{af}(i)$ is EB	(1)	

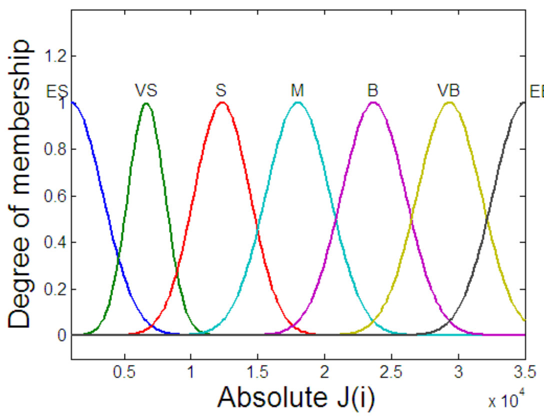

(a) Input: $|J(i)|$

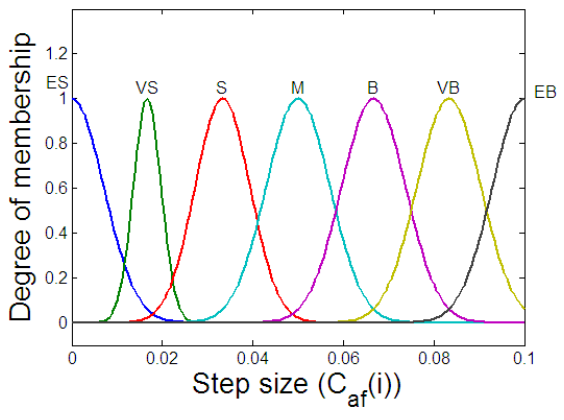

(b) Output: $C_{af}(i)$

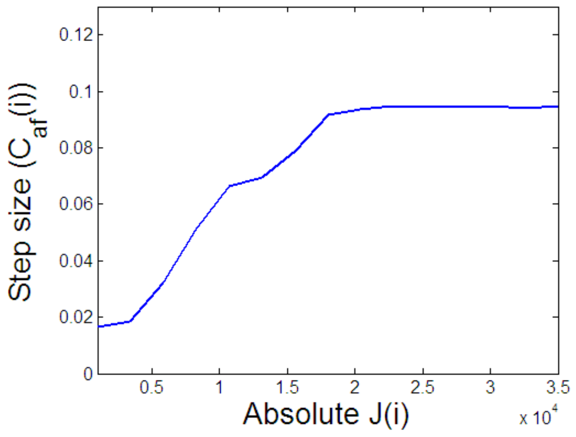

(c) Fuzzy surface

Figure 7.7: Fuzzy membership functions and surface of FABFA for JBC PD control

Using the formulations in equations (7.12)-(7.15), the adaptable chemotactic step sizes were in the range of [0.0164, 0.2], [0.0027, 0.2], [0.0019, 0.2] and [0.0167, 0.09] for LABFA-JBC PD, QABFA-JBC PD, EABFA-JBC PD and FABFA-JBC PD respectively. The convergence plots of controllers depicted in Figure 7.8(a) show that all ABFA-JBC PD controls were significantly faster in convergence than SBFA-JBC PD which converged in 87 steps. QABFA-JBC PD, which converged in 14 steps, was the fastest in convergence among them. It is also noted that there were no oscillations in the optimum point for QABFA-JBC PD and EABFA-JBC PD because they used very small chemotactic step size while there was small oscillation in LABFA-JBC PD but still much smaller than that of SBFA-JBC PD. Figure 7.8(b) presents the time-domain hub-angular displacement output with the controllers.

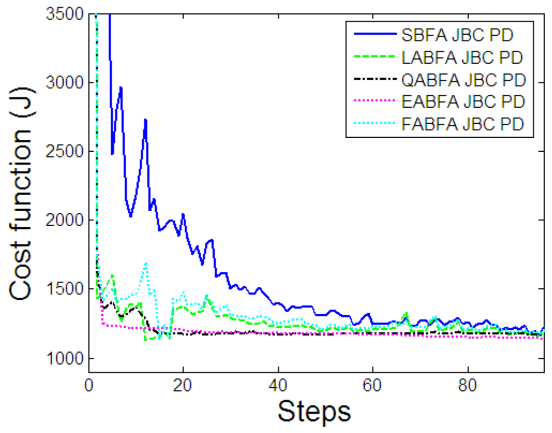

(a) Convergence plots

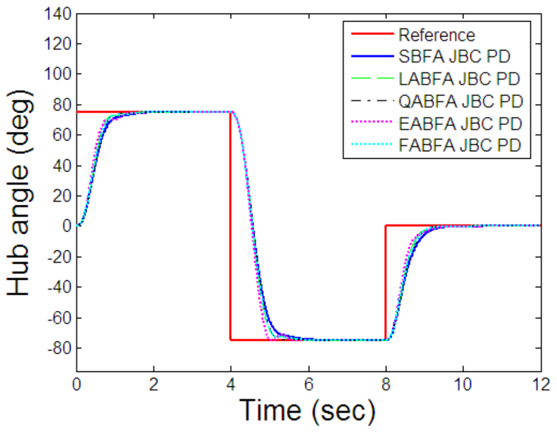

(b) Time-domain hub-angle

Figure 7.8: Simulation results with the BFA-JBC PD controls

As an impact of lower J value, numerical results presented in Table 7.5 and Table 7.6 show that ABFA-based controls result in better time-domain hub-angle output performance, i.e. shorter rise time, decline time and settling time both in the positive and negative pulses in comparison to that with SBFA-JBC PD. The controllers were able to suppress the presence of unwanted overshoot and undershoot as well as steady state error. Compared to using PID-GA control in (Md Zain and Tokhi, 2009), all the controllers in this work achieved much faster settling time, because settling time in (Md Zain and Tokhi, 2009) was 3.264 second

Table 7.5: Numerical results of optimum J of the controllers

Control	$C(i)$ **range**	**Convergence (steps)**	**Optimum J**
SBFA-JBC PD	0.02	87	1.1855×10^3
LABFA-JBC PD	[0.0164, 0.2]	49	1.1403×10^3
QABFA-JBC PD	[0.0027, 0.2]	**14**	1.1679×10^3
EABFA-JBC PD	[0.0019, 0.2]	23	$\mathbf{1.1266 \times 10^3}$
FABFA-JBC PD	[0.0167, 0.09]	51	1.1562×10^3

Table 7.6: Time-domain hub-angle responses of the controllers

Control	K_p	K_v	t_{ri} (s)	t_{si} (s)	t_{rd} (s)	t_{sd} (s)
SBFA-JBC PD	0.9394	0.4887	0.8432	1.4370	1.1167	1.7290
LABFA-JBC PD	1.1793	0.5343	0.7291	1.3121	0.9803	1.6000
QABFA-JBC PD	0.9499	0.4663	0.7820	1.0178	1.0167	1.1960
EABFA-JBC PD	1.8297	0.7325	0.6957	1.2703	0.8877	1.5004
FABFA-JBC PD	1.0376	0.4957	0.7626	1.2594	1.0093	1.5741

B. Experimental results

The BFA-based JBC PD controls obtained in the simulation above were implemented on the single-link flexible manipulator experimental rig. The time-domain hub-angle responses for the controllers are plotted in Figure 7.9.

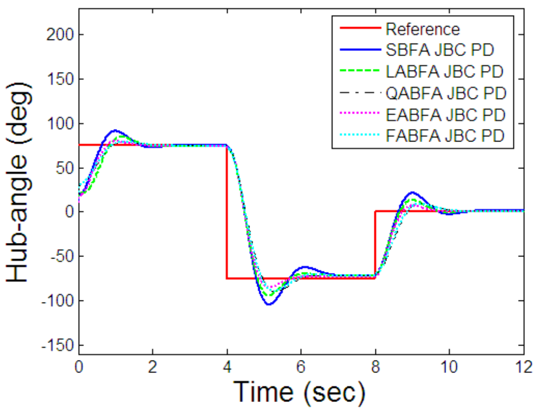

Figure 7.9: Experimental time-domain hub-angle responses

It is noted from the plots that responses with the ABFA-based controls were slightly slower with lower overshoot, undershoot and smaller steady state error than with SBFA-based control. The numerical results presented in Table 7.7 show that all the BFA-based JBC PD controls resulted in acceptable steady-state error, e.g. below 2% with overshoot and undershoot are fall between 4.7819% and 28.8287% respectively.

Table 7.7: Experimental time-domain hub-angle responses parameters with BFA-JBC PD controls

Control	t_{ri} (s)	t_{si} (s)	M_{pi} (%)	e_{ssi} (%)	t_{rd} (s)	t_{sd} (s)	M_{pd} (%)	e_{ssd} (%)	M_{p0} (%)	e_{ss0} (%)
SBFA-JBC PD	0.555	2.233	21.571	0.297	2.544	3.187	28.829	1.913	25.35	1.762
LABFA-JBC PD	0.745	0.823	9.684	0.2923	0.790	2.4	12.265	0.546	10.213	0.3651
QABFA-JBC PD	0.738	0.878	5.086	0.263	0.900	2.145	9.703	0.676	6.739	0.623
EABFA-JBC PD	0.633	0.732	5.602	0.008	0.834	2.114	7.745	0.061	5.592	0.347
FABFA-JBC PD	0.709	0.848	4.782	0.208	0.884	2.243	8.554	0.84	5.592	0.359

7.5. Vibration reduction using end-point acceleration feedback

7.5.1. Controller structure and computation

When a flexible manipulator is moved to follow a desired trajectory, because of its flexible nature, the end-point of the manipulator oscillates around its expected position. This oscillation, or vibration, needs to be minimised. In this work, end-point acceleration feedback control is used to reduce the vibration. The control structure of end-point acceleration feedback (α) is depicted in Figure 7.10.

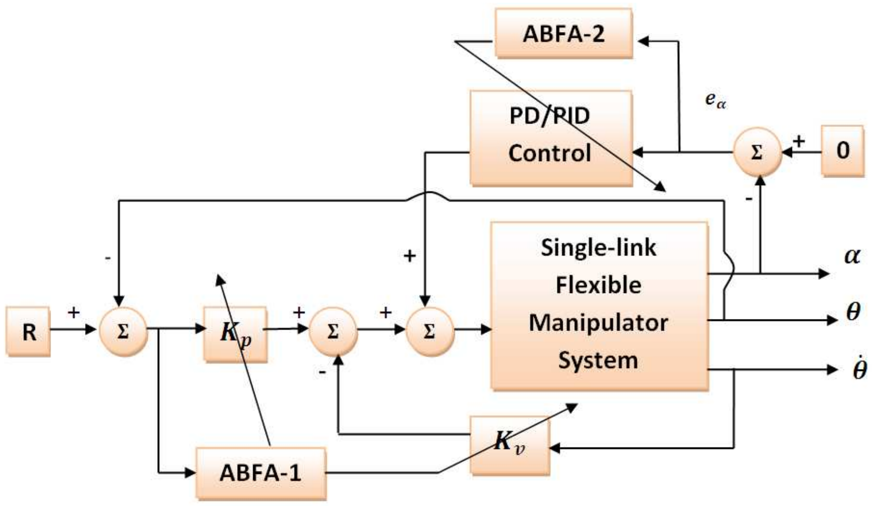

Figure 7.10: End-point acceleration feedback for vibration reduction

A band pass filter (BPF) is installed in the end-point acceleration path to allow vibration with high frequency in the feedback loop. The ideal condition is when there is no vibration, α equals to zero. There are two optimisation processes, i.e. optimisation for input tracking controller using ABFA-1 and optimisation for end-point acceleration feedback using ABFA-2. Similar to input tracking control presented in the previous section, the investigations are focused on the performance of ABFA compared to SBFA.

There are two controls considered in the end-point acceleration feedback loop, PD and PID controls. The output signal of PD and PID controls in the end-point acceleration feedback loop are given as:

$$\text{PD:} \qquad u_\alpha(t) = K_p e_\alpha(t) + K_d \frac{de_\alpha(t)}{dt} \tag{7.16}$$

$$\text{PID:} \qquad u_\alpha(t) = K_p e_\alpha(t) + K_i \int e_\alpha(t)dt + K_d \frac{de_\alpha(t)}{dt} \tag{7.17}$$

where $e_\alpha = 0 - \alpha$ is the end-point acceleration error. In the optimisation process, ABFA-2 used MSE of end-point acceleration error (e_α) as cost function. This is formulated as:

$$J_\alpha = \frac{1}{N}\sum_{k=1}^{N}\left(e_\alpha(k)\right)^2 \tag{7.18}$$

In general, the computation steps are the same as optimising JBC PD above.

7.5.2. Protocol of simulations and experimentations

In this work, the simulations and experimentations are carried out as:

1. Bang-bang input depicted in Figure 7.3 is used as the input trajectory.
2. The best ABFA-1 based controller in the input tracking control discussed in section 8.4 is used as the input tracking control loop. The selection is based on the J value achieved because smallest J means it has the smallest error.
3. Both PD and PID controls with end-point acceleration feedback are optimised using ABFA-2.
4. For the same reasons for input tracking control (ABFA-1), the parameters of ABFA-2 are chosen so that bacteria have enough life time (steps) to find global minimum of the cost function.
5. The performances of ABFA are compared to SBFA based on the optimum J_α achieved, convergence speed, time-domain and frequency responses of end-point acceleration. Moreover, the performances of controller with end-point acceleration feedback are compared to open loop-control and JBC PD control without end-point acceleration feedback based on the J_α value achieved, time-domain and frequency-domain responses.
6. Finally, the parameters of PD / PID controls obtained in the simulations are applied in the flexible manipulator rig. The investigations are focused on the performances of ABFA-based controls compared to SBFA-based control based on J_α value achieved, time-domain and frequency-domain responses.

7. For frequency-domain responses, main attentions are paid on the comparison of vibration reduction between open loop control and closed loop control, effect of PD and PID control of end-point acceleration feedback on vibration reduction and performance comparison of ABFA-based and SBFA-based control of end-point acceleration feedback. The rate of vibration reduction (in per cent) of end-point flexible arm with closed loop control of end-point acceleration feedback against open-loop control is formulated as follow:

$$R_{\alpha\_l} = \frac{M_{o\alpha}-M_{l\alpha}}{M_{o\alpha}} \times 100 \tag{7.19}$$

where R_{α_l} is the vibration reduction rate for closed loop control with control of end-point acceleration feedback against open-loop control, $M_{o\alpha}$ is the vibration magnitude of open loop control, $M_{c\alpha}$ is the vibration magnitude of closed loop control without control of end-point acceleration feedback and $M_{l\alpha}$ is the vibration magnitude of closed loop control with control of end-point acceleration feedback. The vibration reduction of closed loop control with control of end-point acceleration feedback against closed loop control without control of end-point acceleration feedback can be formulated as:

$$R_{\alpha\_cl} = \frac{M_{c\alpha}-M_{l\alpha}}{M_{c\alpha}} \times 100 \tag{7.20}$$

where R_{α_cl} is the vibration reduction rate of EABFA-JBC PD with control of end-point acceleration feedback against EABFA-JBC PD without control of end-point acceleration feedback.

7.5.3. Open-loop simulation

The responses of end-point acceleration for open-loop simulation using bang-bang input depicted in Figure 7.3 are shown in Figure 7.11(a) and Figure 7.11(b) in the time-domain and frequency-domain respectively. The time-domain response show that the maximum vibration only occurs in early stage due to fast movement of the manipulator. It confirms that faster and bigger angular movement result bigger vibration of end-point acceleration. The numerical results of frequency-domain responses are presented in Table 7.8.

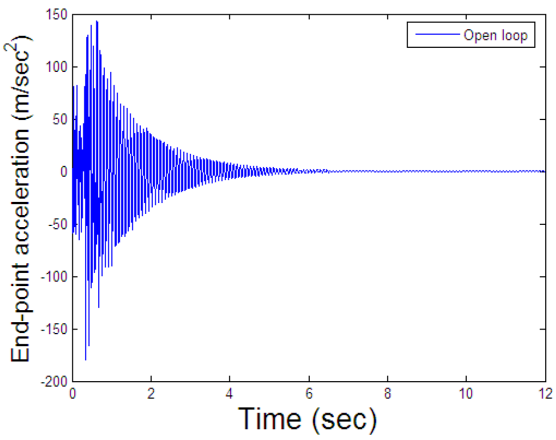

(a) End-point acceleration time-domain

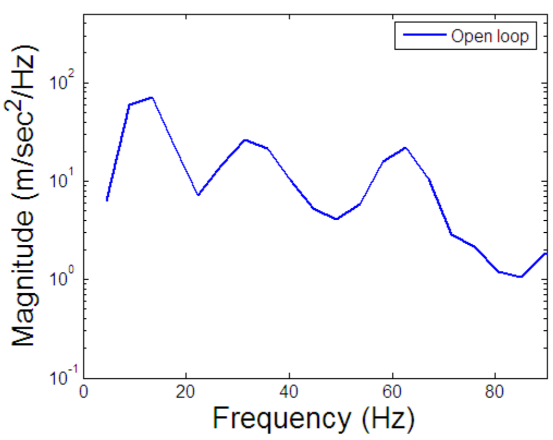

(b) End-point acceleration frequency-domain

Figure 7.11: Open-loop end-point acceleration response to bang-bang input

Table 7.8: Numerical results of end-point acceleration response in open-loop (F is frequency (Hz) and M is magnitude ($m/sec^2/Hz$))

J_α **value**	**Mode 1**	**Mode 2**	**Mode 3**

456.8778	F = 13.42 Hz
	M = 71.96
		F=31.31 Hz
		M=26.01
			F=62.62
			M=21.9

7.5.4. End-point acceleration feedback with PD control

A. Simulation results

In this part, PD controller optimised by BFAs with end-point acceleration feedback is used to reduce the vibration at the end-point of the flexible arm. Since there are only two parameters to be optimised, i.e. K_p and K_d, the nutrient media (cost function) of BFA is a two-dimension search space. It is noted from the numerical results of input tracking control presented in Table 7.6 that EABFA JBC PD had the smallest cost function J value. Thus, in this investigation EABFA-JBC PD is used as the input tracking controller. The two parameters of EABFA-JBC PD are K_{p1} = 1.8297 and K_{v1} = 0.7325. In the optimisation process, the BFA-2 used the same general parameter as:

• $p = 2$	• $N_c = 10$	• $N_{re} = 3$	• $N_{ed} = 3$
• $S = 4$	• $N_s = 2$	• $S_r = S/2$	• $P_{ed} = 0.25$

The initial positions of bacteria were selected randomly across the search space. For SBFA, the chemotactic step size was chosen manually by trial and error and the best result was achieved when $C(i)$ was equal to 0.002. For ABFAs, the best results were achieved when the adaptable chemotactic step size for LABFA-PD, QABFA-PD and EABFA-PD were set up as:

$$C_{al}(i) = \frac{0.05}{1+\frac{1}{0.00024|J(i)|}} \tag{7.21}$$

$$C_{aq}(i) = \frac{0.05}{1+\frac{1}{0.00005\left((0.165J(i))^2+0.165|J(i)|\right)}} \tag{7.22}$$

$$C_{ae}(i) = \frac{0.05}{1+\frac{1}{0.0014e^{(0.02|J(i)|)}}} \tag{7.23}$$

For FABFA-PD, the fuzzy structure contained one input, i.e. absolute cost function of every bacterium $|J(i)|$ and one output, i.e. fuzzy adaptable chemotactic step size for every bacterium $C_{af}(i)$. Seven Gaussian membership functions were used for both input and output. The membership functions for input and output are plotted in Figure 7.12(a) and Figure 7.12(b) respectively. The fuzzy rules result the relationship between input and output shown in Figure 7.12(c) were formulated as:

R_1	:	IF $|J(i)|$ is ES THEN $C_{af}(i)$ is ES	(1)	
R_2	:	IF $|J(i)|$ is VS THEN $C_{af}(i)$ is ES	(1)	
R_3	:	IF $|J(i)|$ is S THEN $C_{af}(i)$ is S	(1)	
R_4	:	IF $|J(i)|$ is M THEN $C_{af}(i)$ is M	(1)	(7.24)
R_5	:	IF $|J(i)|$ is B THEN $C_{af}(i)$ is B	(1)	
R_6	:	IF $|J(i)|$ is VB THEN $C_{af}(i)$ is VB	(1)	
R_7	:	IF $|J(i)|$ is EB THEN $C_{af}(i)$ is EB	(1)	

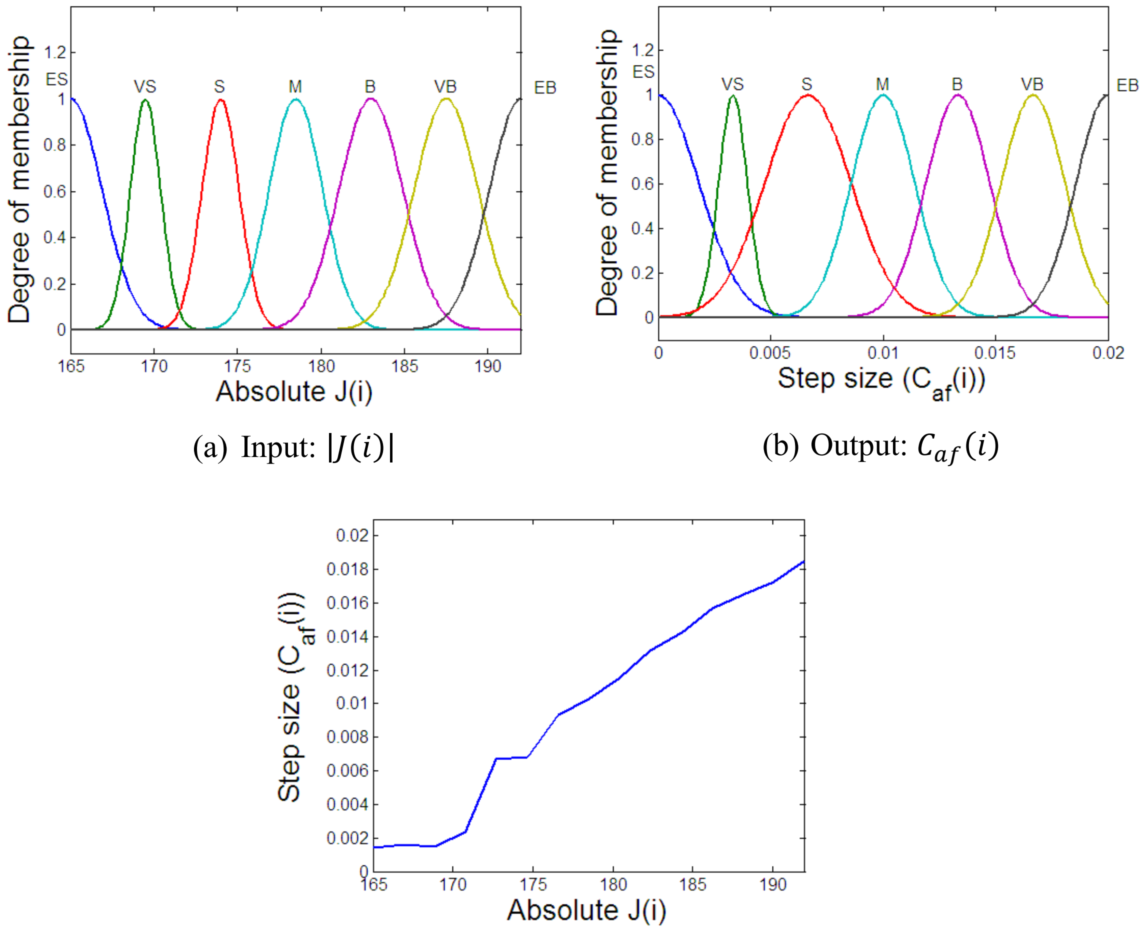

(c) Fuzzy surface

Figure 7.12: Fuzzy membership function and surface of FABFA-PD of end-point acceleration feedback

By using these formulations the chemotactic step size of ABFA-PD were in the ranges [0.002, 0.005], [0.002, 0.005], [0.002, 0.005] and [0.0016, 0.0185] for LABFA-PD, QABFA-PD, EABFA-PD and FABFA-PD respectively. The convergence plots depicted in Figure 7.13(a) show that FABFA-PD had the fastest convergence speed with SBFA-PD, LABFA-PD, QABFA-PD and EABFA-PD having the same convergence speed. This was probably due to the cost function landscape being rather flat and FABFA-PD was able to converge faster because it applies human logic to choose the step size. The numerical results presented in Table 7.9 show that FABFA-PD converged in 18 steps compared to other BFAs, which converged in 37 steps.

Time-domain end-point acceleration responses are depicted in Figure 7.13(b). It is noted that, with PD control in the end-point acceleration feedback loop, the manipulator vibration was damped faster than without PD control. The cost function J_α

values presented in Table 7.9 show that all PD controls with end-point acceleration feedback achieved smaller values than open-loop control and without PD control in the end-point acceleration feedback loop with the lowest cost function J_α value 170.2501 achieved by EABFA JBC PD-EABFA PD. PSD of end-point acceleration depicted in Figure 7.13(c) shows that the resonance frequencies for the first three vibration modes were 13.42 Hz, 31.31 Hz and 62.62 Hz.

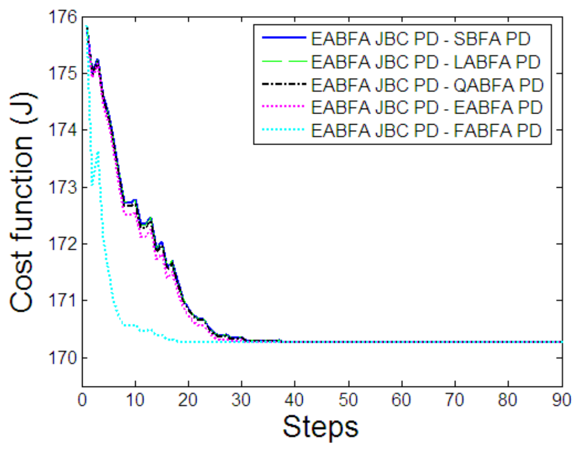

(a) Convergence plots

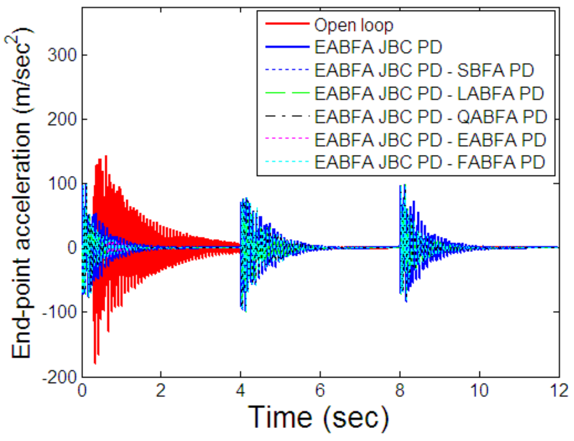

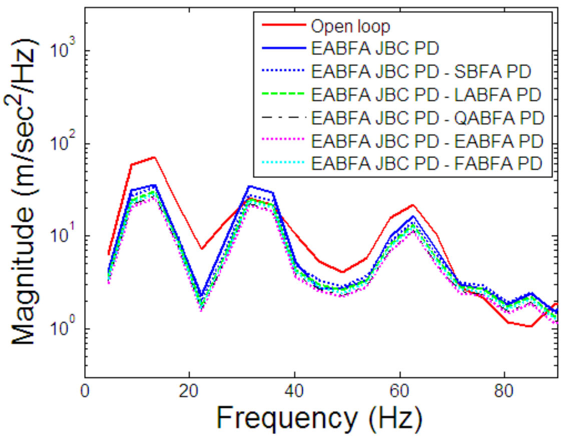

(b) Time-domain end-point acceleration

(c) Frequency-domain end-point acceleration

Figure 7.13: Simulation results for PD end-point acceleration feedback controls

Table 7.9: Numerical results for PD end-point acceleration feedback controls

Control	$C(i)$	$\boldsymbol{K_{p2}}$	$\boldsymbol{K_{d2}}$	**Optimum $\boldsymbol{J_{\alpha}}$**	**Convergence (steps)**
Open loop control	-	-	-	456.8778	-
EABFA JBC PD	-	-	-	202.6463	-
EABFA JBC PD – SBFA PD	0.002	0.1402	0.0840	170.2637	37
EABFA JBC PD LABFA-PD	[0.002, 0.005]	0.1397	0.1129	170.2593	37
EABFA JBC PD – QABFA PD	[0.0020, 0.005]	0.1403	0.0827	170.2537	37
EABFA JBC PD – EABFA PD	[0.002, 0.005]	0.1398	0.1076	**170.2501**	37
EABFA JBC PD – FABFA PD	[0.0016, 0.0185]	0.1401	0.0943	170.2562	**18**

The response magnitudes at the first and third vibration modes were reduced with PD controller in end-point acceleration feedback loop, whereas reinforcement occurred at the second mode. Table 7.10 shows the vibration reduction achieved at the resonance modes with BFA-PD controllers in the end-point acceleration loop. It is noticed that for all controllers with end-point acceleration feedback, all ABFA-based PD controls have bigger vibration reduction than that of SBFA-based with the biggest reduction percentage for the first three resonance mode is achieved by EABFA JBC PD-EABFA PD, i.e. 63.910 %, 18.185 % and 48.767 % for the first, second and third modes respectively.

Table 7.10: Spectral attenuation at resonance modes with BFA-PD end-point acceleration feedback controls against open-loop control ($m/sec^2/Hz$)

Control	**Mode 1 (dB)**	**Mode 2 (dB)**	**Mode 3 (dB)**
EABFA JBC PD-SBFA PD	38.16 (53.029 %)	-1.68 (-6.459 %)	7.3 (33.333 %)
EABFA JBC PD-LABFA PD	41.36 (57.476 %)	0.94 (3.614 %)	8.69 (39.680 %)
EABFA JBC PD-QABFA PD	45.82 (63.674 %)	3.86 (14.840 %)	9.76 (44.566 %)
EABFA JBC PD-EABFA PD	**45.99 (63.910 %)**	**4.73 (18.185 %)**	**10.68 (48.767 %)**
EABFA JBC PD-FABFA PD	43.14 (59.950 %)	2.4 (9.227 %)	9.45 (43.150 %)

The effect of end-point acceleration feedback control in the vibration reduction against EABFA JBC PD in per cent is shown in the numerical results presented in Table 7.11 show that all ABFA-based PD controls have bigger vibration reduction percentage than that of SBFA PD and the biggest vibration percentage is obtained by EABFA JBC PD-EABFA PD, i.e. 27.01 %, 39.511 % and 32.572 % for the first, second and third resonance modes respectively.

Table 7.11: Spectral attenuation at resonance modes with BFA PD end-point acceleration feedback controls against EABFA JBC PD without feedback loop ($m/sec^2/Hz$)

Control	Mode 1 (dB)	Mode 2 (dB)	Mode 3 (dB)
EABFA JBC PD – SBFA PD	1.78 (5.003 %)	7.49 (21.296 %)	2.04 (12.259 %)
EABFA JBC PD – LABFA PD	4.98 (13.997 %)	10.11 (28.737 %)	3.43 (20.613 %)
EABFA JBC PD – QABFA PD	9.44 (26.532 %)	13.03 (37.038 %)	4.5 (27.043 %)
EABFA JBC PD – EABFA PD	**9.61 (27.01 %)**	**13.9 (39.511 %)**	**5.42 (32.572 %)**
EABFA JBC PD – FABFA PD	6.76 (18.999 %)	11.57 (32.888 %)	4.19 (25.180 %)

B. Experimental results

The time-domain and frequency domain end-point acceleration responses of experimental rig with PD control in the end-point acceleration feedback loop are shown in Figure 7.14. It is noted that the manipulator vibration at the end-point has been reduced with the PD end-point acceleration feedback controls. Numerical results of time-domain responses presented in Table 7.12 show that the J_α values with PD end-point acceleration feedback controls were smaller than open loop and without feedback control with the smallest J_α value achieved by EABFA JBC PD-EABFA PD.

Table 7.12: Experimental results of time-domain end-point acceleration responses

Control	J_α value
Open loop	1.5843
EABFA JBC PD	0.3514
EABFA JBC PD – SBFA PD	0.2659
EABFA JBC PD – LABFA PD	0.2385
EABFA JBC PD – QABFA PD	0.2459
EABFA JBC PD – EABFA PD	**0.2273**
EABFA JBC PD – FABFA PD	0.2375

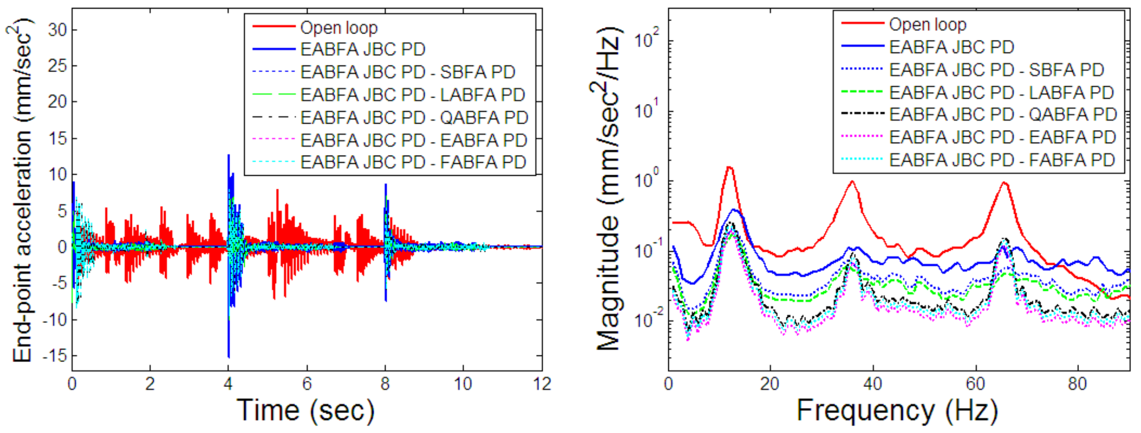

(a) Time-domain End-point acceleration

(b) Frequency-domain end-point acceleration

Figure 7.14: Experimental results of end-point acceleration responses

The numerical results presented in Table 7.13 shows the spectral attenuations achieved at the first three resonance modes with BFA PD end-point acceleration feedback controls with the biggest vibration reduction for the first and second resonance modes is achieved by EABFA JBC PD-EABFA PD, e.g. 89.707 % and 94.059 % while for third resonance mode is achieved by EABFA JBC PD-LABFA PD, e.g. 95.293 %. Moreover, in general, ABFA-based PD controls of end-point acceleration feedback have bigger vibration reduction rate compared to SBFA-based

Table 7.13: Spectral attenuations achieved at resonance modes with BFA-PD end-point acceleration feedback controls against open-loop control ($m/sec^2/Hz$).

Control	Mode 1 (dB)	Mode 2 (dB)	Mode 3 (dB)
EABFA JBC PD-SBFA PD	1.407 (86.045 %)	0.945 (93.143 %)	0.924 (92.939 %)
EABFA JBC PD-LABFA PD	1.465 (89.523 %)	0.9545 (94.039 %)	**0.947 (95.293 %)**
EABFA JBC PD-QABFA PD	1.373 (83.936 %)	0.9194 (90.581 %)	0.833 (83.826 %)
EABFA JBC PD-EABFA PD	**1.468 (89.707 %)**	**0.9547 (94.059 %)**	0.89 (83.826 %)
EABFA JBC PD-FABFA PD	1.407 (86.033 %)	0.9318 (91.813 %)	0.854 (83.927 %)

The numerical results presented in Table 7.14 show that for the first and second vibration resonance mode all with controllers of end-point acceleration feedback are able to significantly damp the vibration and the biggest reduction is achieved by EABFA JBC

PD-EABFA PD, i.e. 57.172 % and 47.55 % respectively while for the third resonance mode is achieved by EABFA JBC PD-LABFA PD, i.e. 64.736 %. Again, this results show that ABFAs-based controller of end-point acceleration feedback is superior compared to SBFA-based.

Table 7.14: Spectral attenuations achieved at resonance modes with BFA-PD end-point acceleration feedback controls against EABFA JBC PD without feedback loop ($m/sec^2/Hz$).

Control	Mode 1	Mode 2	Mode 3
EABFA JBC PD-SBFA PD	0.164 (41.887 %)	0.045 (39.530 %)	0.0625 (47.108 %)
EABFA JBC PD-LABFA PD	0.222 (56.409 %)	0.0546 (47.42 %)	**0.086 (64.736 %)**
EABFA JBC PD-QABFA PD	0.132 (33.418 %)	0.0195 (16.92 %)	-0.028 (-21.084 %)
EABFA JBC PD-EABFA PD	**0.225 (57.172 %)**	**0.0547 (47.55 %)**	0.0279 (21.009 %)
EABFA JBC PD-FABFA PD	0.165 (41.989 %)	0.0319 (27.75 %)	-0.007 (-5.271 %)

7.5.5. End-point acceleration feedback with PID control

A. Simulation results

In this section, PID control optimised by BFA with end-point acceleration feedback is used to reduce the vibration at the end-point of the flexible arm. Since there are three parameters to tune in a PID control, the cost function of BFA will form a three-dimensional search space. Similar to the case of PD end-point acceleration feedback control, here EABFA JBC PD is used as the input tracking controller. The two parameters of EABFA JBC PD are K_{p1} = 1.8297 and K_{v1} = 0.7325. In the optimisation process, the BFA-2 used the general parameters:

• p = 3	• N_c = 10	• N_{re} = 3	• N_{ed} = 2
• S = 4	• N_s = 2	• $S_r = S/2$	• P_{ed} = 0.25

The initial positions of bacteria were selected randomly across the cost function. For SBFA, the chemotactic step size was chosen manually by trial and error and the best result was achieved when $C(i)$ was equal to 0.005. For ABFA, the best results were achieved with chemotactic step size for LABFA, QABFA and EABFA set up as:

$$C_{al}(i) = \frac{0.2}{1+\frac{1}{0.0001|J(i)|}} \quad (7.25)$$

$$C_{aq}(i) = \frac{0.2}{1+\frac{1}{0.0021\left(\left(0.01J(i)\right)^2+0.01|J(i)|\right)}} \tag{7.26}$$

$$C_{ae}(i) = \frac{0.2}{1+\frac{1}{0.0225e^{(0.00005|J(i)|)}}} \tag{7.27}$$

For FABFA, the fuzzy structure contained one input, i.e. absolute cost function of every bacterium $|J(i)|$ and one output, i.e. fuzzy adaptable chemotactic step size for every bacterium $C_{af}(i)$. Seven Gaussian membership functions were used for both input and output. The membership functions for input and output are plotted in Figure 7.15(a) and Figure 7.15(b) respectively. Fuzzy rules result the relationship between input and output can be shown in Figure 7.15(c) were formulated as:

R_1	:	IF $|J(i)|$ is ES THEN $C_{af}(i)$ is VS	(1)	
R_2	:	IF $|J(i)|$ is VS THEN $C_{af}(i)$ is S	(1)	
R_3	:	IF $|J(i)|$ is S THEN $C_{af}(i)$ is VB	(1)	
R_4	:	IF $|J(i)|$ is M THEN $C_{af}(i)$ is EB	(1)	(7.28)
R_5	:	IF $|J(i)|$ is B THEN $C_{af}(i)$ is EB	(1)	
R_6	:	IF $|J(i)|$ is VB THEN $C_{af}(i)$ is EB	(1)	
R_7	:	IF $|J(i)|$ is EB THEN $C_{af}(i)$ is EB	(1)	

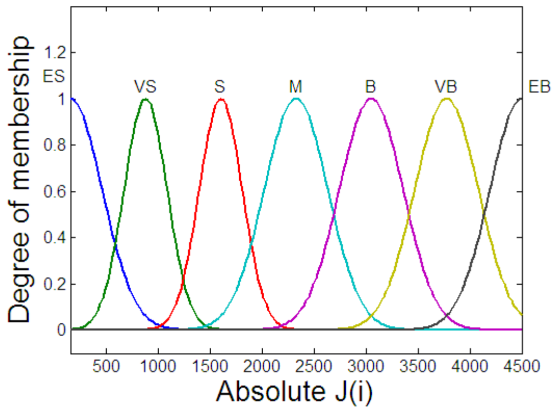

(a) Input: $|J(i)|$

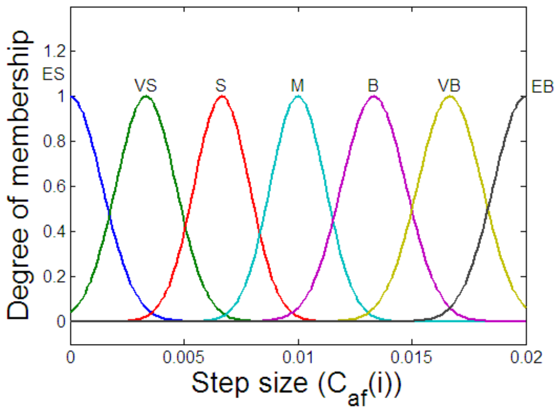

(b) Output: $C_{af}(i)$

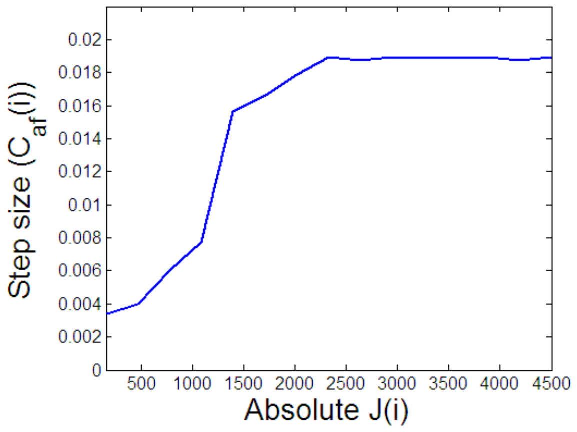

(c) Fuzzy surface

Figure 7.15: Fuzzy membership function and surface of FABFA PID end-point acceleration feedback control

By using these formulations the chemotactic step size of ABFA were in the range [0.0034, 0.2], [0.0019, 0.2], [0.0044, 0.2] and [0.0034, 0.0189] for LABFA PID, QABFA PID, EABFA PID and FABFA PID respectively. The convergence plots depicted in Figure 7.16(a) show that all ABFA achieved faster convergence speed than SBFA. The numerical results presented in Table 7.15 show that ABFA converged in 11 steps compared to SBFA which converged in 22 steps. Time-domain and frequency-domain end-point acceleration responses depicted in Figure 7.16(b) and Figure 7.16(c) show that the system vibration was reduced with the PID end-point acceleration feedback controls.

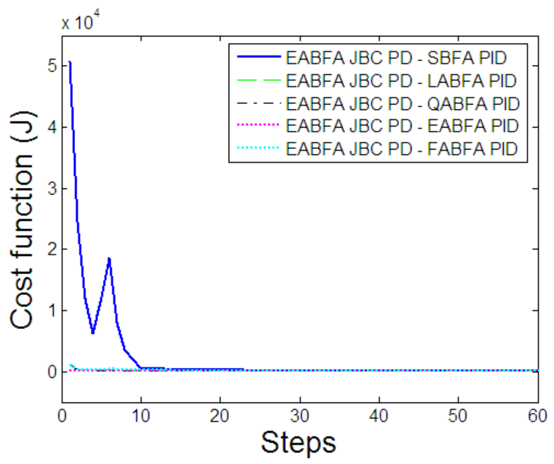

(a) Convergence plots

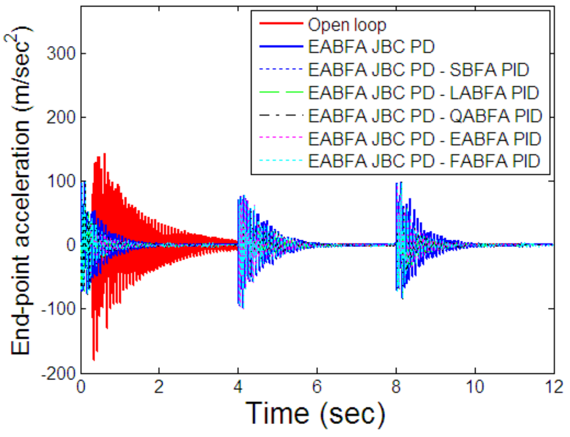

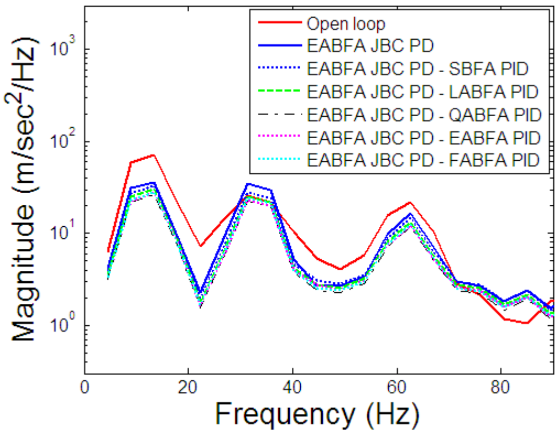

(b) Time-domain end-point acceleration

(c) Frequency-domain end-point acceleration

Figure 7.16: Simulation results of BFA PID end-point acceleration feedback controls

Cost function J_α values presented in Table 7.15 show that all controllers with end-point acceleration feedback achieved smaller value than open-loop control and without PID controller of end-point acceleration feedback, with the lowest cost function J_α value (170.2573) achieved by EABFA PID. PSD of end-point acceleration depicted in Figure 7.16(c) shows that the resonance frequencies of the first three modes were 13.42 Hz, 31.31 Hz and 62.62 Hz. Vibration's reduction occurred at the first and third modes and the vibration was reinforced at the second mode.

Table 7.15: Numerical results for BFA PID end-point acceleration feedback controls

Control	$C(i)$	K_{p2}	K_{i2}	K_{d2}	**Optimum J**	**Convergence (steps)**
Open loop	-	-	-	-	456.8778	-
EABFA JBC PD	-	-	-	-	202.6463	-
EABFA JBC PD-SBFA PID	0.005	0.0875	0.0048	0.0400	171.5426	22
EABFA JBC PD-LABFA PID	[0.0034, 0.2]	0.0957	0.0046	0.0445	171.3446	11
EABFA JBC PD-QABFA PID	[0.0019, 0.2]	0.0872	0.0082	0.0681	171.4794	11
EABFA JBC PD-EABFA PID	[0.0044, 0.2]	0.1399	0.0814	0.1304	**170.2573**	11
EABFA JBC PD-FABFA PID	[0.0034, 0.0189]	0.0804	0.0102	0.0378	171.5290	11

The numerical results in Table 7.16 show the spectral attenuations against open-loop achieved at the resonance modes with the BFA PID end-point acceleration feedback controls. ABFA-based PID end-point acceleration feedback controls have bigger reduction rate compared to EABFA JBC PD-SBFA PID and the biggest reduction is achieved by EABFA JBC PD-QABFA PID, e.g. 62.924 %, 11.496 % and 44.566 % for the first, second and third vibration modes respectively.

Table 7.16: Spectral attenuations achieved at resonance modes with BFA-PID end-point acceleration feedback controls against open-loop control ($m/sec^2/Hz$)

Control	**Mode 1**	**Mode 2**	**Mode 3**
EABFA JBC PD-SBFA PID	38.64 (53.697 %)	-2.219 (-8.535 %)	7.16 (32.694 %)
EABFA JBC PD-LABFA PID	41.67 (57.907 %)	0.589 (2.268 %)	9.3 (42.511 %)
EABFA JBC PD-QABFA PID	**45.28 (62.924 %)**	**2.99 (11.496 %)**	**9.76 (44.566 %)**
EABFA JBC PD-EABFA PID	43.85 (60.937 %)	2.55 (9.804 %)	9.45 (43.150 %)
EABFA JBC PD-FABFA PID	43.66 (60.673 %)	1.85 (7.113 %)	9.39 (42.877 %)

Against EABFA JBC PD, numerical results presented in Table 7.17 show that all ABFA-based PID end-point acceleration feedback controls achieved bigger vibration reduction level than SBFA PID and the biggest reduction rate is achieved by EABFA JBC PD-QABFA PID, i.e. 23.6405 %, 34.5651 % and 27.0433 % for the first, second and third vibration resonance modes respectively.

Table 7.17: Spectral attenuations achieved at resonance modes with BFA-PID end-point acceleration feedback controls against EABFA JBC PD without feedback loop $(m/sec^2/Hz)$

Control	Mode 1	Mode 2	Mode 3
EABFA JBC PD-SBFA PID	1.62 (4.636 %)	6.95 (19.755 %)	1.9 (11.418 %)
EABFA JBC PD-LABFA PID	4.65 (13.309 %)	9.76 (27.743 %)	4.05 (24.339 %)
EABFA JBC PD-QABFA PID	**8.26 (23.641 %)**	**12.16 (34.565 %)**	**4.5 (27.043 %)**
EABFA JBC PD-EABFA PID	6.83 (19.548 %)	11.72 (33.314 %)	4.19 (25.180 %)
EABFA JBC PD-FABFA PID	6.64 (19.004 %)	11.01 (31.325 %)	4.13 (24.82 %)

B. Experimental results

Time-domain numerical results presented in Table 7.18 show that all BFA PID end-point acceleration feedback controls achieved smaller J_α values than open-loop control and without end-point acceleration feedback control with the lowest J_α value (0.1968) achieved by EABFA JBC PD-EABFA PID.

Table 7.18: Experimental results for BFA PID end-point acceleration feedback controls

Control	J_α value
Open loop	1.5843
EABFA-JBC PD	0.3514
EABFA JBC PD-SBFA PID	0.2592
EABFA JBC PD-LABFA PID	0.2329
EABFA JBC PD-QABFA PID	0.2046
EABFA JBC PD-EABFA PID	**0.1968**
EABFA JBC PD-FABFA PID	0.2126

The experimental responses obtained by using parameters of PID control obtained in the simulations above with the flexible manipulator rig are shown in Figure 7.17. It is noted that significant vibration reduction has been achieved with the BFA PID end-point acceleration feedback controls.

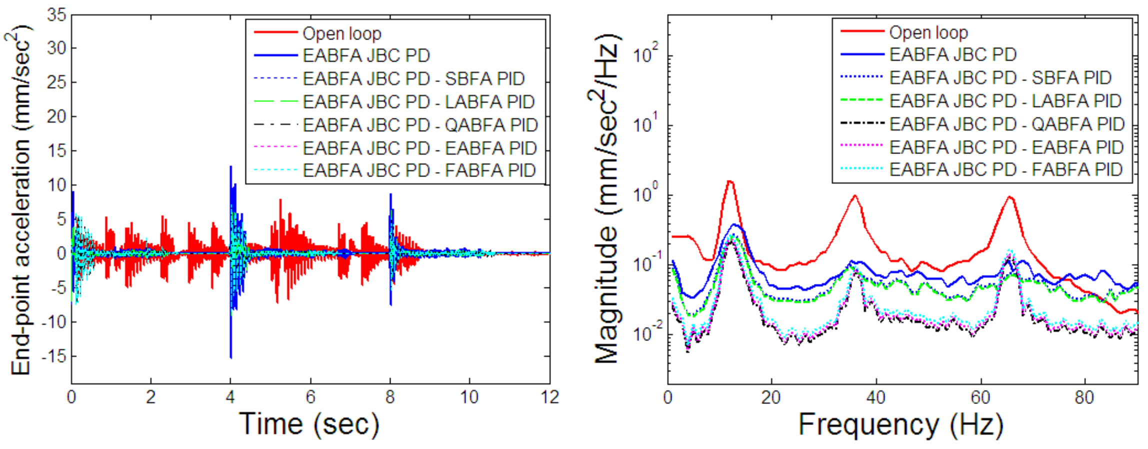

(a) Time-domain end-point acceleration

(b) Frequency-domain end-point acceleration

Figure 7.17: Experimental results for BFA PID end-point acceleration feedback controls

It is noted in the frequency-domain responses that the vibration was reduced at the first three resonance modes with BFA PID end point acceleration feedback controls. Against open-loop control, the numerical results for frequency-domain responses presented in Table 7.19 shows the spectral attenuations achieved at the first three modes with the BFA PID end-point acceleration feedback controls and the biggest vibration reduction for the first and second resonance modes are obtained by EABFA JBC PD-QABFA PID, e.g. 88.564 % and 93.192 %, while for the third resonance mode is achieved by EABFA JBC PD-LABFA PID, e.g. 92.939 %.

Table 7.19: Spectral attenuations achieved at resonance modes with BFA-PID end-point acceleration feedback controls against open-loop control ($m/sec^2/Hz$)

Control	Mode 1	Mode 2	Mode 3
EABFA JBC PD-SBFA PID	1.351 (82.585 %)	0.924 (91.074 %)	0.919 (92.466 %)
EABFA JBC PD-LABFA PID	1.362 (83.24 %)	0.93 (91.695 %)	**0.924 (92.939 %)**
EABFA JBC PD-QABFA PID	**1,449 (88.564 %)**	**0.95 (93.192 %)**	0.858 (86.350 %)
EABFA JBC PD-EABFA PID	1.428 (87.262 %)	0.938 (92.384 %)	0.857 (86.240 %)
EABFA JBC PD-FABFA PID	1.427 (87.209 %)	0.935 (92.148 %)	0.837 (84.158 %)

Against EABFA JBC PD without control of end-point acceleration feedback results depicted in Table 7.20 that the biggest vibration reduction for the first and second vibration resonance mode is obtained by EABFA JBC PD-QABFA PID, e.g. 57.41 %

and 58.147 % respectively while for the third resonance mode is provided by EABFA JBC PD-LABFA PID, e.g. 47.139 %.

Table 7.20: Spectral attenuations achieved at resonance modes with BFA-PID end-point acceleration feedback controls against EABFA JBC PD without feedback loop $(m/sec^2/Hz)$

Control	Mode 1	Mode 2	Mode 3
EABFA JBC PD-SBFA PID	0.154 (35.146 %)	0.052 (45.124 %)	0.057 (43.599 %)
EABFA JBC PD-LABFA PID	0.165 (37.582 %)	0.056 (48.94 %)	**0.063 (47.139 %)**
EABFA JBC PD-QABFA PID	**0.252 (57.41 %)**	**0.067 (58.147 %)**	-0.003 (-2.184 %)
EABFA JBC PD-EABFA PID	0.23 (52.561 %)	0.061 (53.18 %)	-0.004 (-3.012 %)
EABFA JBC PD-FABFA PID	0.225 (51.172 %)	0.06 (51.726 %)	-0.025 (-18.599 %)

7.6. Summary

New chemotactic step size adaptation schemes of BFA proposed and discussed in Chapter 4 have been adopted for tuning of JBC PD, for hub-angle trajectory control and for tuning PD and PID end-point acceleration feedback controls for end-point vibration reduction. In case of JBC PD control tuning, all ABFA-JBC PD controls outperformed SBFA-JBC PD since they could converge faster to optimum value, were able to achieve better optimum value, and result in better time-domain hub-angle response. The addition of maximum undershoot with appropriate weighting value in the cost function has allowed to suppress the presence of unwanted overshoot and undershoot. Since all of ABFA and SBFA used the same general parameters and the initial positions of bacteria were selected randomly across the nutrient media, the superior results achieved with ABFA are thus attributed to the adaptable chemotactic step sizes.

For tuning end-point acceleration feedback control, in general, ABFA were able to converge faster than SBFA. For the best J_α achieved, in both simulation and experimentation ABFA achieved lower J_α value compared to SBFA. It has also been demonstrated that significant vibration reduction at the end-point of the manipulator can be achieved by realising ABFA-based end-point acceleration feedback control into the control structure.

CHAPTER 8
CONCLUSION AND FUTURE WORK

8.1. Summary and conclusion

Investigations into the development of biologically-inspired soft computing approaches based on bacterial foraging algorithm (BFA) for modelling and control of dynamic systems have been presented. The work has focused on the modification of BFA so that it could have faster convergence speed and better accuracy. The convergence speed has been defined as the number of steps needed by algorithm to converge to the optimum value. To validate their performances, the modified BFAs have then tested both on benchmark functions and in dynamic modelling and control of a flexible manipulator system.

The original BFA proposed by Passino (2000, 2002) has been described in detail together with its current applications and current modifications. It can be noted from the preliminary simulation on the parameter selection and its impact that the most influential factors on convergence are initial positions of bacteria and chemotactic step size ($C(i)$) while the most influential factors for accuracy are the number of chemotactic steps per bacterium lifetime between reproduction steps (N_c), the number of reproduction steps (N_{re}), the number of elimination and dispersal events (N_{ed}) and chemotactic step size ($C(i)$). If initial positions of bacteria are chosen randomly in the nutrient media and adequate N_c, N_{re} and N_{ed} values are provided, then the most influential factor for both convergence and accuracy is the chemotactic step size ($C(i)$).

The original BFA uses a constant chemotactic step size ($C(i)$) regardless of the nutrient value. In a minimisation case, if the nutrient value is big it means that bacteria are in the places which are far away from the global minimum. Bigger $C(i)$ makes BFA converge to the optimum value faster. It can be noted from the literature that the chemotaxis mechanism of BFA results in oscillation around the global optimum point or global minimum point in the minimisation case. In order to make bacteria head to the global minimum point without oscillation, very small chemotactic step size $C(i)$) is needed. As a consequence, very small $C(i)$ value requires BFA needing larger number of steps to converge to the optimum value. Thus the strategy adopted in this work for achieving faster convergence without oscillation around the global minimum has been to use large $C(i)$ when the nutrient value is big and very small $C(i)$ when the nutrient value is very small near the global minimum point. Four novel approaches which allow $C(i)$ change regarding the nutrient value have been presented and discussed. The BFA with adaptation schemes based on three functions, namely linear, quadratic, exponential and fuzzy logic referred to as LABFA, QABFA, EABFA and FABFA respectively have been investigated. In order to evaluate their performances, these four proposed algorithms have been used to find optimum point of seven commonly used benchmark test functions and the results compared to that of SBFA. In the comparison process, all ABFAs and SBFA used the same general parameters, the only difference has been that SBFA used constant $C(i)$ while ABFAs have used adaptable chemotactic step size. It has been demonstrated that the BFAs with the adaptable chemotactic step size, referred to as ABFA, have performed faster in convergence speed to global optimum and have been able to achieve better nutrient value as compared to SBFA. Thus, all the four proposed algorithms can potentially be used in the applications to replace the constant chemotactic step size in SBFA.

A thorough investigation of modelling of a single-link flexible manipulator system with ABFAs has been carried out. ABFAs have been used for finding optimal parameters of ARX models characterising the manipulator from torque input to hub-angle, hub-velocity and end-point acceleration outputs. While the developed models have represented the dynamic behaviour of the system well, it has further been demonstrated that the ABFAs have outperformed SBFA in terms of convergence speed and accuracy.

Investigations have been carried out for using the proposed ABFAs to optimise NN-based models characterising the dynamic behaviour of the flexible manipulator. Three SISO models have been constructed to represent the dynamic behaviour of the single-link flexible manipulator: from torque input to hub-angle, hub velocity and end-point acceleration. While the ABFA-NN based models have represented the dynamic behaviour of the system well, a comparative assessment of the results has revealed the ABFAs have outperformed the SBFA in terms of convergence speed and optimal cost function value.

Further investigations of using ABFAs in a modelling context has involved for optimising FL-based models to represent the dynamic behaviour of the single-link flexible manipulator system. ABFAs have been used to develop three FL-based SISO models to represent the system behaviour from torque input to hub-angle, hub-velocity and end-point acceleration outputs. It has been demonstrated that the system behaviour has been characterised well with using Mamdani type fuzzy rules and Gaussian type membership functions. Furthermore, a comparative assessment of the results has revealed superiority of the ABFAs over SBFA in terms of speed of convergence and optimal cost function value reached.

In a control context, the proposed ABFAs have been used for control application, ABFAs proposed and discussed in Chapter 4 have been initially adopted to tune parameters of JBC PD control for hub-angle trajectory tracking of the single-link flexible manipulator system. A cost function including MSE and weighted response overshoot and undershoot has been developed and investigations have revealed that with such a cost function the response overshoot/undershoot is significantly reduced. The control structure has been extended further to incorporate end-point acceleration feedback for end-point vibration reduction. Two type of controllers, namely PD and PID have been designed using ABFAs and placed in the end-point acceleration feedback loop. Investigations have revealed that the system has performed well at set-point tracking as well as end-point vibration reduction with the developed control approaches. Moreover, comparative assessment of the results has revealed superiority of the ABFAs over SBFA in terms of speed of convergence, optimal cost function value reached and system response. In the comparative assessment carried out throughout this work the same general BFA parameters have been used for ABFAs and SBFA and all bacteria have initially been placed randomly across the nutrient media. This implies that the superior performance achieved with the ABFAs over SBFA can be attributed to the adaptable chemotactic step size in the ABFAs.

8.2. Future work

In line with present work, the potential works to be explored in the future including the following:

8.2.1. Applications of BFAs for vibration control of a single-link flexible manipulator systems and other flexible structures

It can be noted from the literature that BFA has not widely been used for vibration control of single-link flexible manipulator systems and other flexible structures such as flexible beam and flexible plate. The potential applications that BFA can be used include optimising vibration controller types such as iterative learning control (ILC), FL control, NN control and command shaping.

8.2.2. Applications of BFAs for modelling and control of a multi-link flexible manipulator systems

Multi-link flexible manipulator system is a flexible manipulator which contains more than one joint. In such case, there are more than one hub-angular movement to be controlled and also mechanism of vibration reduction will be much more very challenging compared to a single-link one. In order to obtain dependable modelling and reliable controller, BFAs could be used for both modelling and controlling task. Literature suggested that only a few works have been reported in this application so that there are still plenty open spaces to fill.

8.2.3. Applications of BFAs for robotic modelling and control

It can be noticed from the literature that only a few applications of BFA in the area robotics have been reported. Thus BFAs may be adopted for modelling and control of robotic systems.

8.2.4. Applications of BFAs in modelling and control paradigms for paraplegic mobility

The literatures show that there are only few works on the application of BFAs in the areas of biomedical engineering especially with paraplegia have been reported. Thus there is potential for BFAs to develop optimal muscle models and associated control for paraplegic mobility purposes.

8.2.5. Hybridisation of BFA with other biologically-inspired soft computing techniques

In the current work, investigations were only focused on the modification of BFA including development of hybrid BFA-FL and BFA-NN to get better accuracy and faster convergence than original BFA. Hybridisation and comparison with other soft computing techniques such as honey bee, ant colony optimisation, clonal expansion etc would be very interesting. The comparison can be made based on several aspects such as their accuracy, convergence speed and possibility for real time application.

8.2.6. Implementation of BFA in real-time

Most of the works reported in the literature have involved used of BFA in simulations and only a few reports indicated the application of BFA in the real time. The main issue is due to the computational time of BFA that does not meet real-time requirements with currently available processors. The potential solutions to solve this is by modifying original BFA algorithms, applying certain computation techniques such as parallel computation, using high performance processing devices and etc. Besides its huge challenge, the application of BFA in the real time application in various areas such as robotics, biomedical engineering, is very promising.

8.2.7. Multi-objective BFA

The current work in this thesis was devoted to single-objective optimisation. For highly complex optimisation tasks, which involve two or more conflicting objectives to be met, multi-objective optimisation technique is needed. It can be noted from the literature that multi-objective evolutionary algorithms were the dominant techniques to be used and only a few works on multi-objective BFA have been reported. Despite its huge challenge, multi-objective BFA offers many potential advantages.

8.2.8. Ensemble computation using BFA

In some applications, such as pattern classification, feature selection, several algorithms need to work together to solve the problem. Collection of algorithms which work together for solving one common task is called as ensemble computing. It looks like many people working together to finish one common task. Reports in the literature suggest that evolutionary algorithm based ensemble computing have been proposed by researchers. However, ensemble computation based on BFA has not been reported yet. The BFA can be used such as for optimising parameters of classifiers used in the ensemble and etc. Thus, investigation on possible BFA based ensemble computing will be interesting to pursue.

8.2.9. Implementation of BFA in grid computing

Grid computing is computation technique by using multi-computer resources to achieve common goal. It can be noticed from the literature that the use evolutionary algorithms have been reported successfully in grid computing. However, the application of BFA in grid computing has not been reported yet. Inspired by the success of evolutionary algorithms in grid computing, possible application of BFA in grid computing could be investigated.

REFERENCES

Acharya, D. P., Panda, G., Mishra, S., and Lakshmi, Y. V. S. (2007). Bacteria foraging based independent component analysis. *Proceedings of International Conference on Computational Intelligence and Multimedia Applications 2007*, pp. 527 – 531.

Akcam, M. O. and Takada, K. (2002). Fuzzy modelling for selecting headgear types. *European Journal of Orthodontics*, **24**, pp. 99 – 106.

Alam, M. S. and Tokhi, M.O. (2007). Dynamic modelling of a single-link flexible manipulator system: a particle swarm optimisation approach. *Journal of Low Frequency Noise, Vibration and Active Control*, **26** (1), pp. 57 – 72.

Alam, M. S. and Tokhi, M.O. (2008). Hybrid fuzzy logic control with genetic optimisation for a single-link flexible manipulator. *Engineering Application of Artificial Intelligence*, **21**, pp. 858 – 873.

Alavandar, S., Jain, T. and Nigam, M. J. (2010). Hybrid bacterial foraging and particle swarm optimisation for fuzzy precompensated control of flexible manipulator. *International Journal of Automation and Control*, **4**(2), pp. 234 – 251.

Aldebrez, F. M., Mat Darus, I. Z. and Tokhi, M. O. (2004). Dynamic modelling of a twin rotor system in hovering position. *Proceedings of The First International Symposium on Control, Communications and Signal Processing (ISCCSP2004),* Hammamet, Tunisia, 21-24 March, 2004, pp. 823 – 826.

Ali, A. and Majhi, S. (2006). Design of optimum PID controller by bacterial foraging strategy. *Proceedings of IEEE International Conference on Industrial Technology ICIT 2006*, 15 – 17 December, 2006, Mumbai, India, pp. 601 – 605.

Ali, E. S. and Abd-Elazim, S. M. (2010). Optimal PID tuning for load frequency control using bacteria foraging optimization algorithm. Proceedings of the 14th International Middle East Power Systems Conference (MEPCON'10), Cairo University, Egypt, December 19 – 21, 2010, pp. 410 – 415.

Auxillia, D. J. and Sundaravadivelu, S. (2011). Fast output sampling control technique via reduced order model for blood perfusion uncertainity in hyperthermia. *European Journal of Scientific Research* ISSN 1450-216X Vol.51 No.1 (2011), pp.97 – 108.

Azad, A. K. M. (1994). *Analysis and design of control mechanisms for flexible manipulator systems*. PhD thesis, Department of Automatic Control and Systems Engineering, The University of Sheffield, UK.

Bakwad, K. M., Pattnaik, S. S., Sohi, B. S., Devi, S., Panigrahi, B. K. and Gollapudi, S. V. R. S. (2009a). Bacterial foraging optimization technique cascaded with adaptive filter to enhance peak signal to noise ratio from single image. *IETE Journal of Research*, **55**(4), July – August, 2009, pp. 173 – 179.

Bakwad, K. M., Pattnaik, S. S., Sohi, B. S., Devi, S. and Lohakare, M. R. (2009b). Parallel bacterial foraging optimization for video compression. *International Journal of Recent Trends in Engineering*, **1**(1), May 2009, pp. 118 – 122.

Bakwad, K. M., Pattnaik, S. S., Sohi, B. S., Devi, S., Panigrahi, B. K. and Gollapudi, S. V. R. S. (2010). Multimodal function optimization using synchronous bacterial foraging optimization technique. *IETE Journal of Research*, **56**(2), March – April, 2010, pp. 80 – 87.

Barpi, F. (2004). Fuzzy modelling of powder snow avalanches. *Cold Regions Science and Technology*, **40**, pp. 213 – 227.

Ben Omrane, I. and Chatti, A. (2010). Training a neural network using hierarchical genetic algorithm for modelling and controlling a nonlinear system of water level regulation. *Nonlinear Dynamics and Systems Theory*, **10**(1), pp. 65–76.

Billings, S.A. and Voon, W.S.F. (1986). Correlation based validity tests for nonlinear models. *International Journal of Control*, **44** (1), pp. 235 – 244.

Biswas, A., Dasgupta, S., Das, S., and Abraham, A. (2007a). A synergy of differential evolution and bacterial foraging optimization for global optimization. *Neural Network*, **6**(7), pp. 607 – 626.

Biswas, A., Dasgupta, S., Das, S., and Abraham, A. (2007b). Synergy of PSO and bacterial foraging optimization – a comparative study on numerical benchmarks. *E.*

Corchado et al. (Eds.): Innovations in Hybrid Intelligent Systems, **ASC 44**, pp. 255 – 263.

Brabazon, A. (2010). Biologically – inspired algorithms for financial modelling. CFA Seminar, 26 February 2010, UCD Natural Computing Research & Applications Group (NCRA), http://ncra.ucd.ie.

Book, W.J. (1984). Recursive Lagrangian dynamics of flexible manipulator arms. *International Journal on Robotics Research*, **3**(3), pp. 87–101.

Book, W. J. and Majette, M. (1983). Controller design for flexible distributed parameter mechanical arms via combined state-space and frequency domain techniques. *Transaction of ASME Journal of Dynamic Systems, Measurement and Control*, **105**(4), 245 – 254 (1983).

Calafiore, G. C. (2008). On 3-D Point Set Matching With MAE and SAE Cost Criteria. *IEEE Transactions on Systems, Man, and Cybernetics – Part A: Systems and Humans*, **38**(2), March 2008, pp. 443 – 450.

Cannon, R.H. and Schmitz, E. (1984). Initial experiment on the endpoint control of a flexible one-link robot. *International Journal of Robotics Research*, **3**(3), pp. 62–75.

Chatterjee, A. and Matsuno, F. (2006). Bacterial foraging techniques for solving EKF-based slam problems. *Proceedings of International Control Conference (Control 2006)*, Glasgow, UK, August 30 – September 01, 2006, pp. 1 – 6.

Chen, M. and Linkens, D. A. (1998). A hybrid neuro-fuzzy controller. *Fuzzy Sets and Systems*, **99**, pp. 27 – 36.

Chen, H., Zhu, Y. and Hu, K. (2009). Cooperative bacterial foraging optimization. *Discrete Dynamics in Nature and Society*, Hindawi Publishing Corporation, 2009, pp. 1 – 17.

Chu, Y. Mi, H., Liao, H., Ji, Z. and Wu, Q. H. (2008). A fast bacterial swarming algorithm for high-dimensional function optimization. *Proceedings of 2008 IEEE Congress on Evolutionary Computation (CEC 2008)*, pp. 3134 – 3139.

Coelho, L. d-S. and Silveira, C. d-C. (2006). Improved bacterial foraging strategy for controller optimization applied to robotic manipulator system. *Procedings of the 2006 IEEE International Symposioum on Intelligent Control*, Munich, Germany, October 4 – 6, 2006, pp. 1276 – 1281.

Das, T. K., Venayagamoorthy, G. K., and Aliyu, U. O. (2008). Bio-Inspired Algorithms for the Design of Multiple Optimal Power System Stabilizers: SPPSO and BFA. *IEEE Transactions on Industry Applications*, **44** (5), pp. 1445 – 1457.

Das, S., Biswas, A., Dasgupta, S., and Abraham, A. (2009). Bacterial foraging optimization algorithm: theoretical foundations, analysis, and applications. *Studies in Computational Intelligence*, **203**, pp. 23 – 55.

Dasgupta, S., Das, S., Abraham, A. and Biswas, A. (2009a). Adaptive computational chemotaxis in bacterial foraging optimization: an analysis. *IEEE Transaction On Evolutionary Computation*, **13**(4), August 2009, pp. 919 – 941.

Dasgupta, S., Biswas, A., Das, S., Panigrahi, B. K. and Abraham, A. (2009b). A micro-bacterial foraging algorithm for high-dimensional optimization. *Proceedings of The Eleventh Conference on Congress on Evolutionary Computation CEC'09*, IEEE Press Piscataway, NJ, USA, 2009, pp. 1 – 8.

Dasgupta, S., Das, S., Biswas, A. and Abraham, A. (2010). Automatic circle detection on digital images with an adaptive bacterial foraging algorithm. *Soft Computing*, **14**, pp. 1151 – 1164.

Dasgupta, S., Biswas, A., Abraham, A., and Das, S. (2008). Adaptive computational chemotaxis in bacterial foraging algorithm. *Proceedings of 2008 International Conference on Complex, Intelligent and Software Intensive Systems CISIS 2008*, March 04 – 07, 2008, pp. 64 – 71.

Datta, T., Misra, I.S., Mangaraj, B. B. and Imtiaj, S. (2008). Improved adaptive bacteria foraging algorithm in optimization of antenna array for faster convergence. *Progress In Electromagnetics Research C*, **l**, pp. 143–157.

DeJong, K. A. (1980). Adaptive System Design: A Genetic Approach. *IEEE Transaction on Systems, Man and Cybernetics*, **SMC-10**(9), September 1980, pp. 566 – 574.

Dote, Y. and Ovaska, S. J. (2001). Industrial applications of soft computing: a review. *Proceedings of The IEEE*, September, 2001, 89(9), pp. 1243 – 1265.

Dou, W., Wu, Q., Chen, Y., Ruan, S. and Constans, J-M. (2005). Fuzzy modelling of different timorous cerebral tissues on MRI images based on fusion of feature information. *Proceedings of the 2005 IEEE Engineering in Medicine and Biology 27th Annual Conference Shanghai*, China, September 1-4, 2005, pp. 3104 – 3107.

Dougherty, E. R. (1994). Optimal mean-absolute-error filtering of Gray-scale signals by the morphological hit-or-miss transform. *Journal of Mathematical Imaging and Vision*, **4**, pp. 255-271.

Dunne, R. A. (2007). Statistical approach to neural networks for pattern recognition. Wiley-Interscience, A John Wiley & Sons, Inc., Publication, Hoboken, New Jersey.

Eldred, M. S., Giunta, A. A., van Bloemen Waanders, B.G., Wojtkiewicz, S. F., Hart, W. E. and Alleva, M. P. (2001). *DAKOTA, A Multilevel Parallel Object-Oriented Framework for Design Optimization, Parameter Estimation, Uncertainty Quantification, and Sensitivity Analysis.* Version 3.0 Reference Manual, Sandia Technical Report SAND2001.

Farhat, I. A. and El-Hawary, M. E. (2010). Dynamic adaptive bacterial foraging algorithm for optimum economic dispatch with valve-point effects and wind power. *IET Generation, Transmission and Distribution*, **4**(9), pp. 989 – 999.

Garcı´a-Ferna´ndez, I., Martı´n-Guerrero, J. D., Pla-Castellsa, M., Soria-Olivas, E., Martı´nez-Dura´, R. J., and Mun˜oz-Marı´, J. (2004). Crane collision modelling using a neural network approach. *Expert Systems with Applications*, **27** (2004), pp. 341–348.

Gharooni, S., Heller, B. and Tokhi, M.O. (2001). A new hybrid spring orthosis for controlling hip and flexion in the swing phase. *IEEE Transaction on Neural Systems Rehabilitation Engineering*, **9**(1), pp. 106 – 107.

Ghoshal, S. P., Chatterjee, A., and Mukherjee, V. (2009). Bio-inspired fuzzy logic based tuning of power system stabilizer. *Expert Systems with Applications*, **36**, pp. 9281–9292.

Goldberg, D. E. (2002). A meditation on the application of soft computing and its future. *Soft Computing and Industry: Recent Applications*, Roy, R., Koopen, M., Ovaska, S., Furuhashi, T., and Hoffman, F., Eds. London, U.K.: Springer – Verlag, 2002, pp. XV – XVIII.

Gollapudi, S. V. R. S., Pattnaik, S. S., Bajpai, O. P., Devi, S., Sagar, Ch. V., Pradyumna, P. K. and Bakwad, K. M. (2008). Bacterial foraging optimization technique to calculate resonant frequency of rectangular microstrip antenna. *International Journal of RF and Microwave Computer-Aided Engineering*, **18**(4), July 2008, pp. 383 – 388.

Gollapudi, S. V. R. S., Pattnaik, S. S., Bajpai, O. P., Devi, S., Bakwad, K. M. and Pradyumna, P. K. (2009). Intelligent bacterial foraging optimization technique to calculate resonant frequency of RMA. *International Journal of Microwave and Optical Technology*, March 2009, **4**(2), pp. 67 – 75.

Gollapudi, S. V. R. S., Pattnaik, S. S., Bajpai, O. P., Devi, S., and Bakwad, K. M. (2011). Velocity modulated bacterial foraging optimization technique (VMBFO). *Applied Soft Computing*, **11**, pp. 154 – 165.

Golmohammadi, D., Creese, R. C., Valian, H., and Kolassa, J. (2009). Supplier selection based on a neural network model using genetic algorithm. *IEEE Transactions on Neural Networks*, **20**(9), September 2009, pp. 1504 – 1519.

Grossberg, S. (1982). *Studies of the mind and brain*. Reidel Press, Drodrecht, Holland.

Guney, K. and Basbug, S. (2008). Interference suppression of linear antenna arrays by amplitude-only control using a bacterial foraging algorithm. *Progress In Electromagnetics Research*, PIER **79**, pp. 475–497.

Guzman, M.A., Delgado, A. and De Carvalho, J. (2010). A novel multiobjective optimisation algorithm based on bacterial chemotaxis. *Engineering Applications of Artificial Intelligence*, **23**, pp. 292 – 301.

Hagan, M. T., Demuth, H. B. and Beale, M. (1996). *Neural network design*. PWS Publishing Company, USA.

Haghizadeh, A., Shui, L. T. and Goudarzi, E. (2010). Estimation of Yield Sediment Using Artificial Neural Network at Basin Scale. *Australian Journal of Basic and Applied Sciences*, **4**(7): pp. 1668 – 1675, 2010.

Han, M. and Yuan, N. (1998). Analysis of UWB echoes using bispectrum model. *International Journal of Infrared and Millimeter Waves*, **19**(8), pp. 1141 – 1149.

Hanmandlu, M., Nath, A. V., Mishra, A. C. and Madasu, V. K. (2007). Fuzzy model based recognition of handwritten hindi numerals using bacterial foraging. *Proceedings of the sixth IEEE/ACIS International Conference on Computer and Information Science (ICIS 2007)*, 11-13 July 2007, Melbourne, Australia, pp. 309 – 314.

Hastings, G. G. and Book, W. J. (1987). A linear dynamic model for flexible robotics manipulator. *IEEE Control Systems Magazine*, **7**, pp. 61 – 64.

Hebb, D.O. (1949). *The organisation of behaviour*. Wiley and Sons, New York.

Hopfield, J.J. (1982). Neural networks and physical systems with emergent computational abilities, *Proceedings of the National Academy of Sciences*, **79**, pp.2554 – 2558.

Hota, P. K., Barisal, A. K. and Chakrabarti, R. (2010). Economic emission load dispatch through fuzzy based bacterial foraging algorithm. *Electrical Power and Energy Systems*, **32**, pp. 794 – 803.

Hung, N. Q., Babel, M. S., Weesakul, S. and N. K. Tripathi, N. K. (2009). An artificial neural network model for rainfall forecasting in Bangkok, Thailand. *Hydrology and Earth System Sciences*, **13**, pp. 1413–1425, 2009.

Ibrahim, B. S. K. S. M. K. (2011). *Modelling and control of paraplegic's knee joint (FES-swinging)*. PhD thesis, Department of Automatic Control and Systems Engineering, The University of Sheffield, UK.

Jain, A.K. and Mohiuddin, K. M. (1996). Artificial neural networks: a tutorial. *Computer: The IEEE Computer Society Magazine*, **29**(3), pp. 31–44.

Jain, T. and Nigam, M. J. (2008a). Optimization of PD-PI controller using swarm intelligence. *International Journal of Computational Cognition*, **6**(4), pp. 55 – 59.

Jain, T. and Nigam, M. J. (2008b). Optimization of PD-PI controller using swarm intelligence. *Journal of Theoretical and applied Information Technology*, **4**(11), pp. 1013 - 1018.

Jain, T., Alavandar, S., Radhamohan, S. V. and Nigam, M. J. (2009). Genetically-bacterial swarm optimization fuzzy pre-compensated PD control of two-link rigid-flexible manipulator. *International Journal of Intelligent Computing and Cybernetics*, **3**(3), pp. 463 – 494.

Jamshidi, M., Akbarzadeh, T. M. and Vadie. N. (1998). Experimental test beds for intelligent robot controllers based on soft-computing approaches with application to waste management. *Technical Report WERC 1207*, *New Mexico Waste-Management Education and Research Consortium*, USA, 1998.

Jang, J-S. R., Sun, C-T. and Mizutani, E. (1997). *Neuro-fuzzy and soft computing a computational approach to learning and machine intelligence*. Prentice Hall Upper saddle NJ, 07458.

Jnifene, A. and Andrews, W. (2005). Experimental study on active vibration control of a single-link flexible manipulator using tools of fuzzy logic and neural networks. *IEEE Transactions on Instrumentation and Measurement*, **54**(3), June 2005, pp. 1200 – 1208.

Karlik, B. and Olgac, A. V. (2010). Performance analysis of various activation functions in generalized MLP architectures of neural networks. International Journal of Artificial Intelligence And Expert Systems (IJAE), 1(4), pp. 111 – 122.

Kim, D. H. and Cho, J. H. (2005). Adaptive tuning of PID controller for multivariable system using bacterial foraging based optimization. *P. S. Sczepaniak et al. (Eds.): AWIC 2005, LNAI 3528*, Springer-Verlag Berlin Heidelberg, pp. 231 – 235.

Kim, D. H. and Cho, J. H. (2006). A biologically inspired intelligent PID controller tuning for AVR Systems. *International Journal of Control, Automation, and Systems*, **4**(5), October 2006, pp. 624 – 636.

Kim, D. H., Abraham, A. and Cho, J. H. (2007). A hybrid genetic algorithm and bacterial foraging approach for global optimization. *Information Sciences*, **177**, pp. 3918 – 3937.

Korani, W. (2008). Bacterial foraging oriented by particle swarm optimization strategy for PID tuning. Proceedings of the 2008 Conference Companion on Genetic and Evolutionary Computation GECCo'08, July 12 – 16, 2008, Atlanta, Georgia, USA, pp. 1823 – 1826.

Kreinovich,, V., Quintana, C. and Reznik, L. (1992). Gaussian membership functions are most adequate in representing uncertainty in measurements. Proc. NAFIPS'92: North American Fuzzy Information Processing Society Conf., *Puerto Vallarta, Mexico* **Vol. II**, NASA Johnson Space Center, Houston, TX (1992), pp. 618–624.

Kumar, M. S. and Renuga, P. (2010). Bacterial foraging algorithm based enhancement of voltage profile and minimization of losses using thyristor controlled series capacitor (TCSC). International Journal of Computer Application (0975 - 8887), 7(2), September, 2010, pp. 21 – 27.

Kwak, M.K., Sciulli, D., 1996. Fuzzy-logic based vibration suppression control experiments on active structures. *Journal of Sound and Vibration*, **191**(1), 15–28.

Leondes, C. T. (1998). Neural network systems techniques and applications. Academic Press, San Diego California.

Li, Y. and Kareem, A. (1993). Parametric modelling of stochastic wave effects on offshore platforms. *Applied Ocean Research,* **15,** pp. 63 – 83.

Lin, W. and Liu, P. X. (2006). Hammerstein model identification based on bacterial foraging. *Electronics Letters*, 9th November, 2006, *42*(23).

Lin, J.-H. and Coyle, E. J. (1990). Minimum Mean Absolute Error Estimation over the Class of Generalized Stack Filters. *IEEE Transactions on Acoustics, Speech and Signal Processing*, **38**(4), pp. 663 – 678.

Liu, Y. and Passino, K. M. (2002). Biomimicry of social foraging bacteria for distributed optimization: models, principles and emergent behaviours. *Journal of Optimization Theory and Applications*, **115**(3), December 2002, pp. 603 – 628.

Ljung, L. (1999). *System identification: theory for the user, 2nd edition*. Englewood Cliffs, NJ: Prentice hall.

Luo, F.L. and Unbehauen, R. (1997). *Applied neural networks for signal processing*. Cambridge University Press, Cambridge, New York, 1997.

Mahfouf, M., Kandiah, S. and Linkens, D. A. (2002). Fuzzy model-based predictive control using an ARX structure with feedforward. *Fuzzy Sets and Systems,* **125**, pp. 39–59.

Mahmoud, K. R. (2010). Design optimization of a bow-tie antenna for 2.45 GHz RFID readers using a hybrid BSO-NM algorithm. Progress *in Electromagnetic Research*, **PIER 100**, pp. 105 – 117.

Majhi, R., Panda, G., Majhi, B. and Sahoo, G. (2009). Efficient prediction of stock market indices using adaptive bacterial foraging optimization (ABFO) and BFO based techniques. *Expert Systems with Applications*, **36**, pp. 10097 – 10104.

Majhi, B. and Panda, G. (2010). Development of efficient identification scheme for nonlinear dynamic systems using swarm intelligence techniques. *Expert Systems with Applications*, **37**, 1 January, 2010, pp. 556 – 566.

Majhi, B. and Panda, G. (2006). Recovery of digital information using bacterial foraging optimization based nonlinear channel equalizers. Proceedings of The 1st International Conference on Digital Information Management, 6 December, 2006, Bangalore, India, pp. 367 – 372.

Mamdani, E.H. and Assilian, S. (1974). Application of fuzzy algorithms for control of simple dynamic plant. *Proceedings of IEE D*, **121**, pp.1585-1588.

Mangaraj, B. B., Misra, I. S. and Barisal, A. K. (2008). Optimizing included angle of symmetric v-dipoles for higher directivity using bacteria foraging optimization algorithm. *Progress In Electromagnetics Research B*, **3**, pp. 295 – 314.

Mangaraj, B. B., Misra, I. S. and Sanyal, S. K. (2010). Application of bacteria foraging algorithm for the design optimization of multi-objective Yagi-Uda array. *International Journal of RF and Microwave Computer-aided Engineering,* **21**(1), DOI: 10.1002/mmce.20483, pp. 25 – 35.

Martins, J.M., Mohamed, Z., Tokhi, M.O., Sa da Costa, J. and Botto, M.A. (2003). Approaches for dynamic modelling of flexible manipulator systems. *IEE Proceedings of Control Theory Application*, **150**(4), July 2003, pp. 401 – 411.

Mat Darus, I.Z. and Tokhi, M.O. (2004). Parametric modelling of a flexible 2D structure. *Journal of Low Frequency Noise, Vibration and Active Control*, **23**(2), pp. 115-131.

Mat Darus, I.Z. and Tokhi, M.O. (2005). Soft computing-based active vibration control of a flexible structure. *Engineering Applications of Artificial Intelligence*, **18**, pp. 93 – 114.

Md Zain, B. A. (2011). Modelling and control of flexible manipulators in 3D motion. PhD thesis, Department of Automatic Control and Systems Engineering, The University of Sheffield, UK.

Md Zain, M. Z. Tokhi, M. O. and Alam, M. S. (2005). Robustness of hybrid learning acceleration feedback control scheme in flexible manipulators. *World Academy of Science, Engineering and Technology*, 6, pp. 143 – 146.

Md Zain, M. Z. Tokhi, M. O. and Mohamed, Z. (2006). Hybrid learning control schemes with input shaping of a flexible manipulator system. *Mechatronics*, **16**, pp. 209 – 219.

Md Zain, B. A. and Tokhi, M. O. (2009). Dynamic simulation and control of a flexible manipulator using genetic algorithms. *Proceeding of the third International Conference on Modeling, Simulation and Applied Optimization*, Sharjah, UAE, January 20 – 22, 2009, pp. ICMSA0/08-1-6.

Md Zain, B.A., Tokhi, M.O. and Abd. Latiff, I. (2009a). Dynamic modelling of a single-link flexible manipulator using particle swarm optimisation. *The Second International Conference on Control, Instrumentation and Mechatronic Engineering (CIM09),* Malacca, Malaysia, June 2 -3, 2009.

Md Zain, B.A., Tokhi, M.O., and Md Salleh, S. (2009b). Dynamic modelling of a single-link flexible manipulator using parametric techniques with genetic algorithms. *Proceedings of 2009 Third UKSim European Symposium on Computer Modelling and Simulation*, Athens, Greece, November 25 – 27, 2009, pp. 373 – 378.

Md Zain, B.A., Tokhi, M.O., and Md Salleh, S. (2009c). PID control with genetic tuning of a single-link flexible manipulator. Proceedings of The Sixteenth International Congress on Sound and Vibration, Krakow, Poland, 5 – 9 July, 2009, pp. 1 – 8.

Menq, C.H. and Chen, J.-S. (1988). Dynamic modelling and payload adaptive control of a flexible manipulator. *Proceedings of IEEE International Conference on Robotics and Automation*, Philadelphia, 24-29 April 1988, pp. 488–493.

Mishra, S. and Bhende, C. N. (2007). Bacterial foraging technique-based optimized active power filter for load compensation. *IEEE Transactions on Power Delivery*, **22**(1), January, 2007, pp. 457 – 465.

Mishra, S. (2005). A hybrid least square-fuzzy bacterial foraging strategy for harmonic estimation. *IEEE Transactions on Evolutionary Computation*, **9**(1), pp. 61 – 73 (2005).

Mohamed, Z. (2003). *Dynamic modelling and control of a flexible manipulator*. PhD thesis, Department of Automatic Control and Systems Engineering, The University of Sheffield, 2003.

Mohamed, Z., Martins, J. M., Tokhi, M. O., da Costa, S. and Botto, M. A. (2005). Vibration control of a very flexible manipulator system. *Control Engineering Practice*, **13**, pp. 267 – 277.

Moudgal, V.G., Passino, K.M. and Yurkovich, S. (1994). Rule-based control for a flexible-link robot. *IEEE Transactions on Control Systems Technology*, **2**(4), December 1994, pp. 392 – 405.

Nazzal, J. M., El-Emary, I. M. and Najim, S. A. (2008). Multilayer perceptron neural network (MLPs) for analyzing the properties of Jordan oil shale. *World Applied Sciences Journal*, **5**(5), pp. 546-552, 2008.

Negnevitsky M. (2005). *Artificial Intelligence: A Guide to Intelligent Systems.* Pearson Education Limited, Edinburgh Gate, Harlow Essex, England, (2nd Edition 2005).

Niu, B., Zhu, Y., and Zeng, X. (2006). Optimum design of PID controllers using only a germ of intelligence. *Proceedings of the Sixth World Congress on Intelligent Control and Automation*, Dalian, China, June 21-23, pp. 3584 – 3588.

Noriega, G., Restrepo, J., Guzman, V., Gimenez, M. and Aller, J. (2010). On line parameter estimation of electric systems using the bacterial foraging algorithm. *Universidad Ciencia y Technologia UCT*, **14**(54), pp. 45 – 54.

Ogata, K. (2002). Modern control engineering fourth edition. Prentice-Hall Inc. Upper Saddle River, New Jersey.

Ovaska, S. J., VanLandingham, H. F. and Kamiya, A. (2002). Fusion of soft computing and hard computing in industrial applications: an overview. *IEEE Transactions on Systems, Man, and Cybernetics – Part C: Applications and Reviews*, May, 2002, **32**(2), pp. 72 – 79.

Ovaska, S. J., Kamiya, A. and Chen, Y-Q. (2006). Fusion of soft computing and hard computing: computational structures and characteristics features. *IEEE Transactions on Systems, Man, and Cybernetics – Part C: Applications and Reviews*, May 2006, **36**(3), pp. 439 – 448.

Padma, S. and Subramanian, S. (2010). Parameter estimation of single phase core type transformer using bacterial foraging algorithm. *Engineering*, **2010**(2), pp. 917 – 925.

Pandi, V. R., Biswas, A., Dasgupta, S. and Panigrahi, B. K. (2010). A hybrid bacterial foraging and differential evolution algorithm for congestion management. *European Transactions on Electrical Power*, **20** (7), DOI: 10.1002/etep.368, pp. 862–871.

Panigrahi, B. K. and Pandi, V. R. (2008). Bacterial foraging optimisation: Nelder-Mead hybrid algorithm for economic load dispatch. *IET Generation, Transmission and Distribution*, **2**(4), pp. 556 – 565.

Panigrahi, B. K. and Pandi, V. R. (2009). Congestion management using adaptive bacterial foraging algorithm. *Energy Conversion and Management*, **50**, pp. 1202 – 1209.

Parlos, A.G., Chong, K.T. and Atiya, A. F. (1994). Application of the recurrent multilayer perceptron in modeling complex process dynamics. *IEEE Transactions on Neural Networks*, **5**(2), March 1994, pp. 255 – 266.

Passino, K. M. (2000). Distributed optimization and control using only a germ of intelligence. *Proceedings of the 2000 IEEE International Symposioum on Intelligent Control*, 17 – 19 July, 2000, Rio Patras, Grrece, pp. p-5 – p-13.

Passino, K. M. (2002). Biomimicry of bacterial foraging for distributed optimization and control. *IEEE Control Systems Magazine*, June 2002, pp. 52 – 67.

Passino, K. M. (2005). *Biomimicry for Optimization, Control, and Automation*. Springer-Verlag London Limited 2005

Piedboeuf, J.-C., Farooq, M., Bayoumi, M., Labinaz, G. and Argoun, M. B. (1993). Modelling and control of flexible manipulators-revisited. *Proceedings of the 36th Midwest Symposioum on Circuits and Systems*, Detroit, Michigan, USA, 1993, pp. 1480 – 1483.

Poerwanto, H. (1998). *Dynamic simulation and control of flexible manipulator systems*. PhD thesis, Department of Automatic Control and Systems Engineering, The University of Sheffield, UK.

Ramos, V., Fernandes, C., Rosa, A. C. and Abraham, A. (2007). Computational chemotaxis in ants and bacteria over dynamic environments. *Proceedings of IEEE Congress on Evolutionary Computation CEC'07*, 25 – 28 September 2007, pp. 1109 – 1117.

Ramirez-llanos, E. and Quijano, N. (2009). E. Coli bacterial foraging algorithm applied to pressure reducing valves control. *Proceedings of 2009 American Control Conference*, Hyatt Regency Riverfront, St. Louis, MO, USA, June 10 – 12, 2009, pp. 4488 – 4493.

Rashtchi, V., Bayat, A. and Vahedi, H. (2009). Adaptive step length bacterial foraging algorithm. *Proceeding of IEEE International Conference on Intelligent Computing and Intelligent Systems ICIS 2009*, 20 – 22 November 2009, Shanghai, China, pp. 322 – 326.

Refenes, A.N., Zapranis, A. and Francis, G. (1994). Stock performance modeling using neural networks: a comparative study with regression models. *Neural Networks*, **7**(2), pp. 375 – 388.

Rumelhart, D.E., Hilton G.E. and Williams, R.J. (1986). Learning representations by back-propagating errors, *Nature*, **323**, pp. 533 – 536.

Saber, A. Y. and Venayagamoorthy, G. K. (2008). Economic load dispatch using bacterial foraging technique with particle swarm optimization biased evolution. *Proceedings of 2008 IEEE Swarm Intelligence Symposium*, St. Louis MO USA, September 21 – 23, 2008, pp. 1 – 8.

Sakkalis, V., Cassar, T., Zervakis, M., Camilleri, K. P., Fabri, S. G., Bigan, C., Karakonstantaki, E., and Micheloyannis, S. (2008). *Computational Intelligence and Neuroscience*, **2008**, pp. 1 – 15, doi:10.1155/2008/462593.

Sakthivel, V. P., Bhuvaneswari, R. and Subramanian, S. (2010). Design optimization of three-phase energy efficient induction motor using adaptive bacterial foraging algorithm. *COMPEL: The International Journal for Computation and Mathematics in Electrical and Electronic Engineering*, **29**(3), pp. 699 – 726.

Shaheed, M. H. (2000). Neural and genetic modelling, control and real-time finite element simulation of flexible manipulators. PhD thesis, Department of Automatic Control and Systems Engineering, The University of Sheffield, UK.

Shaheed, M. H., Poerwanto, H. and Tokhi, M. O. (2004). Adaptive inverse-dynamic and neuro-inverse-dynamic active vibration control of a single-link flexible manipulator. *Proceedings of IMechE 219 Part I: Journal of Systems and Control Engineering,* pp. 431 – 448 (2004).

Shaheed, M.H. and Tokhi, M.O. (2002). Dynamic modelling of a single-link flexible manipulator: parametric and non-parametric approaches. *Robotica*, **20**, pp. 93 – 109.

Shaheed, M. H., Poerwanto, H. and Tokhi, M. O. (2005). Adaptive inverse-dynamic and neuro-inverse-dynamic active vibration control of a single-link flexible manipulator. *Proceedings of IMechE Vol. 219 Part I: Journal of Systems and Control Engineering*, **219**, pp. 431 – 448.

Shaheed, M. H., Tokhi, M. O., Chipperfield, A. J. and Azad, A. K. M. (2001). Modelling and open-loop control of a single-link flexible manipulator with genetic algorithms. *Journal of Low Frequency Noise, Vibration and Active Control,* **20**(1), pp. 39 – 55.

Sharma, S. K., Irwin, G. W., Tokhi, M. O. and McLoone, S. F. (2003). Learning soft computing control strategies in a modular neural network architecture. *Engineering Applications of Artificial Intelligence,* **16**, pp. 395 – 405.

Shen, H., Zhu. Y., Zhou, X., Guo, H., and Chang, C. (2009). Bacterial foraging optimization algorithm with particle swarm optimization strategy for global numerical optimization. Proceedings of The 1st ACM/SIGEVO summit on Genetic and Evolutionary Computation GEC'09, June 12 – 14, 2009, Shanghai, China, pp. 497 – 504.

Siddique, M.N.H. (2002). Intelligent control of flexible-link manipulator systems. PhD thesis, Department of Automatic Control and Systems Engineering, The University of Sheffield, UK.

Siddique, M.N.H. and Tokhi, M.O. (2006). GA-based neural fuzzy control of flexible-link manipulators. *Engineering Letters Special issue on Hybrid Intelligent Systems using Neural Networks, Fuzzy Logic and Genetic Algorithms, Oscar Castillo Edt,* **13**(2).

Simani, S. and Bonfe, M. (2009). Fuzzy modelling and control of the air system of a diesel engine. *Advances in Fuzzy Systems*, **2009**, pp. 1 – 14. doi:10.1155/2009/450259.

Sinha, A. (2007). Optimal filter design for face classification using bacteria foraging algorithm. *Proceedings of the 6th WSEAS International Conference on Circuits, Systems, Electronics, Control and Signal Processing,* Cairo, Egypt, December 29 – 31, 2007, pp. 399 – 403.

Sivanandam, S. N., Sumathi, S. and Deepa, S. N. (2007). *Introduction to fuzzy logic using MATLAB*. Springer-Verlag Berlin Heidelberg.

Sowell, F. (1992). Modelling long-run behaviour with the fractional ARIMA model. *Journal of Monetary Economics*, **29**, pp. 277 – 302.

Sreenivasa Rao, K. and Yegnanarayana, B. (2007). Modelling durations of syllables using neural networks. *Computer Speech and Language*, **21**, pp. 282–295.

Su, T-J., Chen, G-Y., Cheng, J-C. and Yu, C-J. (2010). Fuzzy PID controller design using synchronous bacterial foraging optimization. *Proceedings of The 3rd International Conference on Information Sciences and Interaction Sciences*, 23 – 25 June, 2010, Chengdu, China, pp. 639 – 642.

Sugeno, M. and Kang, G.T., (1988). Structure identification of fuzzy model. *Fuzzy Sets and Systems*, Vol. 28, pp. 15-33.

Sumanbabu, B., Mishra, S., Panigrahi, B. K. and Venayagamoorthy, G. K. (2007). Robust tuning of modern power system stabilizers using bacterial foraging algorithm. *Proceedings of IEEE congress on Evolutionary Computation*, 25 – 28 September, 2007, Singapore, pp. 2317 – 2324.

Sun, Y.L., and Er, M.J. (2004). Hybrid fuzzy control of robotics systems. *IEEE Transactions on Fuzzy Systems*, **12**(6), pp. 755–765.

Suzuki, Y., Ovaska, S. J., Furuhashi, T., Roy, R. and Dote, Y. Eds. (2000). *Soft Computing in Industrial Applications*. London, U.K.: Springer – Verlag.

Sze, T.L. (1995). *System identification using radial basis neural networks*. PhD thesis Department of Automatic Control and Systems Engineering, The University of Sheffield, Sheffield, U.K.

Takagi, T. and Sugeno, M. (1985). Fuzzy identification of systems and its application to modeling and control. *IEEE Transaction on Systems, Man and Cybernetics***,** **15**, pp. 116-132.

Talebi, H.A., Patel, R.V. and Asmer, H. (1998). Dynamic modeling of flexible-link manipulators using neural networks with application to the SSRMS. *Proceedings of the 1998 IEEE/RSJ International Conference on Intelligent Robots and Systems*, Victoria, B.C., Canada October 1998, pp. 673 – 678.

Talebi, H.A., Khorasani, K. and Patel, R. V. (2002). Tracking control of a flexible-link manipulator using neural networks: experimental results. *Robotica*, **20**, 417 – 427.

Tatli, H. and Sen, Z. (1999). A new fuzzy modelling approach for predicting the maximum daily temperature from a time series. *Turkish Journal of Engineering and Environmental Science*, **23**, pp. 173 – 180.

Tokhi, M.O. and Azad, A. K.M. (2008). *Flexible manipulators: modelling, simulation and control*. Institution of Engineering and Technology. UK.

Tokhi, M. O. Md zain, M. Z., Alam, M. S. and Mohamed, Z. (2004). An iterative learning control approach for vibration suppression of flexible manipulator systems. Proceedings of Control 2004, University of Bath, UK, September 2004, ID-091, pp. 1 – 5.

Tokhi, M. O. and Md Zain, M. Z. (2006). Hybrid learning control schemes with acceleration feedback of a flexible manipulator system. *Proceedings of IMechE Vol. 220 Part I: Journal of Systems and Control Engineering*, 220, pp. 257 – 267.

Tokhi, M. O. and Azad, A. K. M. (1995). Real time finite difference simulation of a single-link flexible manipulator incorporating hub inertia and payload. *Proceedings of I MechE-I: Journal of Syatems and Control Engineering*, **209**(11), pp. 21 – 33.

Tokhi, M.O., Azad, A.K.M. (1997). Design and development of an experimental flexible manipulator system. *Robotica*, **15**(Part 3), pp. 283–292.

Tokhi, M. O., Poerwanto, H. and Azad, A. K. M. (1995). Dynamic simulation of flexible manipulator incorporating hub inertia, payload and damping. *Machine Vibration*, **4**, pp. 106 – 124.

Tokhi, M. O., Mohamed, Z. and Azad, A. K. M. (1997). Finite difference and finite element approaches to dynamic modelling of a flexible manipulator. *Proceedings of I MechE-I: Jornal of Systems and Control Engineering*, **211**(12), pp. 145 – 156.

Tokhi, M.O., Mohamed, Z. and Shaheed, M. H. (2001). Dynamic characterisation of a flexible manipulator system. *Robotica*, **19**, pp. 571 – 580 (2001).

Tokhi, M.O. and Mohamed, Z. (1999). Finite element approach to dynamic modelling of a flexible robot manipulator: Performance evaluation and computational requirements. *Communications in Numerical Methods in Engineering,* **15**, 669–676 (1999).

Tripathy, M., Mishra, S. and Venayagamoorthy, G. K. (2006). Bacteria foraging: a new tool for simultaneous robust design of UPFC controllers. *Proceedings of 2006 International Joint Conference on Neural Networks*, Sheraton Vancouver Wall Centre Hotel, Vancouver, BC, Canada, July 16 – 21, 2006, pp. 2274 – 2280.

Tripathy, M. and Mishra, M. (2007). Bacteria foraging-based solution to optimize both real power loss and voltage stability limit. *IEEE Transactions on Power Systems*, **22**(1), pp. 240 – 248.

Tripathy, M., Mishra, S., Lai, L. L., and Zhang, Q. P. (2006). Transmission loss reduction based on FACTS and bacteria foraging algorithm. *T. P. Runarsson, et. al. (Eds.): PPSN IX, LNCS*, **4193**, pp. 222–231.

Tse, F. S., Morse, I. E. and Hinkle, T. R. (1980). *Mechanical Vibrations Theory and Applications,* Allyn and Bacon Inc., Boston.

Ulagammai, M., Venkatesh, P., Kannan, P. S., and Padhy, N. P. (2007). Application of bacterial foraging technique trained artificial and wavelet neural networks in load forecasting. *Neurocomputing*, **70**, pp. 2659 – 2667.

Usoro, P.B. Nadira, R. and Mahil, S.S. (1986). A finite element / Lagrange approach to modelling lightweight flexible manipulators. *Transactions of ASME: Journal of Dynamic Systems, Measurement and Control*, **108**, pp. 198–205 (1986).

Verspecht, J. (1996). Black box modelling of power transistors in the frequency domain. *Conference Record of the INMMC 1996 Workshop - Duisburg (Germany),* pp. 1 – 7.

Yamano, M., Konno, A. and Uchiyama, M. (2000). Experiments on capturing a floating object by two flexible manipulators. *Proceedings of the IEEE International Conference on Robotics and Automation*, San Francisco, California, USA, April 2000, pp. 482 – 487.

Ying, C., Hua, M. and Zhen, J. (2008). BFA based neural network for image compression. Journal of Electronics (China), **25**(3), May 2008, pp. 405 - 408.

Yong, S., Zhimin, L. and Dongsheng, Z. (2009). Optimal multi-objective design of power system damping controller using synergy of bacterial foraging and particle swarm optimization. *Proceedings of The 1st ACM/SIEGEVO Summit on Genetic and Evolutionary Computation GEC'09,* June 12 – 14, 2009, Shanghai, China, pp. 1037 – 1040.

Yu, R. Lim, K. P., Wu, D., Pan, F., Li, Z. G., Feng, G. and Wu, S. (2002). A 2-stage partial distortion search algorithm for block motion estimation. *Y.-C. Chen, L.-W. Chang, and C.-T. Hsu (Eds.): PCM 2002*, LNCS 2532, Springer-Verlag Berlin Heidelberg 2002, pp. 127−134.

Yurkovich, S. (1992). Flexibility effects on performance and control. M.W. Spong, F.L. Lewis & C.T. Abdallah (Eds.), *Robot Control (Part 8),* pp.321–323. New York: IEEE Press.

Widrow, B. (1987). ADALINE and MADALINE – 1963, Plenary speech. *Proceedings of 1st IEEE International Conference on Neural Networks*, San Diego, CA, pp. 143 – 158.

Zadeh, L.A.(1965). Fuzzy sets. *Information and Control*, **8**, pp. 338 – 353.

Zadeh, L.A. (1968). Fuzzy algorithms. *Information and Control*, **12**, pp. 94 – 102.

Zadeh, L.A. (1973). Outline of a new approach to the analysis of complex systems and decision process, *IEEE Transaction on Systems, Man and Cybernetics (SMC)*, **3**, pp. 28 – 44.

Zalzala, A. M. and Morris, A.S. (1991). A neural network approach to adaptive robot control. *International Journal of Neural Networks*, **2**(1), March 1991, pp. 17 – 35.